Faculty of Science and Engineering
Department of Civil Engineering

Design of Ballasted Railway Track Foundations using Numerical Modelling with Special Reference to High Speed Trains

Md. Abu Sayeed

This thesis is presented for the Degree of
Doctor of Philosophy
of
Curtin University

June 2016

ABSTRACT

The research presented in this thesis focuses on the development of a new design method for ballasted railway track foundations using advanced numerical modelling, with special reference to high speed trains. In recent years, congestion on highways symptomizes that railways have become the most popular means of public transportation, which has increased the demand for heavier and faster trains. Heavy axle loads and high speed trains increase vibrations in railway tracks and possible nearby structures. As a consequence, both the risk of train operations and cost of maintenance have recently increased significantly. In order to avoid such risks and to minimise the construction and maintenance costs, new design methods for ballasted railway track foundations are immensely needed.

Proper design of ballasted railway track foundations entails accurate estimation of the thickness of granular layer (i.e. ballast and sub-ballast) in such a way that it can provide protection against subgrade failure and limit the excessive track deformation induced by the train repeated moving loads. Therefore, a comprehensive study is timely warranted to investigate the influence of repeated loading on the subgrade failure and the corresponding cumulative plastic (permanent) deformation of different track layers. In order to provide stability to railway tracks against failure, the total deformation of track substructure (i.e. granular media and subgrade) has to be limited to a tolerable value. Existing design methods have not captured the critical fact that ballast can be liable for up to 40% of the total track deformation. Besides, available design methods usually calculate the subgrade stresses from models based on static loading multiplied by an impact factor to capture the train dynamic loading; however, this inevitably fails to capture the true effects of train moving loads.

In this thesis, a new practical design method for ballasted railway track foundations was inspired from the shortcomings of the existing design methods. The proposed design method was developed based on improved empirical models and sophisticated three-dimensional (3D) finite element (FE) numerical analyses. The improved empirical models were used for predicting the cumulative plastic deformations of the track, whereas the stress behaviour of ballast and subgrade under applications of train

repeated loadings were determined from the 3D FE numerical modelling. In the improved empirical models, the effects of number of load applications, stress state, physical state and material type were considered. The impact of stress state was explicitly represented by the induced deviator stress while the material physical state was indirectly specified by its monotonic strength obtained from the conventional triaxial compression tests. The material type was considered through certain material parameters involved. In the 3D FE modelling, the dynamic response of railway tracks under a variety of train-track-ground conditions was investigated and quantified. The FE modelling was also used to investigate the impact of train speed on the behaviour of ballasted railway track foundations and to evaluate the critical speed under various conditions of the train-track-ground system. The practical implications of the obtained results were critically analysed and discussed to facilitate the development of the proposed design method.

The results obtained from the study were synthesised into a new design method comprised of two design procedures that aim at preventing the progressive shear failure of the subgrade and the excessive plastic deformation of the track. All governing parameters that significantly affect the selection of the granular layer thickness for preventing the track failure were carefully considered in the proposed design method. The method was then evaluated against field data of several track sites and the results were found to be in excellent agreement with the field observations. The proposed design method is expected to provide a significant contribution to the current railway track code of practice.

PUBLICATIONS

The following publications are produced from the research work conducted in this PhD thesis:

Referred Journal Papers

Sayeed, M. A., and Shahin, M. A. (2016). "Three-dimensional numerical modelling of ballasted railway track foundations for high-speed trains with special reference to critical speed." *Transportation Geotechnics*, 6, 55-65.

Sayeed, M. A., and Shahin, M. A. "Design of Ballasted Railway Track Foundations using Numerical Modelling: Part I-Development." *Canadian Geotechnical Journal*, (to be submitted).

Sayeed, M. A., and Shahin, M. A. "Design of Ballasted Railway Track Foundations using Numerical Modelling: Part II-Applications." *Canadian Geotechnical Journal*, (to be submitted).

Referred Conference Paper

Sayeed, M. A., and Shahin, M. A. (2015). "Modelling of ballasted railway track under train moving loads." *Proceedings of the 12th Australia New Zealand Conference on Geomechanics*, Wellington, New Zealand, Paper No. 132: 1-8.

Sayeed, M. A., and Shahin, M. A. (2016). "Investigation into impact of train speed for behavior of ballasted railway track foundations." *Proceedings of the 3rd International Conference on Transportation Geotechnics*, Procedia Engineering, 143, 1152-1159. .

Sayeed, M. A., and Shahin, M. A. (2017). " Investigation into Some Design Aspects of Ballasted Railway Track Foundations" *Tenth International Conference on the Bearing Capacity of Roads, Railways and Airfields*, Athens, Greece, (Submitted).

ACKNOWLEDGEMENTS

In the name of Allah, the most gracious, the most merciful. I would like to express my enormous gratitude to my supervisor, Associate Professor Mohamed Shahin, Department of Civil engineering, Curtin University, for his encouragement, thoughtful guidance, continual support in professional and personal matters and invaluable help throughout this research. His patience and availability to answer my queries whenever needed with his heavy workload are deeply appreciated. In addition, his numerous comments, constructive criticisms, suggestions, encouragement and friendship have been of great value to me, and this work would not be possible without his contribution.

My gratitude is also extended to my co-supervisor, Professor Hamid Nikraz, Department of Civil engineering, Curtin University, for his kind support, precious suggestions and comments during my candidature. I would also like to thank Dr Wasiul Bari for his valuable comments, suggestions and help in preparing this thesis. I am also grateful to Dr Mostafa Ismail for his professional editing of this thesis.

I wish to thank the Department of Civil Engineering, Curtin University, for the provision of excellent research support and facilities. Heartfelt acknowledgements are expressed to all academic and non-academic members of the Department of Civil Engineering and in particular, Mrs Diane Garth and Mr Frankie Sia for their tireless assistance and warm-hearted cooperation during my study. My special thanks are also extended to my fellow postgraduate students for their friendship and company. The scholarship awarded to this research project by Curtin University is sincerely acknowledged.

Finally, I am indebted to my family and in particular my parents, Md. Tojammul Hoque and Mst Khairun Nessa. Without their encouragement, guidance and sacrifices, I may never have come this far in my study. Very special and sincere gratitude is offered to my wife, Farjana Binte Hye, and to my daughter, Wazifa Binte Sayeed, for their constant love, patience, understanding and strength throughout my PhD program. Their supports, spoken or unspoken, have helped me to negotiate all the twists and turns of my PhD work.

TABLE OF CONTENTS

LIST OF FIGURES

LIST OF TABLES

LIST OF SYMBOLS

a	material parameter depends on soil type
a_r	deformation at the reference tonnage
$a_0^{/}$	slope of the semi-logarithmic relation
A	area coefficient
A_{sb}	sleeper/ballast effective contact area
b	material parameter depends on soil type
b_t	track width
c	cohesion
c_d	viscous damping of the foundation
C	train speed
$[C]$	damping matrix
C_{cr}	critical speed
$C_{cr\,(particular\,train)}$	critical speed of the desired particular train
$C_{cr\,(X-2000\,HST)}$	critical speed of the X-2000 HST
$C_{cr\,(Thalys\ HST)}$	critical speed of the Thalys HST
$C_{\max}$	maximum train speed
C_n	Courant number
C_p	compression wave velocity
C_R	Raleigh waves velocity
C_s	shear wave velocity
d	super elevation deficiency
D	empirical coefficient
D_w	wheel diameter
E	dynamic modulus of elasticity
E_b	ballast modulus
E_i	Young's modulus of elasticity at the *i*th layer
EI	flexural stiffness of the Winkler beam
E_s	subgrade modulus
E_{sb}	sub-ballast modulus

f_c	carriage passing frequency
$f_{c(particular\ train)}$	carriage passing frequency of a particular train
$f_{c(X\text{-}2000\ HST)}$	carriage passing frequency of the X-2000 HST
$f_{c(Thalys\ HST)}$	carriage passing frequency of the Thalys HST
F_2	coefficient depending on the sleeper type and track maintenance
FI	fouling index
g	acceleration due to gravity
G	static axle load
$G_{s\text{-}b}$	specific gravity of ballast material
$G_{s\text{-}f}$	specific gravity of fouling material
h	thickness of ballast and sub-ballast layer
$\tilde{h}$	equivalent depth below the sleeper
h_i	thickness of the *i*th layer
h_s	super elevation
h_v	vertical distance between the rail top and the vehicle's centre of gravity
H	material thickness
H_b	thickness of granular ballast layer
H_{bi}	thickness of each sublayer for the ballast
H_s	subgrade thickness
H_{sb}	sub-ballast thickness
H_{si}	thickness of each sublayer of the subgrade
H_w	crosswind force
I	moment of inertia
I_ε	strain influence factor
I_{ε_b}	ballast strain influence factor
I_{ε_s}	subgrade strain influence factor
I_{ρ_s}	subgrade deformation influence factor
k	stiffness of the Winkler foundation
K	modulus number
$[K]$	stiffness matrix
l	total length of sleeper

l_e	effective length of sleeper supporting the maximum rail seat load
L	length coefficient
L_a	distance between axles
L_b	distance between two bogies
L_c	carriage length
L_{min}	distance between two adjacent *loading nodes*
$L_{particular\ train}$	carriage length of the desired particular train
$L_{X-2000\,HST}$	carriage length of the X-2000 HST
$L_{Thalys\,HST}$	carriage length of the Thalys HST
m	material parameter depends on soil type
$[M]$	mass matrix
M_b	mass of ballast materials
M_f	mass of fouling materials
n	modulus exponent
N_b	number of load cycles on ballast
N_{bi}	numbers of P_{si} load cycles in the ballast
N_s	number of load repetitions in the subgrade layer
N_{si}	numbers of P_{si} load cycles in the subgrade
N_{si}^{o}	equivalent load cycles of maximum static wheel load P_s in subgrade
P	static wheel load
P_c	vertical distance between centre of gravity of train and centre of rail
P_d	design wheel load
P_F	front wheel load of carriage
P_L	applied load essential to introduce the lateral displacement
P_{Lc}	lateral force at curved track on the outer rail
P_R	rear wheel load
P_s	static wheel load
$P_d^{/}$	dynamic wheel load
P_w	distance between the centre of wind force and centre of the rail
P_4	percentage of ballast particle passing the 4.75 mm (no. 4) sieve
P_{200}	percentage of ballast particle passing the 0.075 mm (no. 200) sieve

q_r	maximum rail seat load
$Q_{centrifugd}$	vertical wheel load due to centrifugal force on the outer rail
$Q_{dynamic}$	dynamic wheel load component resulting from train speed
$Q_{quasi-static}$	vertical quasi-static wheel load
Q_{static}	vertical static wheel load
Q_{total}	total vertical wheel load
Q_{wind}	vertical wheel load due to wind force on the outer rail
r_c	radius of a circle whose area is equivalent to the sleeper bearing area
$R_{b\text{-}f}$	relative ballast fouling ratio
R_c	radius of track curvature
R_f	failure ration
s	standard deviation of applied loading or deflection
S	ballast settlement
$Se(t')$	mean ballast deformation over a unit length at tonnage t'
t	time
t_r'	reference tonnage taken as two million tonnes.
T_i	total traffic tonnage for the wheel load P_{si}
u	coefficient subjected to the upper confidence limit
u_v	vertical displacement of track
V_1	volume of contaminated void taken from the ballast profile
V_2	volume of total void taken from ballast profile
w	sleeper width
x	material parameter depends on ballast type
x'	mean rail stress
X	maximum applied load or deflection
X'	empirical constants depending on the ballast conditions
y	material parameter depends on ballast type
Y'	empirical constant depending on the ballast conditions
$Y_{centrifugd}$	lateral load caused by centrifugal force on the outer rail
$Y_{dynamic}$	dynamic lateral wheel load component
$Y_{e_{max}}$	maximum quasi-static lateral force

Y_{flange}	lateral load in curve caused by flanging against the outer rail
$Y_{quasi-static}$	quasi-static lateral wheel load
Y_{total}	total lateral wheel load
Y_{wind}	lateral load due to cross wind
z	material parameter depends on ballast type
Z	empirical constant
α	mass proportional damping coefficient
$\alpha^{/}$	speed coefficient
β	stiffness proportional damping coefficient
$\beta^{/}$	speed coefficient
γ	unit weight,
$\gamma^{/}$	speed coefficient
δ	impact factor dependent upon the track condition
Δt	time step
η	speed factor
ϕ	friction angle
φ	dimensionless dynamic impact (or amplification) factor
σ_1	major principal stress
σ_3	confining pressure
σ_d	deviatoric stress
σ_{d_b}	deviatoric stress in the ballast layer
σ_{d_s}	deviatoric stress in the subgrade soil
$\sigma_{(d\_s)a}$	allowable deviatoric stress at the subgrade surface
$(\sigma_d)_{TS}$	threshold stress of soil at yield in a standard test at σ_3 = 0.35 kg/cm^2
$(\sigma_d)_{TP}$	threshold stress of soil at any other confining pressure
σ_s	subgrade stress
σ_{sb}	average stress at the sleeper/ballast contact surface
σ_{s_b}	compressive strength of the ballast under 50 kPa confining pressure
σ_{s_s}	unconfined compressive strength of subgrade soil

ε_1	average vertical strain after the first load cycle
ε_N	plastic strain after the N_b load cycle
ε_{p_b}	cumulative plastic strain in the ballast
$\varepsilon_{(p\_b)i}$	plastic strain at the centre of each ballast sublayer
ε_{p_s}	cumulative plastic strain of subgrade
$\varepsilon_{(p\_s)a}$	allowable cumulative plastic strain at the subgrade surface
$\varepsilon_{(p\_s)i}$	plastic strain at the centre of each subdivided layer of subgrade
ρ_b	track deformation by the ballast layer
ρ_{b1}	ballast deformation after the first load cycle
ρl	mass per unit length of the beam
ρ_s	cumulative plastic deformation of the subgrade layer
ρ_{sa}	allowable subgrade deformation for the design traffic tonnage
ρ_t	total cumulative plastic deformation of the track under repeated load
ρ_{ta}	allowable plastic deformation of the track
ω_i	natural frequency of mode-1 of the full model
ω_j	natural frequency of mode-2 of the full model
v	Poisson's ratio
v_i	Poisson's ratio at the *i*th layer
$\delta(x-Ct)$	Dirac delta function of the moving load at speed C
∞	infinity
ξ	hysteretic damping ratio

ABBREVIATIONS

AAR	Association of American Railroads
AREA	American Railway Engineering Association
BE	Boundary element
BEM	Boundary element method
BR	British Railways
CTRL	Channel Tunnel Rail Link
CWR	Continuously welded rail
DAF	Dynamic amplification factor
DC	Duncan-Chang
DEM	Discrete element method
FDM	Finite difference method
FE	Finite element
FEM	Finite element method
HALs	Heavy axle loads
HAT	Heavy axle train
HST	High speed train
HSTs	High speed trains
HTL	Heavy Tonnage Loop
JNR	Japanese National Railways
LE	Linear elastic
LTM	Low track modulus
MC	Mohr-Coulomb
MGT	Million gross tonnes
NC	Northeast Corridor
ORE	Office of Research and Experiments
PVC	Percentage void contamination
SBFEM	Scaled boundary finite element method
TLTM	Trial low track modulus
UCL	Upper confidence limit
UCS	Unconfined compressive strength
WSF	Wheel spacing factor
1D	One-dimensional
2D	Two-dimensional
3D	Three-dimensional

CHAPTER 1

INTRODUCTION

1.1 PREFACE

Recent traffic congestion on highways in many countries around the world has led railways to become the most popular means of public transportation, which has increased the demand for heavier and faster trains. An introduction of heavy axle loads and high speed trains in modern railway traffic creates high stresses in the track layers and causes excessive vibrations under dynamic loading. As a consequence, the risk associated with train operations has increased significantly in the form of train safety, degradation/deformation of track foundations, fatigue failure of rails and interruption of power supply to trains (Madshus and Kaynia, 2000). To avoid such risks and to fulfil the demand of modern railway traffic, advanced design methods for ballasted railway track foundations are necessary and timely warranted.

A conventional ballasted railway track is comprised of superstructure (rails, fastening system and sleepers) and substructure (ballast, sub-ballast and subgrade). The rails transfer the wheel loads to the supporting sleepers, which are spaced evenly along the rail length. The sleepers hold the rails in designated positions with a fastening system and anchor the superstructure into the ballast layer. The ballast and sub-ballast layer (often referred to as the granular layer) transmit the high imposed stress at the sleeper/ballast interface to the subgrade layer at a reduced level by spreading. In the design of ballasted railway track foundations, the thickness of the granular layer needs to be specified so that stresses applied to the subgrade are sufficiently reduced to prevent subgrade failure (Selig and Waters, 1994). Conventionally, the design of ballasted railway track foundations is also referred to as design of the granular layer thickness.

In the literature, several empirical and simplified theoretical methods have been proposed to calculate the granular layer thickness. These methods include the American Railway Engineering Association (AREA) manual (AREA, 1996); the Canadian Modified Method suggested by Raymond (1978); the Japanese National

Railways developed by Okabe (1961); the British Rail method proposed by Heath et al. (1972); and the UIC 719 R method offered by the International Union of Railways (1994). However, most of these design methods were based on stress analyses where all track layers were assumed as a homogeneous half-space (i.e. no allowance for the effect of stiffness of the individual track layers). Furthermore, the effect of repeated loading on the track settlement was not included as a design parameter. Thus, the application of these over-simplified methods for modern railway track design often only provides ballpark estimates and may lead to poor design in most cases.

The latest and probably the most robust design method currently available in the literature was developed about two decades ago by Li and Selig (1998a, b), which emphasised on preventing the progressive shear failure and excessive plastic deformation of the track subgrade. This method was based on the combined use of a multilayered analytical model (called GEOTRACK) together with extensive cyclic loading laboratory testing. This method provided some improvements; however, frequent maintenance is still required for tracks designed by most up-to-date standards that adopt existing design methods including Li-Selig method. The study reported by Burrow et al. (2007) and Gräbe (2002) confirmed the argument of Shahu et al. (2000) that existing design methods may not be appropriate for modern railway traffics. Accordingly, there is an immense need to develop advanced design methods that can carefully consider the factors affecting the response of railway track systems, leading to more reliable design.

In order to provide strong, safe, reliable and efficient pathway for train traffic, the total track deformation should not exceed a prescribed tolerable limit (Shahin, 2009). However, the critical factor of the deformation of granular layer was virtually overlooked in all available design methods, despite the fact that ballast can be responsible for up to 40% of the total track deformation, as indicated by many researchers (e.g. Li et al., 2002; Selig et al., 1981; Stewart, 1982). To avoid such a limitation, improved empirical models for predicting both the deformation of granular ballast and subgrade materials can be used for the development of an advanced design method for track foundations.

Furthermore, when a train runs along a track, the ballast and subgrade soil elements become subjected to complex loading, including the principal stress rotation (Brown, 1996; Powrie et al., 2007). Accordingly, train moving loads (i.e. cyclic loading with principal stress rotation) may affect the material stiffness and degree of cumulative plastic strain (Inam et al., 2012; Lekarp et al., 2000a; Lekarp et al., 2000b). However, in existing design methods, the models used to calculate the subgrade stresses were mostly based on static loading that cannot fully capture the dynamic effects of moving loads induced by the trains, which is a serious shortcoming of the available methods.

Over the years, the necessity to overcome the shortcomings of the analytical approaches has led to the development of numerical methods, which are facilitated by today's computers high processing capacity. Among the various available numerical methods [e.g. boundary element (BE) method (Andersen and Nielsen, 2003), finite element (FE) method (Banimahd et al., 2013; El Kacimi et al., 2013; Hall, 2003; Sayeed and Shahin, 2015) and 2.5D FE-BE method (Adam et al., 2000; Bian et al., 2014; Galvín et al., 2010; O'Brien and Rizos, 2005)], the FE method has been found to be the most useful tool for simulating the critical features of the train-track-ground interaction problem. Accordingly, sophisticated three-dimensional (3D) FE numerical modelling can be used to determine the induced stresses in the ballast and subgrade layers for the development of an advanced design method for ballasted railway track foundations.

Existing design methods also consider the effect of train speed by simply utilising several empirical formulas for estimating the dynamic amplification factor (DAF). Most of the DAF empirical formulas only consider the impact of train speed and loading characteristics, and neglect the characteristics of the train-track-ground condition. However, recent studies carried out by several researchers (e.g. Alves Costa et al., 2015; Sayeed and Shahin, 2016a) indicated that the DAF is significantly influenced by the characteristics of the subgrade. Moreover, due to resonance, catastrophic track deflection may occur when the train approaches the critical speed (Krylov, 1994; Madshus and Kaynia, 1999; Yang et al., 2009), which is also significantly influenced by the modulus and thickness of the subgrade medium and train geometry (Alves Costa et al., 2015; Sayeed and Shahin, 2016b). Unfortunately,

there is no proper guideline for considering the critical speed in the available design methods. Again, such limitations emphasise the need for developing an advanced design method that can consider the DAF carefully, and provide guidelines to determine the critical speed of the train-track-ground system to avoid undesirable scenario.

1.2 OBJECTIVES AND SCOPE OF THE THESIS

Inspired by the limitations discussed above, this research aimed to develop a new practical design method for ballasted railway track foundations that can overcome most shortcomings of existing design methods. The new design method was developed based on improved empirical equations and sophisticated 3D FE numerical modelling. The improved empirical equations were used for calculating the cumulative plastic deformations of the track substructure (ballast and subgrade) layers, whereas the stress parameters of these layers under train moving load were obtained from the 3D FE numerical modelling. The outcomes of the investigations were synthesised into a set of design charts that formed the core of the proposed method so that it can readily be used by railway geotechnical engineers for routine design practice. The specific objectives of this research can be summarised as follows:

1. To perform sophisticated 3D FE numerical modelling for analysis and prediction of the behaviour of railway track foundations, with special reference to high speed trains.

2. To categorise and understand the influence of key factors affecting the dynamic response of railway track foundations, including the impact of train critical speed.

3. To develop a new design method for railway track foundations based on 3D FE analyses and improved empirical models. The design method will be developed in the form of simple design charts and procedures so as to facilitate the use of the method by railway engineers for routine design practice.

4. To validate the developed design method using true case studies available in the literature.

1.3 ORGANISATION OF THE THESIS

This thesis is divided into six chapters, including the introductory chapter. An overview of the work presented in each chapter is described below.

Following this introductory chapter, Chapter 2 provides a brief overview of the different components of track structure, various modes of track failure and the possible remedial measures. Chapter 2 also includes a summary of past studies regarding the analysis and design methods of ballasted railway tracks, with emphasis on their limitations to identify the scope of the present work.

Chapter 3 presents the previous studies that dealt with the effect of repeated loading on the cumulative plastic deformation of granular ballast and also illustrates the proposed improvements to the existing empirical models for better estimation of the cumulative plastic strain and deformation of granular materials.

Chapter 4 describes the development and validation of a sophisticated 3D FE numerical modelling and analyses, which can accurately simulate and predict the dynamic response of railway tracks subjected to train moving loads. A comprehensive parametric study to investigate the track dynamic response and behaviour over a wide range of train-track-ground parameters is also presented in this chapter. In addition, a thorough investigation into the impact of various conditions of the train-track-ground system on the dynamic amplification factor (DAF) and critical speed are presented.

Chapter 5 formulates the design methodology including design charts based on improved empirical models for predicting the cumulative plastic strain of ballast and subgrade materials, and sophisticated 3D FE modelling employed for the stress analysis.

The summary, conclusions and recommendations for further studies based on the current research are given in Chapter 6. Finally, a list of references and appendices follow Chapter 6.

CHAPTER 2

LITERATURE REVIEW

2.1 INTRODUCTION

Ballasted railway track is designed and built to provide a strong, safe, reliable and efficient pathway for the movement of trains; hence, the track should be durable enough in lateral, longitudinal and vertical directions under various conditions of wheel loading and train speed. For design of ballasted railway track foundations, the thickness of granular layer (i.e. combined thickness of ballast and sub-ballast) has to be estimated precisely so that the train induced stress applied to the subgrade is decreased adequately to provide protection against track failures. Generally, the thickness of granular layer is estimated on the basis of experience or using empirical equations recommended by various railway authorities. However, these methods are not suitable for modern railway traffic requirements (Burrow et al., 2007; Gräbe, 2002). Therefore, to develop a reliable design method, detailed cross-disciplinary knowledge is needed to advance the design process. This includes the fundamental characteristics of track components, various modes of track failure and their remedy measures and state-of-the-art analysis and design methods of ballasted railway track foundations. Accordingly, the aim of this chapter is to provide an overview of the relevant literature and present a background for this thesis. It is not intended to cover every piece of the literature on track design; rather it is meant to broadly review the more important aspects of ballasted railway track design in relation to the present research.

2.2 RAILWAY TRACK COMPONENTS

Ballasted railway track is the most traditional and universally preferred railway track structure, because of its low construction cost and simplicity of maintenance (Kaewunruen and Remennikov, 2008). It is a layered discrete system that consists of rails, fasteners, rail pads, sleepers, ballast, sub-ballast and subgrade, as shown in Figure 2.1. In general, a ballasted railway track structure can be divided into two main groups, namely the track superstructure and substructure. The track

superstructure refers to rails, rail pads, fastening systems and sleepers or ties, whereas the track substructure is associated with the geotechnical system, which is composed of a granular media of ballast and sub-ballast overlying a subgrade soil. In the sections that follow, the components of railway track structure and their relevant functions are briefly discussed.

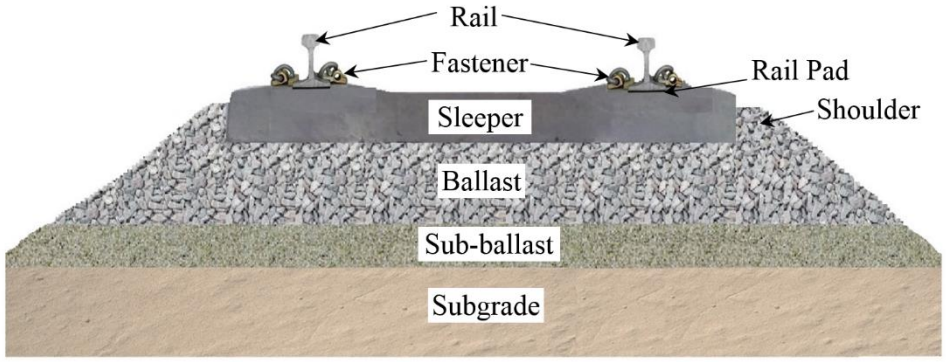

(a) Transverse Section

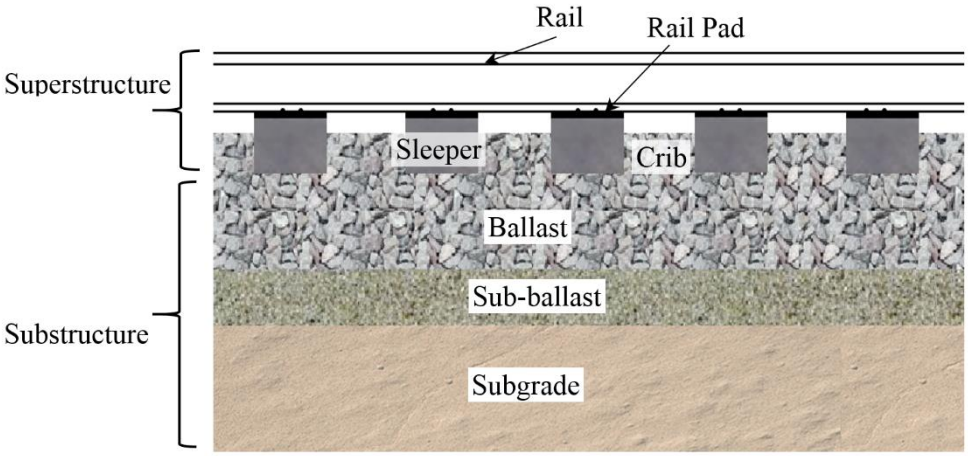

(b) Longitudinal Section

Figure 2.1: Typical ballasted railway track cross section.

2.2.1 Rails

The rails are a pair of parallel steel beams laid along the longitudinal direction of the track that support the train wheels vertically and laterally, and provide a stable platform for circulation of wheels as smoothly as possible (Selig and Waters, 1994). The main function of rails is to transfer the contacted wheel loads (i.e. vertical forces as well as lateral forces and any accelerating or braking forces) to the supporting sleepers, which are spaced evenly along the rail length. Besides, rails in modern track

are used for transferring signals and act as a conductor on an electrified line (Esveld, 2001). In order to perform the main functions stated above, the rails should have sufficient stiffness. For this purpose, over the world, the standard section profile of rail is 'I' shaped, which has the least cross-sectional area but the higher moment of inertia that delivers greater flexural strength. In addition of having sufficient stiffness, the rail and wheel surfaces should be smooth enough, as unevenness in these surfaces generates additional dynamic load on the track structure, especially in the case of running high speed trains (HST).

The rail beams are usually connected by bolted joints or welding. In bolted connection, the rails are joined using bolts and drilled plates named as 'fishplate'. The discontinuity of rails resulting from the joints creates unwanted vibrations and additional dynamic loads, which reduces the passengers' comfort and may cause failure at the joints. The impact of dynamic load and lower rail stiffness at these joints cause higher stress on the ballast and subgrade, and consequently the rate of degradation and deformation of substructure materials increases, which demands frequent maintenance of the track (Salim, 2004). On the other hand, continuously welded rail (CWR) reduces wear and tear of rolling stocks and track damages, and provides better passenger comfort. Thus, CWR has replaced the use of bolted joints in most of the main passenger and freight train tracks (Selig and Waters, 1994).

2.2.2 Rail Fastening System and Pads

In ballasted railway tracks, the rails are discretely held by sleepers that are spaced along the longitudinal direction of the railway. The rail and sleepers are usually secured by steel fasteners against vertical, lateral and longitudinal movement. A typical fastening system is shown in Figure 2.2. Depending on the rail section and type of sleepers, different types of fasteners (e.g. e-clip, fast clip, tension clamp, bolt clamped, etc.) are used by railway authorities throughout the world. With the present railway technology, the rail is not placed just on top of the sleeper; instead, a rail pad of 10 to 15 mm thickness, which consists of an elastic material, is used between the rail and sleeper. The major functions of the rail pad include providing resiliency in the rail-sleeper system, damping the train-induced vibration, and preventing or decreasing rail-sleeper contact attrition (Selig and Waters, 1994).

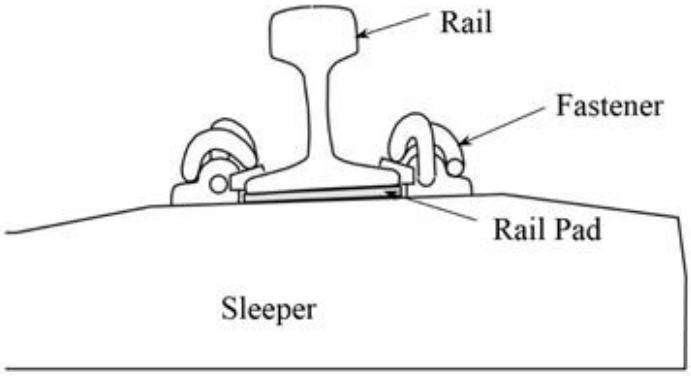

Figure 2.2: Typical fastening system in railway tracks (Dahlberg, 2003).

2.2.3 Sleepers or Ties

The sleepers (or ties) receive the wheel load through the rail and distribute it in the transverse direction of the track to the wider ballast area, to reduce the stress to a permissible level. They hold the rails in designated position with the fastening system and anchor the superstructure in the ballast layer, thus preventing the longitudinal and lateral movements. The sleepers can be made of wood (timber), steel or concrete. Esveld (2001) classified the timber sleepers into two groups based on the strength of wood: softwood (e.g. pinewood) and hardwood (e.g. oak, beech, tropical tree). Based on the geometry, the concrete sleepers are categorised as twin-block or mono-block (Figure 2.3). The various types of the sleepers, their dimension and spacing are summarised in Table 2.1. Timber sleepers are generally used in the conventional or older railway tracks, as they are inexpensive and available worldwide. Prestressed mono-block concrete sleepers are more dominantly used in the recent tracks for high speed trains as they are more durable, stronger, and therefore provide better fastening than timber sleepers. The main drawback of the prestressed concrete mono-block sleepers is their handling, as they are considerably heavier than the timber sleepers. Besides, they should have rail pads between the rail and sleeper to provide sufficient resiliency. In Europe, another extensively used sleeper is the twin-block sleeper, which consists of two reinforced concrete blocks connected with a steel bar. This type of sleeper is much lighter than the mono-block sleeper, but its handling and placing are still limited due to its tendency to twist during lifting. However, although the handling of steel sleepers is not difficult, they are hardly used due to the fear of corrosion and high cost (Bonnett, 2005).

(a) Mono-block concrete sleeper (b) Twin-block concrete sleeper

Figure 2.3: Types of concrete sleepers (Kaewunruen and Remennikov, 2008).

Table 2.1: Typical sleeper dimensions (Selig and Waters, 1994).

Location	Material	Width (mm)	Length (mm)	Spacing (mm)
Australia	Wood	210-260	2000-2743	610-760
	Concrete	-	-	600-685
China	Wood	190-220	2500	543-568
	Concrete	240-290	2500	568
Europe	Wood	250	2600	630-700
	Concrete	250-300	2300-2600	692
North America	Wood	229	2590	495
	Concrete	286	2629	610
South Africa	Wood	250	2100	700
	Concrete	203-254	2057	700
		230-300	2200	600

2.2.4 Ballast

Ballast is the crushed granular material used in railway track in which the sleepers are embedded to support the superstructure. It is the top layer of track substructure, placed above the sub-ballast or subgrade layer, which anchors the track in place and reduces the stress transmitted to the subgrade, as reported by various researchers (e.g. Selig, 1998). Conventionally, crushed, angular, clean, strong stones and rocks (igneous or well-cemented sedimentary rocks) are been considered as a source of good quality ballast. In addition, good ballast materials should be uniformly graded,

and without the possibility of cementing action (Selig and Waters, 1994). The particle size should be 28-50 mm as aggregates finer than 28 mm do not provide adequate drainage, whilst particles larger than 50 mm do not offer suitable stress distribution (Bonnett, 2005). Generally, no particular specification for the index characteristics of ballast has been established to date. Therefore, a wide variety of materials are used as ballast, such as crushed granite, dolomite, rhyolite, basalt, limestone, gneiss, slag and gravel. The choice of ballast materials depends mainly on the quality and availability of materials and cost.

Ballast performs the following fundamental functions to serve as a stable platform for the sleeper and rail (Esveld, 2001; Salim, 2004; Selig and Waters, 1994):

- Provide a firm and stable foundation, and support the sleeper evenly with high bearing strength.
- Transfer the stress on the ballast layer to the subgrade surface to a reduced and tolerable level.
- Provide adequate support to the sleepers against vertical, lateral and longitudinal forces induced by moving train load.
- Reduce the total plastic deformation of track.
- Provide dynamic resiliency and energy absorption for the track.
- Provide adequate hydraulic conductivity for immediate drainage of water falling onto the track.
- Facilitate renovation operation (readjust the track geometry by ballast tamping or stoneblowing), redesign or reconstruction of the track.
- Relieve frost weathering by not being frost-vulnerable and by applying an insulation coat to guard the underlying layers.
- Prevent weed growth by providing a protection layer that is incompatible for weeds.
- Provide adequate electrical resistance between rails.
- Absorb airborne noise.

2.2.5 Sub-ballast

Sub-ballast is a layer of aggregates usually comprised of locally available well graded crushed rock or sand-gravel mixtures, which is placed between the ballast and subgrade. They must be durable enough to bear the train-induced dynamic

loads imposed via the rail-sleeper-ballast layer. Besides, it should have the proper filtering function. The sub-ballast layer can be used economically to fulfil the following key functions of ballast (Shahu et al., 2000):

- Transfer and distribute the train-induced stress from the ballast layer to the underlying subgrade soil over a wider area to an acceptable level.
- Extend the subgrade frost protection by providing an insulation layer.

In addition, the sub-ballast layer has some other essential functions for satisfactory track performance that cannot be achieved by the ballast layer alone. These are as follows (Selig and Waters, 1994):

- Separate the ballast layer from the subgrade, and hence prevent penetration of the coarse ballast materials into the subgrade layer, and also prohibit upward migration of the fine subgrade materials into the ballast layer.
- Resist clay particles to mix with the infiltrated water, which may lead to slurry (mud) formation. This function prevents mud pumping, which is one of the major problems of ballast fouling and subgrade disgrace.
- Receive the rain water flowing through the ballast and drain it away to trenches at the sides of the track.
- Provide drainage of the underlying subgrade water that might flow upward.

2.2.6 Subgrade

The subgrade is the bottom layer of track substructure upon which the other component of railway track is built. In general, it could be the naturally deposited soil or a specially stabilised soil when the naturally deposited soil cannot bear the train-induced load. In some special cases (e.g. rail embankment), the subgrade may be made of available fill materials, provided that they are firm enough so that no shear failure can occur due to its own weight and train dynamic loads (Jain et al., 2003). The key function of the subgrade is to provide a firm platform for the ballast and sub-ballast layers. In case of running a high speed train, the train-induced stresses spread out as much as seven meters beneath the bottom of the sleepers (Li, 1994). This stress zone is significantly larger than the thickness of the granular layer (i.e. ballast and sub-ballast). Therefore, the subgrade layer is deemed as the most critical substructure layer with a significant influence on the track performance. For

instance, the subgrade stiffness and thickness are supposed to influence rail, sleeper and ballast degradation and deformation (Selig and Li, 1994). A low subgrade stiffness results in greater elastic deformation and provides less stability to the ballast layer and other components of the track structure (Liang et al., 2001). In addition, the variability of the subgrade stiffness causes differential track settlement and increases higher dynamic impact loading (Raymond, 1978).

2.3 TRACK FAILURE AND MAINTENANCE

Movements in the ballast, sub-ballast and subgrade caused by train dynamic loads under different speeds and loadings deform the railway track in both vertical and lateral directions (Selig and Cantrell, 2001). Although the distortions of the track are normally small, they are usually non-uniform in nature, which increases the dynamic load and gradually deteriorates the riding quality. Therefore, track maintenance is often invoked, and a large portion of maintenance cost is usually due to geotechnical problems (Fair, 2004; Hay, 1982; Indraratna et al., 1998; Indraratna et al., 2011a; Tennakoon et al., 2014; Woodward et al., 2007). In the following sections, the reasons for track deterioration due to geotechnical problems and techniques used for its maintenance are discussed.

2.3.1 Ballast Fouling

Contamination of ballast with the presence of fines is defined as ballast fouling (Salim, 2004). It is one of the main causes of deterioration of track geometry. When the ballast becomes fouled, higher settlement occurs due to the reduction of the angle of shearing resistance, leading to performance reduction.

There are numerous reasons of ballast fouling, which can be categorised into five groups as follows (Selig and Waters, 1994):

a) Ballast particle breakage
b) Subgrade upward migration
c) Infiltration from underlying sub-ballast layer
d) Infiltration from ballast surface
e) Sleeper wear

The sources of ballast fouling mentioned above are briefly described in Table 2.2 based on Selig and Waters (1994). According to field and laboratory investigations in North America, Selig and Waters (1994) concluded that ballast particle breakage is the most significant source of ballast fouling, as depicted in the pie chart shown in Figure 2.4.

Table 2.2: Sources of ballast fouling (Selig and Waters, 1994).

Category of Fouling	**Sources of Ballast Fouling**
a) Ballast particle breakage	i) Rail traffics • Repeated loading • Train induced vibration • Hydraulic action of subgrade slurry ii) Handling iii) Compaction machines iv) Tamping operation v) Chemical weathering vi) Freezing water in voids vii) Thermal stress
b) Subgrade upward migration	i) Insufficient drainage ii) Poor sub-ballast layer iii) Saturation iv) Pumping action from underlying layer
c) Infiltration from underlying sub-ballast layer	i) Migration of sub-ballast particle due to inadequate gradation ii) Breakdown in the old track bed
d) Infiltration from ballast surface	i) Delivered with ballast ii) Water borne iii) Wind blown iv) Meteoric dirt v) Splashing from adjacent wet spot vi) Dropped from passenger and freight trains
e) Sleeper wear	i) Attrition between sleeper and ballast due to lateral ballast deformation

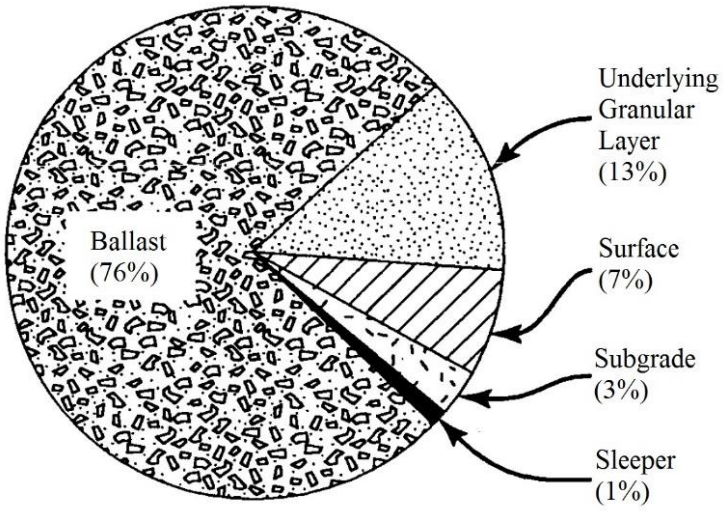

Figure 2.4: Percentage source of ballast fouling in North America (Selig and Waters, 1994).

Usually, porosity in a ballast layer is about 25-50%; therefore, fouling is not considered to be significant until the presence of fines increases to 10% or more. In order to quantify the degree of fouling, Selig and Waters (1994) defined the fouling index (FI) as follows:

$$FI = P_4 + P_{200} \tag{2.1}$$

where, P_4 and P_{200} are the percentage of ballast particle passing the 4.75 mm (No. 4) and 0.075 mm (No. 200) sieve, respectively.

Alternatively, Feldman and Nissen (2002) introduced a different fouling indices, i.e. the percentage void contamination (PVC) for the measurement of ballast fouling as follows:

$$\text{PVC} = \frac{V_1}{V_2} \times 100\% \tag{2.2}$$

where, V_1 and V_2 are the volume of contaminated void and total void of a ballast sample taken from the total depth of the ballast profile, respectively. Although this method is a straightforward measurement of the percentage of void occupied by the fines, it overestimates the degree of fouling (Indraratna et al., 2011a). For this reason,

Indraratna et al. (2011b) proposed a new parameter named the relative ballast fouling ratio, R_{b-f}. It is defined as the ratio of the volumes of fouling particles (passing a 9.5 mm sieve) and ballast particles (particles being retained on a 9.5 mm sieve). The R_{b-f} can be expressed as follows:

$$R_{b-f} = \frac{M_f \times \frac{G_{s-b}}{G_{s-f}}}{M_b} \times 100\% \tag{2.3}$$

where, M_b and M_f, and G_{s-b} and G_{s-f} are the mass and specific gravities of ballast and fouling materials, respectively. To quantify the R_{b-f}, the mass and specific gravity of the ballast and fouling materials need to be measured. This assessment method is quicker and more attractive than the PVC method. The degrees of foulness of ballast based on the fouling index, FI, and relative ballast fouling, R_{b-f}, are listed in Table 2.3.

Table 2.3: Categories of ballast based on the fouling index (Indraratna et al., 2011a).

Ballast Category	Fouling Index (%)	Relative Ballast Fouling (%)
Clean	$FI < 1$	$R_{b-f} < 2$
Moderately Clean	$1 \leq FI < 10$	$2 \leq R_{b-f} < 10$
Moderately Fouled	$10 \leq FI < 20$	$10 \leq R_{b-f} < 20$
Fouled	$20 \leq FI < 40$	$20 \leq R_{b-f} < 50$
Highly Fouled	$FI \geq 40$	$R_{b-f} \geq 50$

2.3.2 Ballast Maintenance

In a ballasted railway track, when the ballast becomes fouled and loses its uniform graded characteristics, the ability of the ballast to perform its important functions decreases and ultimately may be lost. Consequently, ballast maintenance is essential. In this section, several techniques for ballast maintenance are briefly described.

2.3.2.1 Ballast tamping

Ballast tamping operation is generally exercised to readjust the track geometry. The sequence of this operation is presented in Figure 2.5. This process is comprised of lifting up the sleeper, and then placing and pressing the ballast below the sleeper to fill the free spaces caused by the lifting action. Both stages are accompanied by vibration, which causes some ballast breakage. In addition, loosening of the particles develops new particle contact, and increases the rate of particle breakage under further traffic loading. Eventually, tamping is required again over a shorter time period (Figure 2.6). After a long run, ballast fouling gradually occurs as result of fines, which damage the drainage system and its capacity to keep the track in its desired position. Ultimately, it is essential to replace the fouled ballast with a fresh one (Selig and Waters, 1994).

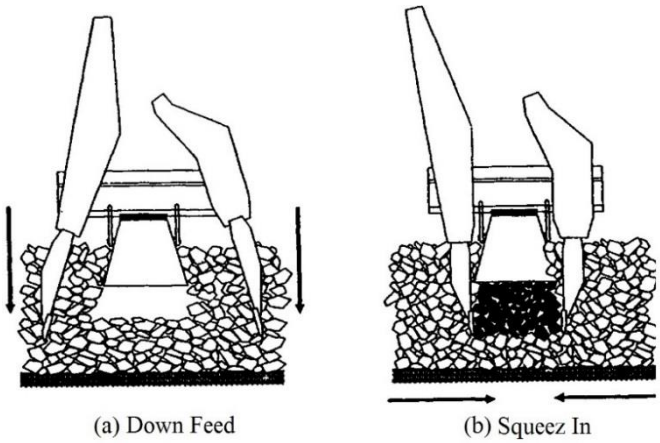

Figure 2.5: Sequence of ballast tamping operation (Selig and Waters, 1994).

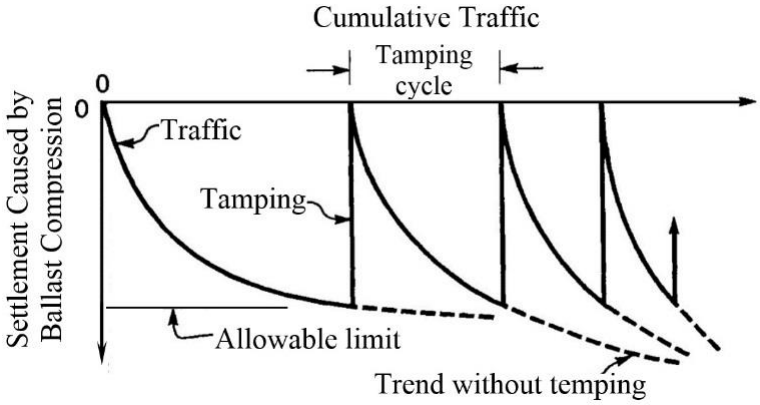

Figure 2.6: Effect of progressive fouling on tamping period (Selig and Waters, 1994).

2.3.2.2 Stoneblowing

Stoneblowing is a new mechanised tamping technique for releveling the track by lifting the sleepers and blowing smaller size stone particles into the voids created below each sleeper (Anderson and Key, 2000). Before the development of this mechanised tamping technique, the measured shovel packing method was used to relevel the railway track to its desired position. This manual method was performed by two groups of labour, where sleepers are lifted up by a group of labour, while smaller stones are shovelled into the free space with minimum disturbance to the well-condensed ballast by another set of labour. The mechanised form of this operation, which is fully computer controlled, is recognised as stoneblowing or pneumatic ballast injection. Figure 2.7 shows a schematic diagram of the stoneblowing operation.

The stoneblowing process builds a two-layer ballast bed. To understand the performance of such a ballast bed under cyclic loading, Anderson and Key (1999) performed a series of large-scale triaxial model tests under cyclic loading and concluded that stoneblowing is an improved version of track maintenance than the commonly used tamping method. However, the size and type of gravel and the depth of the inserted layer are of critical importance in deciding the post maintenance behaviour.

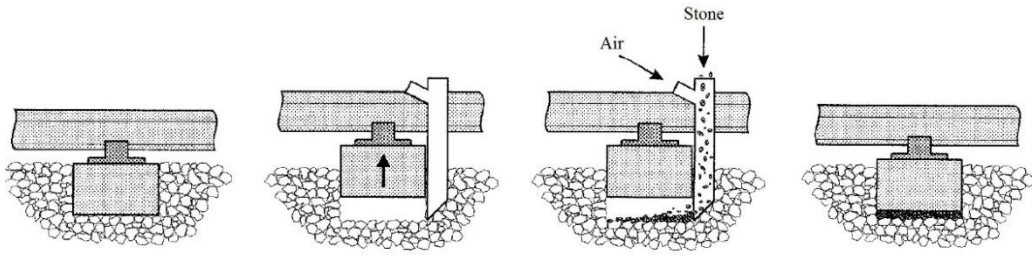

Figure 2.7: Schematic diagram of stoneblowing operation (Anderson and Key, 2000).

2.3.2.3 Ballast cleaning and renewal

As stated earlier, when ballast fouling (contamination) occurs excessively, the function of ballast (i.e. the capacity of holding the track in its desired position) gets impaired, even after performing other maintenance operations (e.g. tamping or

stoneblowing). Ultimately, it is essential to clean the ballast or replace the fouled ballast with a fresh one to maintain the desired bearing capacity, track stiffness and track alignment (Fair, 2004). The operation of ballast cleaning or renewal is time consuming and expensive. In addition, it interrupts the traffic flow, and consequently, it is not possible to operate this maintenance regularly.

In general, ballast cleaning operation is performed by a truck mounted cleaning machine, as presented in Figure 2.8. This machine digs away the fouled ballast beneath the sleepers by a conveyor chain with excavating teeth attached and brings it to a vibration screen, which separates the usable ballast material from the fines. The usable ballast is then returned to the track for reuse and the dirt materials are taken away to the spoil lorry for disposal. During this operation, care must be taken to confirm that the existing sub-ballast layer is not unintentionally eradicated or damaged by the cutter bar of the cleaning machine (Selig and Waters, 1994).

When the ballast layer is excessively fouled, it may need replacement with fresh ballast. In this circumstance, the cleaning machine digs out the dirty ballast and conveys it into the wagon, and a fresh ballast is placed to fill the void after removing the dirty ballast. The waste ballast can be cleaned and reused to minimise further demand of fresh ballast in the track and reduce the environmental impact. Experimental studies were carried out by Indraratna et al. (2005) and Indraratna et al. (2007) to investigate the performance of recycled ballast stabilised with the geo-synthetics material. These studies concluded that recycled ballast stabilised with appropriate geo-synthetics can be used as an alternative material of commonly used fresh ballast.

Figure 2.8: The C750 ballast cleaning machine (Courtesy Strukton Rail).

2.3.3 Subgrade Failure and Remedial Measures

As mentioned earlier, the subgrade layer has the most significant influence on track performance. The key function of the subgrade is to provide a stable platform for the track structure. Subgrade failure must be avoided so that it can continue performing its functions properly. However, under adverse conditions, numerous modes of subgrade disgrace can develop, which lead to failure or repeated requirement of track maintenance. Some of the most common subgrade failures are as follows:

- Massive shear failure
- Progressive shear failure
- Excessive plastic settlement
- Excessive consolidation settlement
- Subgrade attrition and mud pumping
- Frost heaves and thaw softening
- Swelling and shrinkage

In the following sections, the above-mentioned modes of subgrade failure and their remedial measures are briefly described, based on the study of Selig and Waters (1994).

2.3.3.1 Massive shear failure

Massive shear failure is the most dramatic failure of railway track; however, it rarely takes place in railway tracks. This type of failure is likely to happen only when the subgrade shearing strength reduces suddenly because of increasing water content. For instance, a railway track may experience massive shear failure shortly after heavy rainfall or flooding, which is characterised by differential settlement, resulting in a sudden loss of track alignment as illustrated in Figure 2.9.

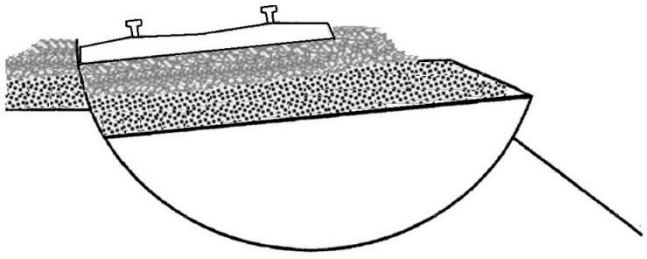

Figure 2.9: Massive shear failure (Selig and Waters, 1994).

Massive shear failure can also happen after excavation of a cut. The mechanism behind this failure is the reduction in shear strength due to dissipation of the negative pore pressure in the slope over time. This failure may also be attributed to an increase in the driving force and drop in the shear strength due to seepage of water through the slope. This type of failure is a typical soil mechanics problem that is analysed in many textbooks (e.g. Das, 2006). A complete analysis and discussion of this mode of failure are beyond the scope of this study.

2.3.3.2 Progressive shear failure

Progressive shear failure is a general subgrade failure of railway track, which is caused mainly by the effect of repeated train loading on the subgrade soil. This type of failure is most likely to occur in the ballast/subgrade interface, where the traffic induced stresses are very high. Overstressing of soil and repeated cyclic loading cause plastic flow of the subgrade soil from below the track to sideways and upward direction and may cause bearing capacity failure. This phenomenon is known as 'Cess Heave', which is presented in Figure 2.10.

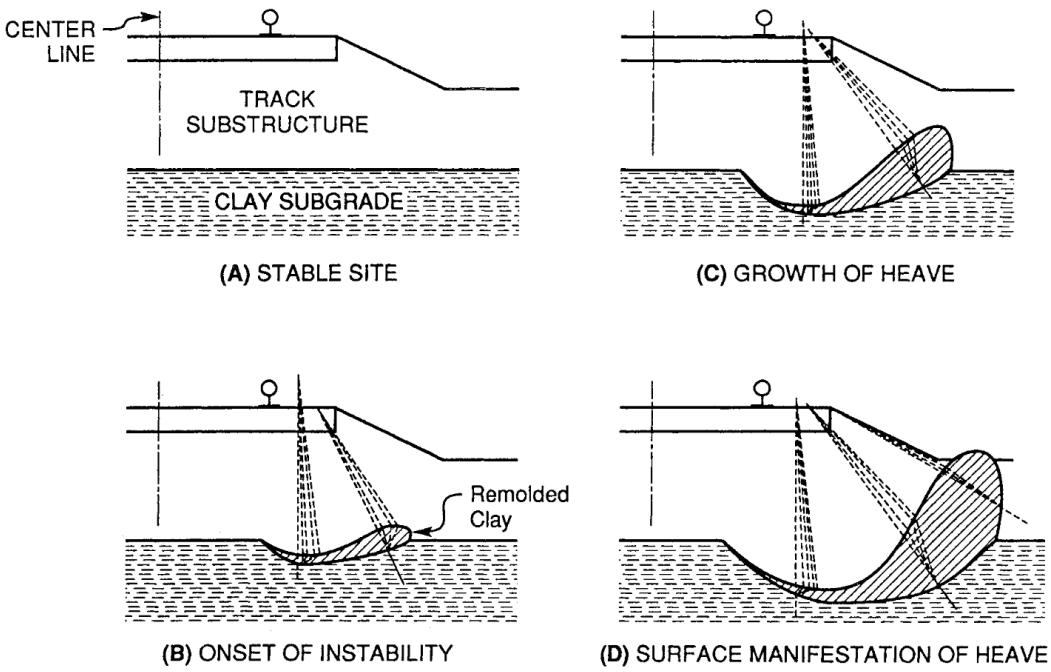

Figure 2.10: Development of progressive shear failure (cease heave) at the top of overstressed clay (Li and Selig, 1995).

In case of fine-grained subgrade with high clay content, progressive shear failure is often accompanied with strength reduction in soil by remoulding its structure and repeated accumulation of pore water pressure under repeated cyclic loading. This type of failure may arise at a stress level less than that required to cause massive shear failure. Therefore, progressive shear failure instead of massive shear failure is the key design criteria of track foundation (Li and Selig, 1995). This mode of subgrade failure can be minimised by:

- Providing an adequate depth of ballast and sub-ballast layer between the sleeper and subgrade soil, so that the distributed stress developed on the subgrade surface become uniform and less than its tolerable stress level.
- Providing an adequate drainage system that maintains a low water table level.

2.3.3.3 Excessive plastic settlement

For a ballasted railway track, excessive plastic settlement (or deformation) is considered as a principal mode of track failure, as it can severely affect the track performance for safe and comfortable train operation. Therefore, the total cumulative plastic deformation under repeated train moving loads should be less than a tolerable limit.

Excessive plastic settlement includes progressive shear deformation as well as progressive compaction and consolidation under repeated cyclic loading. The plastic settlement developed by a single load application may be negligible under general condition. However, the total cumulative plastic settlement after millions of load cycles may develop to such a significant extent that it can severely affect the track performance. In addition, the accumulation of plastic settlement along and across the track is generally non-uniform. Therefore, excessive plastic settlement may lead to an undesirable change in the track geometry.

To balance the damage of track elevation affected by the excessive plastic settlement in the subgrade, more ballast material must be added to the track, which increases the thickness of ballast layer. If ballast material is continually added to solve this problem, a severe appearance of accumulated subgrade plastic deformation can occur as shown in Figure 2.11, which is known as ‘ballast pocket’. Li and Selig (1995)

demonstrated that when a cavity at the subgrade surface occurs, it gathers water, which in turn softens the subgrade near the cavity. The soft subgrade soil squeezes out and the underlying soil becomes softer under repeated train moving loads; thus, the cavity deepens and the edges of soft subgrade material collect around the pocket, which forms a larger water-filled pocket. Moreover, the ballast may become fouled with the subgrade soil particles, thus degrading the characteristics of the ballast material.

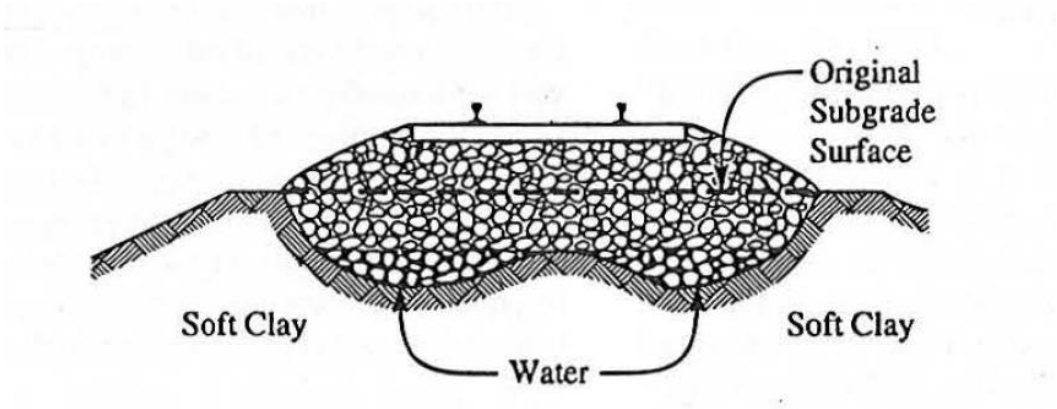

Figure 2.11: Cross section showing ballast pocket (Li and Selig, 1995).

In general, to mitigate this mode of track failure, the thickness of the ballast layer should be increased to reduce the traffic induced stress in the subgrade layer; consequently, the cumulative plastic deformation in the track will be less than the threshold value. However, the ballast layers also degrade and deform under repeated cyclic loading. Many researchers (e.g. Li et al., 2002; Selig et al., 1981; Stewart, 1982) suggested that about 40% of the total track deformation may come from the ballast layer. Therefore, a more detailed study is needed to consider the total track deformation (i.e. deformation of ballast and subgrade layer) occurred under repeated loading in the development of an advanced design method, which will be discussed in Chapter 3.

2.3.3.4 Excessive consolidation settlement

Railway tracks are often constructed on high embankments. Under such circumstances, a high stress is developed in the embankment foundation due to the new weight of both the embankment and track structure. As the excess pore water pressure dissipates through seepage, the track settles with the decrease in the soil

void ratio. The rate of dissipation of the pore water pressure is usually fast in the coarse-grained soil, and the settlement normally ceases by the end of the construction period of the embankment and track structure. On the other hand, the excess pore water pressures dissipate slowly in fine-grained or low pervious subgrade. As a result, consolidation settlement of the track continues for a long time after construction. This type of failure can be found if the track embankment is constructed on a clay subgrade soil. Detailed description of the consolidation settlement problem is beyond the scope of this study and can be found in many textbooks (e.g. Das, 2005).

2.3.3.5 Attrition and mud pumping

Subgrade soil attrition and mud pumping are local subgrade failures. This type of subgrade failure usually takes place under poorly maintained rail joints, where ballast comes into direct contact with fine-grained materials. The stress developed in the contact of the ballast and subgrade points results in wearing of the subgrade surface. In saturated conditions, the attrition products and water mix together and form slurry (mud) at the ballast/subgrade interface (see Figure 2.12a). Under the repeated cyclic loading, the slurry pumps upward into the ballast layer. When the mud reaches the sleeper/ballast interface, further repeated movement of the sleeper within the ballast causes the mud to eject from below the sleeper up towards the surface of the ballast to give a condition known as ‘pumping’ (Figure 2.12b). Ultimately, the slurry flows away into the trackside drainage.

Although this type of failure is very common in low maintained tracks, it can be prevented easily by providing a sub-ballast layer between the ballast and subgrade layer during the construction of the track (Figure 2.12c). The sub-ballast layer protects the subgrade from attrition and stops the development of slurry by preventing the penetration of the coarse-grained ballast into the subgrade. In addition, the sub-ballast layer work as a filtering medium which prevents the upward migration of any slurry that develops in the sub-ballast/subgrade interface.

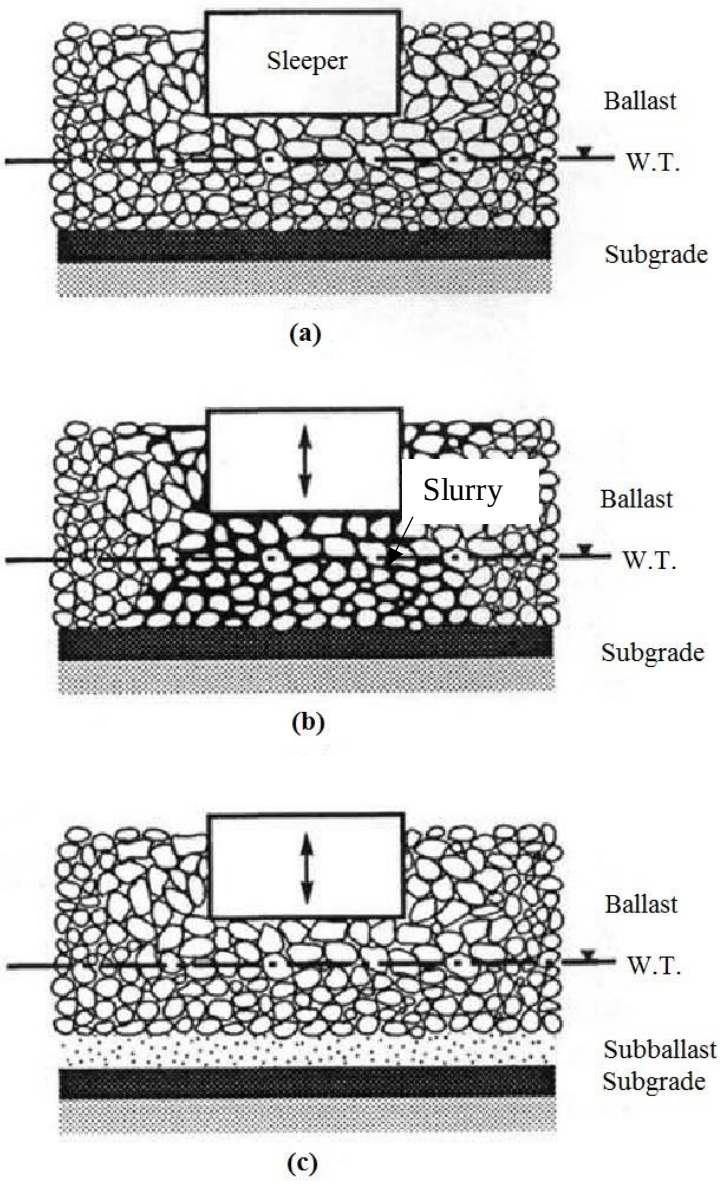

Figure 2.12: Cause and prevention of subgrade attrition and pumping (Selig and Waters, 1994).

2.3.3.6 Frost heaves and thaw softening

The occurrence of frost heave problem is associated with concurrent presence of frost-susceptible soil, pore water and freezing temperatures. Frost-susceptible soils include silts, silty sands and low plasticity clays. These soils are adequately fine-grained and porous, so that they facilitate sufficient flow of water by the capillary action to promote the development of ice lenses. When the pore water freezes and grows into lenses under freezing temperatures, the volume of the subgrade increases significantly. Afterwards, when the temperature increases, the ice melts and the

volume reduces. The excess pore water pressure in the subgrade reduces the subgrade soil strength significantly. This frost heave and thaw softening problem causes severe vertical differential settlement and accelerates the damages of track components.

A proper drainage system is required to protect the track from the frost heave and thaw softening problem by keeping the ground water table low. Besides, an adequate thick insulating layer of non-frost susceptible soil (i.e. the ballast and sub-ballast layer) can be used to prevent attainment of the freezing temperature in the subgrade.

2.3.3.7 Swelling and shrinkage

A ballasted railway track built on expansive subgrade soil may be substantially affected by the swelling and shrinking behaviour of the subgrade soil. Expansive soils are those plastic soils that swell considerably in the presence of water and then shrink with the loss of water. This problem involves severe differential settlement in the track. Numerous techniques, such as replacement of the expansive soil under the track, installation of moisture barrier, and ground improvement by pre-wetting, compaction control and chemical stabilisation can be employed to prevent this problem.

2.4 METHODS OF ANALYSIS OF RAILWAY TRACK

To analyse and design a ballasted railway track foundations, the type and magnitude of forces and stresses imposed on the different components of the track must be known. Different methods that are used by various railways organisations to compute different types of forces and stresses are briefly described below.

2.4.1 Design Vertical Wheel Load

The nominal wheel load is usually measured for a stationary situation; however, in the design of a railway track, the forces and stresses applied to the various track layers must be determined considering the movement of train at a certain specified speed. Esveld (2001) indicated that the total vertical load imposed on a rail is the sum of a quasi-static load that has three components and a dynamic load, as given below:

$$Q_{total} = Q_{quasi\text{-}static} + Q_{dynamic} \tag{2.4}$$

$$Q_{quasi\text{-}static} = Q_{static} + Q_{wind} + Q_{centrifugd} \tag{2.5}$$

where, Q_{total} is the total vertical wheel load; $Q_{quasi\text{-}static}$ is the quasi-static wheel load; Q_{static} is the static wheel load; Q_{wind} and $Q_{centrifugd}$ are respectively the increment of wheel load due to wind force and non-compensated centrifugal forces on the outer rail; and $Q_{dynamic}$ is the dynamic wheel load component resulting from the train speed, wheel diameter, unsprung mass, rail joint, etc.

The static wheel load is half of the static axle load (G), hence:

$$Q_{static} = \frac{G}{2} \tag{2.6}$$

Considering equilibrium of forces acting on a vehicle moving along a curved track, as depicted in Figure 2.13, Esveld (2001) suggested the following equation for calculating the wind forces and centrifugal forces:

$$Q_{wind} + Q_{centrifugd} = H_w \frac{P_w}{b_t} + G \frac{P_c}{b_t^{\,2}} \left(\frac{b_t C^2}{g R_c} - h_s \right) \tag{2.7}$$

where, H_w is the crosswind force; P_w is the distance between the centre of the resultant wind force and centre of the rail; b_t is the track width; P_c is the vertical distance between the centre of gravity of the train and centroid of the rail; C is the train speed; g is the acceleration due to gravity; R_c is the radius of track curvature; h_s is the superelevation.

When the superelevation is not provided on the rail track properly, the maximum wheel force usually occurs in the outer rail; hence, the total vertical load in the outer rail obtained from Equations (2.4) to (2.7) can be calculated as:

$$Q_{total} = \frac{G}{2} + H_w \frac{P_w}{b_t} + G \frac{P_c}{b_t^{\,2}} \left(\frac{b_t C^2}{g R_c} - h_s \right) + Q_{dynamic} \tag{2.8}$$

In Equation (2.8), the dynamic contribution is the most uncertain portion of the total wheel load. To consider the dynamic component of wheel load, the static wheel load may be multiplied by an influence coefficient generally known as the dynamic amplification factor (DAF). Many factors affect the DAF, including train speed, static wheel load and wheel diameter, unsprung vehicle mass, condition of vehicle and track-ground system, etc.

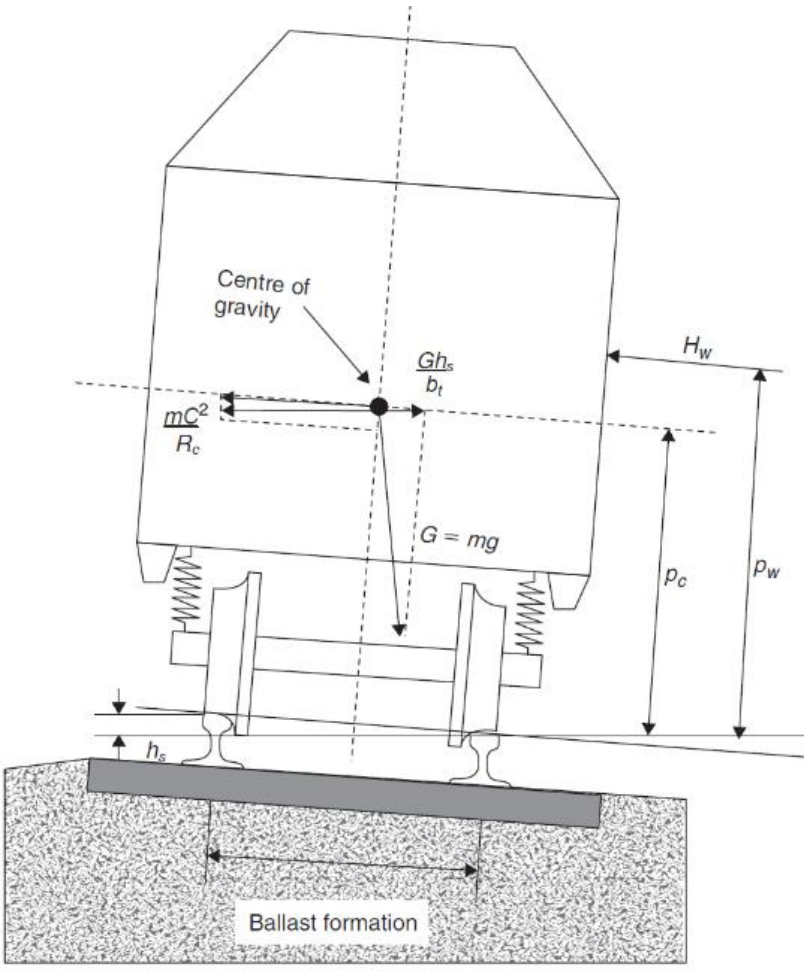

Figure 2.13: Quasi-static vehicle forces on a curved track (Esveld, 2001).

In the existing design methods, a variety of empirical equations are usually used for determining the design vertical wheel load by different railway authorities. In these methods, the design dynamic wheel load is generally expressed as a function of the static wheel load. Various expressions used for estimating the design vertical wheel load are discussed below.

2.4.1.1 AREA impact factor

To determine the design vertical wheel load, Li and Selig (1998a) used the following simple expression recommended by the American Railway Engineering Association (AREA):

$$P_d^{/} = \varphi P_s \tag{2.9}$$

where, $P_d^{/}$ and P_s are the dynamic and static wheel load (kN), respectively; and φ is the dimensionless DAF, which is given by the following equation:

$$\varphi = 1 + \frac{0.0052C}{D_w} \tag{2.10}$$

where, C is the train speed (km/h); and D_w is the wheel diameter (m).

2.4.1.2 ORE impact factor

The Office of Research and Experiments (ORE) of the International Union of Railway (UIC) suggested a more detailed method for determining the dynamic amplification factor, φ, of Equation (2.9) (Jeffs and Tew, 1991). According to ORE, the value of φ depends on three dimensionless speed coefficients $\alpha^{/}$, $\beta^{/}$ and $\gamma^{/}$, and is given by Equation (2.11).

$$\varphi = 1 + \alpha^{/} + \beta^{/} + \gamma^{/} \tag{2.11}$$

where, $\alpha^{/}$ and $\beta^{/}$ are correlated to the average value of the dynamic impact factor; and $\gamma^{/}$ is related to the standard deviation of the impact factor. The coefficient $\alpha^{/}$ is influenced by the irregularities of the track, vehicle compactness and train speed. Although developing relationship between $\alpha^{/}$ and track irregularities is very difficult, it was empirically found that for the worst condition; $\alpha^{/}$ increases with the cubic function of the train speed, C, thus:

$$\alpha^{/} = 0.04\left(\frac{C}{100}\right)^3 \tag{2.12}$$

where, C is the train speed (km/h). The numeric coefficient (0.04) is reliant mainly on the type of train and resilience of the vehicle suspension.

The coefficient β' is correlated with the wheel load shift in the curve, and can be presented by either:

$$\beta' = \frac{2d.h_v}{b_t^{\,2}} \tag{2.13}$$

or

$$\beta' = \frac{2d.h_v}{b_t^{\,2}} \tag{2.14}$$

where, d is the superelevation deficiency (m); h_v is the vertical distance between the rail top and vehicle's centre of gravity (m); b_t is the centre-to-centre horizontal distance between rails (m); h_s is the superelevation (m); g is the acceleration due to gravity (m/s^2); R_c is the radius of track curvature (m).

The last coefficient γ' is influenced by the condition of track, design and maintenance conditions of the train and train speed. It was empirically found that for the worst condition, γ' increases with the train speed, C, and can be expressed by the following equation:

$$\gamma' = 0.10 + 0.017\left(\frac{C}{100}\right)^3 \tag{2.15}$$

The value of φ under different train speeds and numerous conditions of tangent track is plotted graphically in Figure 2.14.

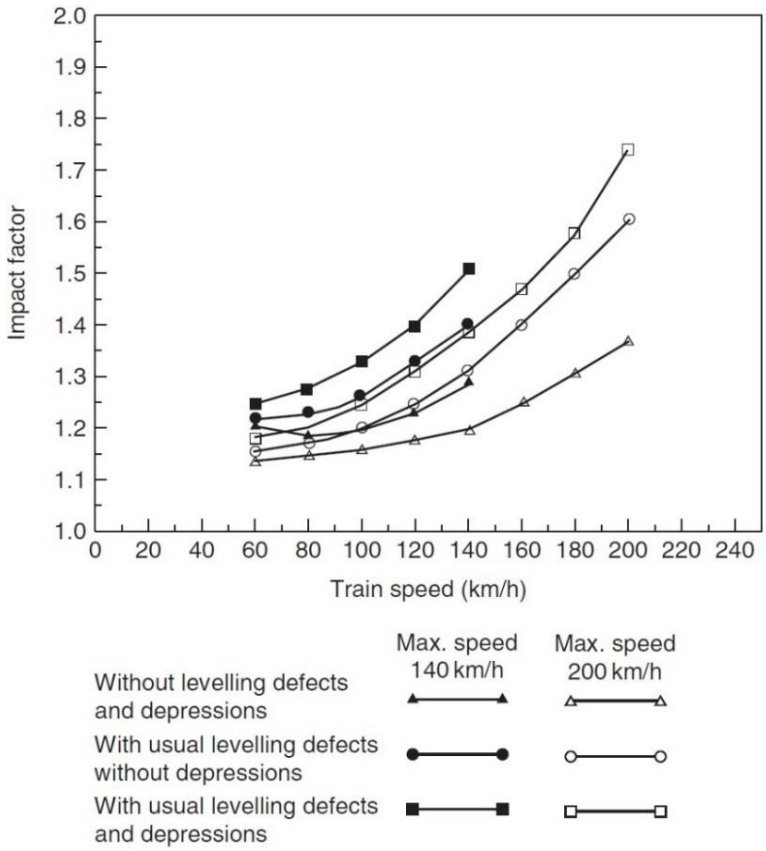

Figure 2.14: The relationship between the ORE impact factor and train speed for different track conditions (Jeffs and Tew, 1991).

2.4.1.3 JNR impact factor

The Japanese National Railways (JNR) adopts the following simple expression to determine the equivalent dynamic wheel load for design of ballasted railway track foundations, as suggested by Atalar et al. (2001):

$$P_d^{/} = p\left(1+\frac{C_{\max}}{100}\right)(1+D) \tag{2.16}$$

where, $P_d^{/}$ is the equivalent dynamic wheel load (kN); P is the static wheel load (kN); $C_{\max}$ is the maximum train speed (km/h); and D is the empirical coefficient ≈ 0.3.

2.4.1.4 Eisenmann's formula

Eisenmann (1972) indicated that the rail deflections and bending stresses are normally distributed, and the mean values can be estimated from the beam on elastic

foundation model. This normal distribution is demonstrated in Figure 2.15 for both the rail deflection and rail stress values.

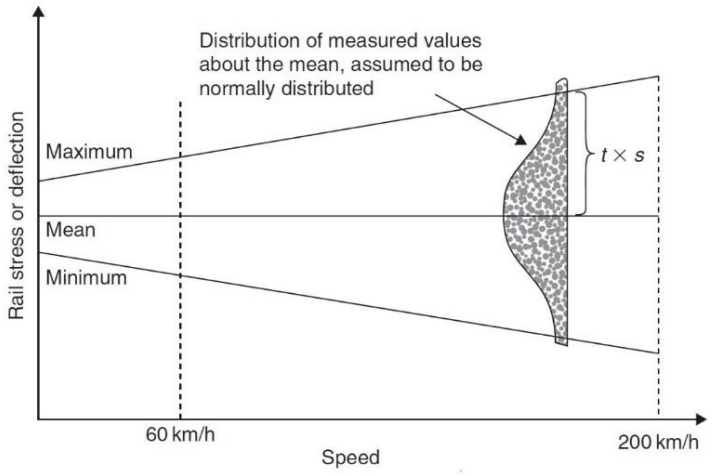

Figure 2.15: Statistical distribution of measured rail stress and deflection values, showing the effect of increased speed upon the range of the standard deviation (Eisenmann, 1972).

The mean rail stress and its relating standard deviation are represented by the following expression:

$$s = x^{/} \cdot \delta \cdot \eta \tag{2.17}$$

where, s is the corresponding standard deviation of applied loading or deflection; $x^{/}$ is the mean rail stress; δ is a factor dependent upon the track condition (0.1 for track in very good condition, 0.2 for track in good condition, and 0.3 for track in poor condition); and η is the speed factor.

The values of η depends on train speed, C (km/h), and can be obtained using the following expressions:

$$\eta = 1 \qquad \text{If } C < 60\,\text{km/h} \tag{2.18}$$

$$\eta = \left(1 + \frac{C - 60}{140}\right) \qquad \text{If } 60 \le C \le 200\,\text{km/h} \tag{2.19}$$

The corresponding maximum applied load (or rail deflection) was given by Jeffs and Tew (1991), as follows:

$$X = x^{/} + s \cdot u \tag{2.20}$$

where, X is the maximum applied load or deflection, u is a value subjected to the upper confidence limit (UCL) defining the possibility that the maximum applied load will not exceed 0 for 50% UCL, 1 for 84.1% UCL, 2 for 97.7% UCL and 3 for 99.9% UCL.

Assuming linearity between the applied load and rail stress or deflection, Equation (2.9) can be rewritten as:

$$X = \varphi \cdot x^{/} \tag{2.21}$$

Combining Equations (2.17) and (2.20), and comparing with Equation (2.21), the expression for the impact factor becomes:

$$\varphi = 1 + \delta \cdot \eta \cdot u \tag{2.22}$$

2.4.2 Design Lateral Wheel Load

Selig and Waters (1994) specified that there are two primary causes of lateral loads applied to rails: (a) lateral wheel load; and (b) buckling reaction load. Lateral wheel loads are originated by both the lateral force component of the friction between the rail and wheel and the lateral force imposed by the wheel flange on the rail. The buckling reaction loads in the lateral direction are exerted by the high compressive stresses accompanied with high temperatures in rail.

Similar to the vertical wheel load (Equations 2.4 and 2.5), the lateral load applied by the wheel on rails is also the summation of the quasi-static and dynamic loads, hence:

$$Y_{total} = Y_{quasi\text{-}static} + Y_{dynamic} \tag{2.23}$$

$$Y_{quasi\text{-}static} = Y_{flange} + Y_{wind} + Y_{centrifugd} \tag{2.24}$$

where, Y_{total} is the total lateral wheel load; $Y_{quasi-static}$ is the quasi-static lateral wheel load; Y_{flange} is the lateral load in curve caused by flanging against the outer rail; Y_{wind} is the increment of the lateral load due to cross wind; $Y_{centrifugd}$ is the increment of the lateral load caused by the non-compensating centrifugal force on the outer rail; and $Y_{dynamic}$ is the dynamic lateral wheel load component.

If both the centrifugal and wind lateral forces entirely affect the outer rail, the equation of maximum quasi-static lateral force, $Y_{e_{\max}}$, obtained from Figure 2.13 can be determined as follows:

$$Y_{e_{\max}} \approx \frac{G}{b_t}\left(\frac{b_t C^2}{gR_c} - h_s\right) + H_w \tag{2.25}$$

Similar to calculation of the design vertical wheel load, the static lateral load can be multiplied by the DAF to estimate the design lateral wheel load.

In order to determine the lateral loads in the track, the Office of Research and Experiments (ORE) performed test programs for train speeds up to 200 km/h. These studies indicated that the lateral load is influenced only by the radius of the curve, and the following empirical equation was suggested to use:

$$P_{Lc} = 35 + \frac{7400}{R_c} \tag{2.26}$$

where, P_{Lc} is the lateral force at curved tracks on the outer rail (kN), and R_c is the radius of curve (m).

In France, a similar empirical equation to determine the design lateral wheel load is usually used, where the lateral force is considered to increase with the axle load, as follows:

$$P_L > 10 + \frac{G}{3} \tag{2.27}$$

where, P_L is the load (kN) essential to introduce the lateral displacement, and G is the axle load (kN).

2.4.3 Load Transfer Method

In a ballasted railway track, the rails transfer the wheel loads to the supporting sleepers, which are spaced evenly along the rail length. Similarly, sleepers transmit the load from the rail to the wider ballast area. The ballast and sub-ballast layers transmit the high imposed stress at the sleeper/ballast interface to the subgrade layer at a reduced level through spreading. Figure 2.16 shows the typical load distribution from the wheel to the rail, sleepers, ballast, sub-ballast and subgrade layers.

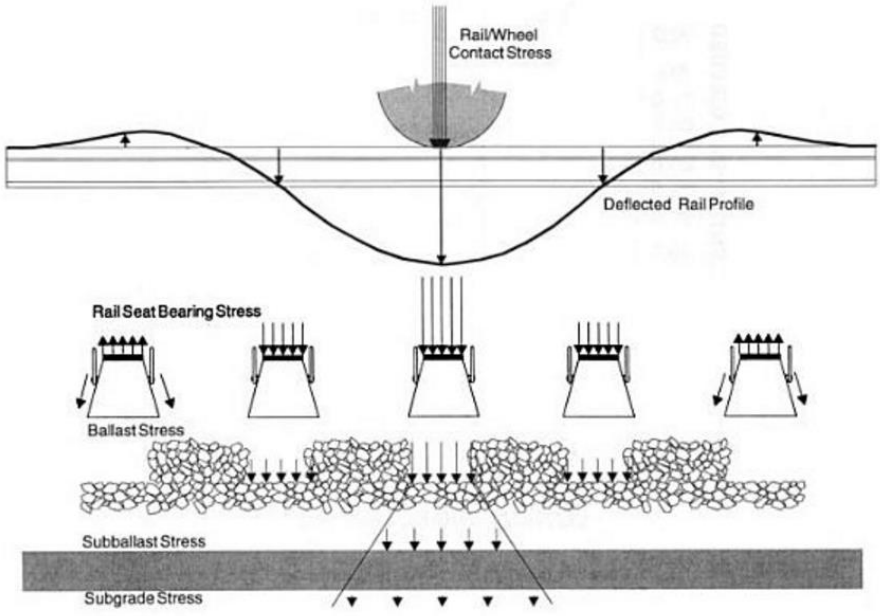

Figure 2.16: Typical wheel load distribution in track (Selig and Waters, 1994).

The stress distribution at the sleeper/ballast interface in practical tracks was investigated by Shenton (1975). This study concluded that the number of ballast particles directly supporting the sleeper is comparatively small, in the range of only 100-200 contacts points, while the ballast size varied from 25 mm to 50 mm, and the width of the sleeper was the usual 250 mm. This study also indicated that precise determination of the sleeper/ballast contact pressure is very challenging. However, the British Railways (BR) took the challenge to quantify the sleeper/ballast contact stress in an actual track. Figure 2.17 shows the pressure distributions in the sleeper/ballast contact surface. Inspection of this figure shows that the pressure distribution is inconsistent and vary from test to test. However, these test results provide clear indication on the maximum stress applied by the sleeper to the underlying ballast for a precise wheel load.

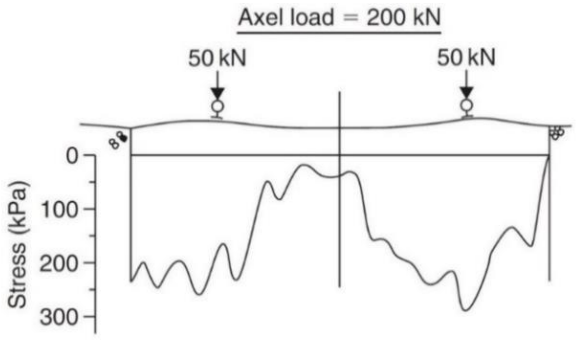

Figure 2.17: Measurement of sleeper/ballast contact pressure (Shenton, 1975).

For design purposes, the sleeper/ballast contact pressure over the estimated effective sleeper area is generally considered to be uniform, and can be expressed by the following equation:

$$\sigma_{sb} = \left(\frac{q_r}{w l_e} \right) F_2 \tag{2.28}$$

where, σ_{sb} is the average sleeper/ballast contact stress; q_r is the maximum rail seat load; w is the sleeper width; l_e is the effective length of sleeper supporting the q_r; and F_2 is a factor depending on the sleeper type and track maintenance.

Considering the effective length of the sleeper supporting the rail seat load, q_r, to be one-third of the total length of sleeper, as shown in Figure 2.18, Equation (2.28) becomes:

$$\sigma_{sb} = \left(\frac{3q_r}{wl} \right) F_2 \tag{2.29}$$

where, l is the total sleeper length.

In the Japanese National Railways (JNR), a similar distribution of contact pressure between the sleeper and ballast was assumed; however, a different effective length of sleeper, l_e, was considered, as shown in Figure 2.19, and can be calculated as:

$$\sigma_{sb} = \left(\frac{q_r}{2l' w} \right) F_2 \tag{2.30}$$

where, l' is the length from the rail centre to the end of sleeper (Figure 2.19).

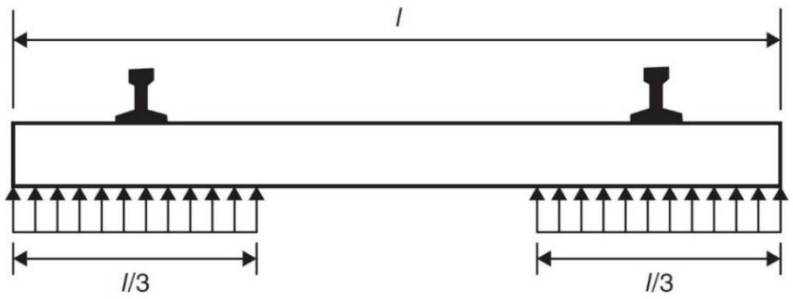

Figure 2.18: Simplified sleeper/ballast contact pressure (Jeffs and Tew, 1991).

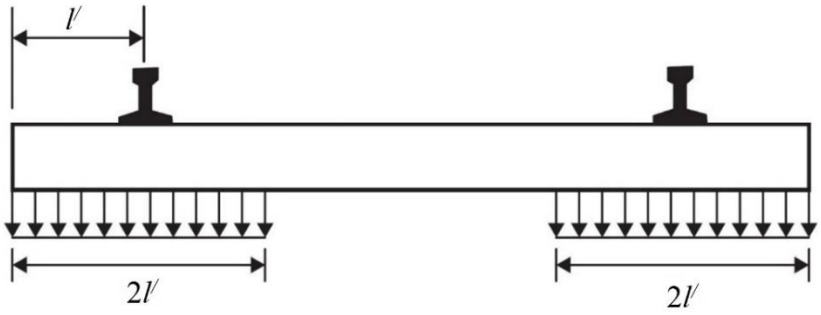

Figure 2.19: Load transfer to ballast assumed by Japanese Standards (Atalar et al., 2001).

AREA recommends that, when calculating the average sleeper/ballast contact stress, the maximum rail seat load should be doubled, and the total sleeper/ballast contact area be used for the concrete sleeper. Hence, the average sleeper/ballast contact stress can be defined by:

$$\sigma_{sb} = \left(\frac{2q_r}{A_{sb}} \right) F_2 \tag{2.31}$$

where, A_{sb} is the sleeper/ballast contact area; σ_{sb}, q_r and F_2 were previously defined. Besides, AREA suggested adopting $F_2 = 2$ to consider the possible excessive contact pressures due to the non-uniform sleeper support caused by possible lack of track maintenance.

It should be noted that in the above equations for determining the average sleeper/ballast contact stress, the rail seat load, q_r, is not equal to the design wheel load, P_d. The USACE railroad design manual suggests that the point wheel load of

the train be transmitted to the adjacent five sleepers, emphasising the highest load on the sleeper below the wheel (Figure 2.20a). However, the deflection pattern of the track subjected to the wheel load indicated that only three sleepers support the load while the other sleepers remain suspended (Selig and Waters, 1994). Furthermore, Atalar et al. (2001) reported that 40% to 60% of the wheel load is supported by the sleeper that is directly below the wheel. Figure 2.20 shows a comparison of the formulas and numerical analyses used for the determination of the maximum rail seat load. It can be seen that the maximum rail seat load varies under different track conditions; consequently, no assumption is believed to be perfect for design of ballasted railway track foundations.

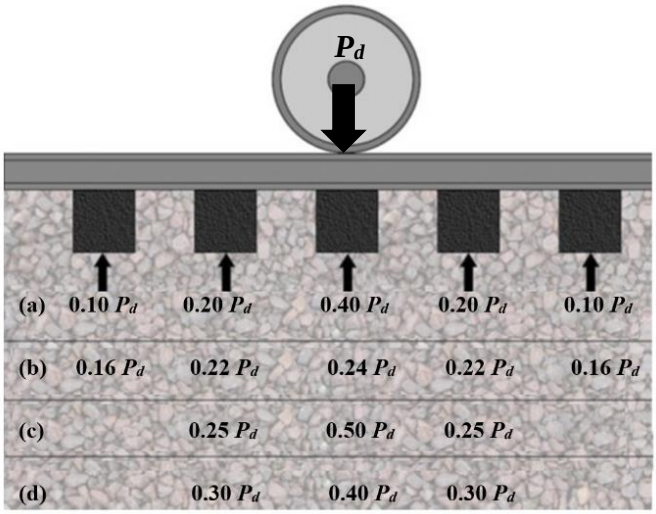

Figure 2.20: Maximum rail seating loads estimated by: (a) five adjacent sleepers' method; (b) FE analysis considering five sleepers; (c) three adjacent sleepers' method; and (d) FE analysis considering three sleepers.

2.4.4 Applied Stress on Subgrade

Numerous methods were proposed by various railway authorities for evaluating the utmost vertical stress on top of the subgrade surface. The most common methods are briefly described below.

2.4.4.1 Trapezoidal approximation (2:1 method)

The trapezoidal approximation is a simple approach for estimating the variation in vertical stress with depth. According to this method, it was presumed that the vertical stress diminishes with depth in the form of a trapezoid that has 2:1 (vertical:

horizontal) inclined sides, as shown in Figure 2.21. Subsequently, the stress at the equivalent depth below the sleeper would be:

$$\sigma_z = \frac{\sigma_{sb} \cdot A_{sb}}{\left(w + \tilde{h}\right)\left(\frac{l}{3} + \tilde{h}\right)} \tag{2.32}$$

where, σ_{sb} is the average value of vertical stress below the sleeper (i.e. above the ballast); A_{sb} is the sleeper/ballast contact area, which is equal to one-third of the sleeper length times its width (i.e. $l/3 \times w$); and $\tilde{h}$ is the equivalent depth below the sleeper.

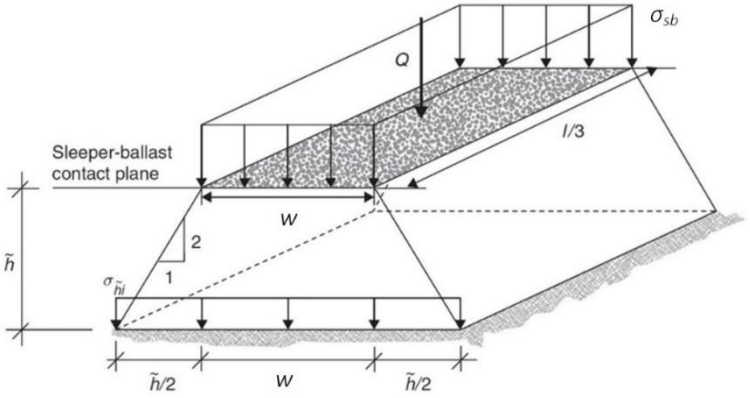

Figure 2.21: Stress distribution on the subgrade comes from sleeper/ballast contact stress by trapezoidal approximation (2:1 method) (Indraratna et al., 2011a)

2.4.4.2 Odemark method

Odemark (1949) suggested an empirical approach to transform a multi-layered (ballast, sub-ballast, and subgrade) system into a single layer system. According to this method, the following equation expresses the equivalent depth of $n-1$ layers:

$$\tilde{h} = \left\{ \begin{array}{l} h_1\left(\frac{E_1}{E_n} \cdot \frac{1-\nu_n^2}{1-\nu_1^2}\right)^{1/3} + h_2\left(\frac{E_2}{E_n} \cdot \frac{1-\nu_n^2}{1-\nu_2^2}\right)^{1/3} + \cdots \\ + h_{n-1}\left(\frac{E_{n-1}}{E_n} \cdot \frac{1-\nu_n^2}{1-\nu_{n-1}^2}\right)^{1/3} \end{array} \right\} \tag{2.33}$$

where, $\tilde{h}$ is the equivalent depth for $n-1$ layers; h_i is the thickness of the *i*th layer; E_i is Young's modulus of elasticity at the *i*th layer; and ν_i is Poisson's ratio at the *i*th layer. According to this technique, once a multi-layer depth is converted into the equivalent depth with respect to the properties of the lowest layer, calculations are only applicable within the lowest layer considered during the transformation (i.e. layer n). If any layers (e.g. layer $n+1$) be present below the layer n, it is supposed that the elastic properties of layer $n+1$ is identical to those found in layer *n*.

2.4.4.3 AREA recommendations

In the design exercise for the North American railway tracks, AREA (1996) suggested the following four empirical equations to estimate the stress imposed on the subgrade by the ballast:

1. Talbot equation:

$$\sigma_s = \frac{16.8\sigma_{sb}}{h^{1.25}} \tag{2.34}$$

2. Japanese National Railways (JNR) equation:

$$\sigma_s = \frac{50\,\sigma_{sb}}{10+h^{1.35}} \tag{2.35}$$

3. Boussinesq elastic equation:

$$\sigma_s = \frac{6q_r}{2\pi h^2} \tag{2.36}$$

4. Love's equation:

$$\sigma_s = \sigma_{sb}\left[1-\left(\frac{1}{1+\frac{r_c^{\,2}}{h^2}}\right)^{3/2}\right] \tag{2.37}$$

In these equations, σ_s is the subgrade stress (psi); σ_{sb} is the average stress at the sleeper/ballast contact surface (psi); h is the thickness of ballast and sub-ballast layers (in inches, except for JNR it is in cm); q_r is the static rail seat load (pounds); and r_c is the radius of a circle whose area is equivalent to the sleeper bearing area, A_{sb} (inches).

Both the JNR and Talbot equations are empirical in nature. The JNR equation was derived for a narrow gauge track, where the Talbot equation was derived from a set of full-scale laboratory tests carried out at the University of Illinois. Several types of granular materials were examined, including gravel, crushed stone, slag and sand, with stresses from the applied static loads measured at different depths and locations under numerous sleepers. The axle loads considered were not as heavy as those commonly used today. The third equation (Equation 2.36) was based on Boussinesq's solution for stress analysis in a semi-infinite, homogeneous elastic body due to an application of a surface point load. Love's formula was a modification of Boussinesq's solution for stress analysis, in which the applied pressure by the sleeper to the ballast was characterised as a uniform stress over a circular area equal to the effective sleeper/ballast contact area, A_{sb}.

2.4.5 Methods for Determining the Dynamic Track Response

A comprehensive review of the literature reveals that the dynamic response of ballasted railway tracks has been generally investigated by three different methods, including empirical, analytical and numerical methods. These methods for determining the dynamic track responses are briefly described below.

2.4.5.1 Empirical method

The dynamic response of a railway track can be analysed using field measurement data, which is known as the empirical method. This method was based on databases of field measurements (e.g. Hall, 2000; Madshus and Kaynia, 2000), and is generally used to predict the environmental impacts on existing or new railway tracks. The method may be suitable for predicting the dynamic track response in some cases that are restricted to particular train speeds, train type and track-ground condition. In this

regard, the mathematical and numerical models might be more beneficial as they are more flexible and not limited to specific conditions.

2.4.5.2 Analytical method

The dynamic response of a railway track due to moving loads on the surface of an elastic medium was studied on a theoretical basis since the start of the 19th century. For instance, Lamb (1904), who is the pioneer of this research area, focused on the dynamic response of elastic half-space and elastic body with an infinite boundary generated by an impulsive load applied at a point or across a line on the surface (Figure 2.22). Subsequently, various analytical models for predicting the dynamic response of the half and full space due to the harmonic point and line loads was developed by other researchers (e.g. Achenbach, 1973; Bortfeld, 1967). A general outcome of these studies states that, due to the influence of a harmonic load on the surface, two types of wave propagate away from the loading point. Primarily, compression waves (*P*-waves) oscillate particles in the direction of the wave propagation. Secondly, shear waves (*S*-waves) oscillate particles in a plane perpendicular to the direction of the wave propagation. The compression wave velocity (C_p) is always higher than the shear wave velocity (C_s). In an elastic half-space, a third type of wave appears at the surface, called Raleigh waves (*R*-waves). The Raleigh wave velocity (C_R) is lower than the C_s, and its amplitude diminishes exponentially in the direction perpendicular to the ground surface.

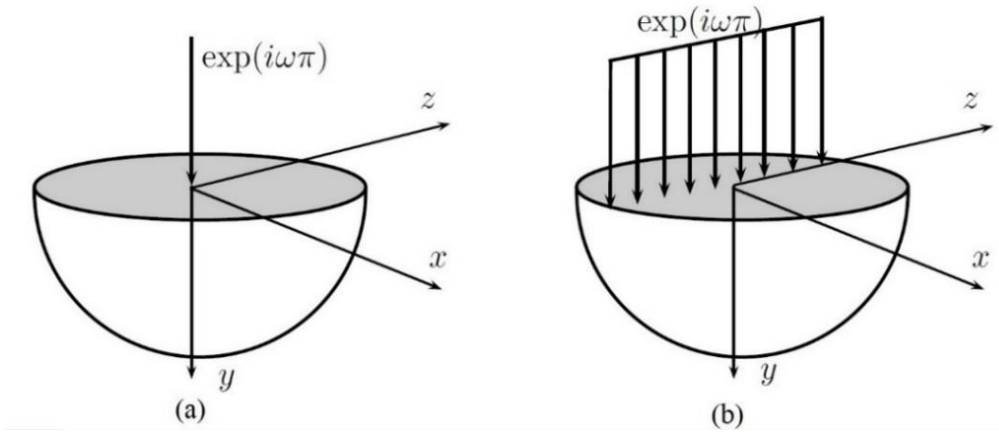

Figure 2.22: Classical Lamb's model with harmonic (a) point load; and (b) line load (Cunha, 2013).

After establishing the dynamic response of an elastic body subjected to harmonic loading, many researchers (e.g. Dieterman and Metrikine, 1996, 1997; Knothe and Grassie, 1993; Krylov, 1995; Madshus and Kaynia, 1999) began to study the dynamic response of a track structure subjected to moving loads. Studies under the train moving loads were appealing, as it was found that the dynamic response increases with the increase in the speed of moving loads. The dynamic response due to moving loads can be expressed by three different terms under three different conditions. Firstly, when the load moves at a speed lower than the speed of *S*-waves of the medium (i.e. $C < C_s$), which is called subsonic condition. Secondly, at the transonic condition, which occurs when the speed of a moving load is lower than the speed of *P*-waves but higher than the speed of *S*-waves (i.e. $C_s < C < C_p$). Lastly, at the supersonic case, which occurs when the speed of a moving load is higher than the *P*-waves in the medium (i.e. $C > C_p$).

Among various analytical models, the beam on Winkler foundation is the simplest and most useful model for simulating railway track with embankment and surrounding soil. This model simulates the track dynamic response by considering a load moving along the infinite beam, which is discretely supported by springs and dashpots, as shown in Figure 2.23.

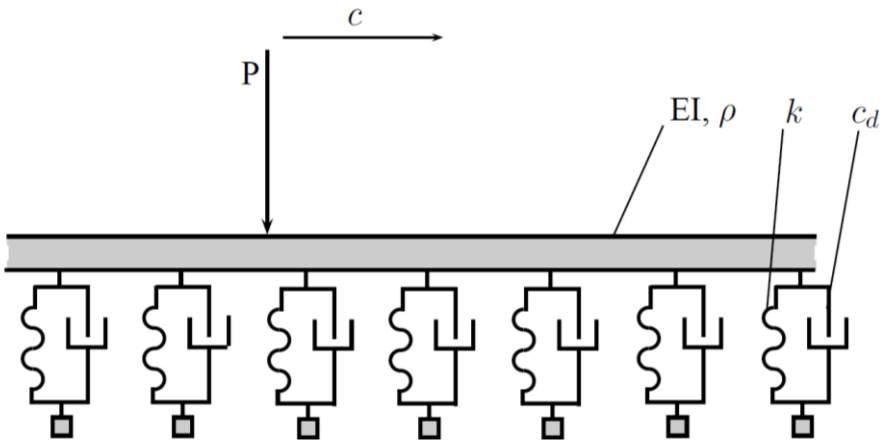

Figure 2.23: Beam on Winkler foundation (Cunha, 2013).

The general differential equation of the track response due to moving loads is given by:

$$EI\frac{d^4u_v(x,t)}{\partial x^4}+\rho l\frac{d^2u_v(x,t)}{\partial x^2}+2c_d\frac{du_v(x,t)}{\partial x}+kdu_v=P\delta(x-Ct) \tag{2.38}$$

where: EI is the flexural stiffness of the Winkler beam (embankment); u_v is the vertical displacement; ρl is the mass per unit length of the beam; k is the stiffness of the Winkler foundation; c_d is the viscous damping of foundation; P is the vertical load and $\delta(x-Ct)$ is the Dirac delta function of the moving load at speed C.

Determination of the analytical model parameters depends on the properties of the track-ground system. In general, there are two approaches to represent the track-ground system. In the first approach, the beam of the model is used to characterise the rails only and the Winkler foundation defines all other components of the track structure (sleeper, ballast, sub-ballast and subgrade). On the other hand, the rails, rail pads, sleepers, ballast, sub-ballast are presented by the beam, and track subgrade is represented by the Winkler foundation.

The beam on Winkler foundation model is useful in predicting the track deflection and can provide a good understanding of well-known theoretical problems, thus it becomes suitable reference for the validation of numerical tools. However, the major drawback of this model is that it cannot allow transfer of shear stresses. Moreover, because of the necessary simplifications and sub-divisions involved, the analytical solutions in general are usually inadequate for practical problems.

2.4.5.3 Numerical method

The requirement to overcome the drawbacks of empirical and analytical approaches led to the development of the numerical methods. These methods are also backed by the computers' high processing capacity. The numerical methods that are commonly used to simulate the dynamic response of railway tracks include the finite element method (FEM), boundary element method (BEM), finite difference method (FDM) and discrete element method (DEM). These numerical methods use different strategies to solve the boundary value problem associated with the track-ground system. A general knowledge of the most common numerical approaches to simulate

the railway track responses and their relative advantages and disadvantages are briefly described below.

2.4.5.3.1 Finite element method (FEM)

The FEM has been widely used by many professionals in different science and engineering fields due to its benefits over other numerical methods. For instance, a finite element (FE) modelling has the advantages of permitting a detailed definition of a track geometry plus the ability to consider sophisticated constitutive models for the track materials. Thus, it can accurately simulate the railway track response and wave propagation by train moving loads within the surrounding soil. However, if the model boundaries are not treated properly, the soil modelling used in the finite elements may provide inaccurate response. Specially, when the boundaries of a FE mesh are kept constrained, the waves generated by the dynamic wheel load will reflect at the mesh boundaries instead of uninterruptedly propagating to outer regions (Kouroussis et al., 2011a). This phenomenon introduces disturbance in the numerical simulation. Therefore, the dynamic model should be sufficiently larger than that used for static analysis to avoid such disturbance. In addition, the model should include absorbing boundaries that mitigates or prevents the wave reflection.

In order to absorb incident waves and avoid reflections in the FE model, Lysmer and Kuhlemeyer (1969) introduced non-reflecting viscous boundaries. These viscous boundaries absorb the incoming waves perfectly if correctly aligned with the incident direction of the waves at the boundaries. Bettess (1977) proposed another way to solve this problem by introducing infinite elements for static and steady-state problems. These infinite elements were derived from the standard finite elements and modified to represent a decay type behaviour as one or more dimensions approach infinity. To address this issue, Wolf and Song (1996) suggested the infinitesimal finite-element cell method, which is also known as the Scaled Boundary Finite Element Method (SBFEM). This method originated from the similarity of the unbounded domain, which is used in the track substructure. Ekevid and Wiberg (2002) used this method to simulate the dynamic response of a typical railway track (Figure 2.24), and reported that utilisation of the SBFEM results in very negligible or no reflections of waves even when support restraints are provided in the nodes of a

soil-structure interface, and the time-history vertical displacements obtained at a point in the track agreed well with the field measurements.

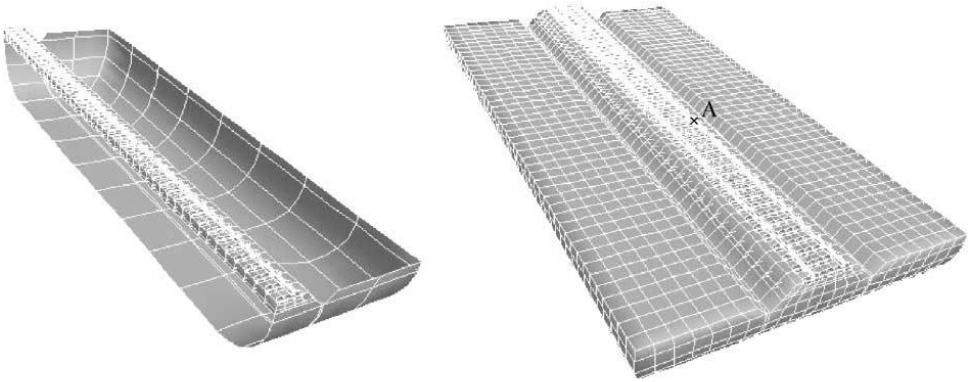

(a) (b)

Figure 2.24: Coupling of FEM and SBFEM for simulating a rail track section: (a) discretisation of the structure-unbounded media interface; (b) the finite element model (Ekevid and Wiberg, 2002).

Although a number of researchers suggested various techniques of absorbing boundaries to mitigate the problem of wave propagation (or reflection) to outer zones in the dynamic FE models, it is still essential to develop a larger model than that used for static analysis. Moreover, the mesh size should be based on the minimum wave length of the train load (i.e. maximum frequency of loading). Consequently, the number of elements becomes much larger than that of the static FE model, which makes the dynamic FE numerical models computationally too costly.

A number of researchers (e.g. Correia et al., 2007) used the two-dimensional (2D) plane strain FE modelling to simulate the dynamic response of ballasted railway tracks. Figure 2.25 shows a typical example of a 2D plane strain modelling of a ballasted railway track. The plane strain railway track modelling requires an assumption that the transversal profile of the track is consistent in the longitudinal direction. However, this is a gross approximation, since the longitudinal rail is discretely supported by the sleepers in the transverse direction of the track.

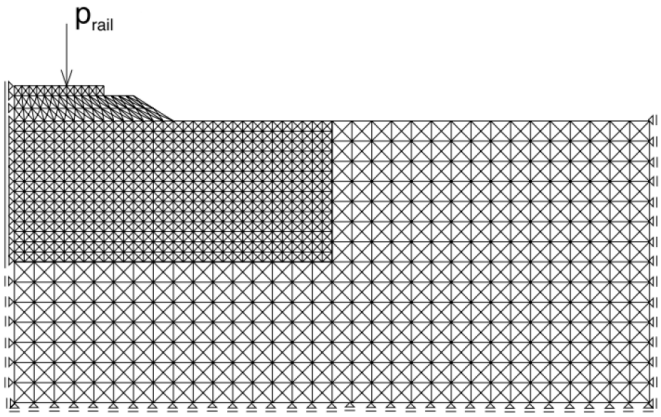

Figure 2.25: Example of a 2D plane strain FE modelling of the track and soil (Suiker, 2002).

The assumption that the load is distributed in the longitudinal direction is another shortcoming of the 2D plane strain modellings. The longitudinal load distribution of the railway track must be accounted beforehand, to calculate accurately the load in the transversal direction of the track. A technique was suggested by Gardien and Stuit (2003) for analysing the dynamic response of the soil from railway tunnels. According to this technique, three complementary models were built instead of developing a three-dimensional (3D) modelling for the dynamic analysis. The first one was a 3D model in which static loads are applied to determine equivalent beam parameters, which were then used in the second model to calculate the force on the ballast surface below the sleeper over time. This force was then applied to the third model, which is a 2D plane strain model of the structure cross section. However, this model cannot accurately predict the stress subjected to train moving loads due to its lack of considering the principle stress rotation.

On the other hand, a 3D FE modelling considers the load distribution in all directions of the track, rendering the simplifications of the 2D FE modelling unnecessary. Obviously, 3D models can also be developed in such a way that the longitudinal rail is supported by discrete sleepers overlying the ballast layer, and can realistically simulate the geometric conditions of the track structure and supporting ground. Figure 2.26 shows an example of a 3D mesh of a railway track model. In this model, the rails and rail-pads are usually simulated by a 1D beam element and an elastic link (spring-dashpot) element, respectively. The remaining components of the model including sleepers, ballast, sub-ballast and subgrade are modelled using 3D solid element. In recent years, a number of researchers (e.g. Banimahd et al., 2013; Hall,

2003) used the 3D FE modelling to simulate the dynamic response of railway tracks, and it was reported that the time-history of the dynamic response predicted by the 3D FE modelling agreed well with the field measurements.

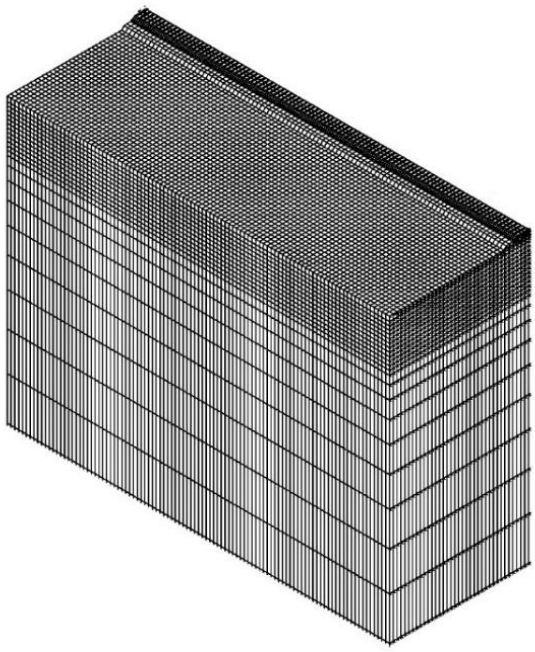

Figure 2.26: Example of a 3D FE model of the track and soil (Hall, 2003).

2.4.5.3.2 FE-BE method

The Boundary Element method (BEM) is an effective way to simulate the wave propagation in soils. Comprehensive information on the BEM can be found in Wrobel (2002). Although, the BEM has the benefit of simulating the wave propagation in half-space, it cannot appropriately deal with the nonlinearity of materials and geometrical complexities. As a result, in simulation of railway tracks, the BEM is usually used to simulate the track foundation only, while the track structure is simulated by different numerical approaches in order to obtain a true track-soil response. In this context, 2.5D is an efficient tool to imply the track-soil interaction, where the soil is modelled using the BEM approach. In the 2.5D model, the transversal geometry of the track structure is only discretised in 2D, and the transversal section of the model is kept invariant in the longitudinal direction.

Sheng et al. (2006) developed a model based on 2.5D FE-BEM to predict the ground vibrations induced by train moving loads. The model considered the arbitrary shape of the transverse geometry of the track. However, the built structures and ground

should be homogeneous in the longitudinal direction. A similar formulation was used by other researchers (e.g. Alves Costa et al., 2012; Fiala et al., 2007; Galvín et al., 2010) to simulate the vibrational response in the track and wave propagation in the surrounding soil induced by high speed train moving loads (Figure 2.27). In addition, a periodic FE-BE coupling method was developed by Clouteau et al. (2000) to predict the dynamic behaviour of very long structures. The same methodology was mostly used by other researchers (e.g. Chatterjee et al., 2003; Clouteau et al., 2004; Degrande et al., 2003; Gupta et al., 2006a; Gupta et al., 2006b) to simulate the track-ground vibration generated from underground railway tracks.

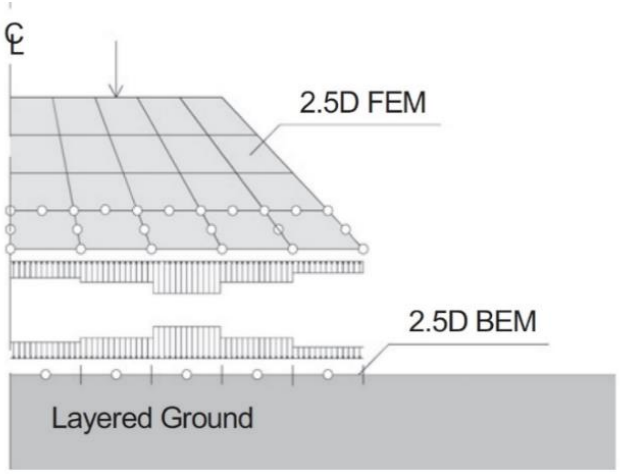

Figure 2.27: 2.5D FEM-BEM coupling (Alves Costa et al., 2012).

2.4.5.3.3 Discrete element method (DEM)

The DEM is another computational tool that has the ability to provide a micro-mechanical insight into the behaviour of granular materials (e.g. ballast). In the DEM scheme, there are only two basic objects: particle and wall. The calculation cycle is a time-stepping algorithm that requires the repeated application of the law of motion to each particle, a constant updating of wall positions and a force-displacement law to each contact. At the start of each time step, the set of contacts is updated from the known particle and wall positions. The force-displacement law is then applied to each contact to update the contact forces based on the relative motion between the two objects at the contact and the contact constitutive model. Afterwards, the law of motion is applied to each particle to update its velocity and position based on the resultant force and moment arising from the contact forces and a body forces acting on the particle. Also the wall positions are updated based on the specified wall

velocities. The typical calculation cycle for the Discrete Element Code YADE is shown in Figure 2.28 (Kozickia and Donzéb, 2008).

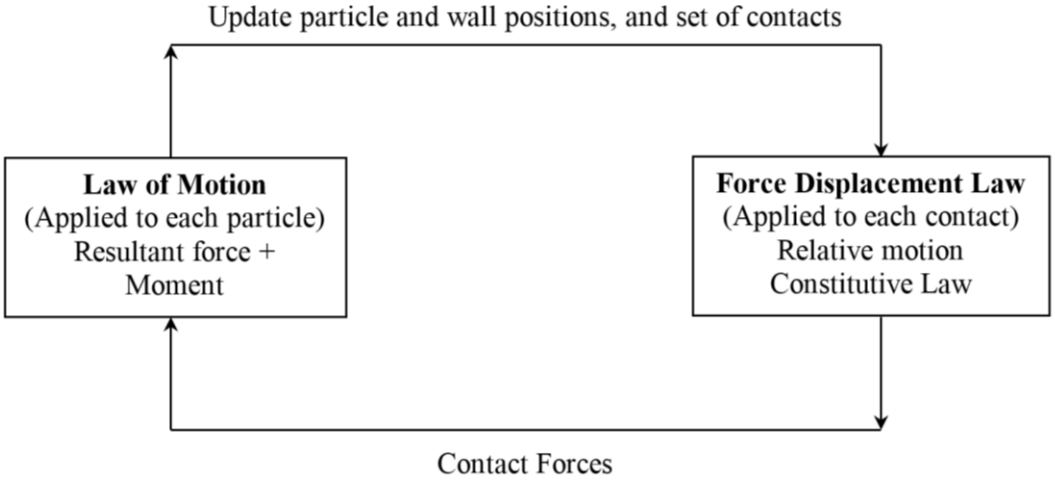

Figure 2.28: The Calculation cycle of DEM in YADE (Kozickia and Donzéb, 2008).

A number of researchers employed DEM to simulate and discover the micro-mechanical behaviour of ballast in the triaxial compression tests (e.g. Hossain et al., 2007; Lu, 2008; Lu and McDowell, 2008) and box tests (e.g. Lim and McDowell, 2005; Lu and McDowell, 2007). However, due to the demand of huge computational cost by DEM, its application to simulate the ballast behaviour in a numerical model of track is rare. Those track models in which the ballast was modelled with DEM only reproduced a small part of the track and the interaction with the subgrade was not simulated. Also, the longitudinal length of the model was reduced to spanning 1 to 5 sleepers in 2D (Lobo-Guerrero and Vallejo, 2006; Saussine et al., 2004) or a single sleeper in 3D (Tutumluer et al., 2007). The limited longitudinal length of these models restricted the simulation of moving loads under the consideration of a single load with a time-dependent modulus.

From the above discussion, it is clear that the 3D FE numerical modelling is the ideal tool compared with other methods (i.e. FE-BE, DEM) in the course of simulating the train-track-ground system under dynamic loads imposed by running trains. Therefore, in the current study, an advanced 3D FE numerical modelling is developed to simulate the dynamic response of railway track foundations, as will be seen in Chapter 4.

2.5 DESIGN METHODS FOR BALLASTED RAILWAY TRACK FOUNDATIONS

Design of ballasted railway track foundations requires accurate estimation of the granular (ballast and sub-ballast) layer thickness that provides protection against track failures induced by train dynamic loads. Thus the design of railway track foundations is also referred to as design of the granular layer thickness. In this section, the main existing design methods are illustrated and their limitations are discussed.

2.5.1 North American Railway Method

Over the years, the minimum granular layer thickness required to prevent subgrade failure was determined on trial-and-error bases in North American railway tracks. From the economic point of view, the minimum thicknesses considered are likely to characterise the average subgrade condition, therefore they often cannot be taken as an appropriate thickness. As the major North American railway tracks have various subgrade conditions, a particular design thickness for the granular layer is not applicable to all conditions.

The manual of the American Railway Engineering Association (AREA, 1996) specified a minimum thickness of ballast and sub-ballast as 300 mm and 150 mm, respectively (i.e. the minimum granular layer thickness is 450 mm). The first step in designing railway track foundations according to the AREA manual involves determination of the maximum rail seat load, q_r. An assumption of q_r = 50% of the design wheel load is considered to be reasonable. The second step is the determination of the sleeper/ballast contact pressure, σ_{sb}, which can be determined using Equation (2.31). In this equation, for wood sleepers, about 2/3 of the total sleeper area is considered as an effective bearing area; the AREA manual recommends that the maximum value of σ_{sb} should be less than 65 psi (450 kPa). On the other hand, the entire sleeper area is considered to be the effective bearing area for concrete sleepers; the AREA manual suggests that the maximum value of σ_{sb} in this case should be less than 85 psi (590 kPa), under the consideration that the track is founded on high-quality ballast.

Once the values of q_r and σ_{sb} are determined, the AREA Manual recommends Equations (2.34) to (2.37) to calculate the required granular layer thickness, in which subgrade stress, σ_s, should be equal to the allowable subgrade bearing pressure. The AREA Manual suggests an allowable subgrade bearing pressure of 20 psi (138 kPa) for all soil conditions. However, as subgrades can vary significantly in strength, the use of a unique value for the bearing pressure (138 kPa) may be either un-conservative in soft soils or too conservative in strong soils.

2.5.2 Canadian Modified Method

Raymond (1978) proposed modifications to the AREA design method discussed above, and resulted in what is now known as the Canadian Modified Method. Casagrande soil classification scheme was used to infer the safe bearing capacity of the subgrade soils, rather than using the single value recommended by the AREA. Although this modification provided some improvement, there are still limitations to the method as the stresses were calculated based on an assumption of a homogeneous half-space for all track layers without considering the properties of each individual layer. Moreover, the effect of repeated (cyclic) loading on the performance of the track substructure was not considered. In order to predict the vertical stress at various depths of the track structure below the sleeper, Boussinesq's elastic equation was used. The wheel load was distributed in such a way that the sleeper directly below the wheel carries 50% of the wheel load, and each of the adjacent sleepers on either side carries 25% of the wheel load. To reflect the dynamic wheel/rail interaction, these loads were arbitrarily doubled. To calculate the granular layer thickness, a uniform pressure distribution in the sleeper/ballast contact surface was assumed along the full length of the sleeper.

Figure 2.29 depicts the simplified design charts for cars of 100 tonnes (90 kN) (Figure 2.29a), and cars of 70 tonnes (63 kN) to 125 tonnes (113 kN) (Figure 2.29b), in which the relationship between the vertical stress and the ratio of ballast thickness to sleeper width is plotted. The range of safe allowable bearing stress for different compacted subgrade soils is superimposed on the chart. The minimum thickness of the granular layer is estimated by identifying the thickness to width ratio at which the vertical stress equals the safe bearing stress of the subgrade soil.

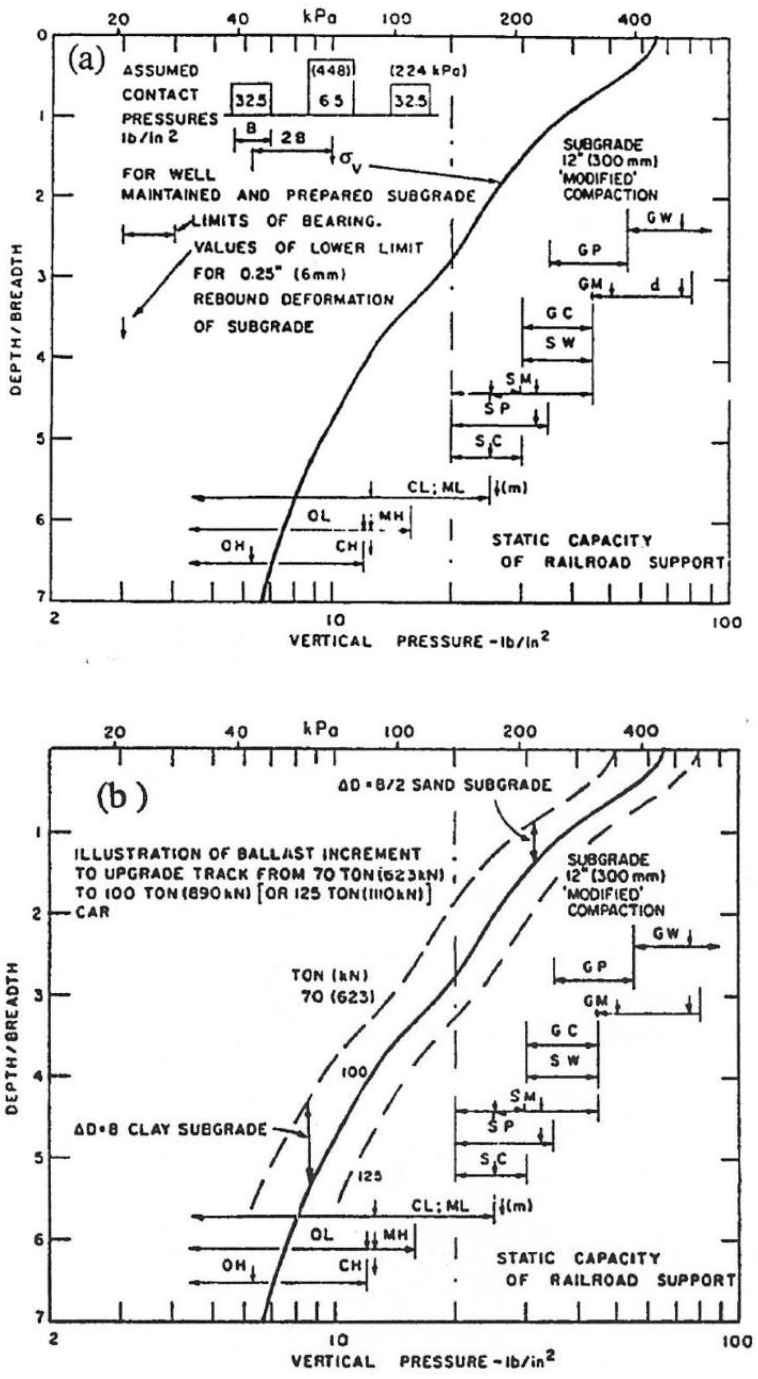

Figure 2.29: Design charts for determining granular layer thickness (Raymond, 1978).

2.5.3 British Railways Method

The British Railways (BR) design method for calculating the granular layer thickness was reported by Heath et al. (1972). The key criterion of this design method is to limit the subgrade surface stress to less than the threshold stress to prevent the excessive plastic deformation of the subgrade soil. In developing this method,

the threshold stress of soil was obtained experimentally by subjecting samples from this soil to cyclic loading. Figure 2.30 shows an example of the results from triaxial compression tests in which the percentage cumulative plastic strain is plotted against the number of loading cycles. Each curve of this figure characterises a specific principal stress difference. It can be seen from Figure 2.30 that there exists a particular principal stresses difference (denoted as the "threshold stress") that divides these curves into two groups. In one group, when the stress level is above the threshold stress, the rate of cumulative plastic strain is found to be extremely rapid, and the deformation increases at an increasing rate until a complete failure of the specimen is reached. On the other hand, when the stress level is below the threshold stress, the rate of cumulative plastic strain is small, and stabilised even after a million cycles.

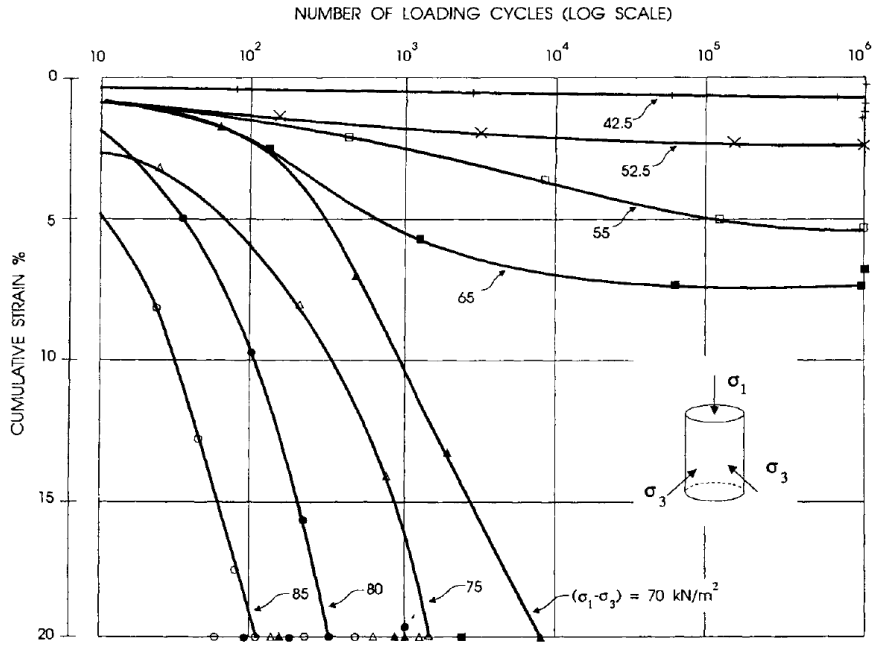

Figure 2.30: Results of repeated load triaxial compression test (Heath et al., 1972).

In order to develop a design chart, Heath et al. (1972) estimated the deviatoric stresses considering the maximum usual axle load using Boussinesq's simple elastic theory for a homogeneous half space to characterise the track substructure. This track design method presumed that a good design is achieved when the deviatoric stress induced in the subgrade soil by the maximum usual

axle load is identical to the threshold stress at the same depth in the subgrade. Figure 2.31 shows a set of solid line curves relating the deviatoric stress to the depth of the subgrade below the sleeper, for a range of axle loads. Also, it displays a set of dashed curves relating the threshold stress with depth for a range of soil threshold stresses determined from the standard cyclic triaxial test, which was performed under a standard ambient pressure. The deviatoric stress distribution, as mentioned earlier, was estimated assuming a substructure of homogeneous half space. The gradients of the threshold stress curves represent the effect of confining pressure.

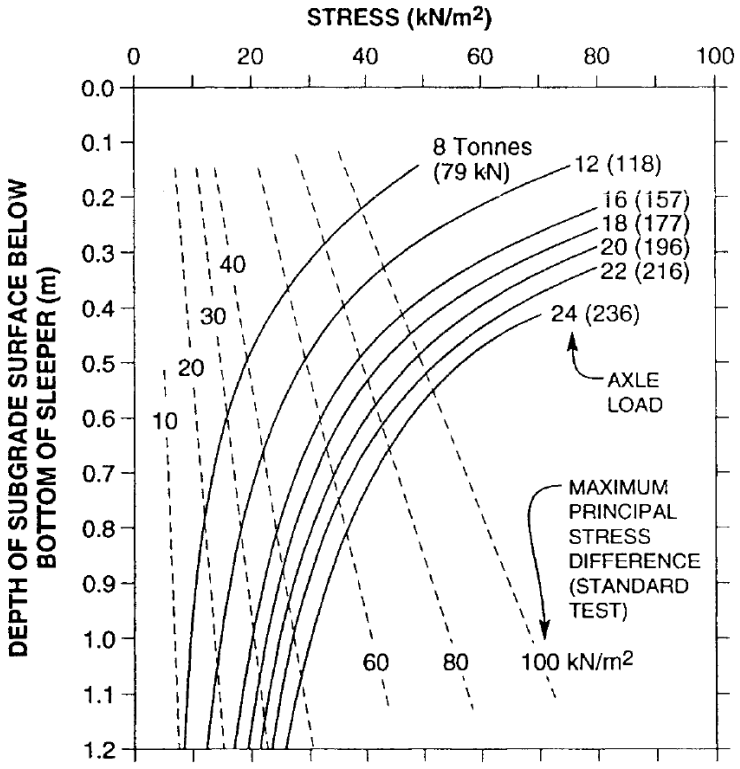

Figure 2.31: Variation of subgrade surface vertical stress and threshold stress with depth bellow bottom of sleeper (Heath et al., 1972).

The threshold stress at various depths can be calculated by the following formula:

$$\frac{\frac{(\sigma_d)_{TS}}{2}}{\frac{(\sigma_d)_{TS}}{2}+0.35+0.1}=\frac{\frac{(\sigma_d)_{TP}}{2}}{\frac{(\sigma_d)_{TS}}{2}+\sigma_3+0.1} \tag{2.39}$$

where, $(\sigma_d)_{TS}$ is the threshold stress of the soil at yield in a standard test at σ_3 = 0.35 kg/cm^2; $(\sigma_d)_{TP}$ is the threshold stress of soil at any other confining pressure, σ_3; and σ_3 is the confining pressure at different depths.

From Figure 2.31, the points at which the two sets of curves intersect represent the required design depth, i.e. the depth at which the induced stress is equal to the threshold strength. For a particular axle load and a particular threshold stress distribution, the required granular layer thickness was then replotted in Figure 2.32 against the threshold stress for that particular axle load. Accordingly, the required thickness of the granular layer can be determined in terms of the threshold stress of the subgrade soil and design axle load.

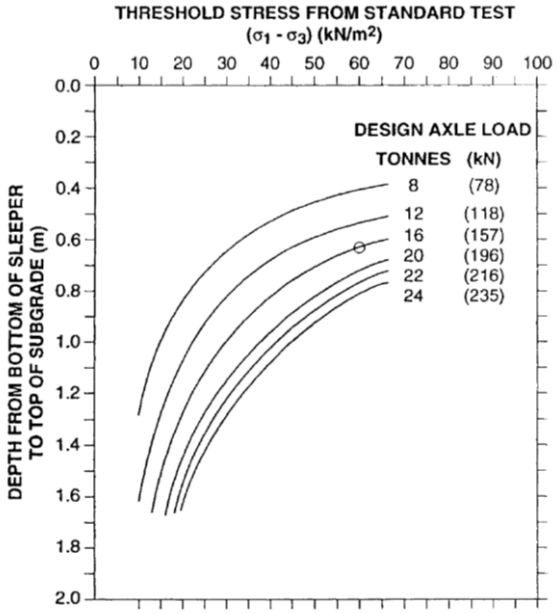

Figure 2.32: Design chart to calculate the granular layer thickness (Heath et al., 1972).

2.5.4 Li-Selig Design Method

The latest innovative design method was developed by Li and Selig (1998a, b), which was based on the combined use of a multilayered analytical model (i.e. GEOTRACK) together with extensive laboratory testing under cyclic loading. The GEOTRACK was used to calculate stresses in the subgrade for different stiffnesses and thicknesses of ballast and subgrade material under static loading situation. The

impacts of the number of repeated loading and the ratio of deviatoric stress to soil strength on the cumulative plastic strain for various soil types were investigated by laboratory testing (Li and Selig, 1996). The results from the analytical model and the laboratory tests were then used to develop design charts for calculating the granular layer thickness for a particular design load and conditions of ballast and subgrade.

In this design method, the subgrade progressive shear failure under repeated loading was correlated with the cumulative plastic strain at the subgrade surface. To prevent such failure, the accumulated plastic strain was considered to be less than an allowable plastic strain for the design traffic tonnage. Accordingly, the design criteria can be mathematically represented by the following equation:

$$\varepsilon_{p\_s} \leq \varepsilon_{(p\_s)a} \tag{2.40}$$

where, ε_{p_s} and $\varepsilon_{(p\_s)a}$ are, respectively, the cumulative plastic strain and allowable plastic strain at the top surface of subgrade for the design traffic tonnage.

Moreover, the excessive plastic deformation failure (ballast pocket) was correlated to subgrade cumulative plastic deformation in this design method. To limit excessive plastic deformations, the cumulative plastic deformation of the subgrade layer was considered to be less than an allowable plastic settlement for the design loading. Thus, the design criterion of this method can be expressed as follows:

$$\rho_s \leq \rho_{sa} \tag{2.41}$$

where, ρ_s is the cumulative plastic deformation of the subgrade layer; and ρ_{sa} is the allowable subgrade deformation for the design traffic tonnage.

Li and Selig (1998a) produced two sets of design charts considering two design criterion as in Equations (2.40) and (2.41). The first set of design charts provides the minimum thickness of the granular layer, H_b, needed to prevent the progressive shear failure of the subgrade under various substructure conditions (Figure 2.33). The granular layer thickness is a function of the ballast modulus, E_b (defined as the repeated deviatoric stress divided by the resilient axial strain), subgrade soil modulus, E_s, soil type, soil physical condition and design load. The second set of design charts gives the thickness of the granular layer needed to prevent excessive

plastic deformation, which is additionally a function of subgrade depth, H_s (Figure 2.34).

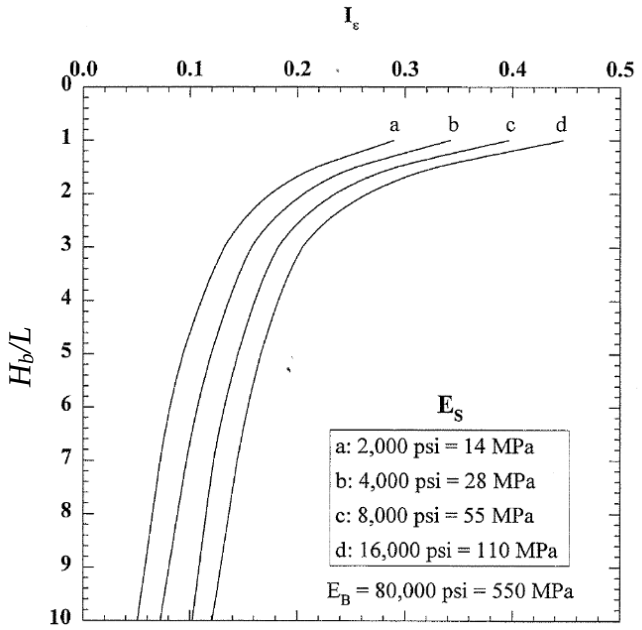

Figure 2.33: An example of design chart to calculate the minimum thickness of granular layer for preventing the progressive shear failure (Li et al., 1996).

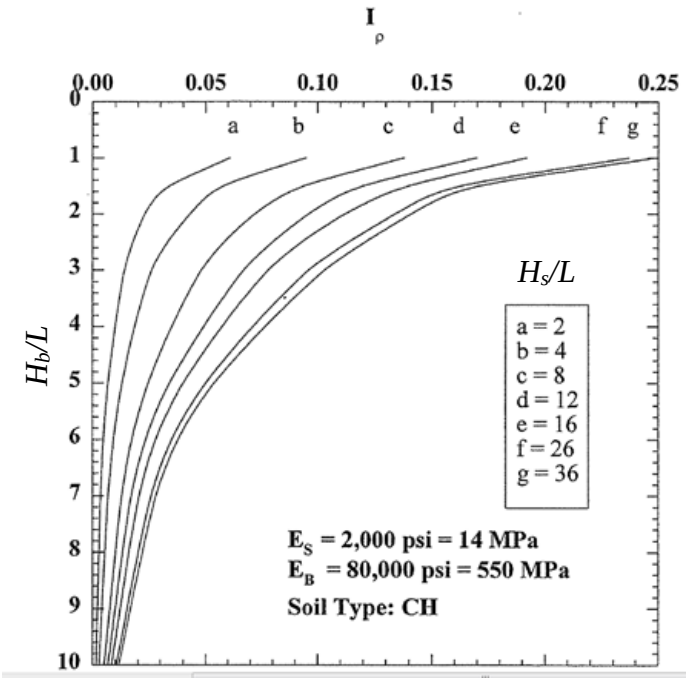

Figure 2.34: An example of design chart to calculate the minimum thickness of granular layer needed to prevent excessive plastic deformations (Li et al., 1996).

2.5.5 The International Union of Railways Method

The International Union of Railways set recommendations for calculating the granular layer thickness, known as the UIC 719 R Method (UIC, 1994), which is an empirical method largely based on the French best practice. The method states that the substructure may consist of some or all of the following layers: ballast, sub-ballast, geotextile and prepared subgrade layers (Figure 2.35). The combined thickness of the granular layers is calculated based on the soil type forming the subgrade, thickness of the prepared subgrade, track configuration and its quality, and loading characteristics. This method does not spell the basis for calculating the individual thicknesses of the ballast and sub-ballast. The prepared subgrade is the top part of the subgrade, which is treated to improve its strength. The inclusion of the prepared subgrade and geotextile in the design is optional.

In this method, the type of soil forming the subgrade was categorised based on the percentage of fines in the soil. Accordingly, there were four soil categories: (1) QS0 which is a soil supposed to be unsuitable without soil stabilisation; (2) QS1 which is a poor soil considered to be acceptable in the natural condition subject to having adequate drainage and maintenance; (3) QS2 is the 'average' quality soil; and (4) QS3 is the 'good' quality soil. The poorer quality subgrade requires higher depth of granular layer.

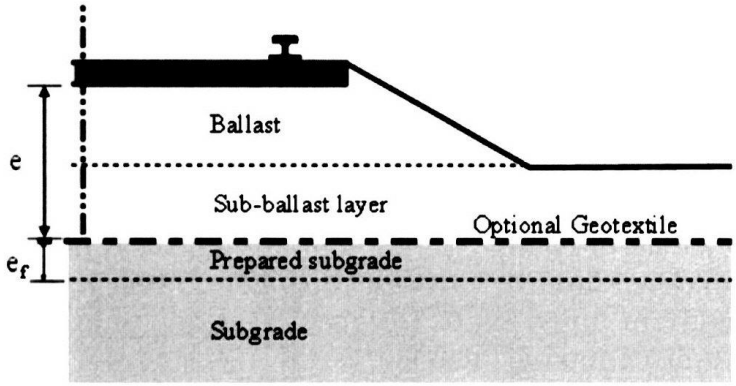

Figure 2.35: Calculation of the minimum thickness of the granular layer (UIC, 1994).

2.5.6 Network Rail Code

The recent Network Rail code of practice (NR/SB/TRK/9039) proposed a set of recommendations for calculating the thickness of the granular layer for design of ballasted railway track (Network Rail, 2005). This code identifies that the track geometry and maintenance requirements are affected by the condition of the substructure. Where the track geometry was not adequate in the past and now needs excessive maintenance, the required granular layer thickness can be obtained from a chart given in the code.

The chart relates the undrained subgrade modulus (i.e. Young's modulus) to the required granular layer thickness for three different amplitudes of the dynamic sleeper support stiffness (namely 30MN/m, 60 MN/m, and 100 MN/m). The minimum value of the dynamic sleeper support stiffness deals with the minimum requirement for the granular layer, for both the existing main lines (with and without geogrid reinforcement) and new track.

2.5.7 Comparison of Available Design Methods

Burrow et al. (2007) presented a comparison between available design methods by calculating the granular layer thickness indicated by each method for different conditions of subgrade, axle load, train speed and cumulative tonnage relating to difference sites in UK. The factors considered in this comparative study are briefly described below.

2.5.7.1 Subgrade modulus

In the abovementioned comparative study, the subgrade was assumed as a high plasticity clay soil, which is a typical problematic soil in the UK. The subgrade soil was characterised by its resilient modulus, which varied within a range from 15 MPa to 100 MPa. As some design methods use properties other than the resilient modulus, these properties were converted into the resilient modulus of soil to make the comparison possible. The compressive strength (σ_s) was related to the resilient modulus (E_s) using a simple relationship as: $E_s \approx 250 \times \sigma_s$. The threshold strength of soil (σ_{TS}) was assumed to be half of its compressive strength, leading to

$E_s \approx 500 \times \sigma_{TS}$. In the European Standard UIC 719 R, soil condition is not characterised by the resilient modulus or strength; rather, this method relates the soil quality to the percentage of fines in the soil. For the clay considered here, it was assumed that the percentage of fine in the soil is about 40%, so the subgrade was classified as a class QS1 soil type.

Regarding the traffic loading, two different circumstances of train speeds were considered. In each case, a mixed traffic loading of 50% freight and 50% passenger was assumed. The characteristics of freight train were representative of the Class 60 locomotive with an axle load of 250 kN travelling at a speed of 125 km/h. The passenger train was assumed to be a HST with an axle load of 170 kN (Kouroussis et al., 2011b). For one circumstance, the passenger HST was assumed to travel at a speed of 200 km/h, and for the other circumstances, the train speed was assumed as 300 km/h. The mixed traffic was only taken into account in the Li-Selig and UIC 719 R design methods. As other design methods do not have the provision to consider mixed traffic, the heavier axle load (i.e. 250 kN) travelling at a speed of 200 km/h or 300 km/h was used to characterise the traffic. A design loading of 900 MGT (i.e. 15 MGT per year for 60 years) was assumed as in the Channel Tunnel Rail Link (CTRL) in the UK (Gibb et al., 1992). Figure 2.36 shows the variation of granular layer thickness with the subgrade condition (Burrow et al., 2011). It can be seen that the design methods show large disparity in the recommended thickness of the granular layer. Because all design methods, except the Li-Selig Method, did not consider the effect of train speeds of 200 km/h and 300 km/h, the obtained granular layer thickness is deemed identical for both train speeds.

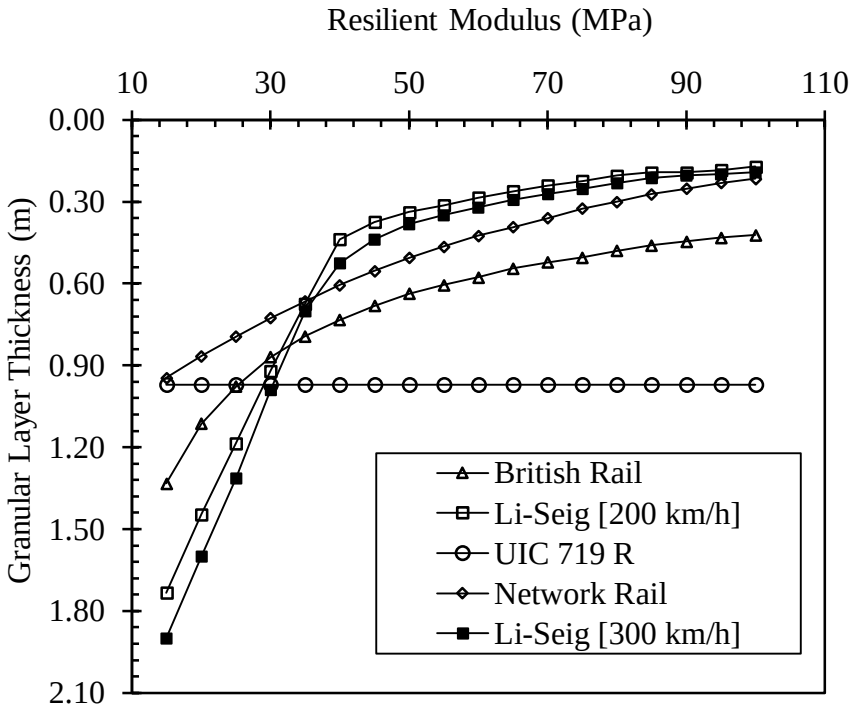

Figure 2.36: Variation of granular layer thickness with subgrade condition (Burrow et al., 2011).

2.5.7.2 Axle load

Burrow et al. (2007) studied the variation of the estimated granular layer thickness with axle load indicated by each method, where the subgrade was assumed to be clay of resilient modulus = 40 MPa. The subgrade soil parameters used in the design methods (i.e. threshold strength and compressive strength) corresponding to a resilient modulus of 40 MPa were determined using the relationship between the resilient modulus and other soil properties (as described earlier in Section 2.5.7.1). To simulate a freight traffic condition, a variation of wheel load from 140 kN to 350 kN was considered. In the UK, the maximum axle load is 250 kN; accordingly, the axle load was limited to this value in the British Rail design method. The design tonnage was considered to be 900 MGT for the design life of the track (60 years). Variation of the estimated granular layer thickness with the axle load is presented in Figure 2.37. It can be seen that there is a significant difference among the various methods in the predicted thickness of the granular layer. It can also be seen that the design thickness is significantly influenced by the axle load, as specified by the Li-Selig method.

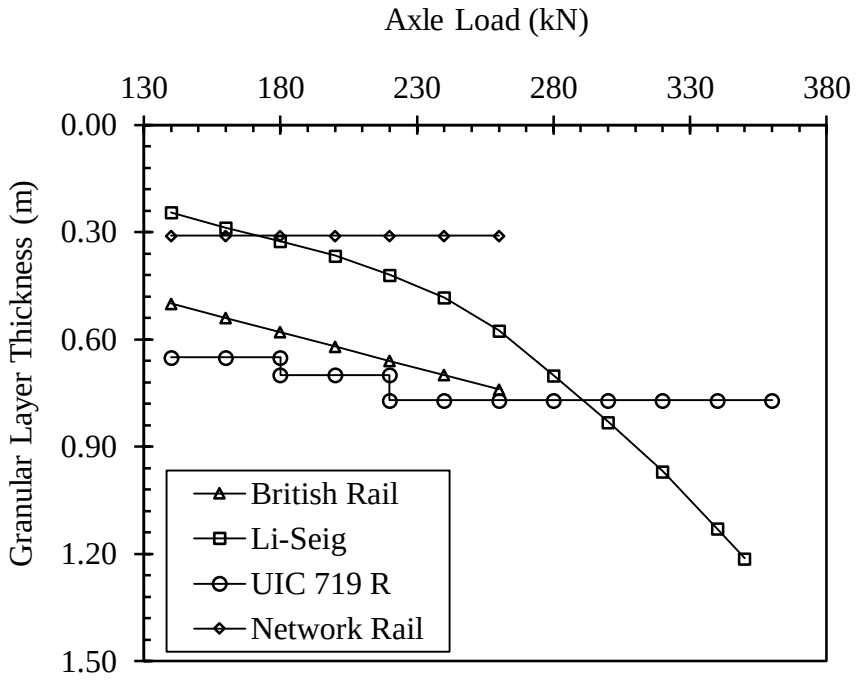

Figure 2.37: Variation of granular layer thickness with axle load (Burrow et al., 2007).

2.5.7.3 Train speed

The design thickness of the granular layer for different train speeds were determined using the different design methods discussed above for a HST with 170 kN axle load (this is similar to Eurostar HST travelling along the CTRL). The required granular layer thicknesses was determined for a speed varying from 80 km/h to 350 km/h. The subgrade properties and design traffic tonnage were considered the same, as described earlier in the Section 2.5.7.2. Variation of the required granular layer thickness with the train speed is presented in Figure 2.38. It can be seen that the required granular layer thickness gradually increases with the increase of the train speed, as indicated by the method developed by Li and Selig (1998a). The design thickness suggested by the Network Rail and the UIC methods depends on the speed limit of 150 km/h and 160 km/h, respectively. However, the design thickness remains independent of train speed as specified by the British Railways method.

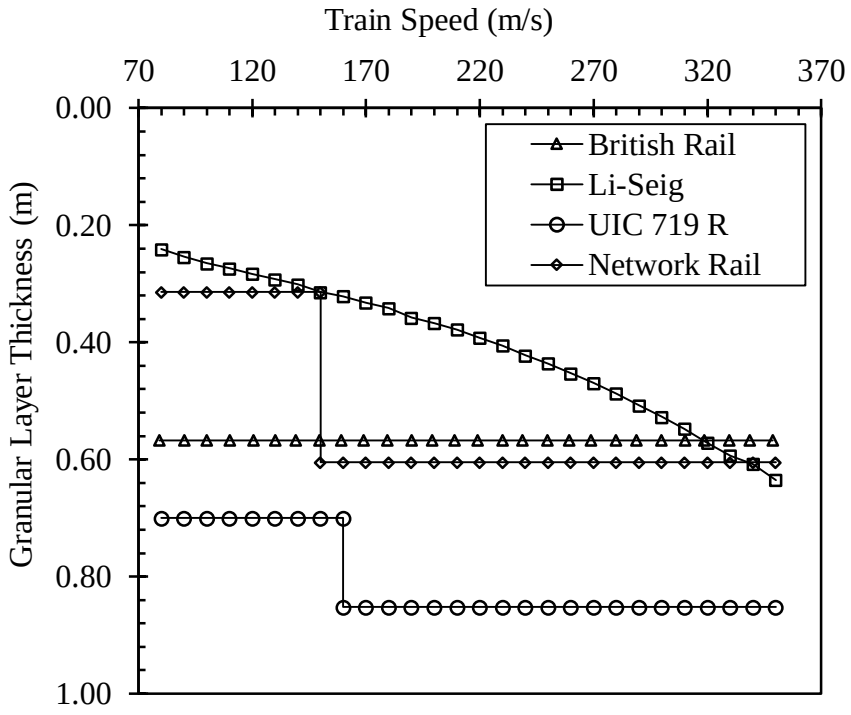

Figure 2.38: Variation of predicted granular layer thickness with train speed (Burrow et al., 2007).

2.5.7.4 Cumulative tonnage

To compare the granular layer thickness required for the cumulative tonnage using existing design methods, a Class 66 locomotive travelling at 125 km/h with axle load of 250 kN was considered. The cumulative tonnage was varied from 30 MGT to 900 MGT with an assumption of 15 MGT/year (Burrow et al., 2007). The subgrade properties were assumed similar to that described earlier in Section 2.5.7.2. Variation of the granular layer thickness with the cumulative tonnage is presented in Figure 2.39. It can be seen that for all design methods, except the Li-Selig method, the required thickness is independent of the cumulative tonnage.

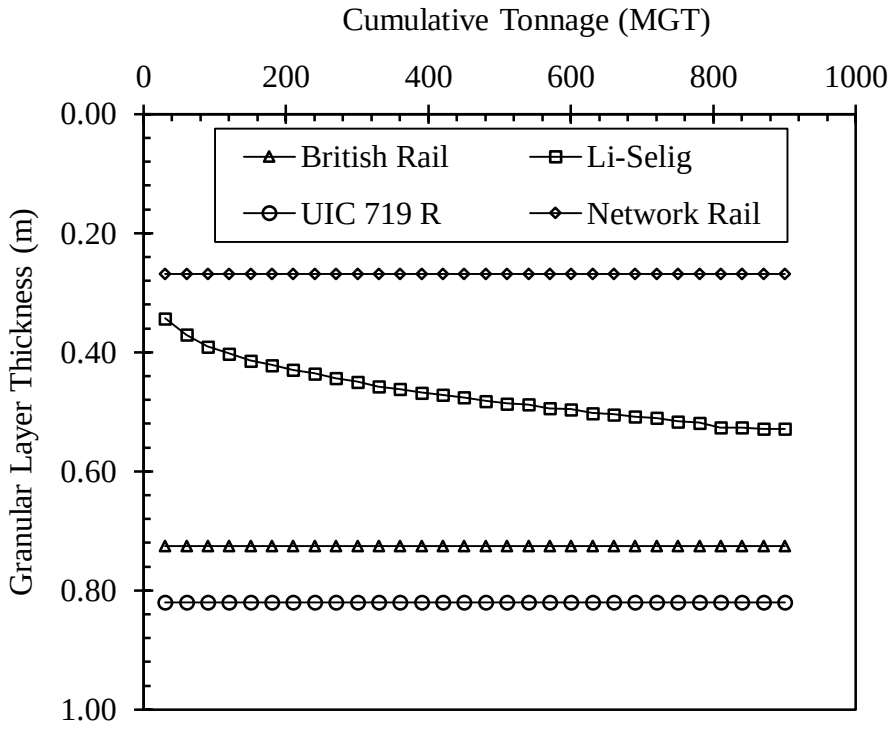

Figure 2.39: Variation of granular layer thickness with cumulative tonnage (Burrow et al., 2007).

2.5.7.5 General observations from the comparative study

From the comparative study presented in Figures 2.36 to 2.39, the following two general remarks can be made:

- The granular layer thickness predicted by existing design methods is a function of at least one of the four parameters; namely the subgrade modulus, axle load, train speed and cumulative tonnage, except for the Li-Selig method, in which in the thickness is a function of all of the four variables.

- The thickness of the granular layer predicted by existing methods varies significantly due to the different design philosophy used in each method.

2.5.8 Applicability of Available Design Methods in Real Sites

In this section, applicability of existing design methods to real sites is discussed. A site of mixed traffic railway track near Leominster in Herefordshir of about 50% freight was investigated by Burrow et al. (2006). The design speed of the train along

the track for the section concerned was 128 km/h, and the annual tonnage at the site was about 6 MGT/year. Lower limit of the subgrade strength and resilient modulus found along the track were 100 kPa and 25 MPa, respectively (O'Riordan and Phear, 2001). Using the data of the field condition and design requirements, the required granular layer thicknesses were calculated using four design methods (Burrow et al., 2007), and the results are provided in Table 2.4.

Table 2.4: Granular layer thickness required in a track near Leominster (Burrow et al., 2007).

Design Method	**Li-Selig**	**UIC 719 R**	**British Rail**	**Network Rail**
Design thickness (m)	0.86	0.82	0.97	0.49

Inspection of Table 2.4 reveals that the required granular layer thickness suggested by Li-Selig and UIC 719 R methods are almost identical. Among these design methods, the British Rail method predicts the maximum granular layer thickness, whereas the Network Rail code predicts the minimum thickness. The actual thickness of the granular layer used along the track was between 0.9 to 1.3 m, and was then increased from its design thickness over time (Burrow et al., 2006). This range of design thicknesses is definitely more than that provided by the existing design methods except the British Rail method. However, it should be noted that to maintain a satisfactory line and level at that site, frequent maintenance is still needed despite the larger thickness adopted.

Gräbe (2002) presented a study related to a site from Broodsnyerplass to Richards Bay COALlink railway track in South Africa, which was originally intended to convey 21 MGT of coal per year using vehicles with an axle load of 20 tonnes. The railway track was recurrently improved, and currently the track conveys over 60 MGT per year with an axle load of 26 tonnes. In 1999, 58% of the capital expenditure was associated with the construction of new track foundations (sub-ballast and subgrade). Up to 68% of the total maintenance costs over the period 1999-2004 were associated with failure of track foundations, even though the line was built using the most up to date standards.

The studies presented by Burrow et al. (2007), Burrow et al. (2007) and Gräbe (2002) state that available design methods for railway track foundations may not be

appropriate for heavy axle loads and high speed trains. There are several limitations in these methods, which need to be addressed to provide an appropriate design of modern railway tracks. In the following section, the limitations of existing design methods are described.

2.5.9 Limitations of Available Design Methods

To compute the minimum granular layer thickness that is adequate to prevent track failures, a number of design methods with numerous drawbacks are provided in the literature. The major characteristics and limitations of these design methods are described here in terms of four aspects: (1) method of analysis; (2) design criterion; (3) material properties; and (4) train load characteristics. All of the four aspects should be carefully considered for a proper design of ballasted railway track foundations.

2.5.9.1 Methods of analysis

Over a long period, the Winkler beam model was used to determine the stress-strain response of track superstructure. However, this model provides a poor prediction for the stresses and strains induced in the substructure layers. AREA recommended the Talbot (Equation 2.34) and JNU (Equation 2.35) empirical formulas for determining the minimum required ballast thickness so that the subgrade failure can be prevented. However, these equations were based on a particular loading and track-ground condition. For example, the JNR equation was derived for a narrow gauge track. Moreover, among the several equations recommended by AREA, the Talbot equation was used more frequently. However, this empirical equation was developed based on experiments performed during the 1910s and 1920s when the axle load was small and train speeds were actually low. Presently, with much heavier wheel loads and higher train speeds, the application of this equation is expected to result in grossly erroneous response of the train-track-ground system. The type and conditions of subgrade soil and ballast as well as effects of repeated loading were not reflected at all in these equations. Moreover, in these equations, the thickness of the ballast was presented as a function of the sleeper/ballast contact stress, which can also be determined using the empirical formula based on the worst condition; this may lead to an uneconomical design of railway tracks.

Most of the existing design methods reviewed herein recommended the use of Boussinesq's elastic theory to analyse the stress developed in substructure layers. Recall that Boussinesq's theory assumes a semi-infinite, homogeneous, elastic body to characterise the ballast, sub-ballast and subgrade layers under a point load or a uniformly distributed load to represent either the rail seat load or sleeper/ballast contact stress. Although this theory may be adequate for approximate estimation of the stress below the wheel load, it is too conservative for designing the railway track. In addition, this theory does not evaluate the effect of the properties of an individual substructure component. As this theory overlooks the stress distribution function of the top rigid layer, it is certain that it will over predict the stress induced in the subgrade layer, leading to more conservative and uneconomical estimation of the thickness required for the granular layer.

On the other hand, the multilayer elastic theories were developed for the stress analysis of individual track components, which can replace the Boussinesq elastic theory for single layer. The design procedure for asphalt railroad track-bed developed by Huang et al. (1987) used the multilayer KENTRACK model. Similarly, Li and Selig (1998a, b) used the GEOTRACK multilayer elastic model for the stress analysis of individual track components, and incorporated the stress analyses results under different track ground conditions to develop design charts. However, these multilayer analytical models were unable to simulate the true train moving loads, and rather provided oversimplified solutions based on a factored static wheel load.

Over the years, railway track analysis and design have been evolved from approximate theoretical calculations to sophisticated numerical solutions. In fact, with the advancement in computer technology, the use of numerical modelling for accurate prediction of railway track response is becoming more popular. A number of researchers (e.g. Chebli et al., 2008; Cunha and Correia, 2012; El Kacimi et al., 2013; Feng, 2011; Hall, 2003) developed 3D FE modellings that can accurately simulate the dynamic response of railway tracks subjected to train moving loads. However, till now, there is no available design method that considers the true train moving loading conditions. Therefore, to develop an advanced design method (to overcome the shortcomings of available design methods), sophisticated 3D FE modelling needs to be developed to simulate the true dynamic response of railway track induced by train moving loads. The methodology of developing and validating

such a sophisticated 3D FE modelling will be discussed in Chapter 4. Finally, the analysis results will be utilised to develop design charts that will facilitate the use of the proposed design method by practitioners for calculating the granular layer thickness, as presented in Chapter 5.

2.5.9.2 Design criteria

The main objective of designing a minimum thickness of granular layer is to prevent failure of track substructure and limit excessive plastic deformation. To satisfy this objective, the AREA method recommends using a universal allowable bearing pressure of 138 kPa. As subgrade soils may vary widely in strength, the use of a single bearing capacity value in design is inappropriate. To overcome this limitation, Raymond (1978) suggested using the allowable subgrade bearing capacity based on the Casagrande soil classification. However, the effect of repeated (cyclic) loading on the track cumulative plastic strain and deformation was not considered in the available design methods, except in the British Railways and Li-Selig methods.

The design criterion of the British Railways method was based on limiting the deviatoric stress at the subgrade surface to be less than a threshold stress, which is an attractive criterion, as it takes into account the effects of repeated loading on the subgrade cumulative plastic strain. Nonetheless, the threshold stress is not a property of soils and cannot be found in all types of soil. Moreover, this criterion does not reflect the effect of subgrade layer thickness on the cumulative plastic deformation.

In order to prevent the progressive shear failure of subgrade, the design criterion of the Li-Selig method limits the total cumulative plastic strain at the subgrade surface to be less than the allowable plastic strain for the design tonnage. Furthermore, to prevent the excessive plastic deformation of the track, another design criterion is used whereby the total cumulative plastic deformation of subgrade soil was limited to less than the allowable subgrade plastic deformation for the design tonnage. However, the deformation of ballast layer was ignored completely, although about up to 40% of the total deformation of railway tracks originates from the ballast layer, as indicated by many researchers (e.g. Li et al., 2002; Selig et al., 1981; Stewart, 1982). Therefore, in this thesis, the total track deformation will be considered as explicit design parameter in the development of the new design method.

2.5.9.3 Material properties

To design a ballasted railway track foundation properly, it is very important to define and quantify the material parameters that indeed affect and reflect the track behaviour. In the AREA method, the track modulus was used to characterise the track structure below the rail, which represents the overall stiffness of the fasteners, sleepers, ballast, sub-ballast and subgrade. However, this parameter was derived from the Winkler beam theory for analysing the superstructure (rails and sleepers). Therefore, it is not expected to be necessarily accurate for calculating the granular layer thickness in the ballasted railway track design.

The key parameter to describe the response of each layer is its resilient modulus or dynamic modulus, which is the stiffness obtained under cyclic loading. Unfortunately, most of the existing design methods were rather based on the static Young's modulus. Transportation Officials (1993) suggested that it is indeed the resilient Young's modulus that should be considered as the main stiffness property for materials in the ballasted railway track design. It is concluded therefore that the static modulus is insufficient for the design of railway tracks.

The properties of ballast and subgrade were represented by the resilient modulus in the design method proposed by Li and Selig (1998a) for design of ballasted railway tracks. In this method, the influence of the soil stress state, soil physical state and its structure as well as soil type on the subgrade performance was represented by deviatoric stress, soil static strength and material parameters, respectively. However, the influence of the ballast stress state, physical state and its type were totally ignored in the formula that calculates the total plastic deformation of the substructure layers. Consequently, in this thesis, the proposed design method will try to overcome the limitations of the available design methods discussed above.

2.5.9.4 Train load characteristics

Proper characterisation of the type and magnitude of traffic loads is essential for accurate design of track foundations. The induced stresses of the adjacent axle loads of the same car or between two adjacent cars overlap, especially in the deeper subgrade. However, most of the existing design methods assumed only one wheel load in the design, except for the design method developed by Li and Selig (1998a)

and Huang et al. (1987). Besides, the influence of the wheel spacing was almost ignored in all existing design methods. Li and Selig (1998a) assumed three wheel loads at a spacing of 1.8 m apart in their stress analysis using the GEOTRAC model. This assumption is very conservative, as the wheel spacing of the most modern passenger train is about 3.0 m or above (Alves Costa et al., 2012; Kouroussis et al., 2011b), which would generate less stress in the subgrade. Thus, the design method developed based on the assumption of less wheel spacing cannot be cost effective.

The design methods recommended by the AREA and Raymond (1978) do not consider the effect of repeated loading. Although the British Railways method considered the stress-strain behaviour under cyclic loading (i.e. threshold stress) as a design criterion, the effect of repeated loading was not included; instead, the maximum single dynamic load was considered as the design wheel load. Only the design method proposed by Li and Selig (1998a) considered the influence of repeated loading on the cumulative plastic strain or deformation as a design criterion. However, this design method was based on a static stress analysis, which cannot represent the effect of moving loads (Brown, 1996; Powrie et al., 2007).

In reality, when a train passes along the track, elements within the substructure layer become subjected to complex loading regime, which involves principal stress rotations (Brown, 1996; Powrie et al., 2007). Train moving loads (i.e. cyclic loading with principal stress rotation) may affect both the material stiffness and rate of accumulation of plastic strain (Gräbe, 2002; Inam et al., 2012; Lekarp et al., 2000a; Lekarp et al., 2000b). The rate of accumulation of plastic strain due to train moving loads is greater for some soils than mere cycling the axial stress alone (Gräbe, 2002). Also, the models used to estimate subgrade stresses were generally based on static analyses, and may not fully represent the effects of moving loads. Therefore, to develop an accurate design method, it is essential to use a model which can properly predict the stress at different layers under the true train moving loads instead of an equivalent static factored load.

Available design methods considered the dynamic wheel load implicitly during the stress analysis and suggested some empirical formulas to calculate the design dynamic wheel load. For example, the AREA and Li-Selig methods recommended Equation (2.10) for calculating the dynamic amplification factor (DAF). In this

equation, the DAF depends only on the train speed and wheel diameter. However, recent studies (e.g. Alves Costa et al., 2015; Sayeed and Shahin, 2016a; Sayeed and Shahin, 2016b) indicated that the DAF is significantly influenced by the subgrade characteristics. Similarly other empirical formulas did not consider the subgrade as an important factor for calculating the DAF, and this is a serious limitation for the available design methods, which needs to be overcome in the development of the advanced design method that will be developed in this thesis.

2.6 SUMMARY

This chapter presented the various components of a typical ballasted railway track, its modes of failure and corresponding remedy measures, particularly those aspects addressed in the present research. This chapter also critically discussed existing methods used to design ballasted railway track foundations, including empirical, analytical and numerical methods. Finally, the current state of available design methods was critically reviewed and the objectives of this thesis were derived by identifying the specific fields in which developments were less profound.

Review of a broad range of relevant literature shows that the analysis and design methods for railway track foundations were generally based on experience or empirical equations, which may be prone to misjudgements and inaccuracy. Among several design methods available in the literature, the Li-Selig method was found to be the most sophisticated design method. This method was based on combined use of GEOTRACK multilayer analytical model coupled with extensive laboratory testing. However, the GEOTRACK analytical model can estimate the stresses based only on static loading and may not fully represent the effect of true train moving loads. Thus, it cannot consider the role of the principal stress rotation on behaviour of substructure material, which is one of the major drawbacks of this design method. Therefore, to improve the existing methods, it is necessary to use more sophisticated numerical models, such as the 3D FE models that can precisely estimate the stresses in track layers under dynamic train moving loads. The dynamic effect due to high speed trains under various train-track-ground conditions can also be analysed using sophisticated 3D FE modelling and can be incorporated in the design method. Moreover, the deformation of ballast layer, which was ignored in almost all available design methods, has to be taken into account.

CHAPTER 3

DEFORMATION OF RAILWAY TRACKS SUBJECTED TO REPEATED LOADING

3.1 INTRODUCTION

Ballasted railway tracks settle as a result of the plastic deformations in the ballast layer and underlying subgrade soil caused by repeated train moving loads. Both the excessive plastic strain at the subgrade surface and the track plastic deformations are the two major problems for railway tracks that increase the maintenance costs and reduce the riding quality. Hence, an accurate prediction of these two parameters is essential for proper design and maintenance planning of railway tracks. In this chapter, past studies on the effects of repeated loading on the cumulative plastic strain and deformation of ballast are briefly reviewed. The chapter also presents an improvement to the existing empirical models for predicting the cumulative plastic strain and deformation of ballast materials. This improvement is based on extensive test results reported in the literature, and considers the major influencing factors such as the number of load applications, stress state, physical state and type of ballast. In addition, an empirical model proposed by Li and Selig (1996) for predicting the cumulative plastic strain of fine-grained subgrade soil is also briefly described. These improved empirical models for predicting the cumulative plastic deformation of ballast and subgrade layers are described herein due to their necessity in developing the new design method for ballasted railway track foundations, which is the main objective of this thesis.

3.2 PLASTIC DEFORMATIONS OF BALLAST

Various researchers investigated the impact of the number of load repetitions on accumulation of plastic deformations of ballast and other granular media. Some of the most important studies in relation to the effects of repeated loading on the cumulative plastic defamation of ballast are briefly described below.

Shenton (1975) indicated that a significant portion of track deformation occurs immediately after ballast tamping; however, the rate of deformation becomes much

slower after the initial rapid deformation, as shown in Figure 3.1(a). Shenton (1975) also noted that the deformation of track may be approximately estimated by a linear relationship with the logarithm of number of load cycles, as shown in Figure 3.1(b).

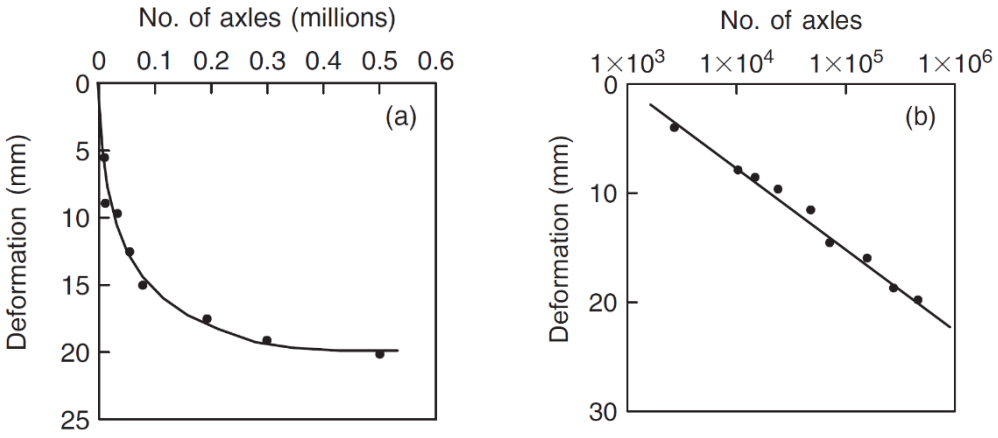

Figure 3.1: Track deformation after tamping: (a) in plain scale; and (b) in semi-logarithmic scale (Shenton, 1975).

Indraratna and Ionescu (2000) conducted a series of true triaxial compression tests on latite ballast and reported highly nonlinear deformation behaviour for ballast under cyclic loading (Figure 3.2). They noticed a rapid rate of ballast deformation (similar to Jeffs and Marich, 1987) during the first 20,000 load cycles, followed by a consolidation stage up to about 100,000 cycles. Indraratna and Ionescu (2000) demonstrated that the ballast bed stabilised during the first 100,000 load cycles, after which the deformation increases at a decreasing rate.

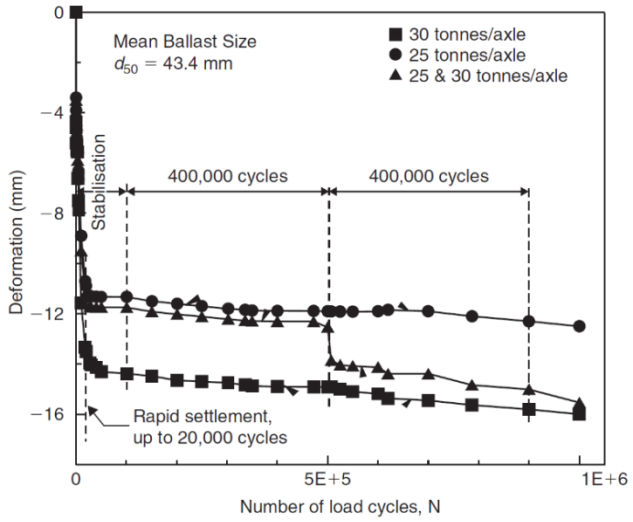

Figure 3.2: Deformation of ballast under cyclic loading (Indraratna and Ionescu, 2000).

Indraratna and Salim (2003) performed a number of cyclic triaxial compression tests on fresh and recycled ballast, and reported a rapid increase in the plastic deformation initially, followed by a stabilised zone with a linear increase in settlement after 100,000 load cycles regardless of the ballast conditions, as depicted in Figure 3.3(a). They also defined a linear relationship between the ballast deformation and logarithm of load cycles, as shown in Figure 3.3(b).

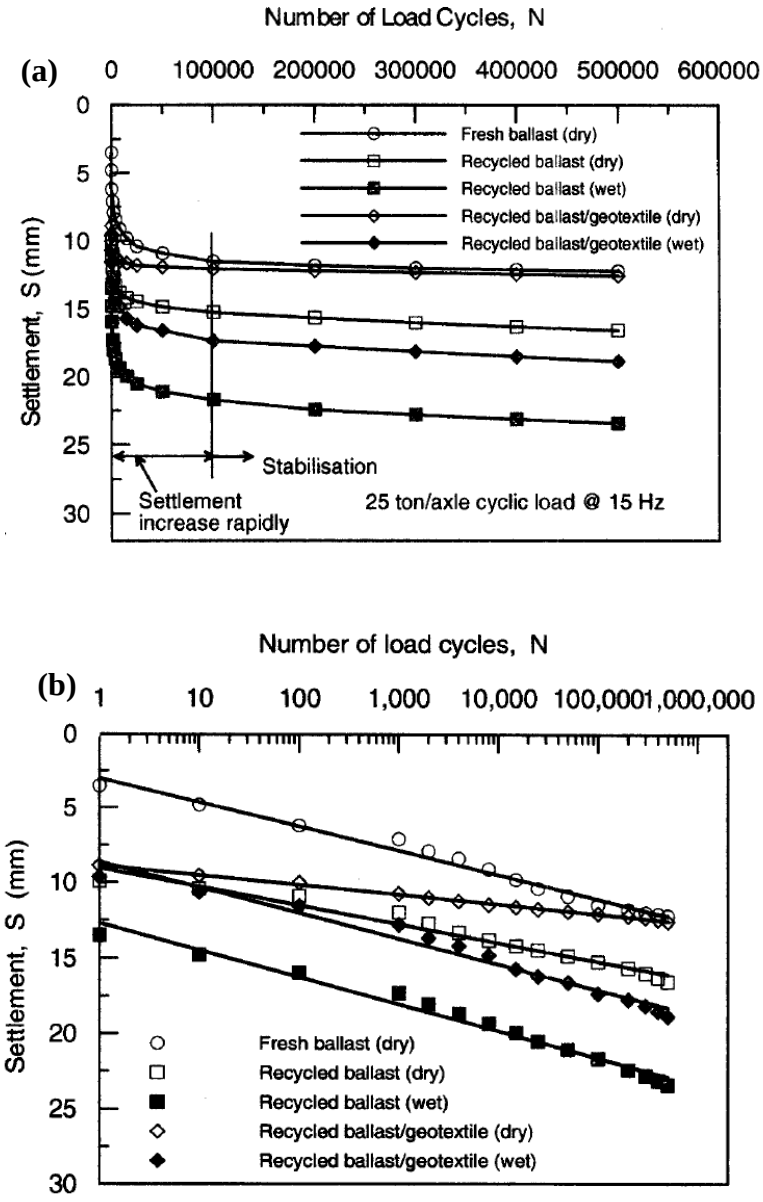

Figure 3.3: Deformation of ballast under cyclic loading: (a) in plain scale; and (b) in semi-logarithmic scale (Indraratna and Salim, 2003).

Raymond and Williams (1978) investigated the influence of load cycles on the axial and volumetric strains of dolomite ballast and concluded that both the axial and

volumetric strains increase linearly with the logarithm of load cycles (Figure 3.4). This study also indicated that the deviatoric stress is the most significant influential factor affecting the cumulative plastic deformation at any number of load cycle. Selig and Waters (1994) and Raymond and Bathurst (1994) also reported similar results.

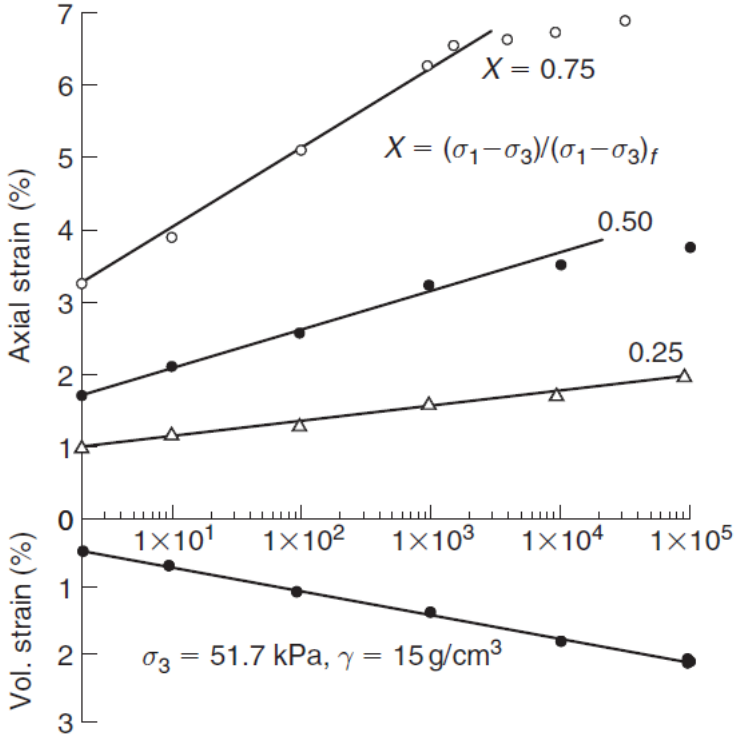

Figure 3.4: Effects of load cycles on axial and volumetric strains (Raymond and Williams, 1978).

In contrast to the trends described above, Raymond and Diyaljee (1979) reported that the relationship between the cumulative plastic strain of ballast and logarithm of load cycles might not be linear for different load magnitudes, grading and ballast types. Diyaljee (1987) concluded that the accumulated plastic strain of ballast is nonlinearly related to the logarithm of the load cycles at a higher cyclic deviatoric stress, as shown in Figure 3.5.

Shenton (1985) analysed a broad range of track settlement data collected from different track sites around the world, and indicated that the relationship between the track settlement and logarithm of load cycles or total tonnage might be linear only for a small number of load cycles, but can lead to significant underestimation of the settlement over a large traffic tonnage (Figure 3.6).

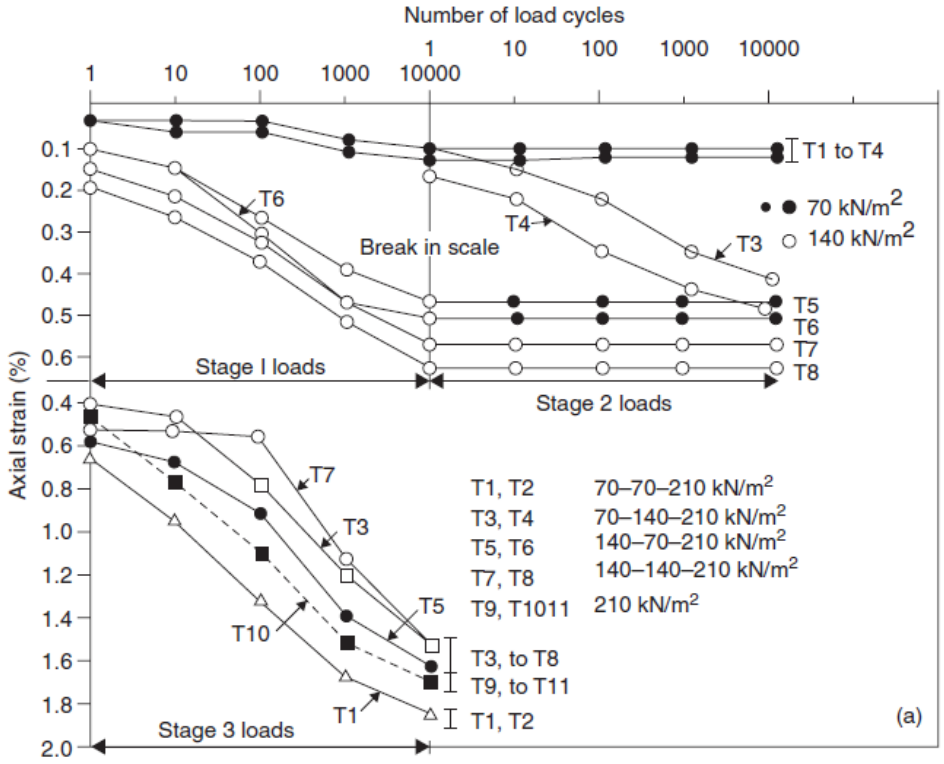

Figure 3.5: Effects of deviatoric stress history on deformation of ballast under cyclic loading (Diyaljee, 1987).

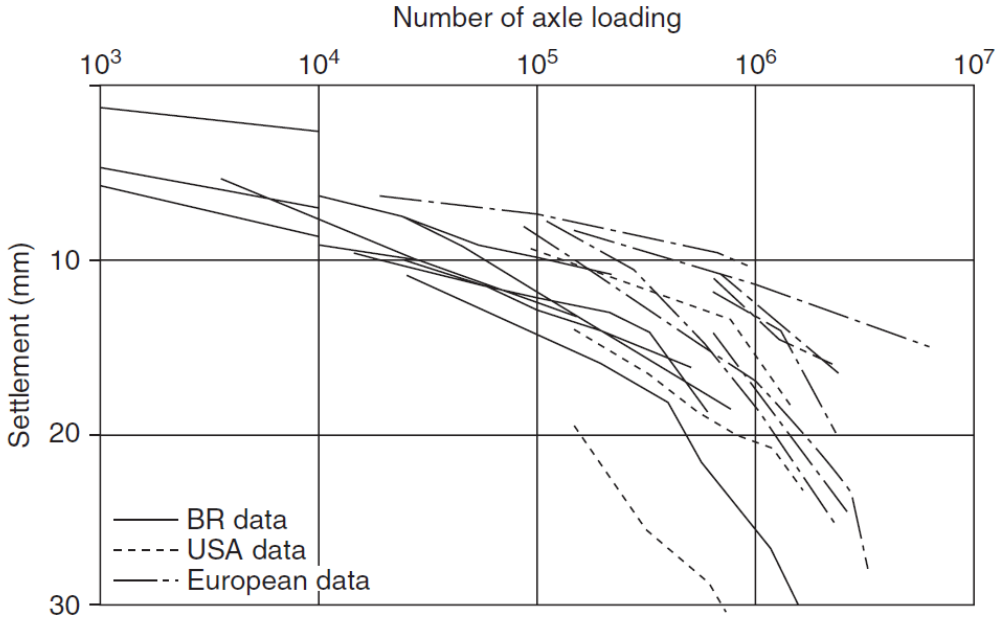

Figure 3.6: Settlement of track at different parts of the world (Shenton, 1985).

3.3 PREDICTION OF BALLAST DEFORMATION

3.3.1 Available Empirical Models

Over the years, a number of studies have investigated the influence of loading characteristics and ballast conditions on the degradation and deformation behaviour of ballast. These studies resulted in the development of several empirical models for determining the accumulated plastic strain of ballast under repeated loading, and some of the most famous models are presented below.

Based on extensive experimental results, an empirical model was developed by Shenton (1975) in which the ballast plastic strain at any number of load cycles with respect to the strain at the first loading cycle and logarithm of the number of load cycles can be expressed as follows:

$$\varepsilon_{p\_b} = \varepsilon_1 \, (1 + \log_{10} N_b) \tag{3.1}$$

where, ε_{p_b} is the average plastic strain in the ballast after the N_b load cycle; and ε_1 is the average vertical strain after the first load cycle. Stewart (1986) conducted a series of cyclic triaxial tests on ballast under variable loading amplitudes and reported that the anticipated strains based on the superposition of ballast strains for various loading magnitudes using a formula similar to Equation (3.1) agree well with the experimental results.

Alva-Hurtado (1980) proposed two empirical models (a linear model for a low number of load cycles and nonlinear model for a large number of load cycles) that can predict the plastic strain as a function of the number of load applications and the vertical plastic strain after the first cycle can be obtained as given below:

$$\varepsilon_{p\_b} = \varepsilon_1 \, (1 + 0.19 \log_{10} N_b) \tag{3.2}$$

$$\varepsilon_{p\_b} = (0.85 + 0.38 \log_{10} N_b)\varepsilon_1 + (0.05 - 0.09 \log_{10} N_b)\varepsilon_1^2 \tag{3.3}$$

where, ε_{p_b} is the average plastic strain of the ballast after N_b load cycle; and ε_1 is the average vertical strain after the first load cycle.

Chrismer and Selig (1993) performed a large number of triaxial compression tests and indicated that ballast accumulated plastic strain can be better represented by a power equation than the logarithmic models, where the ballast cumulative plastic strain is given by:

$$\varepsilon_{p\_b} = \varepsilon_1 N_b^Z \tag{3.4}$$

where, ε_N is the plastic strain after N_b load cycle; ε_1 is the strain after first load cycle; and Z is an empirical constant.

Similarly, Indraratna et al. (2001) reported that the deformation behaviour of ballast can be represented more accurately by a power function as follows:

$$\rho_b = \rho_{b1} N_b^Z \tag{3.5}$$

where, ρ_b is the ballast deformation after N_b number of load cycle; ρ_{b1} is the deformation after the first load cycle, and Z is an empirical constant.

Indraratna and Salim (2003) proposed a logarithmic function of the number of loading cycles for modelling the plastic deformation of ballast with and without geo-synthetic reinforcement (similar to Equation 3.1), where the deformation of ballast is given by:

$$\rho_b = X' + Y' \log N_b \tag{3.6}$$

where, ρ_b is the ballast deformation; N_b is the number of load cycles applied to the ballast; and X' and Y' are empirical constants depending on the ballast conditions, including moisture content and quality.

From a further study, Shenton (1985) derived an empirical model for predicting the ballast settlement based on extensive field data (Figure 3.6), which is given by the following equation:

$$S = K_1 N_b^{0.2} + K_2 N_b \tag{3.7}$$

where, S is the ballast settlement; K_1 and K_2 are empirical constants; and N_b is the total number of load cycles. The deformation of ballast layer is combined of two parts: up to one million stress applications, the first part ($K_1 N_b^{0.2}$) dominate, and the second part ($K_2 N_b$) has a small contribution; and after one million stress applications, the second part becomes negligible.

Raymond and Bathurst (1994) developed a model to correlate the track deformation to the logarithm of total traffic tonnage based on available test results, as follows:

$$S_e(t') = a_r + a_0' \log\left(\frac{t'}{t_r'}\right) \tag{3.8}$$

where, $Se(t')$ is the mean ballast deformation over a unit length at tonnage t'; a_r is the deformation at the reference tonnage; a_0' is the slope of the semi-logarithmic relation; and t_r' is the reference tonnage taken as two million tonnes.

Following the discussion presented above, it can be concluded that most of the existing models that can be used to predict the deformation of ballast are based on strain or deformation incurred after the first load cycle and also on the total number of load cycles. Also, the applicability of these models is apparently limited to certain ballast types and conditions. Therefore, an improved model that can predict the plastic deformation of ballast with consideration of the major influencing factors (including ballast physical state, ballast stress state and ballast type) is still warranted.

3.3.2 Proposed Empirical Model

In the current study, an improved empirical model is proposed for better prediction of the accumulated plastic deformation of ballast. For this purpose, the factors that have been considered to achieve better prediction and the development of the proposed empirical model are described below.

For the ballast stress state, many researchers (e.g. Alva-Hurtado, 1980; Indraratna et al., 2010; Stewart, 1982) indicated that the deviatoric stress is the main stress factor influencing the cumulative plastic strain of ballast under repeated loading rather than

vertical stress or lateral confining stress alone. The plastic strain increases with the increase in the deviatoric stress. Note that the deviatoric stress (σ_d) is the difference between the major and minor principal stresses $(\sigma_d = \sigma_1 - \sigma_3)$. As the shear stress of ballast is basically half the deviatoric stress, the deviatoric stress can be considered to represent the physical meaning of the shear stress. Therefore, the value of the minor principal stress or confining pressure (σ_3) is a secondary factor.

In the current study, the physical state of ballast is defined by its void ratio, gradation, moisture content and ballast structure. Many test results (e.g. Indraratna and Salim, 2003; Raymond and Diyaljee, 1979) reported significant effects of the ballast physical state on the cumulative plastic strain. For example, ballast materials having a small initial void ratio are stronger in shear and generate a smaller deformation than their counterparts with a higher initial void ratio. In order to consider the influence of the ballast physical state, it is not useful nor common to introduce ballast parameters, including the void ratio, gradation, moisture content and ballast structure, directly into an empirical model. However, the influence of these parameters can be indirectly represented by the strength of ballast under monotonic loading; as the ballast strength depends on the void ratio, gradation, moisture content and ballast structure. In addition, the monotonic triaxial tests can be routinely performed.

In this chapter, the empirical model for predicting the cumulative plastic strain is developed for three different types of ballast, namely basalt, granite and dolomite. The model is based on the results of a series of large-scale triaxial, isotropically-consolidated, drained cyclic compression tests available in the literature (e.g. Alva-Hurtado, 1980; Lackenby et al., 2007; Raymond and Williams, 1978). The proposed model is a modification of a model previously suggested by Shahin (2009). The model proposed here is given below:

$$\varepsilon_{p\_b} = x(\alpha)^y [1 + \ln(N_b)]^z / 100 \tag{3.9}$$

where, ε_{p_b} is the cumulative plastic strain of ballast; α is the ratio of σ_{d_b} to σ_{s_b} (i.e. $\alpha = \sigma_{d\_b} / \sigma_{s\_b}$); σ_{d_b} is the applied cyclic deviatoric stress; σ_{s_b} is the compressive strength of ballast under a nominal confining pressure of 50 kPa, which

can be obtained from a monotonic triaxial test; N_b is the number of load applications on the ballast; and *x*, *y* and *z* are regression parameters depending on the ballast type as summarised in Table 3.1.

Table 3.1: Material parameters for various types of ballast.

Ballast Type	***x***	***y***	***z***
Basalt	4.82	1.42	0.49
Granite	1.27	2.41	0.48
Dolomite	4.23	1.15	0.32

Figure 3.7 shows the calibration of predicted (using the proposed model) and experimental cumulative plastic strains for different ballast types, including basalt (Figure 3.7a), granite (Figure 3.7b) and dolomite (Figure 3.7c). It can be seen that the influence of the deviatoric stress, ballast physical state and ballast type on the cumulative plastic strain are reflected well in the prediction.

For a particular ballasted track, ε_{p_b} after N_b load cycles can be determined by knowing the value of σ_d applied on the ballast layer. In the current study, it is recommended to determine the σ_d from a sophisticated three dimensional (3D) finite element (FE) numerical modelling similar to the one described in Chapter 4. Then, the accumulation of plastic deformation can be determined by summing up the deformations of all subdivided layers using the following equation:

$$\rho_b = \sum \varepsilon_{(p\_b)i} H_{bi} \tag{3.10}$$

where, ρ_b is the plastic deformation of ballast layer; $\varepsilon_{(p\_b)i}$ is the plastic strain at the centre of each ballast sublayer; and H_{bi} is the thickness of each sublayer of ballast.

It should be noted that when a train passes along the track, the ballast particles are subjected to a complex loading that involves principal stress rotation. However, the empirical model was developed based on data obtained from traditional cyclic triaxial tests in which the major principal stresses are not rotated. Therefore, it is useful in the future to examine the deformation behaviour of ballast under real loading conditions by considering cyclic loading with principal stress rotation, and incorporating this effect into the empirical model.

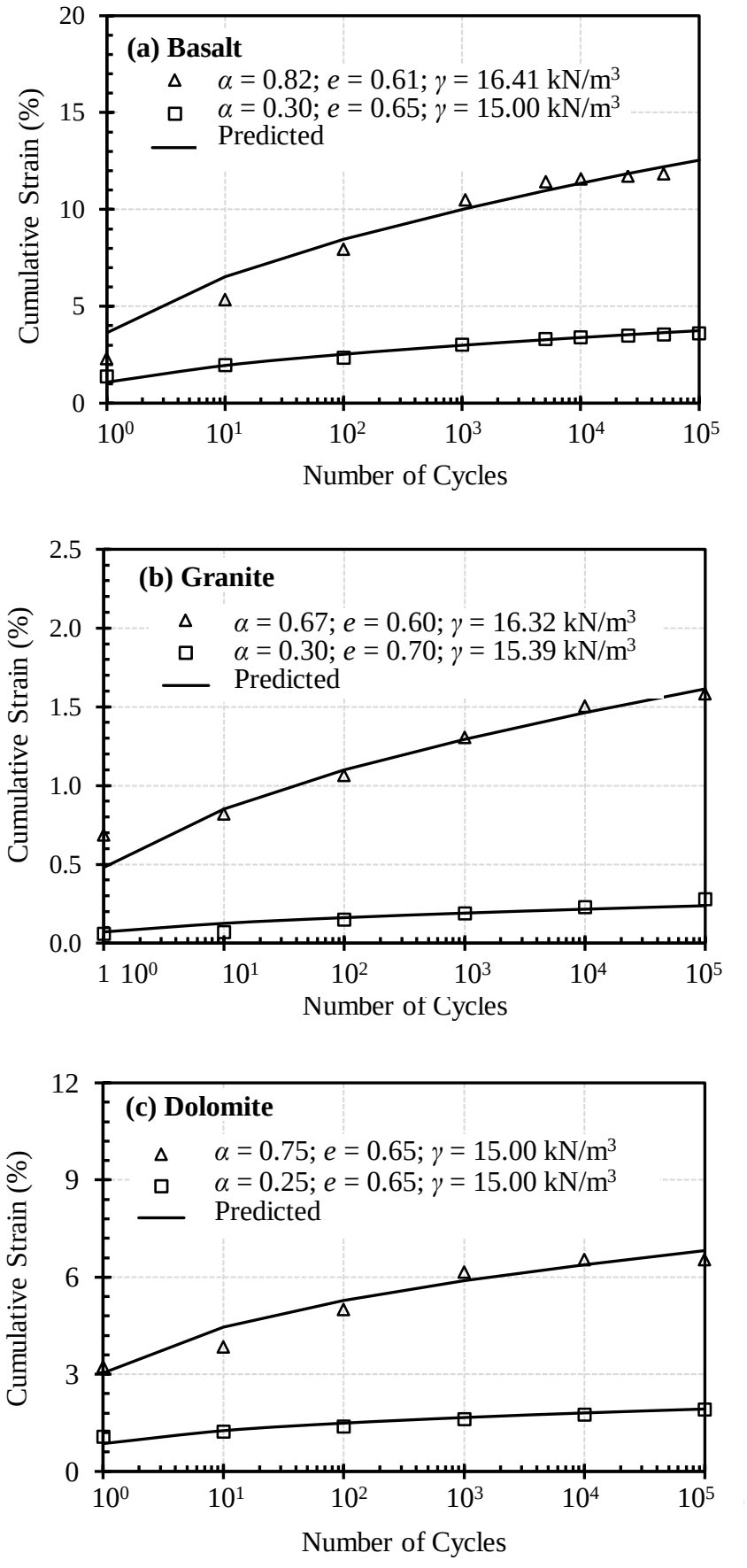

Figure 3.7: Calibration of empirical model with the experimental results.

3.4 PREDICTION OF SUBGRADE DEFORMATION

In the past, a large number of cyclic loading triaxial or direct shear tests were conducted on either unsaturated or saturated soil samples in undrained or drained conditions to investigate the plastic deformation of fine-grained soils under repeated loading. Based on experimental data collected from these tests, various models were proposed for estimating the cumulative plastic strain of fine-grained soils under repeated loading. Among these models, the most advanced ones that are currently used to predict the cumulative plastic strain and cumulative plastic deformation of track fine-grained subgrade soils are as follows (Li, 1994; Li and Selig, 1996):

$$\varepsilon_{p\_s} = \frac{a}{100}\left(\frac{\sigma_{d\_s}}{\sigma_{s\_s}}\right)^{m} N_s^{b} \tag{3.11}$$

$$\rho_s = \sum \varepsilon_{(p\_s)i} H_{si} \tag{3.12}$$

where, ε_{p_s} is the cumulative plastic strain of track subgrade soil; σ_{d_s} is the deviatoric stress applied to the subgrade; σ_{s_s} is the unconfined compressive strength of the subgrade soil; N_s is the number of load repetitions in the subgrade layer; and *a*, *m* and *b* are material parameters given in Table 3.2; ρ_s is the total cumulative plastic deformation of the track subgrade; $\varepsilon_{(p\_s)i}$ is the plastic strain at the centre of each subdivided layer calculated by Equation (3.11); H_{si} is the thickness of each sublayer of the subgrade.

Table 3.2: Material parameters for various types of soil (Li, 1994; Li and Selig, 1996).

Ballast Type	***a***	***m***	***b***
Fat Clay (CH)	1.20	2.4	0.18
Lean Clay (CL)	1.10	1.8	0.16
Elastic Silt (MH)	0.84	2.0	0.13
Silt (ML)	0.64	1.7	0.10

In Equations (3.11) and (3.12), the effect of the soil stress state (i.e. deviatoric stress) on the relationship between the cumulative plastic strain and number of load

applications was considered directly. In addition, the influence of the soil physical state (e.g. water content, dry density and soil structure) on the subgrade performance was represented indirectly by the static soil strength, σ_{s_s}, which was directly linked to the soil physical state and its structure. The influence of soil type was also implied by the material parameters (*a*, *m* and *b*). Thus, the effect of all major influencing factors on the cumulative plastic strain of subgrade soil (i.e. number of repeated stress applications, soil stress state, soil type, and soil physical state) that need to be considered in the prediction model was indeed reflected by the model proposed by Li and Selig (1996). Therefore, this empirical model is adopted herein (i.e. Equations 3.11 and 3.12) and will be used for the development of the new design method in the form of design charts, as described in Chapter 5.

3.5 SUMMARY AND CONCLUSIONS

In this chapter, an enhancement to the existing empirical models for predicting the cumulative plastic deformation of ballast under repeated loading was proposed, which will be used in the development of the new design method in Chapter 5. The improved empirical model was developed based on experimental results available in the literature. In this model, the effect of the most important influencing factor (i.e. deviatoric stress) on the relationship between the cumulative plastic strain of ballast and number of load applications was directly considered. In addition, the ballast physical state as defined by the void ratio, gradation, moisture content and ballast structure was taken into account by the ballast strength obtained from the monotonic triaxial test. The model material parameters (*x*, *y* and *z*) for three different types of ballast were recommended in the absence of test results. These values were determined by regression analysis of available test results in the literature. Comparison between the predicted and available test results showed good agreement and indicated that the improved empirical model can indeed account for the major influencing factors.

CHAPTER 4

NUMERICAL MODELLING OF BALLASTED RAILWAY TRACKS AND PARAMETRIC STUDY

4.1 INTRODUCTION

In recent years, the competition among various traffics in terms of speed, carrying capacity, comfortability, safety and cost has substantially increased the demand for heavier and faster trains. This demand implies foreseeable pressure to construct railway tracks suitable for high speed trains (HSTs) and heavy axle loads (HALs) using innovative technologies. This trend is expected to increase the design demand on railway track foundations. Therefore, a thorough investigation into the impact of various design parameters affecting the overall railway track performance is required. Such investigation is paramount for railway geotechnical engineers to arrive at an optimum plan for both the track design and lifelong maintenance. In this chapter, sophisticated three-dimensional (3D) finite element (FE) modelling is developed as a precursor to understand the dynamic response of ballasted railway tracks subjected to true train moving loads. The FE modelling is validated using field measurement data reported in the literature. A comprehensive parametric study is then carried out to investigate the impact of some important factors on the track performance, including the modulus and thickness of the track foundation layers (namely the ballast, sub-ballast and subgrade) as well as train loading characteristics. Additional FE analyses are carried out to investigate the impact of train speed on the behaviour of ballasted railway track foundations and to evaluate the critical speed (i.e. the train speed at which extraordinary large vibration occurs due to resonance) under various conditions of the train-track-ground system. These conditions include the nonlinearity of track materials; modulus and thickness of the subgrade soil; modulus and thickness of the ballast material; amplitude of train loading; and train geometry. The practical implications of the results obtained on track design are critically analysed and discussed.

4.2 FINITE ELEMENT MODELLING OF RAILWAY TRACK FOUNDATION SYSTEMS

In this thesis, the dynamic response of railway track foundations subjected to train moving loads is simulated via three dimensional (3D) finite element (FE) numerical modelling using the commercial software package Midas-GTS (MIDAS IT. Co. Ltd., 2013). This software is used as it has the provision to simulate the true train moving load. The aim of the numerical modelling performed in the current study is to investigate the dynamic response of railway tracks under various conditions of the train-track-ground system and the obtained results are then used to develop practical design charts as part of the proposed design method for calculating the granular layer thickness needed to provide protection against track failure. Therefore, it is critically prudent to ensure that the FE modelling process is capable of providing reliable outcomes. To this end, initial analyses are performed for two case studies, which are well documented in the literature, to ascertain that the FE modelling can reproduce field observations of compiled measurements obtained from these case studies. Then for the sake of simplicity and ease of simulation, another track with a simplified substructure than that of the case studies is adopted to investigate the track response in a parametric study, as will be seen in the next section.

4.2.1 Case Study 1: Thalys HST Track at a Site near Ath South of Brussels

This selected case study is for a ballasted railway track of the Thalys high speed train (HST) at a site between Brussels and Paris, near Ath, 55 km south of Brussels. This case study is selected because it contains detailed description of all track components and material properties needed for the FE modelling, as well as field measurements of the track and ground vibration parameters in terms of the acceleration of the rail and nearby soil that were measured during the train passage.

4.2.1.1 Track geometry and materials (Thalys HST Track)

The geometry and subgrade profile of the Thalys HST track at the Ath site are shown in Figure 4.1(a) (Degrande and Schillemans, 2001), whereas the corresponding 3D FE model developed to simulate the problem is depicted in Figure 4.1(b), which is composed of layers of ballast and sub-ballast as well as a capping layer founded on

the natural subgrade soil. The FE model dimensions are 80 m, 36 m and 12 m in the longitudinal, horizontal and vertical directions, respectively. The rail is modelled using one-dimensional (1D) I-beam section running across the length of the modelled track. A *UIC*-60 section is assumed for the rail, which is fixed to the sleepers by rail pads characterised by an elastic link (spring-like) element of stiffness equal to 100 MN/m. All other track components (i.e. sleeper, ballast, interface and subgrade) are modelled using 3D solid elements. For model geometry, a total of 133 sleepers are placed along the rail at 0.6 m interval. The rail and sleepers are considered as linear elastic (LE) materials, whereas the ballast and interface layer are modelled using elastoplastic Mohr-Coulomb (MC) materials. Due to the lack of information about the plasticity characteristics of the subgrade soil, it is assumed to be elastic. This assumption is reasonable as the thickness of the granular media (i.e. ballast and sub-ballast) is usually selected so that the level of stress on the track subgrade soil is relatively low; hence, no (or only small) plastic yielding can be developed. The material properties of all track components are summarised in Table 4.1.

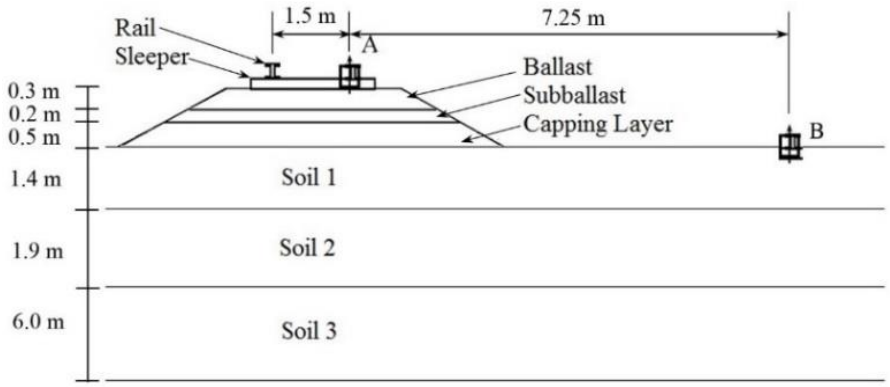

(a)

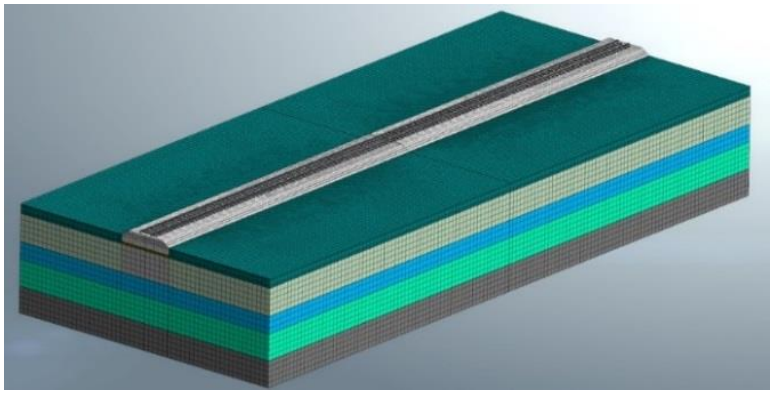

(b)

Figure 4.1: The Thalys HST railway track at the Ath site: (a) track geometry and soil profile (Degrande and Schillemans, 2001); and (b) track FE model.

Table 4.1: Material properties for the case study 1 (Degrande and Schillemans, 2001).

Track Component	Material Property	Value
Rail	Dynamic Modulus of Elasticity, E (MPa)	210,000
	Poisson's Ratio, ν	0.30
	Moment of Inertia, I (m^4)	3.04×10^{-5}
Sleeper	Dynamic Modulus of Elasticity, E (MPa)	30,000
	Poisson's Ratio, ν	0.20
	Unit Weight, γ (kN/m^3)	20.2
	Length, l (m)	2.50
	Width, w (m)	0.27
	Thickness (m)	0.20
Ballast	Dynamic Modulus of Elasticity, E (MPa)	400
	Poisson's Ratio, ν	0.10
	Unit Weight, γ (kN/m^3)	17.7
	Cohesion, c (kPa)	0.00
	Friction Angle, ϕ^o	50.0
	Damping Ratio, ξ	0.02
Subballst	Dynamic Modulus of Elasticity, E (MPa)	300
	Poisson's Ratio, ν	0.20
	Unit Weight, γ (kN/m^3)	21.6
	Cohesion, c (kPa)	0.00
	Friction Angle, ϕ^o	40.0
	Damping Ratio, ξ	0.02
Capping Layer	Dynamic Modulus of Elasticity, E (MPa)	200
	Poisson's Ratio, ν	0.20
	Unit Weight, γ (kN/m^3)	21.6
	Cohesion, c (kPa)	0.00
	Friction Angle, ϕ^o	36.0
	Damping Ratio, ξ	0.02
Soil 1	Dynamic Modulus of Elasticity, E (MPa)	48.0
	Poisson's Ratio, ν	0.30
	Unit Weight, γ (kN/m^3)	18.2
	Shear Wave Velocity, C_s (m/s)	100
	Damping Ratio, ξ	0.03
Soil 2	Dynamic Modulus of Elasticity, E (MPa)	85.0
	Poisson's Ratio, ν	0.30
	Unit Weight, γ (kN/m^3)	18.2
	Shear Wave Velocity, C_s (m/s)	133
	Damping Ratio, ξ	0.03
Soil 3	Dynamic Modulus of Elasticity, E (MPa)	250
	Poisson's Ratio, ν	0.30
	Unit Weight, γ (kN/m^3)	18.2
	Shear Wave Velocity, C_s (m/s)	266
	Damping Ratio, ξ	0.03

4.2.1.2 FE mesh and boundary conditions (Thalys HST Track)

In dynamic analysis, the finite element size, model boundaries and time step have to be selected carefully to ensure accuracy of the results (Galavi and Brinkgreve, 2014). In the current study, the element size of the FE model is generally estimated based on the smallest wavelength that allows the high frequency motion to be simulated correctly. Accordingly, the sizes of the 3D finite elements are taken as: 0.167 m × 0.137 m × 0.2 m; 0.2 m × 0.2 m × 0.2 m; and 0.6 m × 0.6 m × 0.6 m for the sleepers, ballast and subgrade, respectively. Overall, the mesh of the FE model is consisted of 285,000 elements. The model vertical boundaries are connected to viscous dampers to absorb the incident *S*- and *P*- waves and to represent infinite boundary conditions, as suggested by many researchers (Kouroussis et al., 2011a; Lysmer and Kuhlemeyer, 1969). The nodes at the bottom boundary are set to be fixed in every direction to simulate bedrock. The material damping of the FE model is characterised by the mass and stiffness proportional coefficients, normally referred to as the Rayleigh damping, which is commonly used in nonlinear dynamic analyses. The generalised equation for the Rayleigh damping is as follows:

$$[C]=\alpha[M]+\beta[K] \tag{4.1}$$

where, [*C*] is the damping matrix; [*M*] is the mass matrix; and [*K*] is the stiffness matrix. The parameters α and β are the mass and stiffness proportional damping coefficients, respectively. These damping coefficients are frequency-dependent and can be computed using the following equations (Chowdhury and Dasgupta, 2003):

$$\alpha=\frac{2\omega_i\omega_j(\xi_i.\omega_j-\xi_j.\omega_i)}{\omega_j^{\,2}-\omega_i^{\,2}} \tag{4.2}$$

$$\beta=\frac{2(\xi_j.\omega_j-\xi_i.\omega_i)}{\omega_j^{\,2}-\omega_i^{\,2}} \tag{4.3}$$

where, ω_i and ω_j are the natural frequency of mode-1 and mode-2 of the full model, respectively, for which the effective modal mass participation factors are high in the loading direction; and ξ_i and ξ_j are the hysteretic material damping ratios in the frequency range of interest (see Table 4.1). It should be noted that the natural

frequency mode of the FE model is obtained by an eigenvalue analysis considering the subgrade reaction at the boundary of the layered material mesh using Midas-GTS software.

4.2.1.3 Simulation of train moving loads (Thalys HST Track)

In the current study, the train moving loads are modelled in accordance with Araújo (2011) in which the rail FE nodes, which are rigidly connected to the sleepers via pads, are subjected to a wheel load (denoted as *loading nodes*) whose value changes in time. As schematically shown in Figure 4.2, the train moving loads can be thought of as triangular pulses distributed among three nodes. The wheel load, *P*, at one certain *loading node*, *N*+1, increases once the wheel leaves node *N*, reaching a peak value when the wheel is directly above node *N*+1, then finally decreasing back to zero when the wheel reaches the next node *N*+2. As a result, the triangular pulse moves from one node to another by a time interval equal to the spacing of the loading nodes divided by the speed, *C*, of the moving loads. For example, for a train speed of 30 m/s (108 km/h), the wheel point load will pass the distance between two consecutive *loading nodes* (note that the spacing between any two *loading nodes* is 0.6 m) in 0.02 sec. This way, a series of train wheels will be moving along the track. It should be noted that all FE analyses in the current study are performed in the time domain, which is more natural to reproduce the transient phenomenon of wave propagation (Kouroussis et al., 2009).

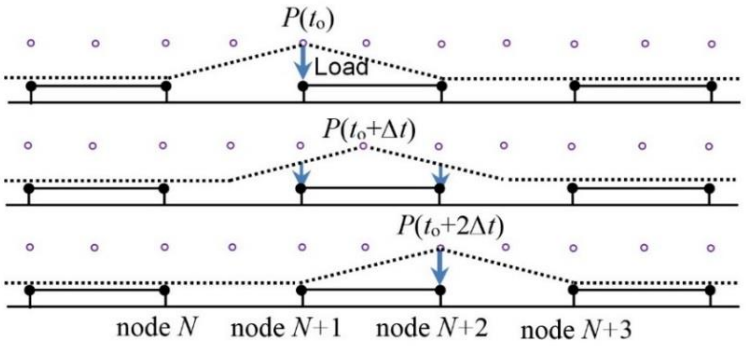

Figure 4.2: Simulation of moving loads (Araújo, 2011).

It should also be noted that during the simulation of the moving loads, the time step is chosen based on the well-known Courant-Friedrichs-Lewy condition, which is mathematically represented as follows (Galavi and Brinkgreve, 2014):

$$C_n = \frac{\Delta t \times C}{L_{\min}} \leq 1 \tag{4.4}$$

where, C_n is called the Courant number, Δt is the time step, C is the train speed and L_{min} is the distance between two adjacent *loading nodes*.

4.2.1.4 Model Validation (Thalys HST Track)

To validate the FE model described above for the Thalys HST, the vibration made (i.e. the time history response of the track) during the passage of train at 87.2 m/s (314 km/h) is predicted at two observation points and the results are compared with field measurements reported by Cunha and Correia (2012). One point of measurements is located at the sleeper, next to the rail (i.e. Point A), and the other point is located on the ground at a horizontal distance equal to 7.25 m from the rail (i.e. Point B), as shown earlier in Figure 4.1(a). The geometry of the Thalys HST is shown in Figure 4.3 and its characteristics including the carriage length (L_c), distance between two bogies (L_b), distance between axles (L_a) and wheel load (P) of each carriage are summarised in Table 4.2.

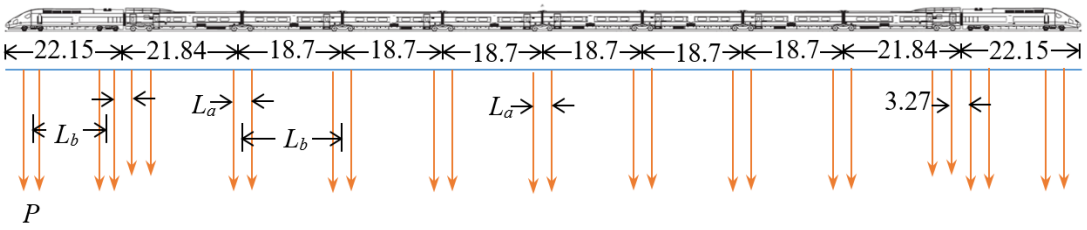

Figure 4.3: Geometry of Thalys HST (Degrande and Schillemans 2001).

Table 4.2: Geometry and load characteristics of Thalys HST (Cunha and Correia, 2012).

Carriage Name	Carriage Number	Axles per Carriage	Spacing			*P* (kN)
			L_a (m)	L_b (m)	L_c (m)	
Locomotive	2	4	3.00	14.00	22.15	84.0
Side Carriage	2	3	3.00	18.70	21.84	71.5
Central Carriage	6	2	3.00	18.70	18.70	84.0

Figure 4.4 shows a comparison between the FE predicted values and field measurements for the vertical acceleration during the train passage at observation points A and B. It should be noted that the field measurements contain some peak vertical acceleration values that are higher than the others and this is explained by Cunha and Correia (2012). Irrespective of this, it can be seen that the developed FE model predicts the track response with appreciative accuracy and agrees well with the field measurements.

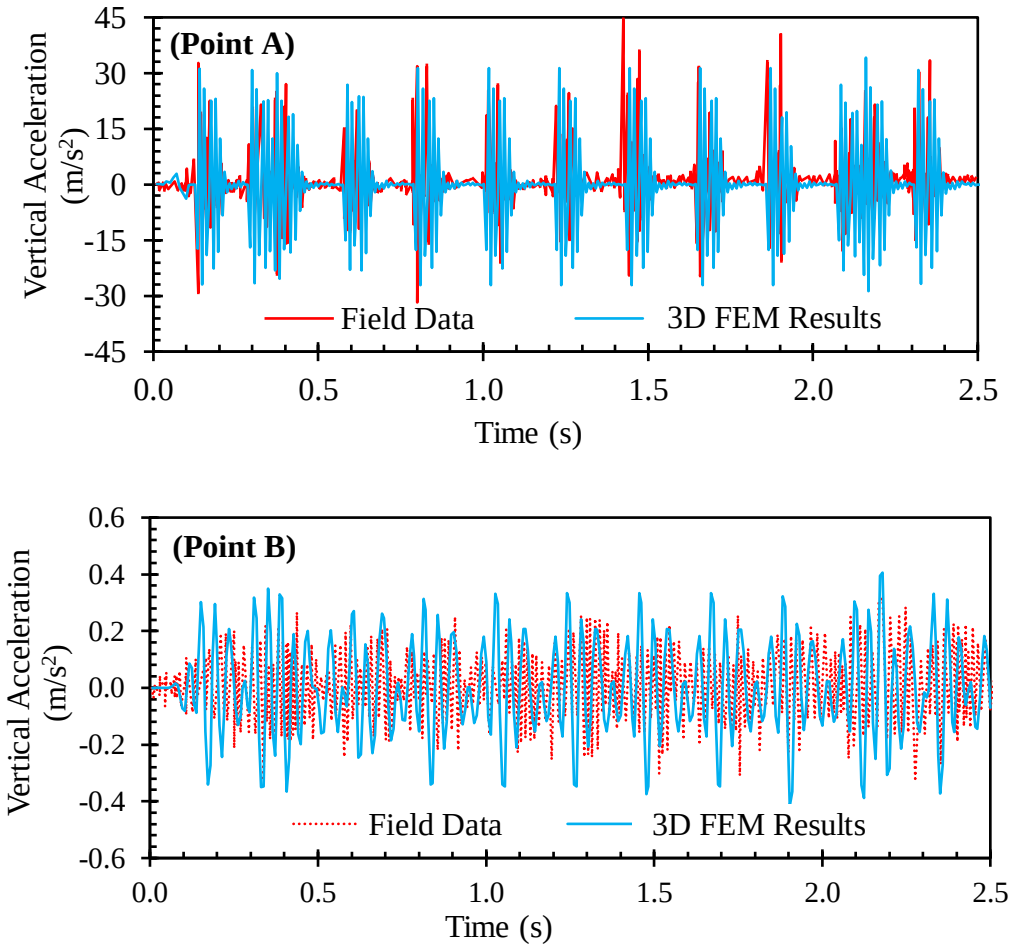

Figure 4.4: Comparison of FE predicted versus field measured responses.

4.2.2 Case Study 2: X-2000 HST Track at the Ledsgard Site

This case study is for a ballasted railway track of the X-2000 HST at Ledsgard site just outside Göteborg (Hall, 2003). Again, the motivation for selecting this case study arose from the fact that detailed description of all needed parameters for the FE modelling are readily available in the literature, including the track material

properties, train loading characteristics and field measurements of track vibration in terms of deflection under various train speeds.

4.2.2.1 Track geometry and materials (X-2000 HST Track)

The geometry and subgrade profile of the X-2000 HST railway track at the Ledsgard site are shown in Figure 4.5(a) (Hall, 2003), while the 3D FE model developed to simulate the track response is depicted in Figure 4.5(b). Here, the model dimensions considered and modelling of track superstructure components (e.g. rail, rail pads and sleepers) are the same as discussed in Section 4.2.1.1 (i.e. case study 1). However, in this model, the subgrade soils (Figure 4.5a) are characterised by nonlinear materials in which the nonlinearity is taken into account via an equivalent linear material in accordance with the approach described by Madshus and Kaynia (1999). The properties of all materials considered in the model are summarised in Table 4.3.

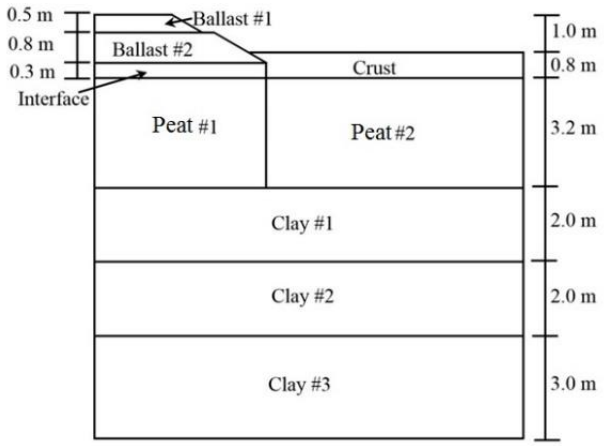

(a)

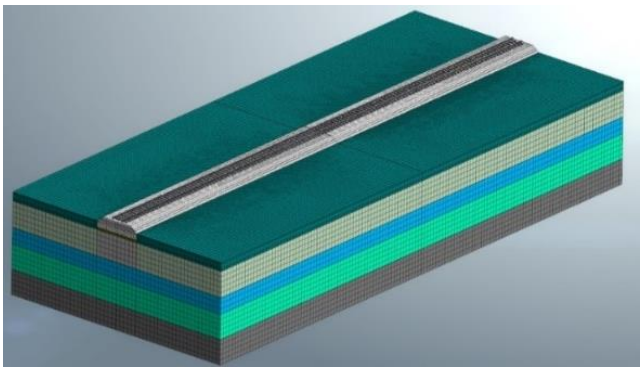

(b)

Figure 4.5: The X-2000 HST railway track at the Ledsgard site: (a) track geometry and soil profile (Hall, 2000); and (b) track FE model.

Table 4.3: Properties of the X-2000 HST track at the Ledsgard site (Hall, 2000).

Track Component	Material Property	Value
Ballast #1 & Ballast #2	Dynamic Modulus of Elasticity, E (MPa)	134
	Poissons Ratio, ν	0.30
	Unit Weight, γ (kN/m^3)	18.6
	Cohesion, c (kPa)	0.00
	Friction Angle, ϕ^o	50.0
	Shear Wave Velocity, C_s (m/s)	165
	Damping Ratio, ξ	0.03
Interface	Dynamic Modulus of Elasticity, E (MPa)	10.0
	Poissons Ratio, ν	0.48
	Unit Weight, γ (kN/m^3)	16.7
	Cohesion, c (kPa)	0.00
	Friction Angle, ϕ^o	30.0
	Shear Wave Velocity, C_s (m/s)	45.0
	Damping Ratio, ξ	0.06
Crust	Dynamic Modulus of Elasticity, E (MPa)	18.0
	Poissons Ratio, ν	0.48
	Unit Weight, γ (kN/m^3)	16.7
	Shear Wave Velocity, C_s (m/s)	60.0
	Damping Ratio, ξ	0.06
Peat #1	Dynamic Modulus of Elasticity, E (MPa)	2.55
	Poissons Ratio, ν	0.49
	Unit Weight, γ (kN/m^3)	12.4
	Shear Wave Velocity, C_s (m/s)	26.0
	Damping Ratio, ξ	0.06
Peat #2	Dynamic Modulus of Elasticity, E (MPa)	7.30
	Poissons Ratio, ν	0.49
	Unit Weight, γ (kN/m^3)	12.4
	Shear Wave Velocity, C_s (m/s)	44.0
Clay #1	Dynamic Modulus of Elasticity, E (MPa)	10.5
	Poissons Ratio, ν	0.49
	Unit Weight, γ (kN/m^3)	14.2
	Shear Wave Velocity, C_s (m/s)	49.0
	Damping Ratio, ξ	0.09
Clay #2	Dynamic Modulus of Elasticity, E (MPa)	13.6
	Poissons Ratio, ν	0.49
	Unit Weight, γ (kN/m^3)	14.2
	Shear Wave Velocity, C_s (m/s)	56.0
	Damping Ratio, ξ	0.09
Clay #3	Dynamic Modulus of Elasticity, E (MPa)	25.3
	Poissons Ratio, ν	0.49
	Unit Weight, γ (kN/m^3)	14.7
	Shear Wave Velocity, C_s (m/s)	75.0
	Damping Ratio, ξ	0.09

4.2.2.2 Simulation of train moving loads (X-2000 HST Track)

In this case study, the approach of simulating the moving loads is the same as that described earlier in Section 4.2.1.3; however, the dynamic responses are simulated herein by considering the loading characteristics of the X-2000 HST. The train geometry and standard axle loads of the X-2000 HST used in the FE modelling are summarised in Table 4.4, which includes (for each car number) the distance between the axles (L_a), distance between two bogies (L_b), carriage length (L_c), front wheel load (P_F) and rear wheel load (P_R). Figure 4.6 shows a schematic diagram of the X-2000 HST showing its components.

Table 4.4: Geometry and axle loads of the X-2000 HST (Takemiya, 2003).

Car Number, *n*	Spacing			Standard Wheel Load	
	L_a (m)	L_b (m)	L_c (m)	P_F (kN)	P_R (kN)
1	2.9	14.5	22.2	81.0	61.3
2	2.9	17.7	24.4	61.3	61.3
3	2.9	17.7	24.4	61.3	61.3
4	2.9	17.7	24.4	61.3	61.3
5	2.9	9.5	17.2	90.0	90.0

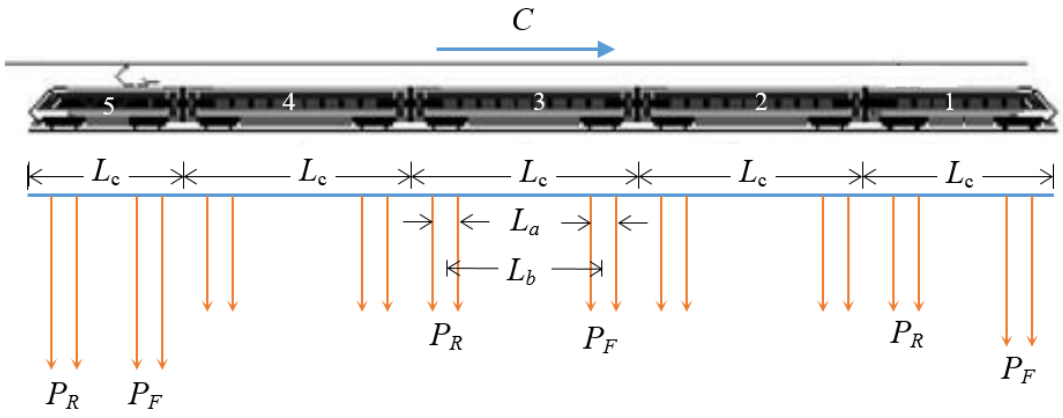

Figure 4.6: Geometry of the X-2000 HST (Takemiya, 2003).

4.2.2.3 Model Validation (X-2000 HST Track)

To validate the FE modelling of the X-2000 HST railway track set out above, the time-history responses of the sleeper deflection during the passage of train at three

different speeds (i.e. 70 km/h, 200 km/h and 252 km/h) are calculated at the centre of the track. The results are then compared with the corresponding field measurements (for train speeds of 70 km/h and 200 km/h) as well as simulation response reported by Kaynia et al. (2000) (for train speed of 252 km/h), as shown in Figure 4.7 (note that the upward deflections are represented by positive values whereas the downward deflections are represented by positive values). It can be seen that when the train loads move over the points of concern for the low speed of 70 km/h (Figure 4.7a), only quasi-static deflections (i.e. downward movements) appear. In contrast, an oscillatory response [see Figure 4.7(b & c)] occurs at higher speeds of 200 km/h and 252 km/h. For all train speeds, however, it is clearly shown that the FE predictions agree reasonably well with the field measurements and published simulated response.

As an additional validation tool, the vertical track deflections are reproduced in the frequency domain, using the Fourier transformation via the software MATLAB, and the results of this exercise are judged against the frequency domain deflections obtained from the field measurements, as shown in Figure 4.8. It can be clearly seen that good agreement exists between the FE predictions and field measurements, for both the low speeds (Figure 4.8a) and high speeds [Figure 4.8(b & c)]. The overall agreement between the FE numerical modelling and measured deflections confirms that the FE modelling process adopted in this study is reliable and can be used with confidence to predict the railway track behaviour, for both the quasi-static and dynamic loading conditions.

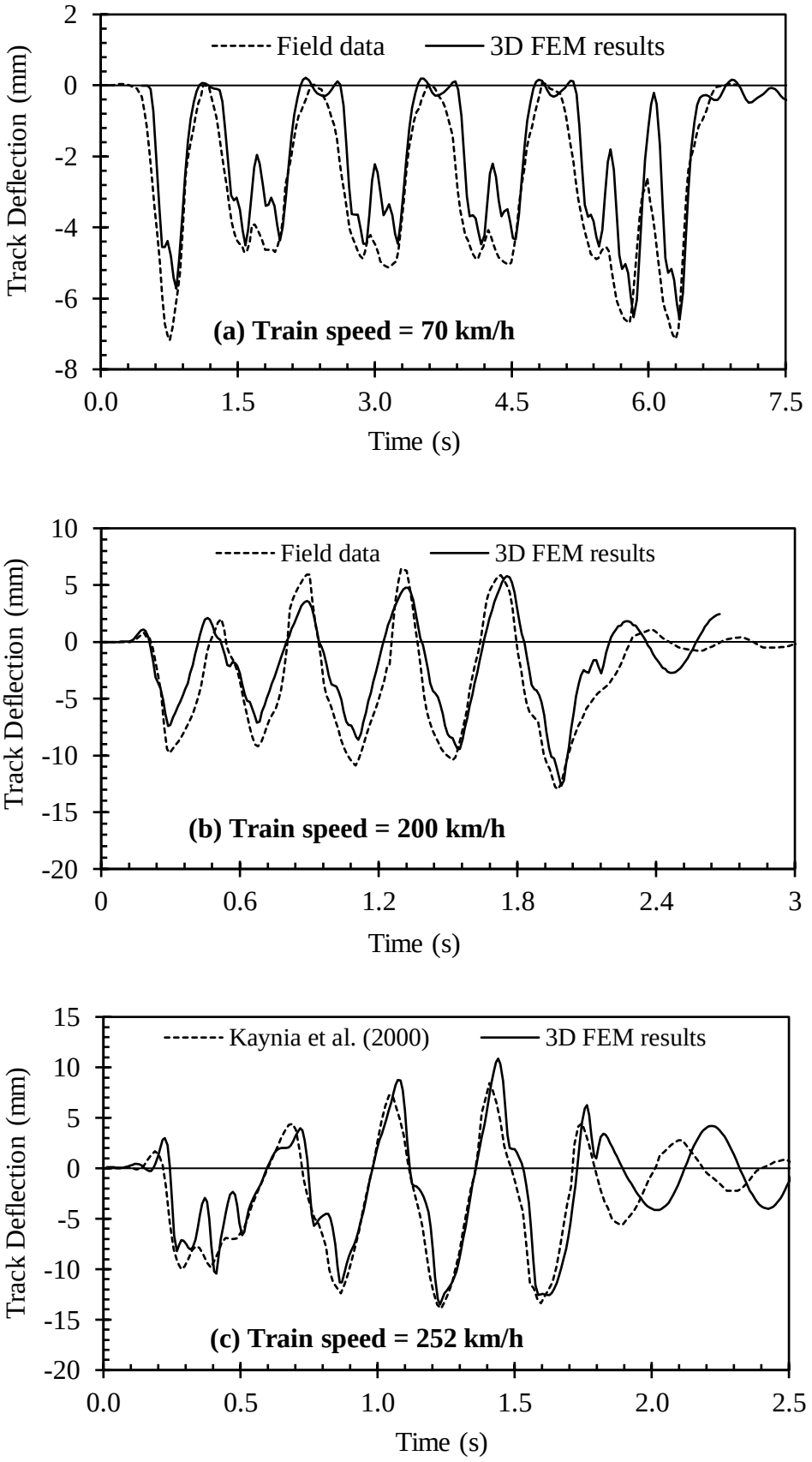

Figure 4.7: Comparison between FE predicted versus field measured deflection responses at the track centre for: (a) train speed of 70 km/h; (b) train speed of 200 km/h; and (c) train speed of 252 km/h.

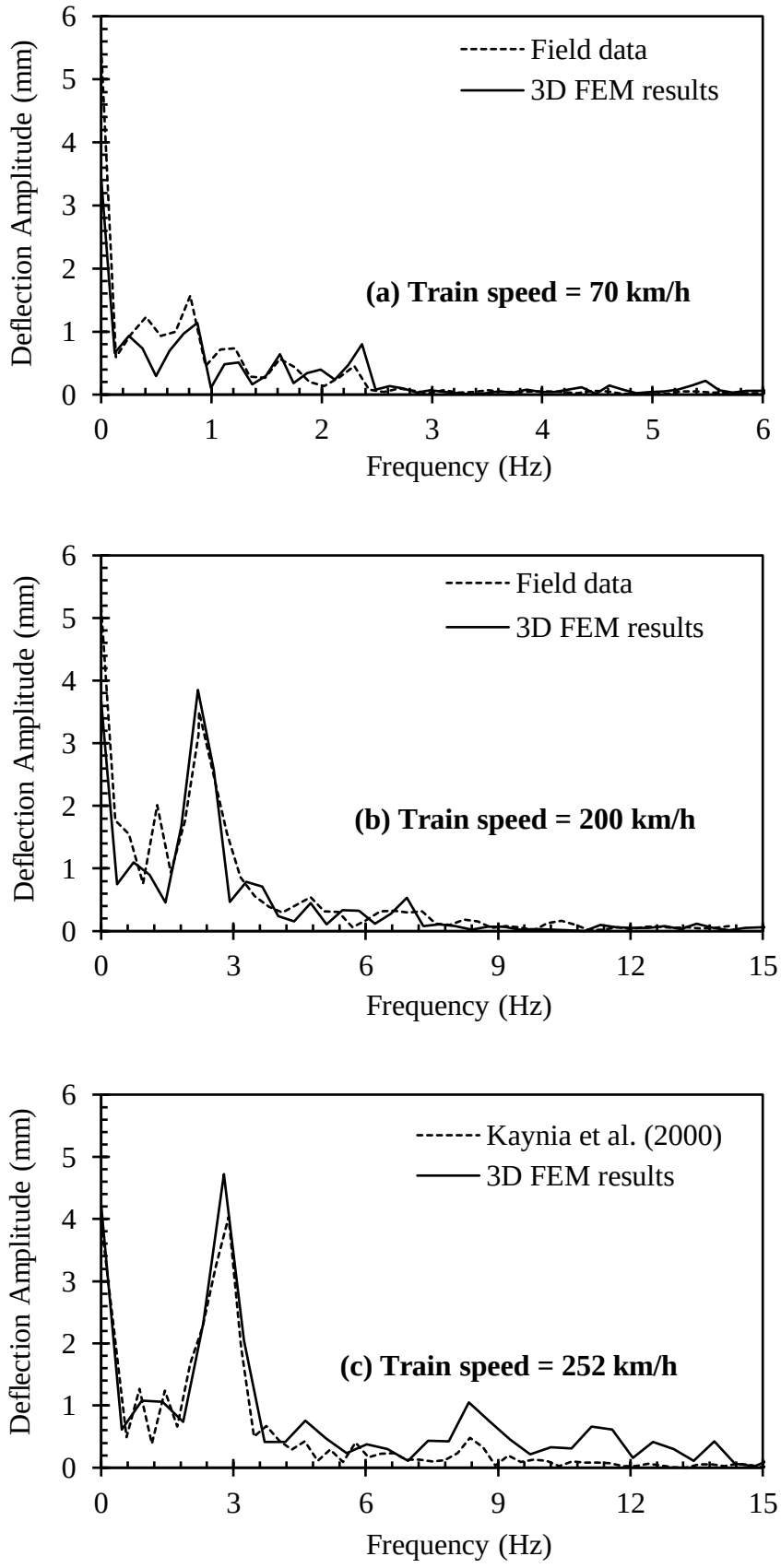

Figure 4.8: Comparison between FE predicted versus field measured deflection responses based on frequency domain at the track centre for: (a) train speed of 70 km/h; (b) train speed of 200 km/h; and (c) train speed of 252 km/h.

4.3 PARAMETRIC STUDY

Several parametric studies on the railway track response over a wide range of track parameters have been reported in the literature by a number of researchers (e.g. Kennedy Jr and Prause, 1979; Li, 1994; Shahin and Indraratna, 2006; Shahu et al., 1999; Stewart, 1982). However, all previous studies addressed unrealistic dynamic situations, thus reported overgeneralised static solutions. Therefore, a comprehensive study on the track responses using the developed 3D FE model subjected to realistic train moving loads is given in this section.

4.3.1 Impact of Track-ground Parameters

In the current parametric study, a FE model similar to that developed earlier for the X-2000 HST is used, but with a simpler substructure profile (see Figure 4.9) that consists of a combined layer of ballast and sub-ballast of 0.45 m founded on a single subgrade layer of 7.5 m, overlying a hard rock. This model is designated as the "nominal model" and will be used as a bench mark for the basis of comparison. The values of different track components are varied in accordance with the practical range and the corresponding track behaviour is compared with respect to the nominal model. The material properties of the nominal model are summarised in Table 4.5, while Table 4.6 shows the range of variables considered in the parametric study. When the impact of a certain parameter is investigated within the range shown in Table 4.6, the other parameters are considered to be constant at their nominal values given in Table 4.5. It should be noted that the values in Tables 4.5 and 4.6 are based on similar values reported in the literature (e.g. Shahu et al., 1999; Stewart, 1982).

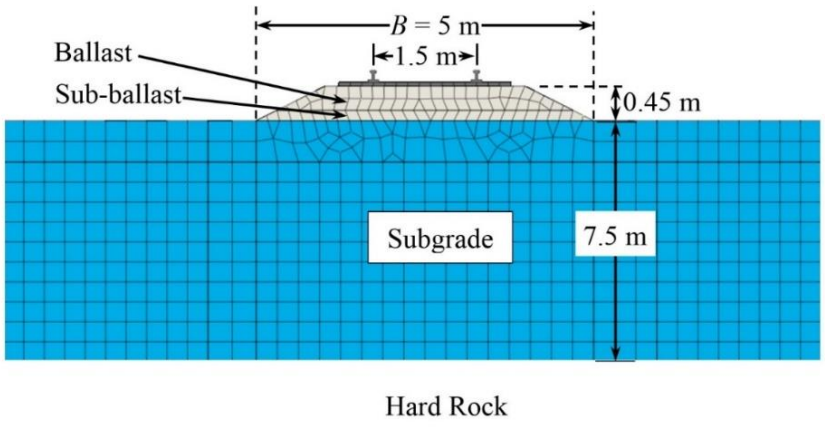

Figure 4.9: Track geometry of the nominal (base case) model.

In this section, the track response corresponding to each of the parameters given in Table 4.6 is investigated in terms of the rail deflection; surface vertical stresses of ballast, sub-ballast and subgrade; surface strain of subgrade; and track stiffness. The observed track response is based on the X-2000 HST moving along the track at a speed of 30 m/s (108 km/h), and the results are shown in Figure 4.10. It should be noted that the horizontal line in each graph of Figure 4.10 represents the track response for the nominal model, as defined by the properties given in Table 4.5, whereas the vertical lines represent the upper and lower ranges of predicted track response for the values of the parameters given in Table 4.6. The numbers inside each graph represent the upper and lower bounds of the parameters considered.

Table 4.5: Substructure material properties of the nominal model.

Track Component	Material Property	Value
Ballast	Dynamic Modulus of Elasticity, E (MPa)	270
	Poissons Ratio, ν	0.30
	Unit Weight, γ (kN/m^3)	17.3
	Cohesion, c (kPa)	0.00
	Friction Angle, ϕ^o	50.0
	Thickness, H (m)	0.30
	Shear Wave Velocity, C_s (m/s)	243
	Damping Ratio, ξ	0.03
Subballst	Dynamic Modulus of Elasticity, E (MPa)	135
	Poissons Ratio, ν	0.35
	Unit Weight, γ (kN/m^3)	21.6
	Cohesion, c (kPa)	0.00
	Friction Angle, ϕ^o	40.0
	Thickness, H (m)	0.15
	Shear Wave Velocity, C_s (m/s)	151
	Damping Ratio, ξ	0.03
Subgrade Soil	Dynamic Modulus of Elasticity, E (MPa)	60.0
	Poissons Ratio, ν	0.35
	Unit Weight, γ (kN/m^3)	18.8
	Thickness, H (m)	7.50
	Shear Wave Velocity, C_s (m/s)	108
	Raleigh Wave Velocity, C_R (m/s)	101
	Damping Ratio, ξ	0.03

Table 4.6: Range of variable track properties used for the parametric study.

Parameter	Lower Bound	Nominal	Upper Bound
Ballast Modulus, E_b (MPa)	135	270	540
Sub-ballast Modulus, E_{sb} (MPa)	80	135	270
Subgrade Soil Modulus, E_s (MPa)	15	60	120
Ballast Thickness, H_b (m)	0.15	0.30	1.20
Sub-ballast Thickness, H_{sb} (m)	0.10	0.15	0.60
Subgrade Thickness, H_s (m)	1.50	7.50	15.00

Figure 4.10(a) shows that the subgrade modulus is the most significant factor affecting the rail deflection. A decrease in the subgrade modulus leads to a dramatic increase in the rail deflection, and similar trend is observed when the modulus and thickness of ballast and sub-ballast are decreased, although their impacts are insignificant. In contrast, a decrease in the subgrade thickness results in a decrease in the rail deflection. Figure 4.10(b) depicts that the ballast modulus and subgrade modulus are found to have the most significant impact on the ballast surface vertical stress. An increase in the ballast modulus causes an increase in the ballast surface vertical stress, while a decrease in the subgrade modulus leads to an increase in the ballast surface vertical stress.

The track response with respect to the sub-ballast and subgrade surface vertical stresses are almost identical, as shown in Figure 4.10(c) & (d) in which the subgrade modulus and thicknesses of ballast and sub-ballast are found to be the most influential factors affecting the track performance. An increase in the subgrade modulus leads to an increase in the sub-ballast and subgrade surface vertical stresses. On the other hand, an increase in the ballast depth causes a reduction in the sub-ballast and subgrade surface vertical stresses. The sub-ballast thickness increases its own surface vertical stress; however, it reduces the stress on the subgrade soil. In Figure 4.10(e), it is evident that the subgrade modulus and ballast depth are the most significant factors influencing the subgrade surface strain. With the increase of these two parameters, the subgrade surface strain reduces dramatically.

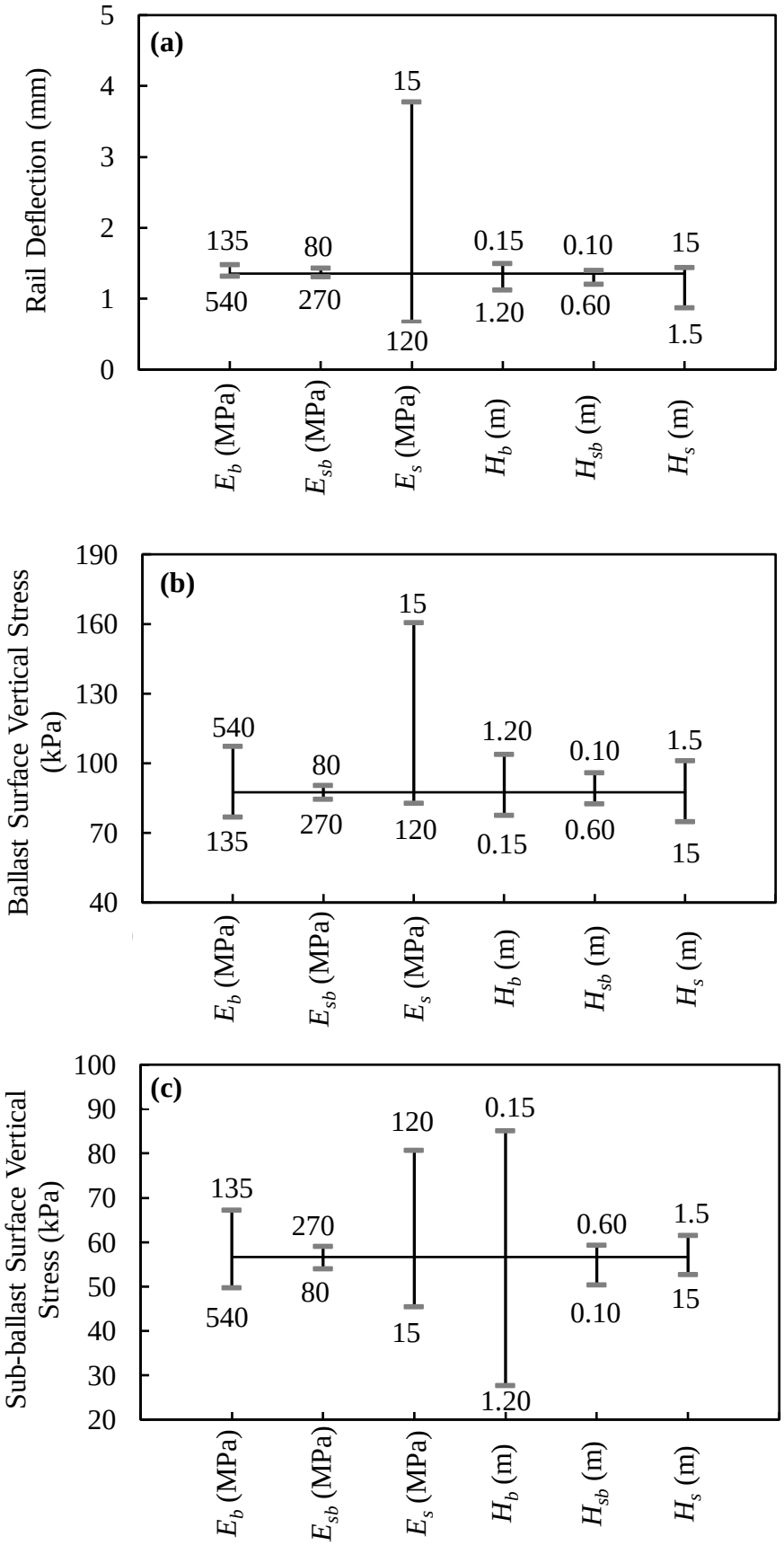

Figure 4.10(a-c): Effect of track influencing parameters on track performance (continued next page).

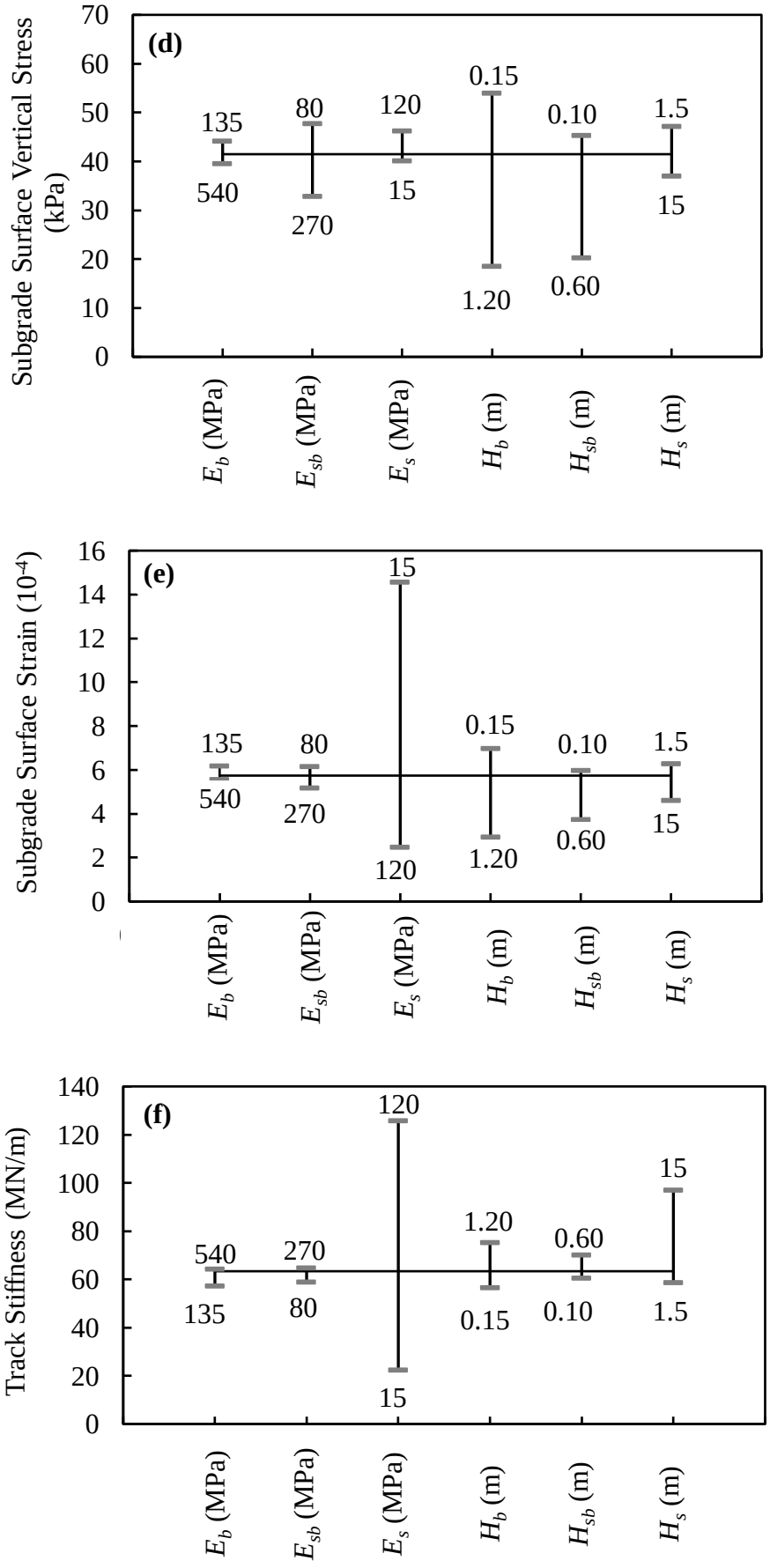

Figure 4.10(d-f): Effect of track influencing parameters on track performance.

Finally, the track performance is measured by a parameter called "track stiffness", which is defined as the force that causes a unit vertical deflection of the track (Selig and Li 1994). Figure 4.10(f) confirms that the most dominating factor influencing the track stiffness is the subgrade modulus. It can be seen that an eight-fold increase in the subgrade modulus from 15 MPa to 120 MPa leads to an increase in the track stiffness of approximately five times. It can also be seen that the depth of the ballast layer plays an important role in increasing the ballasted track stiffness, whereas a decreases in the subgrade thickness leads to an increase in the track stiffness. Overall, it is clearly evident from Figure 4.10 that the subgrade modulus has the greatest influence on the track response.

4.3.2 Impact of Train Loading Characteristics

In this section, the impact of train loading characteristics on the track deflection response is investigated. For this purpose, the FE model for the X-2000 HST with the nominal properties given in Table 4.5 is used unless otherwise specified. In order to investigate the influence of the amplitude of the train moving loads on the track deflection, six different percentages (50%, 75%, 100%, 125% and 150%) of the standard wheel loading of the X-2000 HST is used. The standard wheel loading are considered to be equivalent to the axle loads that are given in Table 4.4. The impact of different percentages of the wheel loading on the track deflection for the nominal model (case) is presented in Figure 4.11. It can be seen that the track deflection increases proportionally with the increase of the percentage of the wheel loading as one would expected.

Similarly, to investigate the impact of the wheel spacing, six different values of the wheel spacing (i.e. L_a = 1.6 m, 1.8 m, 2.2 m, 2.6 m, 3.0 m and 3.4 m) is considered in the X-2000 HST. It should be noted that the values of the wheel spacing considered herein are based on similar values reported in the literature (e.g. Hall, 2003; Jeffs and Tew, 1991; Kouroussis et al., 2011b). The effect of varying the wheel spacing on the track deflection for the nominal model is presented in Figure 4.12. It can be seen that the track deflection increases with the decrease in the wheel spacing, as expected.

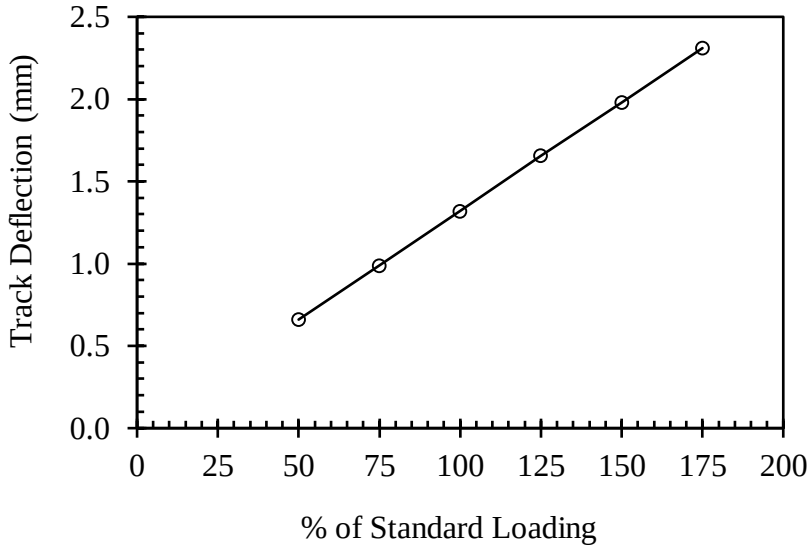

Figure 4.11: Relationship between track deflection and loading amplitude for the nominal model except those specified.

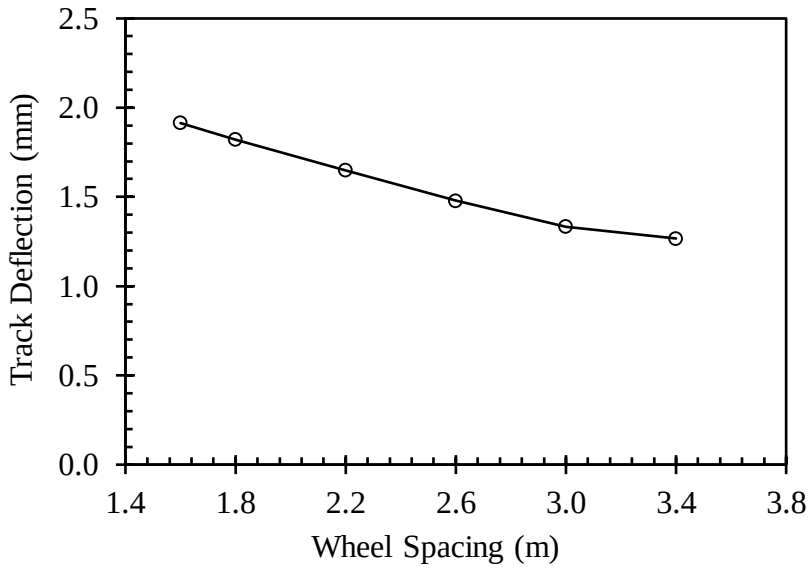

Figure 4.12: Relationship between track deflection and wheel spacing for the nominal model.

Furthermore, to quantify the impact of the wheel spacing so as to be used in the proposed design method that will be described later in Chapter 5, a relationship between the wheel spacing and wheel spacing factor (WSF) are developed and presented in Figure 4.13. The WSF is defined as the ratio of the track deflection at particular wheel spacing to the track deflection for the standard wheel spacing of the X-2000 HST. It can be seen from Figure 4.13 that the effect of wheel spacing can be reduced significantly by increasing the spacing between the train wheels.

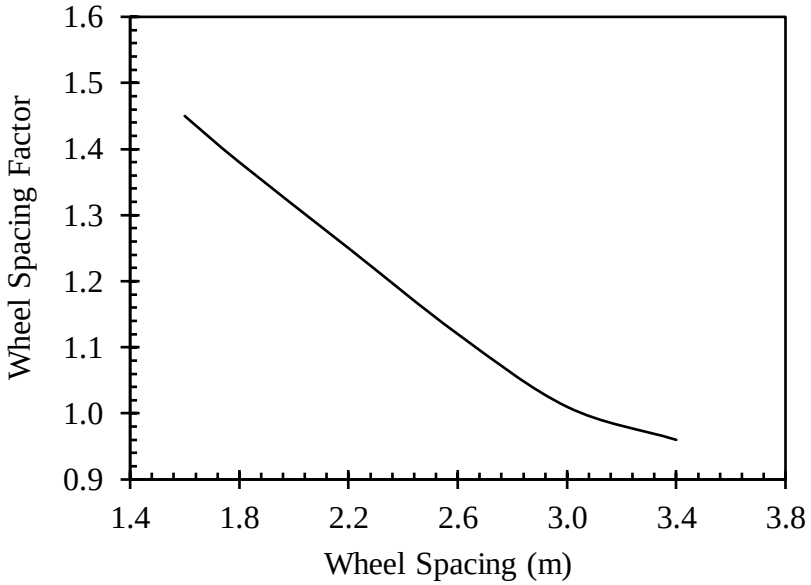

Figure 4.13: Effect of wheel spacing with respect to standard wheel spacing of the X-2000 HST.

4.4 INVESTIGATION INTO THE IMPACT OF TRAIN SPEED

The development of railway networks for high speed trains (HST) is rapidly growing in many countries around the world, as a sustainable solution for increasing the demand of faster transportation. For instance, the Japanese railways authority has constructed the *Shinkansen* HST network of 4,072 km long for trains running at a speed of 320 km/h. Recently, using the magnetic levitation technology, the Japanese bullet train broke the world train speed record in a test conducted in 2015 for a train running at a blazing speed of 603 km/h (Wener-Fligner, 2015). On the other hand, China has the world largest HST network, which is about 16,000 km long, and the Chinese railway authority expects that the train speed in China will increase to up to 400 km/h in the foreseeable future. As train speeds continue to increase, new challenges and problems relating to the performance of railway foundations may arise, primarily due to the significant amplification effects of the train-track-ground vibration (Priest and Powrie, 2009; Wanming et al., 2010). The train-induced ground vibration is dictated mostly by the relationship between the train speed and the corresponding propagating wave velocity of the ground medium. The train speed at which the dynamic response of railway track and surrounding ground are intensely amplified and extraordinary large vibration occurs due to resonance is called the "critical speed" (Krylov, 1994; Madshus and Kaynia, 1999; Yang et al., 2009).

The tremendous increase of the vibration level associated with the critical speed is not only a possible source of detrimental environmental effect and human disturbance, but can also increase the risk of several train operation issues. Such issues include the train safety, degradation/deformation of track foundations, fatigue failure of rails and interruption of the power supply to trains (Madshus and Kaynia, 2000). Therefore, an investigation into the behaviour of ballasted railway track under different train speeds becomes a key research issue, for both avoiding the track resonance and reducing the associated possible vibrations.

The problem associated with soil vibrations due to the dynamic response of moving loads on a surface of an elastic medium has been a subject of research based on a theoretical basis (Dieterman and Metrikine, 1996, 1997; Lamb, 1904). However, failure in operating the X-2000 passenger HST at the Ledsgard site of the West Coast Line between Goteborg and Malmo brought the problem of the impact of high speed trains to the attention of engineering communities. Subsequently, several formulations including analytical approaches (Degrande and Schillemans, 2001; Dieterman and Metrikine, 1997; Sheng et al., 2004), boundary element (BE) modelling (Andersen and Nielsen, 2003), FE modelling (Banimahd et al., 2013; El Kacimi et al., 2013; Hall, 2003), and 2.5D FE-BE modelling (Adam et al., 2000; Bian et al., 2014; Galvín et al., 2010; O'Brien and Rizos, 2005) were proposed for the prediction of train-induced ground vibrations. However, to investigate the effect of train speed on track behaviour and performance, most available studies considered a single cyclic or moving point (or surface) load rather than true (dynamic) train moving loads. The assumption of a single cyclic or moving point load is highly questionable, as the amount of dynamic amplification and critical speed depend on the wavelength of the site and distance between the axles and bogies of the car, thus, the role of frequency comes into an effect (Madshus and Kaynia, 2000). Therefore, the actual train geometry and magnitude of individual axle load need to be accounted for in the analysis of effect of train speed, which will be the case in the current presented work.

In the following sections, the dynamic response of the train-track-ground system subjected to train moving loads at different speeds, namely the critical speed, subcritical speed (i.e. speed less than the critical speed) and supercritical speed (i.e.

speed higher than the critical speed) is investigated. In addition, various conditions of the train-track-ground system affecting the critical speed are examined, including the nonlinearity of track material, modulus and thickness of track subgrade soil, modulus and thickness of ballast materials, amplitude of train loading and train geometry. The obtained results are synthesised into simple sensitivity charts from which the critical speed under various conditions of the train-track-ground system can be readily obtained.

4.4.1 Influence of Train Speed

In order to investigate the effect of train speed on the train-track-ground system, the nominal model of the X-2000 HST (Figure 4.9) is used herein. The sleeper downward and upward deflections versus train speed are depicted in Figure 4.14. It can be seen that the sleeper deflection generally increases with the increase in the train speed, reaching its maximum value at the critical speed, before it decreases with further increase in the train speed. As can be seen, the critical speed is found to be higher than both the Rayleigh wave and shear wave velocities of the subgrade soil overlying the hard rock (the critical speed ≈ 175 m/s versus C_R = 101 m/s and C_s = 108 m/s of the subgrade soil). This result suggests that the critical speed is not always equal to the Rayleigh wave velocity of the top subgrade medium as sometimes thought, and this can be attributed to the existence of the bottom hard rock layer. This behaviour confirms a good consistency (in the qualitative sense) with the results reported by Alves Costa et al. (2015).

It can also be seen from Figure 4.14 that the effect of train speed on the sleeper upward and downward deflections is negligible for train speeds lower than 30% of the critical speed, whilst the dynamic effects commence after that level. However, it can be observed that the sleeper deflection increases sharply when the train speed exceeds around 75% of the critical speed and maintains the same trend until it reaches the critical speed. Therefore, based on the above results, a train speed equivalent to about 75% of the critical speed may be assumed as the practical speed limit for ballasted railway tracks.

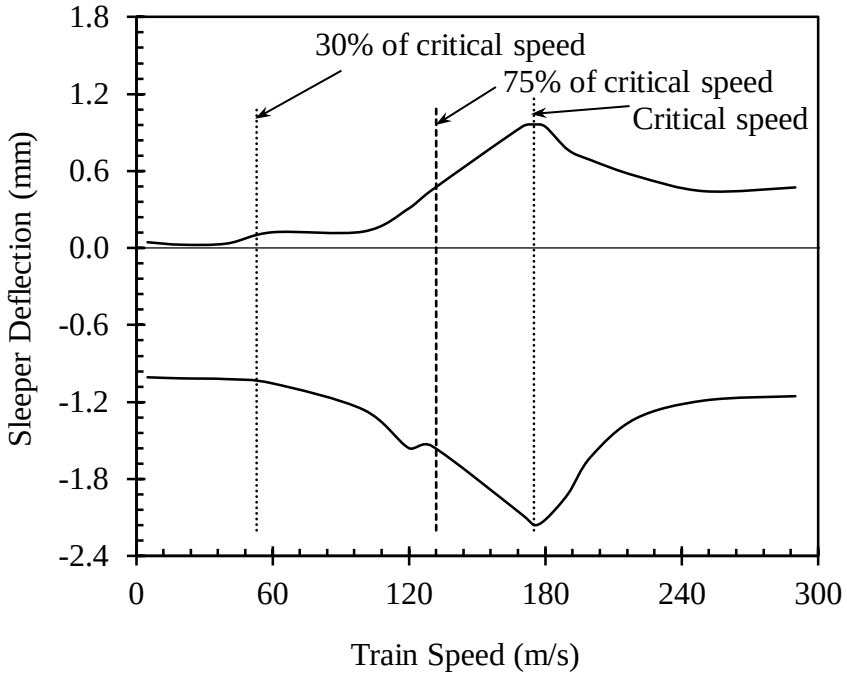

Figure 4.14: Effect of train speed on sleeper deflection.

In Figure 4.15, the time-history of the sleeper deflection response is presented for three typical speeds, including the subcritical speed (100 m/s), critical speed (175 m/s) and supercritical speed (250 m/s). To compare the dynamic response of the railway track to these three selected train speeds, they are all plotted along a common space axis, converted from the time axis, *t*, through multiplication by the train speed, *C*. It can be seen from Figure 4.15 that larger sleeper deflections occur at the train critical speed (175 m/s) than at the other two train speeds (100 m/s and 250 m/s). It can also be seen that for the subcritical train speed (100 m/s), the peaks of the sleeper deflections appear at the moment of passage of the respective axle load of the point under consideration. However, for higher train speeds (i.e. critical and supercritical speed), the contribution of the four axle loads (adjacent two bogies) superimposes to give rise to almost one predominant peak, and the track oscillates after the train passage. This behaviour agrees well with previous published simulated response carried out by Kaynia et al. (2000).

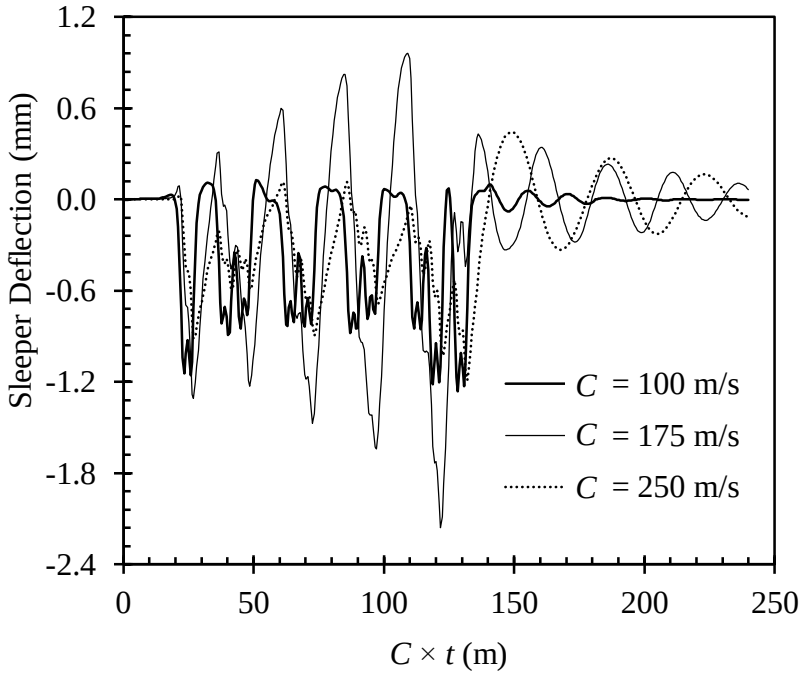

Figure 4.15: Time-history dynamic response of sleeper deflection for different train speeds.

For illustration purpose of the impact of the critical speed on the railway track as compared to the lower speed (i.e. subcritical speed), contour plots of the obtained vertical deflections along the track are depicted in Figure 4.16 at the subcritical speed and critical speed. It can be seen from Figure 4.16(a) that at train subcritical speed of 50 m/s, the vertical deflection is mainly induced near the axle positions, and there is a slight propagation of wave to the surrounding ground, as expected. On the contrary, it can be seen from Figure 4.16(b) that at the critical speed of 175 m/s, the vertical deflection is not only induced near the axle positions but also in the surrounding ground. It can also be seen that a series of wave fronts radiate from the load positions showing a shockwave in the ground, which is known as the "Mach cone"; this phenomenon is similar to the case of sonic boom normally associated with supersonic aircraft (Krylov, 2001). The above results confirm that the FE modelling is trustworthy and can be used with confidence to predict the railway track behaviour at the critical and at other speeds.

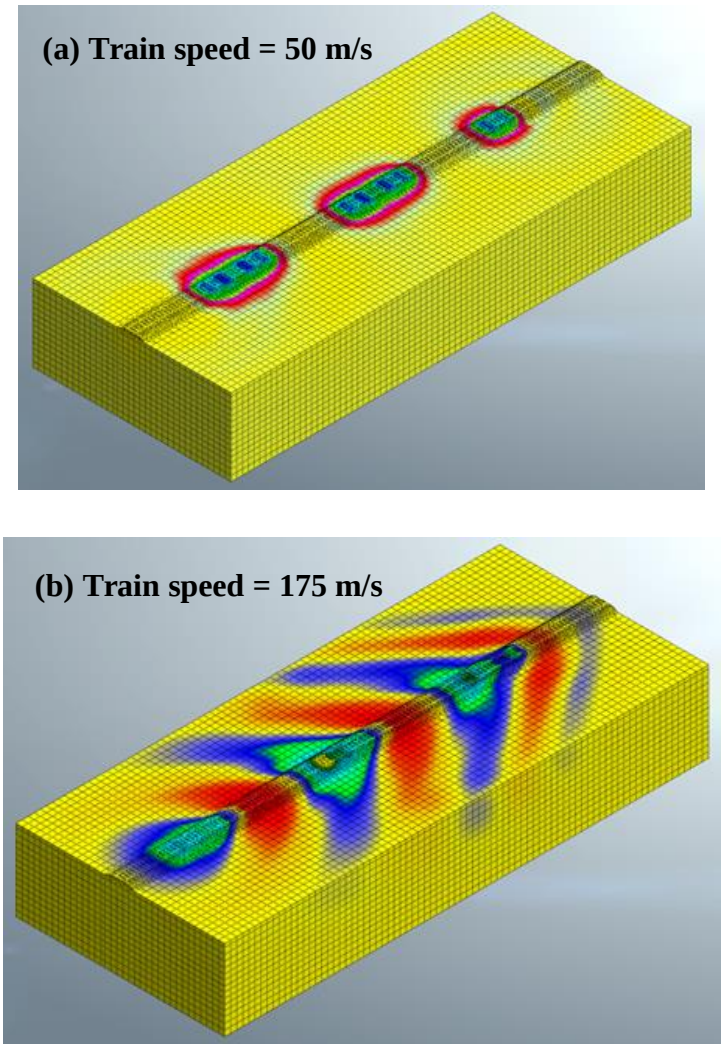

Figure 4.16: Typical contour plots of vertical track deflection for: (a) train speed of 50 m/s; and (b) train speed of 175 m/s.

Figure 4.17 presents the ground vibrations in terms of the vertical displacement of the ground surface measured from the track centre to the neighbouring ground, for the three different train speeds considered above. It can be seen that the critical speed (175 m/s) provides the highest amplitude of ground vibrations compared to the subcritical speed (100 m/s) and supercritical speed (250 m/s). It can also be seen that, for any train speed, the peaks of ground vibrations occur at the track centre and reduces away from it, as would be expected. In addition, it can be observed that the zone from the track centre until about 8 m away experiences a considerable level of ground vibrations for all train speeds, particularly for the critical speed, which could be detrimental for train operation and may also be a possible source of failure for the neighbouring structures.

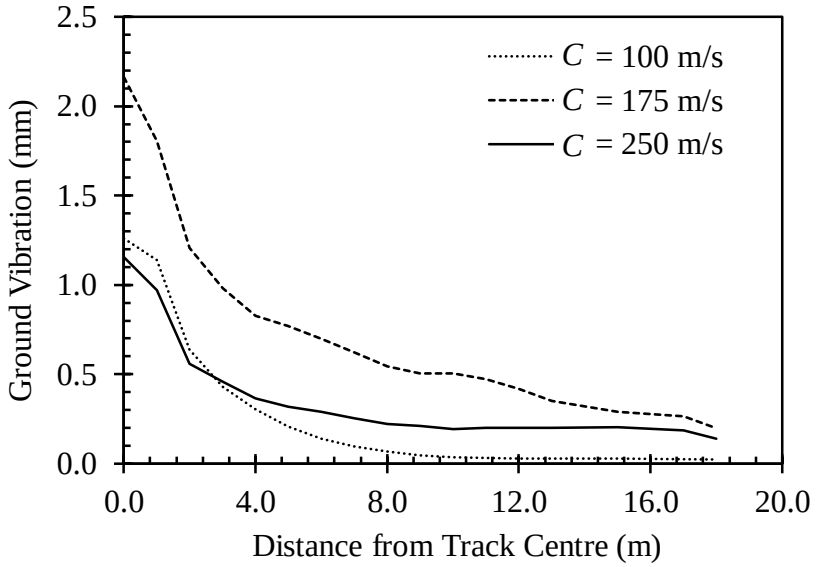

Figure 4.17: Variation of ground vibration in terms of vertical displacement from the track centre at different train speeds.

4.4.2 Factors Affecting Critical Speed of Train-Track-Ground System

As mentioned earlier, when the train speed reaches the critical speed for the train-track-ground system, large vibrations occur, leading to possible track failure, train derailment and damages to the neighbouring structures. To avoid such undesirable scenario, an investigation into the influence of various factors of the train-track-ground system on the critical speed is essential for railway geotechnical engineers, which are presented in some detail next. These factors include the stiffness and thickness of track subgrade, stiffness and thickness of ballast, and amplitude and geometry of train moving loads. For this purpose, the FE model of the X-2000 HST using the nominal properties given in Table 4.5 is utilised unless otherwise specified.

4.4.2.1 Effect of nonlinearity of track materials

The impact of the nonlinearity of track materials on the critical speed is investigated separately for two different subgrades: one with soft soil (i.e. fat clay of the Monroe dam) and the other with stiff soil (i.e. low density sand). Each type of the subgrade soil is modelled for two different scenarios (i.e. linear and nonlinear). In the first scenario, the subgrade soil (i.e. clay or sand) and ballast are represented by a linear elastic materials, whereas in the second scenario the subgrade soil is modelled using the hyperbolic Duncan-Chang (DC) constitutive model (Duncan and Chang, 1970) whilst the ballast is simulated by the elastoplastic Mohr-Coulomb (MC) model.

Accordingly, a total of four models are considered; a summary of which is presented in Table 4.7 and the properties of the two different subgrade used are summarised in Table 4.8. It should be noted that the ballast properties of this model is the same as that used in the nominal model described earlier, whereas the subgrade used is assumed to be the fat clay of the Monroe dam and its properties are obtained from Duncan et al. (1980). On the other hand, the sand subgrade properties are obtained from Al-Shayea et al. (2003). These materials are assumed to be typical of soft and stiff subgrades.

Table 4.7: Material constitutive model used to investigate the impact of nonlinearity of track materials on the critical speed.

Railway Track model	**Subgrade Type**	**Material Model**	
		Ballast	**Subgrade**
Model-1	Soft (Fat clay)	LE	LE
Model-2	Soft (Fat clay)	MC	DC
Model-3	Stiff (Low density sand)	LE	LE
Model-4	Stiff (Low density sand)	MC	DC

Table 4.8: Properties used to investigate the impact of nonlinearity of track materials on the critical speed.

Material Type	γ (kN/m^3)	**Elastic Properties**		**Plastic Properties**		**DC Nonlinearity Properties**			**Dynamic Properties**	
		E (MPa)	ν	c (kPa)	ϕ^o	K	n	R_f	C_s (m/s)	C_R (m/s)
Ballast	17.3	270	0.30	0.0	50	–	–	–	243	225
Soft Subgrade	15.4	6.9	0.38	67.6	0.0	65	0.14	0.77	40	37
Stiff Subgrade	15.6	58.5	0.35	0.0	38	586	1.07	0.90	117	109

Note: γ is unit weight; E is dynamic Young's modulus; ν is Poisson's ratio; c is cohesion; ϕ is the friction angle; K and n is modulus number and modulus exponent, respectively; R_f is failure ration; C_s and C_R are the shear and Rayleigh wave velocity, respectively.

Figure 4.18 shows the sleeper downward and upward deflections versus the train speed, for both subgrades used (i.e. Figure 4.18a for soft subgrade and Figure 4.18b for stiff subgrade). It can be seen that the upward movement profile is insensitive to

the subgrade nonlinearity. In general, the subgrade nonlinearity resulted in higher downward movement than that of the linear subgrade; however, the difference is relatively small in the case of stiff subgrade compared to soft subgrade, which is obvious as soft materials usually show higher nonlinearity than stiff materials. Fortunately, the difference in the magnitude of the critical speed between the linear and nonlinear subgrade tracks is almost negligible, for both the soft and stiff subgrades. Consequently, it is decided that the remaining part of the current study will be conducted only on linear track materials.

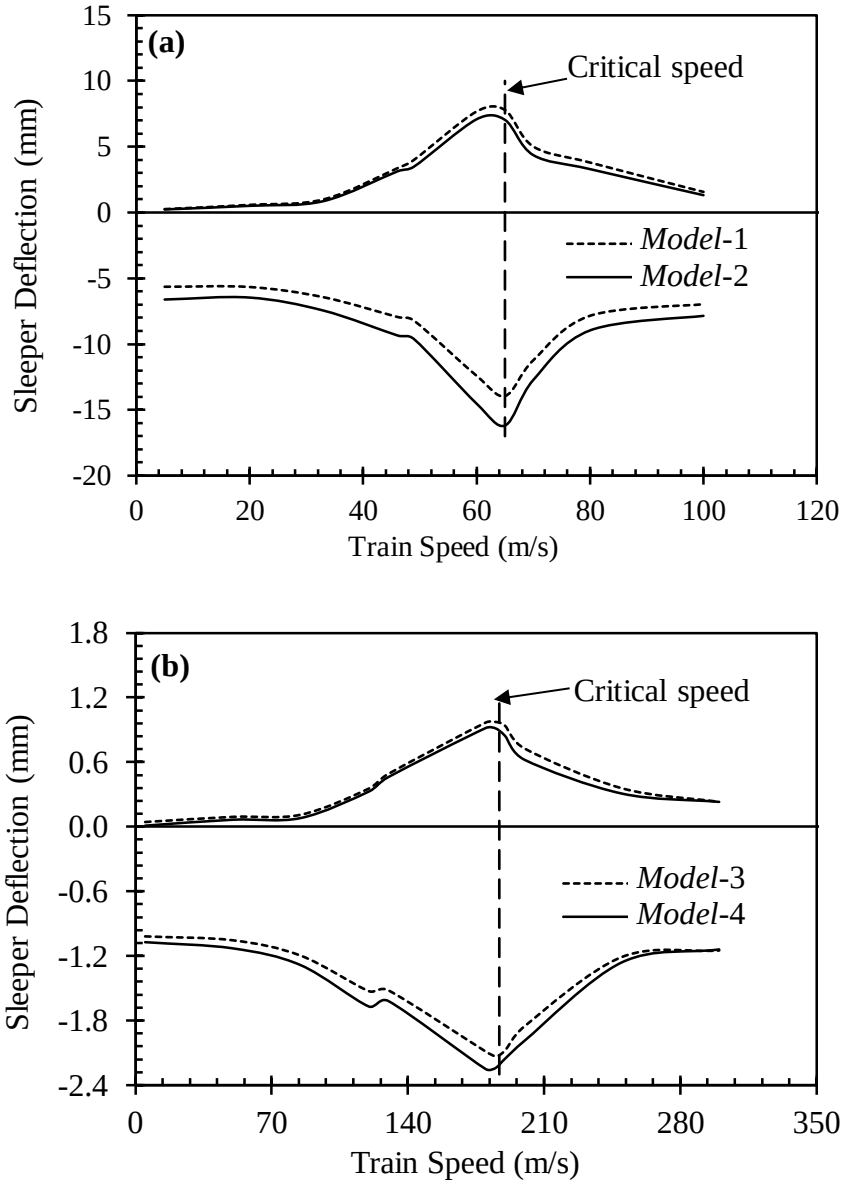

Figure 4.18: Evolution of sleeper deflection versus train speed for: (a) soft subgrade (*Model* 1 versus *Model* 2); and (b) stiff subgrade (*Model* 3 versus *Model* 4), to investigate the impact of nonlinearity of track materials on the critical speed.

4.4.2.2 Stiffness and thickness of track subgrade

Because the wave propagation velocity of any soil medium is highly dependent on its stiffness and thicknesses (Alves Costa et al., 2015), the effect of the subgrade stiffness (or soil modulus), E_s, and thickness, H_s, on the critical speed of train operation is investigated herein. It is well known that the influence of the critical speed is more significant for reduced subgrade stiffness, which means that railway tracks built on soft subgrade usually yield high ground vibrations at low train speed than those founded on stiff subgrade. To investigate the impact of the track subgrade stiffness, five different values of the subgrade modulus are considered (i.e. E_s = 15 MPa, 30 MPa, 60 MPa, 90 MPa and 120 MPa). Similarly, the impact of the track subgrade thickness is investigated for four different track subgrade thicknesses (i.e. H_s = 5 m, 7.5 m, 10 m and ∞ m) overlying a hard rock.

The impact of the track subgrade stiffness and thickness is presented in Figure 4.19, in terms of the relationship between the train speed and dynamic amplification factor (DAF). The DAF is defined as the ratio of the maximum dynamic sleeper deflection at a particular train speed to the maximum quasi-static sleeper deflection (i.e. sleeper deflection at a nominal train speed of 5 m/s). It can be seen from Figure 4.19 that, for all values of E_s and H_s, the DAF increases with the increase of the train speed until it reaches a peak value corresponding to the critical speed, after which it decreases with further increase in the train speed. Figure 4.19(a) shows that, while the critical speed increases with the increase in the track subgrade stiffness, the DAF exhibits an opposite effect. The practical implication of this finding is that the localised ground improvement to spots of the soft soil along the rail track can be very beneficial in increasing the critical speed of trains.

Figure 4.19(b) shows that the magnitude of the critical speed and DAF increases with the decrease in the track subgrade thickness. It can also be seen that the critical speed determined for each subgrade thickness is higher than the Rayleigh wave and shear wave velocities of the top subgrade soil overlying the hard rock, except when $H_s = \infty$. This result is consistent with the finding reported by Alves Costa et al. (2015). Note that details of the evolution of dynamic amplification factor of sleeper downward deflection versus train speed for different subgrade stiffnesses and thicknesses are presented in *Apendix A*.

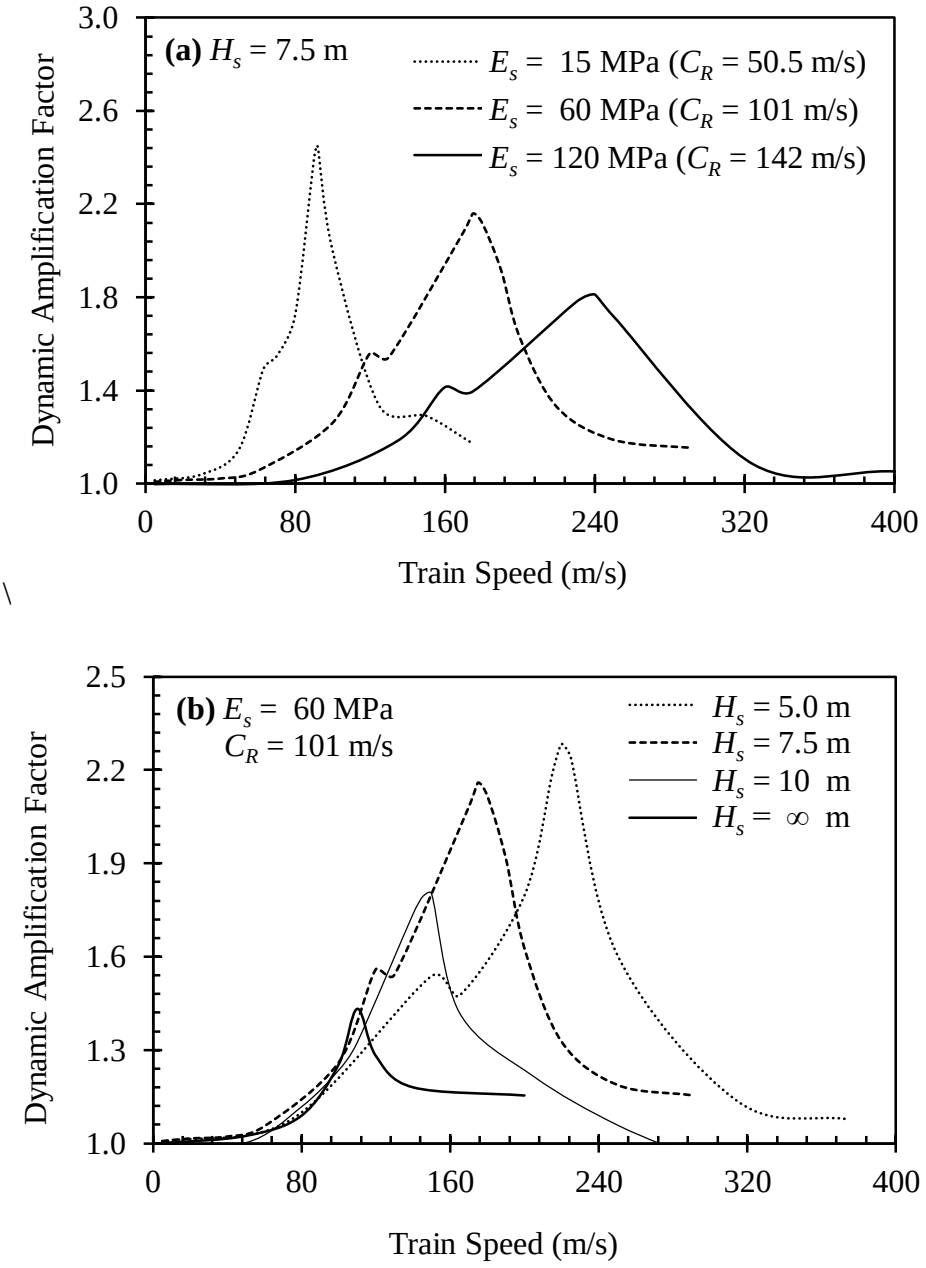

Figure 4.19: Evolution of dynamic amplification factor for sleeper downward deflection versus train speed, for different: (a) subgrade stiffnesses; and (b) subgrade thicknesses.

4.4.2.3 Stiffness and thickness of ballast layer

To investigate the influence of ballast stiffness on the critical speed, three different values of ballast modulus (i.e. E_b = 150 MPa, 300 MPa and 500 MPa) are considered. Besides, the influence of ballast thickness is investigated by considering three different ballast thicknesses (i.e. H_b = 0.35 m, 0.60 m and 0.90 m). The relationships between the DAF of sleeper deflection and train speed for the different values of ballast stiffness and thickness are shown in Figure 4.20. It can be seen that the

evolution of the DAF of sleeper deflection with the train speed and critical speed are not affected by the ballast stiffness or thickness, which is in contrast to the impact of track subgrade stiffness and thickness, as presented earlier in Figure 4.19. This can be attributed to the limited width of the ballast layer compared with the infinite width of the track subgrade, and this prevents the ballast layer to contribute to the increase of the Rayleigh wave of the train-track-ground system; hence, its impact on the critical speed is negligible.

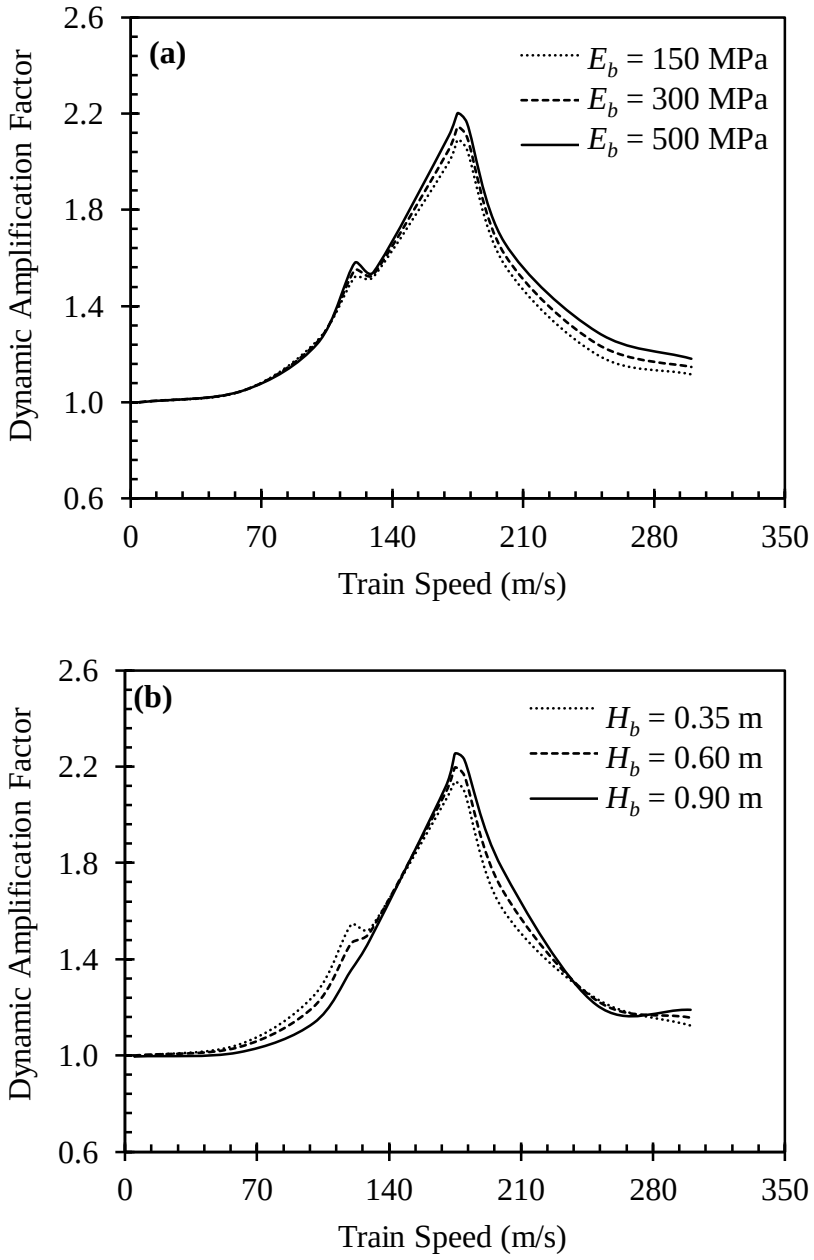

Figure 4.20: Evolution of dynamic amplification factor of sleeper downward deflection versus train speed, for different: (a) ballast stiffnesses; and (b) ballast thicknesses.

4.4.2.4 Amplitude of train moving loads

The influence of the amplitude of train moving loads on the critical speed is investigated using three different loading values denoted herein as *standard*, *light* and *heavy*. The standard loading is considered to be equivalent to the axle load given in Table 4.4, whereas the light loading is considered to be 75% of the standard loading and the heavy loading is taken as 125% of the standard loading. The relationships between the sleeper deflection and train speed for the three considered loading amplitudes are shown in Figure 4.21. As predicted, it can be seen that the sleeper deflection increases with the increase in the train loading amplitude for all train speeds. On the other hand, it can also be seen that the critical speed is almost the same regardless of the train loading amplitude, indicating that the critical speed is independent of the magnitude of train loading.

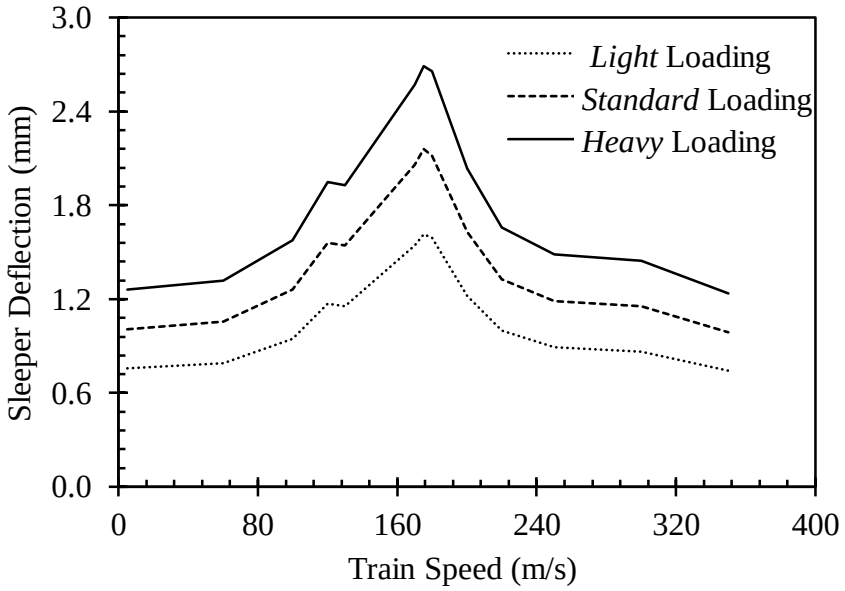

Figure 4.21: Evaluation of sleeper downward deflection versus train speeds for different amplitudes of loading.

4.4.2.5 Effect of geometry of train loading

The effect of the geometry of train loading regime on the critical speed is important for railway transport authorities, since it can guide to the choice of a suitable train for a particular track-ground condition. In this part, the influence of geometry of train loading regime on the critical speed is investigated by considering two trains of different loading geometries, i.e. the X-2000 HST (see Figure 4.6) and Thalys HST

(see Figure 4.3). The geometry and loading characteristics of the X-2000 HST and Thalys HST are previously given in Tables 4.4 and 4.2, respectively. Again, the track of the X-2000 HST with the nominal properties given in Table 4.5 is used in this study. The results are shown in Figure 4.22 in terms of the evolution of the DAF of sleeper deflection with the train speed. It can be seen that both the maximum DAF and corresponding critical speed for the two trains are different. The critical speed obtained for the X-2000 HST and Thalys HST are found to be equal to 175 m/s and 134 m/s, respectively, implying that the critical speed is actually affected by the geometry of train loading.

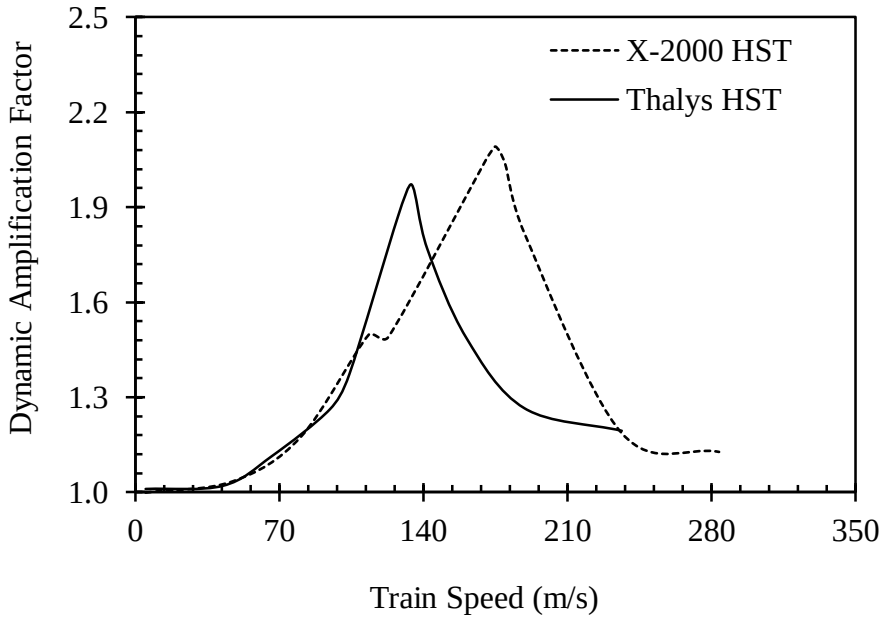

Figure 4.22: Evolution of dynamic amplification factor (DAF) of sleeper downward deflection with train speed for two trains of different geometry.

4.4.3 Development of Sensitivity Charts for Calculation of Critical Speed

It is now useful to synthesise the results of the current study into suitable formulations that can be used in practice to determine the critical speed for any train. As concluded in the preceding section, the critical speed is affected by the train loading geometry. Therefore, the results of the study are manipulated to develop a relationship that allows calculation of the critical speed for any train with respect to the critical speed of the X-2000 HST. However, before developing such a relationship, the discussion presented below is deemed necessary.

Figure 4.23 shows the distance-history of sleeper deflection at the centre of track for the X-2000 HST and Thalys HST, for the same track-ground condition (i.e. nominal model). In this figure, the distance in the *x-axis* coordinate is calculated by multiplying the critical speed (C_{cr}) of each individual train by the corresponding time of the train passage. In Figure 4.23(a), each deflection peak represents the deflection generated for the X-2000 HST due to the overlap of the induced stresses of four wheels of two consecutive bogies. The distance between any two peaks for the X-2000 HST would be equal to the carriage length, L_c, defined earlier or the distance of the centre-to-centre of two consecutive sets of four wheels. So, the load application frequency or the carriage passing frequency (f_c) at the critical speed of the X-2000 HST can be computed by dividing the train critical speed by the carriage length, L_c; hence, f_c for the X-2000 HST would be equal to 7.2 Hz (i.e. 175 m/s divided by 24.4 m), which is equivalent to the natural frequency of the track-ground system. On the other hand, each deflection peak for the Thalys HST (Figure 4.23b) represents the deflection generated due to the overlap of the induced stresses of only two wheels of one bogie. Thereby, the distance between any two peaks for the Thalys HST would be equal to the carriage length, L_c, or the distance of the centre-to-centre of two consecutive bogies, L_b. Accordingly, f_c for the Thalys HST would be equal to 7.2 Hz (i.e. 134 m/s divided by 18.7 m), which is also equivalent to the natural frequency of the track-ground system.

The above results show that at the critical speed condition, the load application (or carriage passing) frequency of trains is usually equal to the natural frequency, f_n, of the track-ground system. This conclusion can be mathematically expressed as follows:

$$f_n = f_{c(any\ particular\ train)} = f_{c(X-2000HST)} = f_{c(ThalysHST)} \tag{4.5}$$

By correlating f_c of any other particular train, i.e. $f_{c(any\ particular\ train)}$, with respect to $f_{c(X\text{-}2000\ HST)}$ or $f_{c(Thalys\ HST)}$ and by replacing it with its corresponding critical speed and carriage length, Equation (4.5) can be rewritten as follows:

$$\frac{C_{cr(particular train)}}{L_{particular train}} = \frac{C_{cr(X-2000HST)}}{L_{X-2000HST}} = \frac{C_{cr(Thalys\ HST)}}{L_{Thalys\ HST}} \tag{4.6}$$

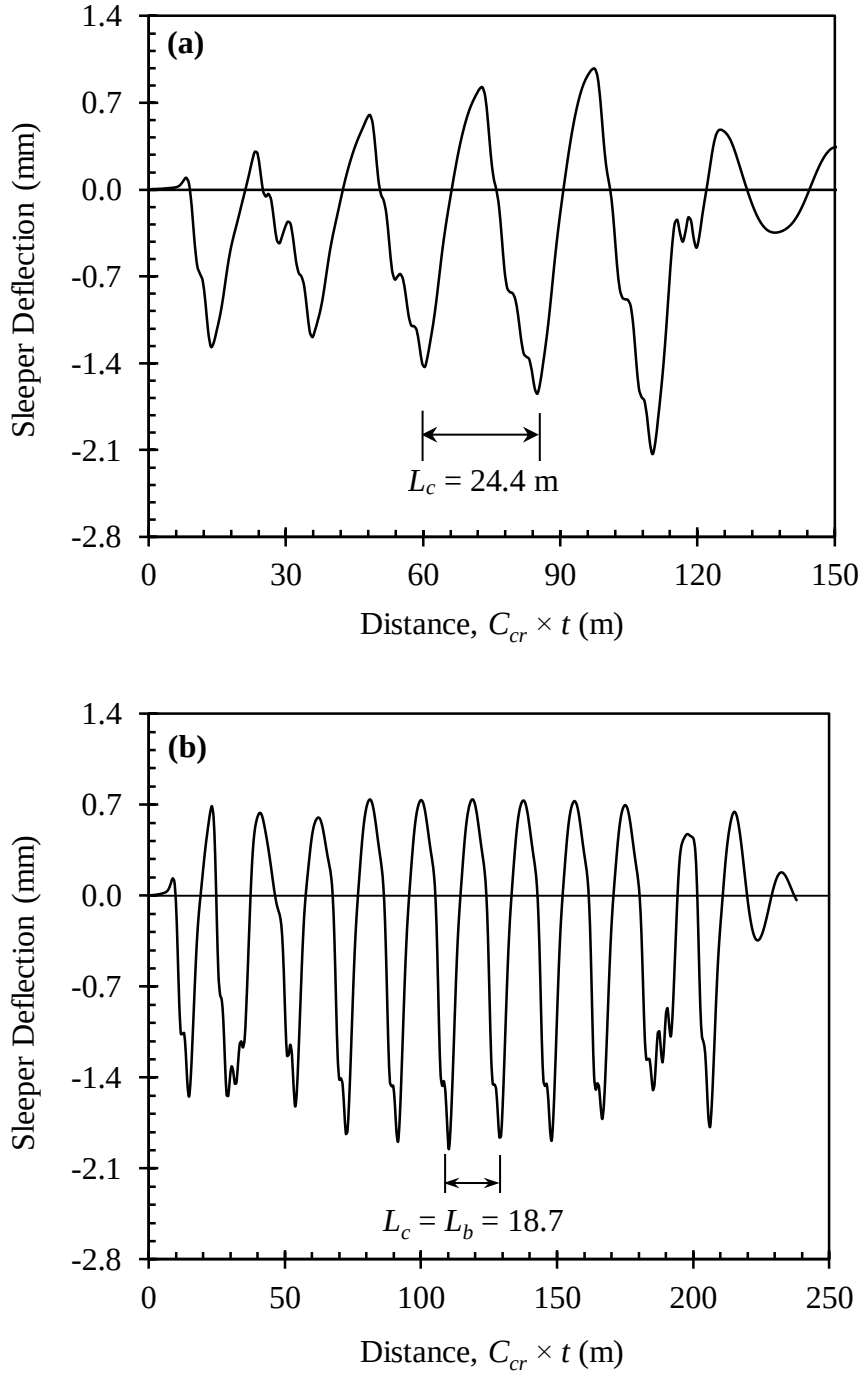

Figure 4.23: Distance-history of sleeper vertical deflection at the critical speeds for: (a) the X-2000 HST; and (b) Thalys HST.

where, $C_{cr(particular train)}$, $C_{cr(X-2000\,HST)}$ and $C_{cr(Thalys\ HST)}$ are the critical speeds of the desired particular trains X-2000 HST and Thalys HST, respectively; and $L_{particular\ train}$, $L_{X-2000\,HST}$ and $L_{Thalys\,HST}$ are the carriage lengths of the desired particular trains X-2000 HST and Thalys HST, respectively. By considering the

length of the central carriage of the X-2000 HST (i.e. $L_{X-2000\,HST}$ = 24.4 m), Equation (4.6) can be simplified as follows:

$$C_{cr\,(particular\ train)} = \frac{C_{cr\,(X-2000\,HST)}}{24.4} \times L_{particular\ train} \tag{4.7}$$

Likewise, by considering the length of the central carriage of the Thalys-HST (i.e. $L_{Thalys\ HST}$ = 18.7 m), Equation (4.6) can also be simplified as follows:

$$C_{cr\,(particular\ train)} = \frac{C_{cr\,(Thalys\ HST)}}{18.7} \times L_{particular\ train} \tag{4.8}$$

Equations (4.7) or (4.8) can then be used to calculate the critical speed of any other train with respect to the critical speed of the X-2000 HST, i.e. $C_{cr\,(X-2000\,HST)}$, or the critical speed of the Thalys HST, i.e. $C_{cr\,(Thalys\ HST)}$.

As mentioned above, either of Equations (4.7) or (4.8) can be used to determine the critical speed for any other particular train. However, this requires the critical speed of either the X-2000 or Thalys HST to be provided. For this reason, the sensitivity charts shown in Figure 4.24 is developed using the results obtained from Section 4.4.3 for the X-2000 HST. Similar sensitivity charts for determination of the critical speed for the Thalys HST are not developed as they are not needed because Equation (4.8) does not have to be used. One of the sensitivity charts is originally developed based on the modulus of the railway subgrade, E_s (Figure 4.24a), and another corresponding sensitivity chart is developed based on the subgrade shear wave velocity, C_s (Figure 4.24b), using the subgrade density, ρ, Poisson's ratio, υ, and the following well-known equation:

$$C_s = \sqrt{\frac{E}{2\rho(1+\nu)}} \tag{4.9}$$

The essence of the sensitivity charts is to readily determine the critical speed of the X-2000 HST for different track subgrade stiffnesses and thicknesses.

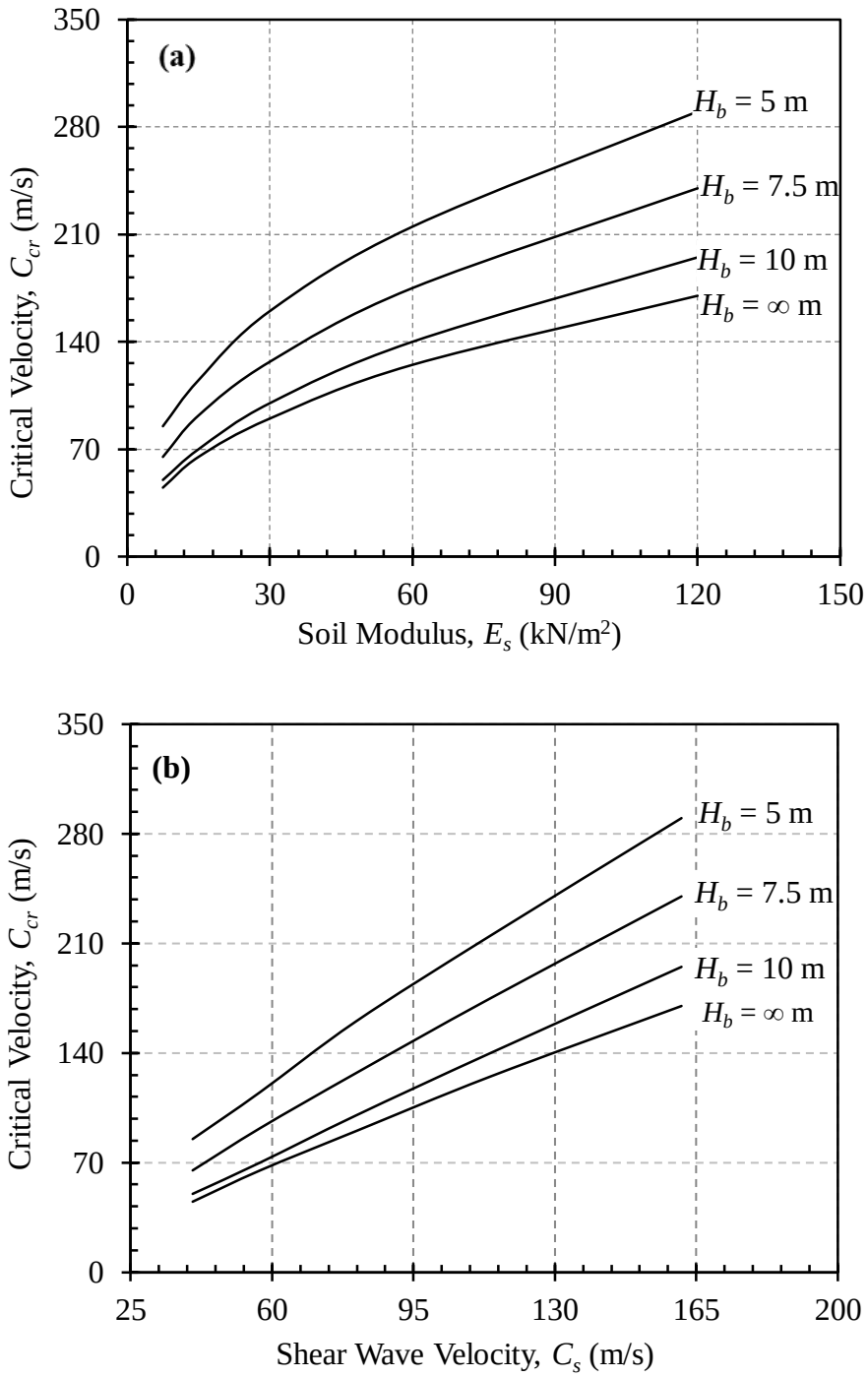

Figure 4.24: Sensitivity charts to calculate the critical speed of the X-2000 HST for different ground conditions: (a) elastic modulus; and (b) shear wave velocity.

4.5 SUMMARY AND CONCLUSIONS

Sophisticated 3D FE modelling was performed in this chapter to simulate and understand the dynamic response of ballasted railway tracks subjected to train moving loads. The respective modelling methodology was successfully predicted the

measurements taken from two well documented case studies available in the literature. The obtained results confirmed that the FE modelling is trustworthy and can be used with confidence to simulate the behaviour of railway track foundations, for both the quasi-static and dynamic loading conditions. A comprehensive parametric study was also performed to investigate the track response over a wide range of track parameters, including the modulus and thickness of ballast, sub-ballast and subgrade. In addition, the developed FE model was used to carry out further analysis to investigate the influence of train speed on the behaviour of ballasted railway track foundations and to evaluate the critical speed under various conditions of the train-track-ground system. The following specific conclusions are drawn from this chapter:

- Subgrade modulus is the dominant influencing factor affecting the overall track performance. A decrease in the subgrade modulus significantly affects the track response, including the rail deflection, ballast and sub-ballast surface vertical stresses, surface subgrade strain and track stiffness. This clearly indicates that maintenance would be a critical issue for tracks built on soft subgrade.

- In general, the track dynamic response in the form of sleeper deflection increases with the increase in the train speed, reaching its maximum value at the critical speed, before it decreases with further increase in the train speed.

- As the underlying hard rock has greater stiffness than the subgrade soil, the critical speed is found to be higher than the Rayleigh wave and shear wave velocities of the top subgrade soil.

- The evolution of sleeper deflection with train speed indicates that when the train speed exceeds 75% of the critical speed, the amplitude of track dynamic response increases rapidly. Therefore, 75% of the critical speed may be assumed as the practical speed limit for ballasted railway tracks.

- The train speed induces significant vibrations at the track centre, which may extend with less magnitude in the transverse direction to a distance equal to 8 m from the track centre, and this may cause detrimental impact on the train-track-ground system and nearby structures especially at the critical speed.

- Due to the nonlinearity of substructure materials, slightly higher downward deflections occur in the nonlinear subgrade track than those of the linear subgrade

track. However, the influence of nonlinearity of substructure materials on the critical speed is almost negligible.

- The subgrade stiffness and thickness are found to have a significant influence on the dynamic amplification factor (DAF) and critical speed of the train-track-ground system. The DAF decreases with the increase of both the subgrade stiffness and thickness. On the other hand, the magnitude of the critical speed is found to increase with the increase in the subgrade stiffness and decreases with the increase in the subgrade thickness.

- The ballast stiffness and thicknesses are found to have little or no influence on the DAF and critical speed of the train-track-ground system.

- The track deformation is found to increase with the increase in train loading magnitudes; however, the critical speed of the train-track-ground system is found to be independent of the train loading amplitude; conversely, it is found to be significantly influenced by the train loading geometry.

- At the critical speed condition, the carriage passing frequency of any particular train is equal to the natural frequency of the track-ground system.

CHAPTER 5

DEVELOPMENT OF NEW DESIGN METHOD AND ITS APPLICATION

5.1 INTRODUCTION

As discussed in the previous chapters, design of ballasted railway track foundations requires accurate estimation of the thickness of the granular layer (i.e. the combined thickness of ballast and sub-ballast layers between the sleeper bottom and the subgrade surface), so that it can provide adequate protection against possible track failure that may be caused by the repeated dynamic action of trains. This is why the design of ballasted railway track foundations is often referred to as the design of the granular layer thickness. In this chapter, a new method is developed for the design of railway track foundations that can sustain the relatively high demand for high speed trains (HSTs) and heavy axle loads (HALs). The design method is based on improved empirical models and sophisticated three-dimensional (3D) finite element (FE) numerical analyses. The improved empirical models are used for predicting the cumulative plastic strain and deformation of the track substructure layers, whereas the stress behaviour of the substructure materials under applications of repeated stresses are determined from the 3D FE numerical modelling. The two most common track failures, namely the subgrade progressive shear failure and excessive plastic deformation of track substructure layers are taken into account during the development of the proposed design method. Accordingly, two design criteria are established to prevent track failure: (1) limiting the cumulative plastic strain; and (2) limiting the track plastic deformation. The design method is then employed to calculate the granular layer thicknesses for four track sites and the results are compared with field measurements available in the literature. The results obtained from the new design method are found to be in reasonable agreement with field measurements.

5.2 DESIGN CRITERIA

As discussed earlier in Chapter 2, among the several modes of track substructure failure, the massive shear failure of the subgrade is the most catastrophic, but it

fortunately rarely occurs in ballasted railway tracks. Since the risk of massive shear failures is very low, the focus of the new design method is directed to prevent the progressive shear failure at the subgrade surface and to limit the excessive deformation of the track substructure under repeated train dynamic load, which are more likely to occur. This simply means that the granular layer thickness should be sufficient so that the stress transferred to the subgrade through the granular media must be less than an allowable value, and this will readily prevent the progressive shear failure of the subgrade and also limit the excessive track deformation.

The deformation of a railway track consists of the combined elastic (resilient) deformation and plastic deformation of each of the granular layer and subgrade soil. The elastic deformation of the track can be reduced by increasing the thickness and stiffness of the granular layer as well as improving the subgrade soil (i.e. increasing the subgrade stiffness), as discussed earlier in Chapter 4. However, in the proposed design method, estimation of the granular layer thickness is mainly intended to limit the excessive plastic deformation of the track substructure layers.

Preventing the progressive shear failure at the top surface of the subgrade (in the form of plastic flow) can be achieved by limiting the excessive cumulative plastic strain at the subgrade surface. On the other hand, limiting the excessive plastic deformation in the track can be achieved by limiting the total plastic deformation accumulated by the ballast and subgrade sublayers. Accordingly, the design criteria of preventing the progressive shear failure and limiting the excessive plastic deformation can be characterised by the following equations:

$$\varepsilon_{p\_s} \leq \varepsilon_{(p\_s)a} \tag{5.1}$$

$$\rho_t = \rho_b + \rho_s \leq \rho_{ta} \tag{5.2}$$

where, ε_{p_s} is the cumulative plastic strain under repeated loading at the subgrade surface; $\varepsilon_{(p\_s)a}$ is the allowable plastic strain at the subgrade surface; ρ_t is the total cumulative plastic deformation of the track under repeated train loading; ρ_b and ρ_s are the contribution to track deformation by the ballast and subgrade layers, respectively; ρ_{ta} is the allowable plastic deformation of the track for the design traffic tonnage.

As discussed in Chapter 3, the key factors influencing the cumulative plastic strain of the ballast and subgrade soil are the distribution of the deviatoric stress with depth in the substructure layers, compressive strength of the substructure materials, types of materials, dynamic wheel load and number of load repetitions. For a specified loading and ground conditions, all of these factors remain fixed except the distribution of the deviatoric stress. Therefore, limiting the cumulative plastic strain or deformation of the track can be achieved by restricting the deviatoric stress to lie within a tolerable level, which in turn depends on imposing an acceptable plastic strain level at the subgrade surface or acceptable deformation values in the track substructure layers.

Recalling from Chapter 3, the cumulative plastic strain of ballast and subgrade layers subjected to repeated loading can be expressed as follows:

$$\varepsilon_{p\_b} = \frac{x}{100}\left(\frac{\sigma_{d\_b}}{\sigma_{s\_b}}\right)^{y}\left[1+\ln(N_b)\right]^{z} \tag{5.3}$$

$$\varepsilon_{p\_s} = \frac{a}{100}\left(\frac{\sigma_{d\_s}}{\sigma_{s\_s}}\right)^{m} N_s^{b} \tag{5.4}$$

where, ε_{p_b} is the cumulative plastic strain in the ballast layer; σ_{d_b} is the deviatoric stress in the ballast; σ_{s_b} is the static strength of ballast under 50 kPa confining pressure, N_b is the number of load repetitions in the ballast layer; *x*, *y* and *z* are the parameters depend on ballast type, as summarised in Table 3.1; ε_{p_s} is the cumulative plastic strain in the subgrade layer; σ_{d_s} is the deviatoric stress in the subgrade; σ_{s_s} is the unconfined compressive strength of the subgrade soil; N_s is the number of load repetitions in the subgrade layer; and *a*, *m* and *b* are constant empirical parameters depend on the type of subgrade soil, as listed in Table 3.2.

Also, recalling from Chapter 3, the total cumulative plastic deformation of track (i.e. the sum of ballast and subgrade deformations) can be expressed as follows:

$$\rho_t = \rho_b + \rho_s = \sum \varepsilon_{(p\_b)i} H_{bi} + \sum \varepsilon_{(p\_s)i} H_{si} \tag{5.5}$$

where, ρ_t is the total plastic deformation of track substructure; ρ_b and ρ_s are the plastic deformation in the ballast and subgrade layers, respectively; H_{bi} and H_{si} are the thickness of each sublayer of the ballast and subgrade layers, respectively; $\varepsilon_{(p\_b)i}$ and $\varepsilon_{(p\_s)i}$ are the plastic strain at the centre of each ballast and subgrade sublayers, respectively.

5.3 DESIGN TRAFFIC

The proposed design method for ballasted railway track foundations emphasises the influence of the following traffic parameters:

- Individual wheel load
- Wheel spacing
- Train speed
- Traffic tonnage

In the current method, these parameters are used to calculate three design variables: (1) design dynamic wheel load, P_d; (2) total equivalent number of design load applications in the ballast layer, N_b; and (3) total equivalent number of design load applications in the subgrade layer, N_s, for the design traffic tonnage. The design dynamic wheel load corresponding to the maximum static wheel load, train speed and wheel spacing of the moving train can be determined as follows:

$$P_d = P_s \times \mathrm{DAF} \times \mathrm{WSF} \tag{5.6}$$

where, P_d is the design dynamic wheel load; P_s is the maximum static wheel load of the traffic assumed to run along the track; DAF is the dynamic amplification factor based on the train speed and subgrade condition (*Appendix A*); WSF is the wheel spacing factor based on the impact of the wheel spacing of any train with respect to the wheel spacing of the X-2000 high speed train (HST), which is considered in the stress analysis for the development of the design charts that will be described in detail later in Section 5.5.

The design traffic tonnage is the total possible amount of load in million gross tonnes (MGT) to be carried along the track without causing track failure. This value should be chosen based on maintenance costs and traffic speed restriction considerations. It

is generally assumed that when a train runs along the track, two axles under the same bogie produce one load cycle in the ballast layer whereas four axles under two adjacent bogies (carriages) produce a single load cycle in the subgrade layer (Li et al., 2002). Therefore, the numbers of load cycles in the ballast (N_{bi}) and in the subgrade (N_{si}) of any wheel load (P_{si}) can be determined as follows:

$$N_{bi} = \frac{T_i}{4P_{si}} \tag{5.7}$$

$$N_{si} = \frac{T_i}{8P_{si}} \tag{5.8}$$

where, T_i is the total traffic tonnage of the wheel load, P_{si}, in the same unit of P_{si}.

In order to consider the influence of different amplitudes of the wheel load on the subgrade performance, the number of the load cycles in the subgrade, N_{si}, for the wheel load, P_{si}, can be converted to an equivalent number of load cycles, N_{si}^{o}, of the design (maximum) static wheel load, P_s, as follows (Li and Selig, 1996):

$$N_{si}^{o} = N_{si}\left(\frac{P_{si}}{P_s}\right)^{m/b} \tag{5.9}$$

where, *m* and *b* are material parameters dependent on the soil type (Table 3.2).

Similarly, the number of load cycles in the ballast, N_{bi}, for the wheel load, P_{si}, can be converted to an equivalent load cycle, N_{bi}^{o}, corresponding to the maximum static wheel load, P_s, as follows:

$$N_{bi}^{o} = N_{bi}\left(\frac{P_{si}}{P_s}\right)^{y/z} \tag{5.10}$$

where, *y* and *z* are material parameters dependent on the ballast type (Table 3.1).

Accordingly, the total number of equivalent load applications in both the ballast layer (N_b) and subgrade layer (N_s) corresponding to the maximum static wheel load, P_s, can be calculated as follows:

$$N_b = N_{bi}^o + N_{bi}^1 + N_{bi}^2 + N_{bi}^3 + - - - - - + N_{bi}^n \tag{5.11}$$

$$N_s = N_{si}^o + N_{si}^1 + N_{si}^2 + N_{si}^3 + - - - - - + N_{si}^n \tag{5.12}$$

5.4 DEVIATORIC STRESS ANALYSIS

As discussed in the preceding section, the purpose of placing an adequate granular layer thickness is to limit the deviatoric stress transferred to the subgrade below a tolerable level so that the progressive shear failure at the subgrade surface and excessive plastic deformation of the track are prevented. Therefore, it is noteworthy to understand how the deviatoric stresses are distributed in the granular layer and subgrade layer under various train-track-ground conditions, including the modulus and thicknesses of ballast and subgrade, and the amplitude of the train load. To this end, this section is devoted to the analyses of the deviatoric stress generation within the track foundation using the developed 3D FE numerical modelling subjected to true train moving loads. The 3D FE modelling is described earlier in Chapter 4. For the analyses of the deviatoric stress in this chapter, the material properties of the nominal track model given in Table 4.5 are used. Table 4.6 demonstrates the range of variables considered in the analyses. In the following analyses, all parameters are assumed to be nominal unless otherwise specified. It is also assumed that the granular layer is characterised only by the ballast layer.

5.4.1 Deviatoric Stress Distribution along the Rail

Based on the FE results, the deviatoric stress distribution characteristics along the rail at the ballast surface (i.e. zero depth below the sleeper) and subgrade surface (i.e. below granular layer) are shown in Figures 5.1 and 5.2, respectively. It can be seen from Figure 5.1 that the maximum deviatoric stresses induced at the ballast surface beneath the sleepers are almost constant after the passage of the X-2000 HST along the track. However, the deviatoric stress at the same depth of the ballast below the crib is less than that beneath the sleeper.

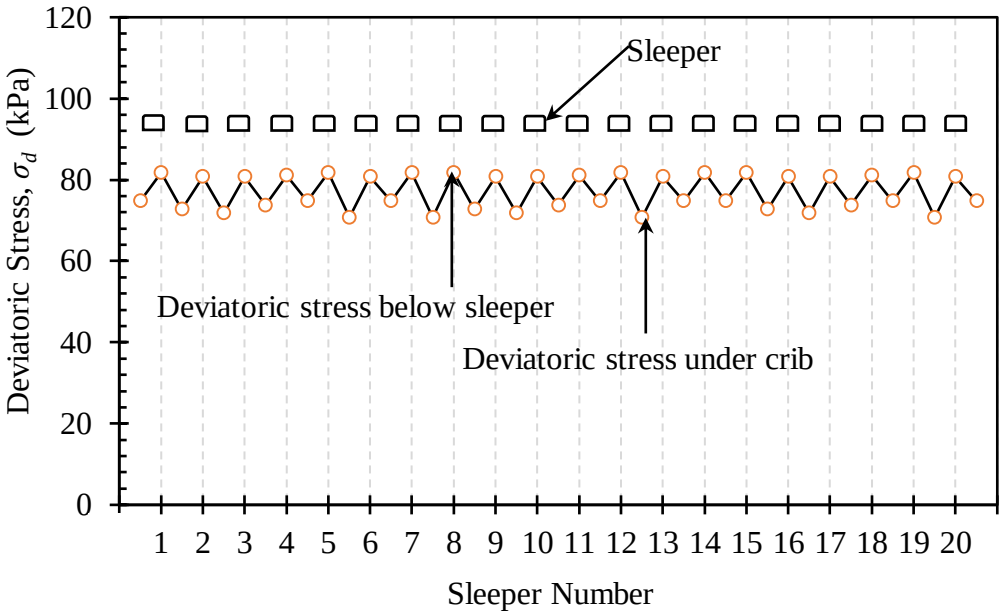

Figure 5.1: Deviatoric stress at the ballast surface along the rail.

On the other hand, it can be seen from Figure 5.2 that the deviatoric stress distribution along the rail at the subgrade surface is invariant. However, for the purpose of railway track foundation design, the deviatoric stress distribution with depth in the ballast and subgrade layers can be selected below the sleeper rather than the crib, which is the zone of maximum deviatoric stress.

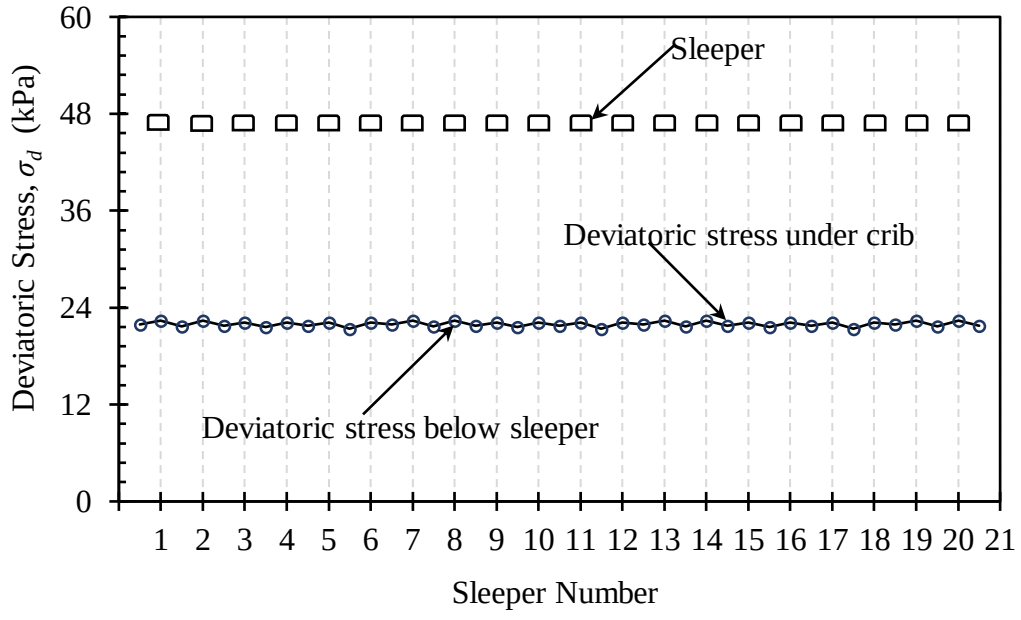

Figure 5.2: Deviatoric stress at the subgrade surface along the rail.

5.4.2 Deviatoric Stress Distribution along the Sleeper

Figure 5.3 shows the deviatoric stress distribution along the sleeper at four different depths of ballast. It can be seen that the deviatoric stress in the ballast at various depths bellow the sleeper is minimum at the track centre and maximum at the end of the sleeper. However, the variation of the deviatoric stress distribution along the sleeper reduces with the depth below the sleeper.

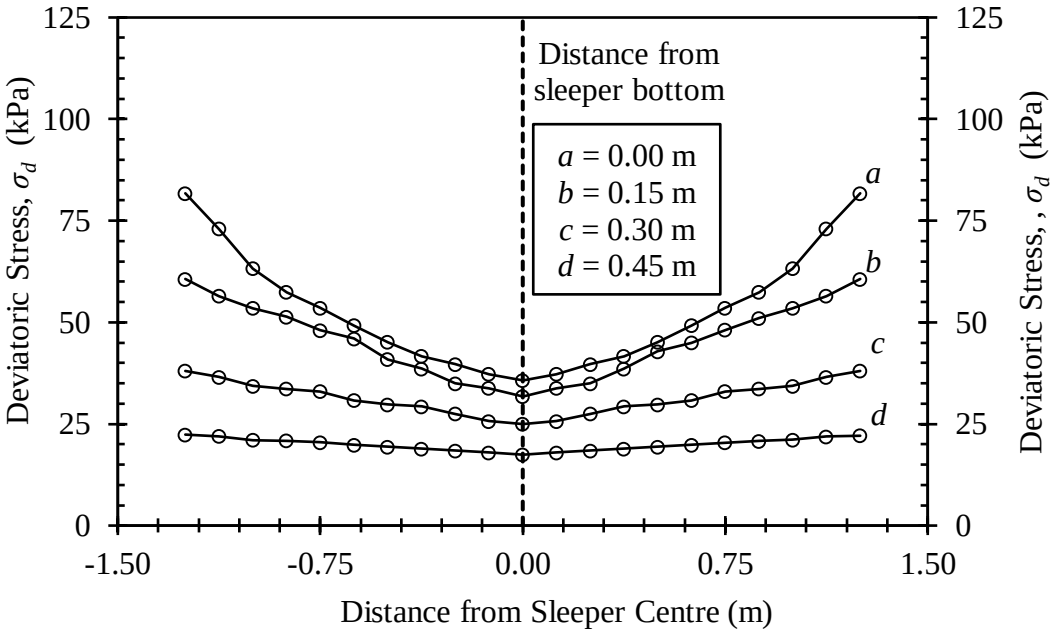

Figure 5.3: Deviatoric stress at different depths of ballast along the sleeper.

The deviatoric stress distribution along the sleeper at three different depths of subgrade from the sleeper bottom is also presented Figure 5.4. It can be seen that the deviatoric stress at a depth of 0.45 m bellow sleeper bottom (i.e. the subgrade surface) is maximum at the end of the sleeper. However, with the increase in depth below the sleeper's bottom, the distribution of the deviatoric stress along the sleeper in the subgrade is almost uniform. Therefore, for the purpose of design of railway track foundations, it is considered that the maximum deviatoric stress at various depths occurs below the end of the sleeper.

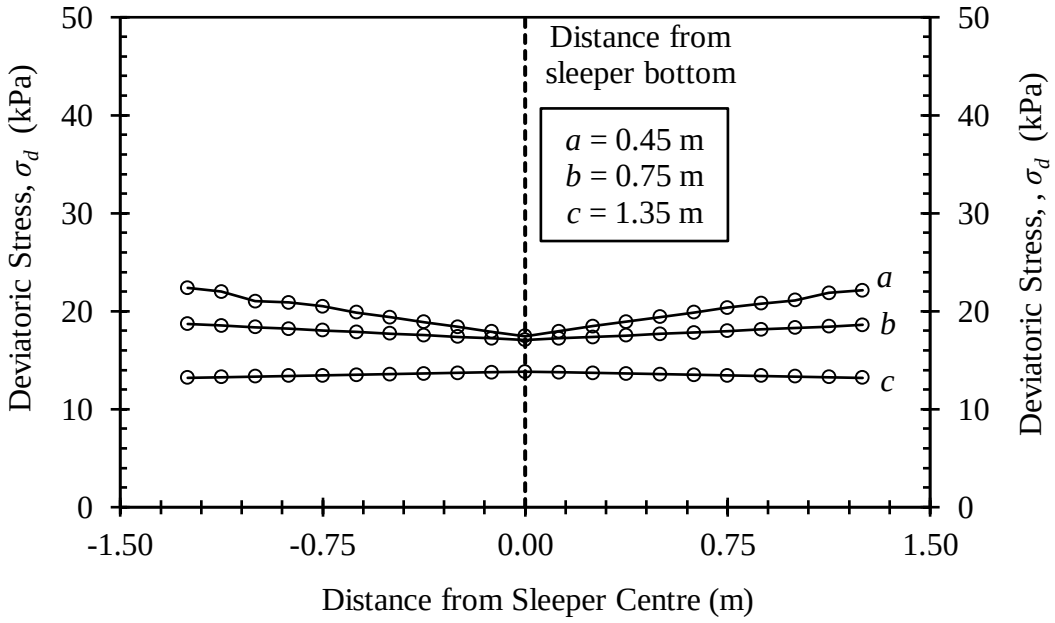

Figure 5.4: Deviatoric stress at different depths of subgrade along the sleeper.

5.4.3 Effect of Ballast and Subgrade Stiffness

In this section, the effects of the ballast and subgrade stiffness on the deviatoric stress distribution with depth in the ballast and subgrade layers are investigated. The herein so called soft ballast is characterised by a dynamic modulus of 135 MPa while the stiff ballast is represented by a dynamic modulus of 540 MPa. Similarly, a dynamic subgrade modulus of 15 MPa represents a soft subgrade while a dynamic subgrade modulus of 120 MPa accounts for a stiff subgrade.

5.4.3.1 Distribution of deviatoric stress within the ballast layer

Figure 5.5 presents the influence of ballast modulus on the distribution of deviatoric stress with depth in the granular layer while the subgrade modulus is 60 MPa. It can be seen that the deviatoric stress diminishes with the depth of the granular layer for all ballast modulus; however, the stress dissipation effect is not the same; it is higher for the stiffer ballast. It can also be seen that the deviatoric stress developed at the ballast surface is greater for higher ballast modulus.

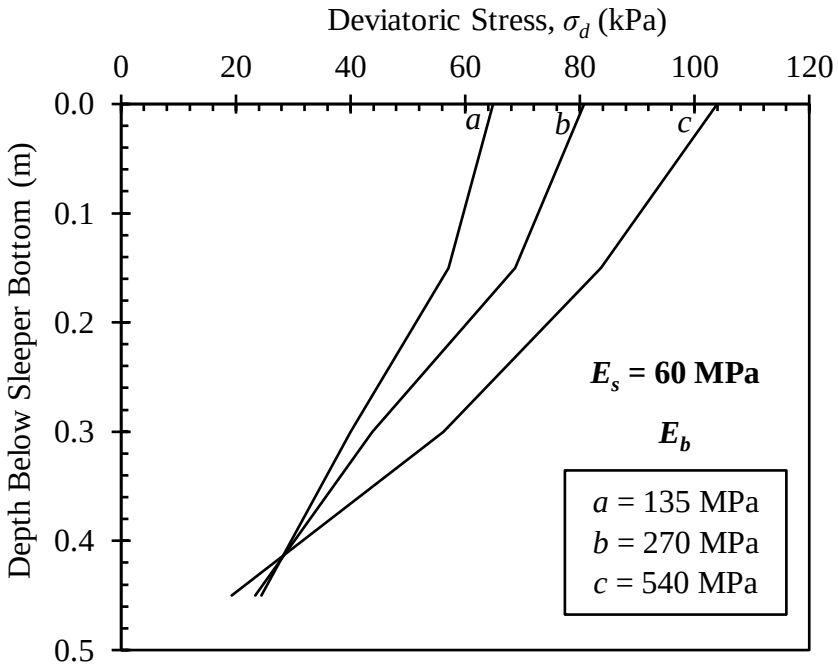

Figure 5.5: Effect of ballast modulus on the distribution of deviatoric stress with depth in the granular layer.

In order to investigate the impact of the subgrade stiffness on the deviatoric stress distribution in the granular layer, five different values of the subgrade dynamic modulus are considered (i.e. E_s = 15 MPa, 30 MPa, 60 MPa, 90 MPa and 120 MPa). The impact of the subgrade stiffness on the deviatoric stress distribution with depth in the granular layer is presented in Figure 5.6. It can be seen that the deviatoric stress induced at the ballast surface increases with the decrease of the subgrade stiffness, indicating that significant stress generates in the ballast layer that is supported by soft subgrade, which might increase the ballast particle breakage and ballast fouling. It can also be seen that the stress distribution efficiency for the ballast layer is higher when the subgrade is softer.

The combined effect of the ballast and subgrade moduli on the distribution of the deviatoric stress in the granular layer is summarised in Figure 5.7, where the solid lines and dotted lines indicate the soft and stiff subgrade conditions, respectively. It can be seen that the maximum deviatoric stress occurs in the ballast surface for the case of combined stiffer ballast and soft subgrade condition. It can also be seen that, with the decrease of the ballast modulus and increase of the subgrade modulus, the stress spreading efficiency of ballast decreases, and vice versa.

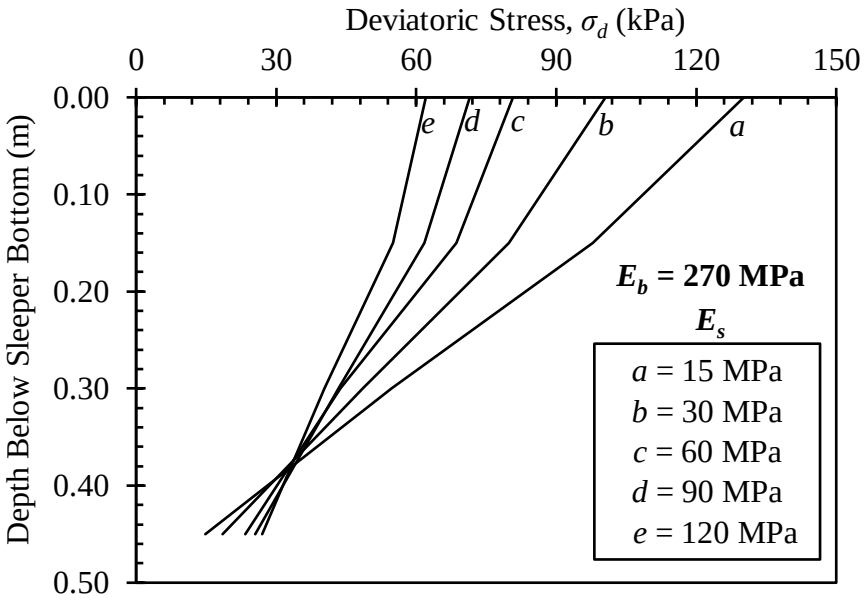

Figure 5.6: Effect of subgrade modulus on the distribution of deviatoric stress with depth in the ballast layer.

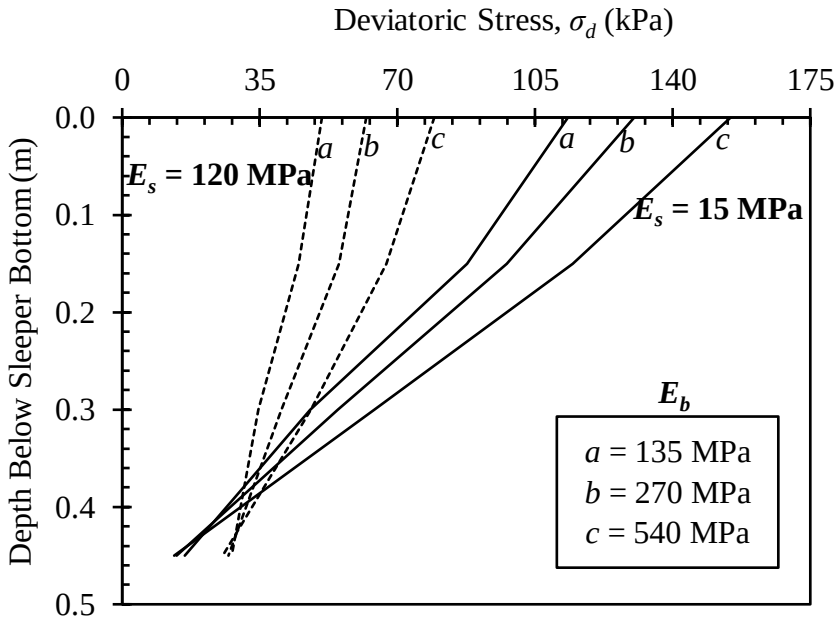

Figure 5.7: Influence of ballast and subgrade moduli on the deviatoric stress distribution in the ballast layer.

5.4.3.2 Distribution of deviatoric stress within the subgrade layer

Figure 5.8(a & b) shows the impact of the ballast modulus on the distribution of the deviatoric stress with depth in the cases of soft and stiff subgrade, respectively. It can be seen that an increase of the ballast modulus decreases the deviatoric stress at the subgrade surface regardless of the subgrade condition; however, the difference in the

deviatoric stress, due to variation of ballast stiffness, at each depth below the sleeper bottom decreases with depth and becomes negligible at about 6 m deep for the soft subgrade condition (Figure 5.8a). On the contrary, in the case of a stiff subgrade, the variation of the deviatoric stress, due to variation of ballast stiffness, at each depth below the sleeper bottom remain same with depth (Figure 5.8b).

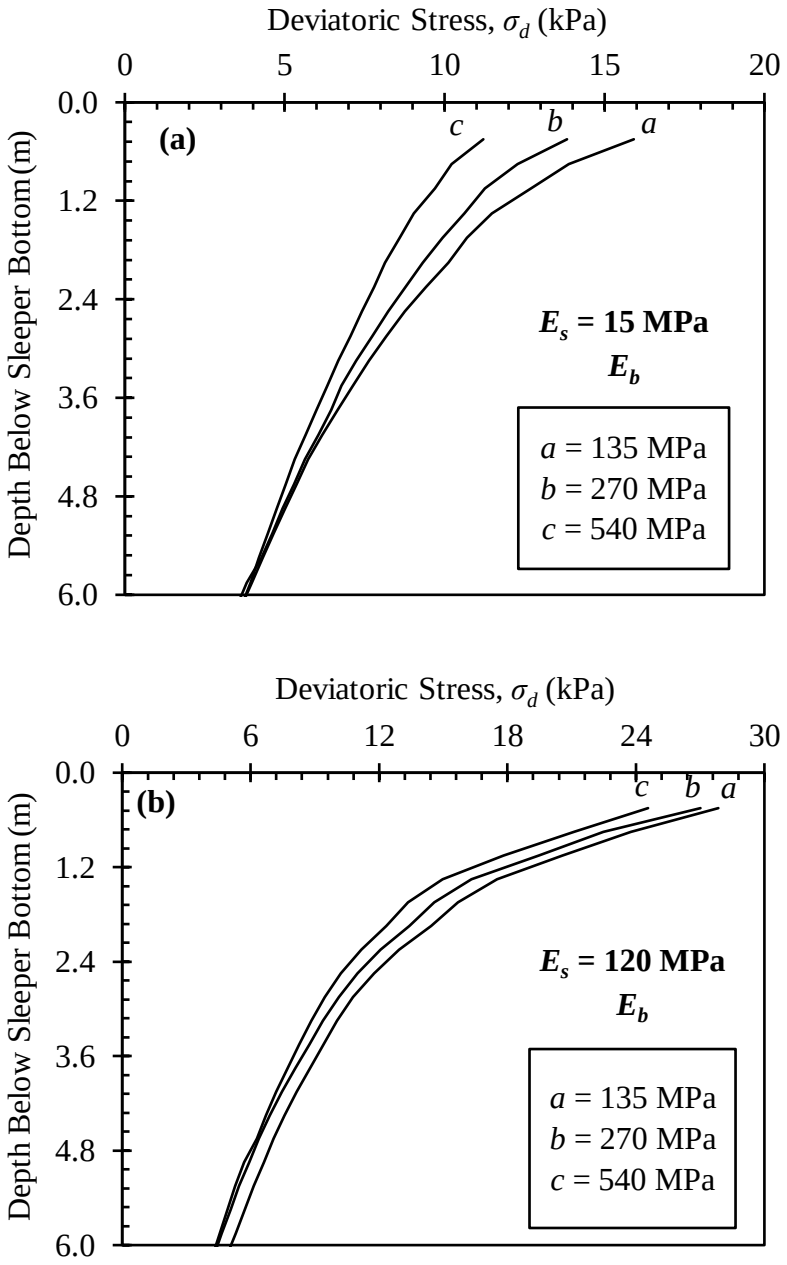

Figure 5.8: Effect of ballast modulus on distribution of the deviatoric stress with depth in the subgrade layer for: (a) a soft subgrade; and (b) a stiff subgrade.

The effect of subgrade modulus on the distribution of the deviatoric stress with depth in the subgrade layer is presented in Figure 5.9. It can be seen that the deviatoric

stress at the subgrade surface increases with the increase of the subgrade stiffness. However, the difference in the deviatoric stress (due to different subgrade stiffness) at each depth below the sleeper bottom decreases with the depth.

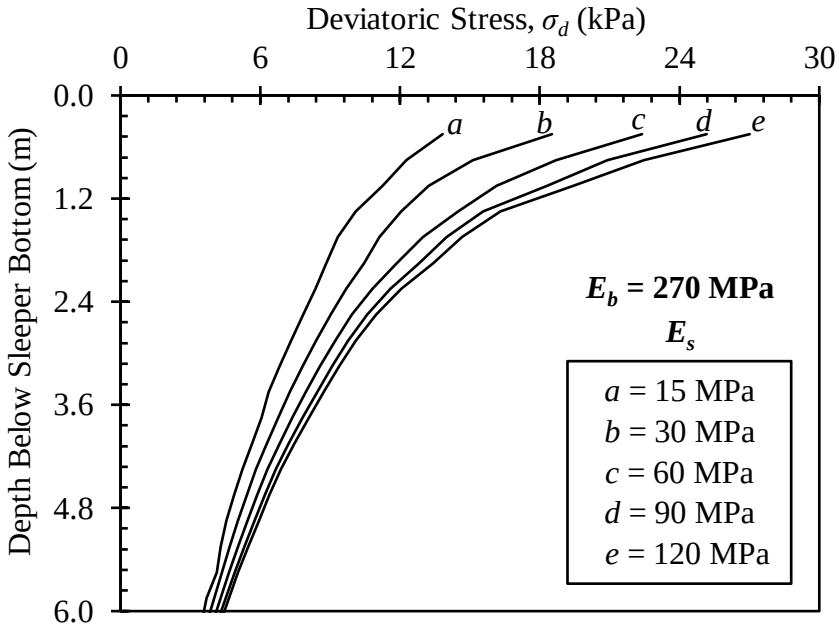

Figure 5.9: Effect of subgrade modulus on the distribution of deviatoric stress with depth in the subgrade layer.

5.4.4 Influence of Granular Layer Thickness

The impact of the granular layer thickness, H_b, on the distribution of the deviatoric stress with depth in the subgrade is investigated considering a range of ballast thickness from 0.15 m to 1.35 m. Figure 5.10 shows the deviatoric stress distribution within the soft subgrade for various granular layer thicknesses. It can be seen that the increase in the granular layer thickness significantly reduces the deviatoric stress at the subgrade surface. It is also evident from the results that a significant difference in the deviatoric stress occurs at each depth below the sleeper bottom due to the corresponding difference in the granular layer thickness, and the difference reduces with the distance below the sleeper.

Figure 5.11 shows the influence of the granular thickness on the distribution of the deviatoric stress with depth in the stiff subgrade. It can be seen that the increase in the granular layer thickness leads to a significant reduction in the deviatoric stress at the subgrade surface. However, in contrast to the soft subgrade condition, the

difference in the deviatoric stress due to change in the granular layer thickness below the sleeper bottom is almost negligible for all depths.

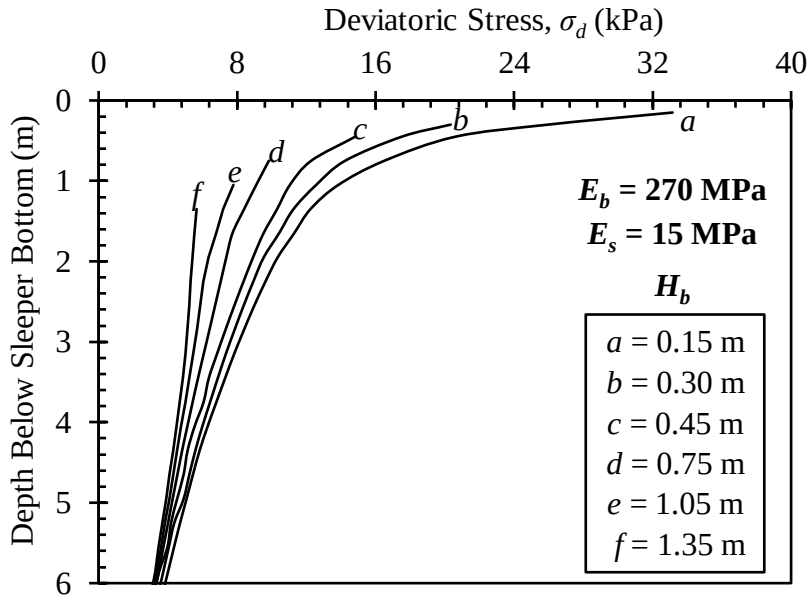

Figure 5.10: Effect of the granular layer thickness on distribution of the deviatoric stress with depth in the soft subgrade.

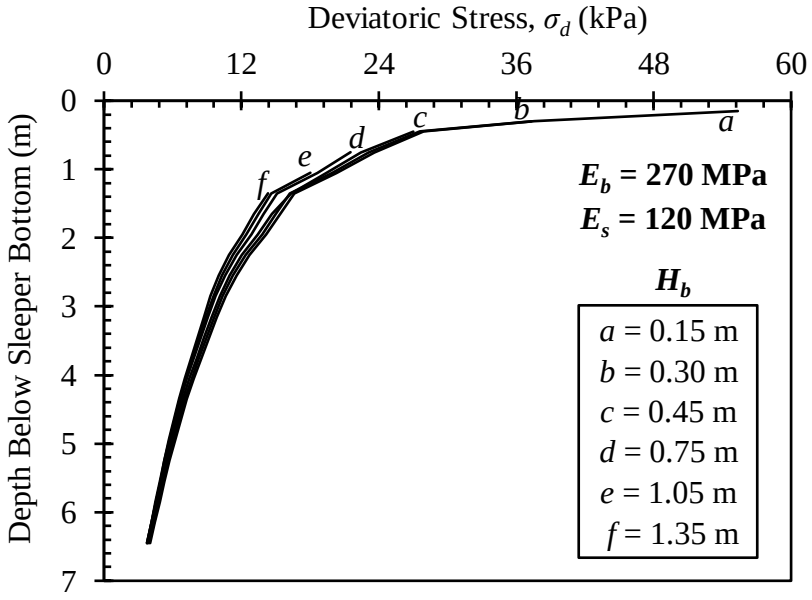

Figure 5.11: Deviatoric stress at different depths of the subgrade layer for stiff subgrade conditions.

In essence, the increase in the granular layer thickness reduces the distribution of the deviatoric stress within the subgrade in two ways. Firstly, when the granular layer thickness increases, the distance of the subgrade surface below the sleeper bottom is

automatically increased. Consequently, the deviatoric stress at the subgrade surface is automatically decreased by virtue of the depth spreading effect. Secondly, with the increase of the granular layer (i.e. stiffer layer) thickness, its stress spreading effect also increases. This leads to a reduction in the deviatoric stress at all depths in the subgrade. However, the second effect weakens when the difference in the stiffness of the granular and subgrade layers becomes smaller. Therefore, when the subgrade soil modulus is closer to that of the ballast, the effect of the granular layer thickness on the distribution of the deviatoric stress in the subgrade becomes insignificant.

5.4.5 Influence of Subgrade Layer Thickness

The impact of the subgrade layer thickness on the distribution of the deviatoric stress within the subgrade is investigated by considering three different subgrade thicknesses (i.e. H_s = 3.5 m, 7.0 m, and 10 m) overlying the hard rock. The distribution of the deviatoric stress for the three subgrade thicknesses considered is shown in Figure 5.12. It can be seen that the difference of the deviatoric stress at each depth of the subgrade is negligible, except at the interface of the subgrade with the hard rock. As the influence of the subgrade thickness on the distribution of the deviatoric stress in the subgrade is insignificant, the subgrade thickness is assumed to be fixed at 7.0 m in the deviatoric analysis performed for development of the upcoming design charts.

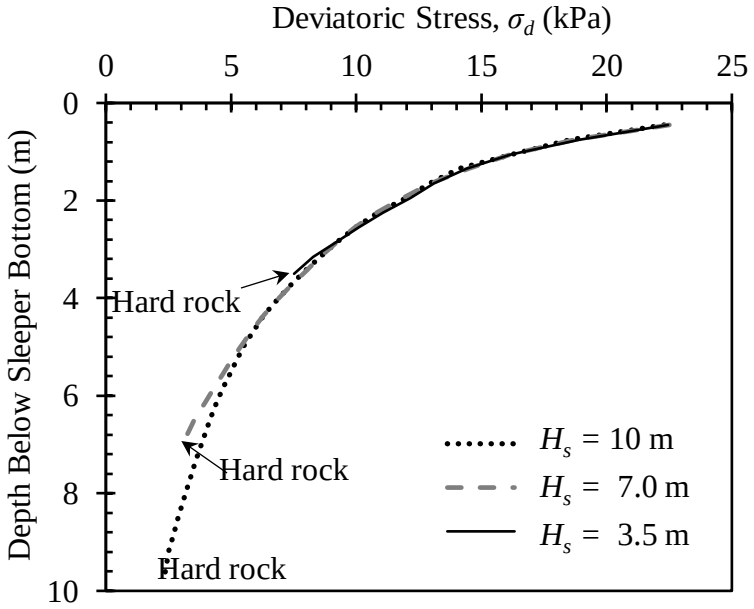

Figure 5.12: Influence of subgrade layer thickness on deviatoric stress distribution with depth in the subgrade layer.

5.4.6 Influence of Amplitude of Train Moving Loads

The influence of the amplitude of the train moving loads on the deviatoric stress distribution within the ballast and subgrade layers is investigated using four different percentages (i.e. 75%, 100%, 125% and 150%) of the standard wheel loading of the X-2000 HST. The standard loading considered to be equivalent to the axle loads is given in Table 4.4. The effect of different percentages of wheel loading on the deviatoric stress distribution with depth in the ballast layer for the nominal model is presented in Figure 5.13. As expected, the deviatoric stress in the ballast layer increases proportionally with the increase in the wheel loading at all depths below the sleeper.

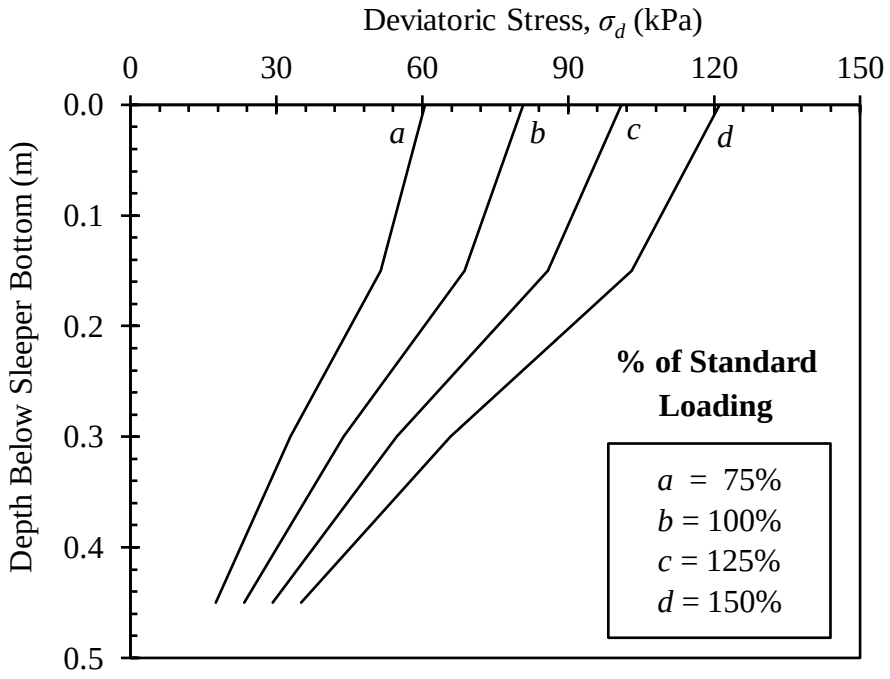

Figure 5.13: Effect of amplitude of wheel loading on the deviatoric stress distribution in the ballast layer.

Figure 5.14 shows the effect of the wheel load on the distribution of the deviatoric stress in the subgrade layer for the nominal model. Again, it can be seen that the deviatoric stress in the subgrade layer also increases proportionally with the increase in the wheel load at each depth below the sleeper.

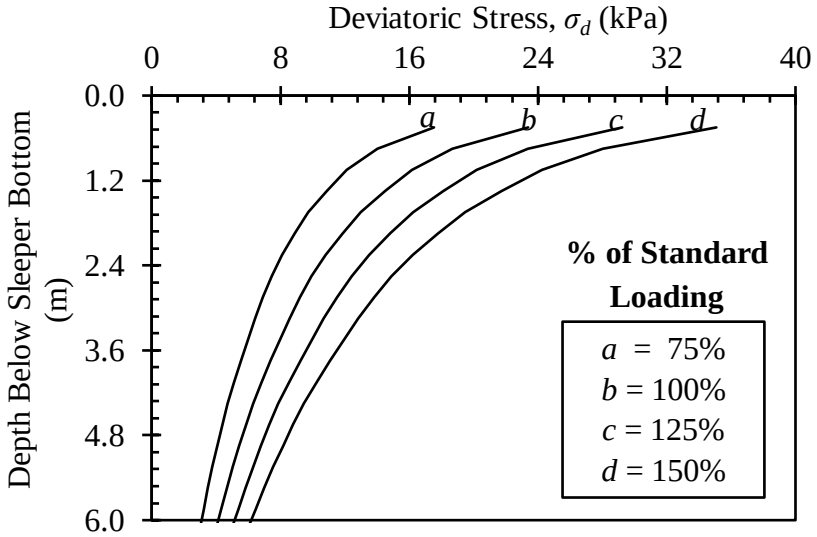

Figure 5.14: Effect of amplitude of wheel loading on the deviatoric stress distribution in the subgrade layer of the nominal model.

The relationship between the ballast surface deviatoric stress and percentage of train loading for the three subgrade conditions is shown in Figure 5.15. It can be seen that the ballast surface deviatoric stress is proportional to the amplitude of the wheel loading for all subgrade conditions. Figure 5.16 presents the relationship between the subgrade surface deviatoric stress and percentage of train loading for the three subgrade conditions. This relationship indicates that the subgrade surface deviatoric stress is also proportional to the amplitude of the wheel loading in a manner similar to the results presented in Figure 5.15.

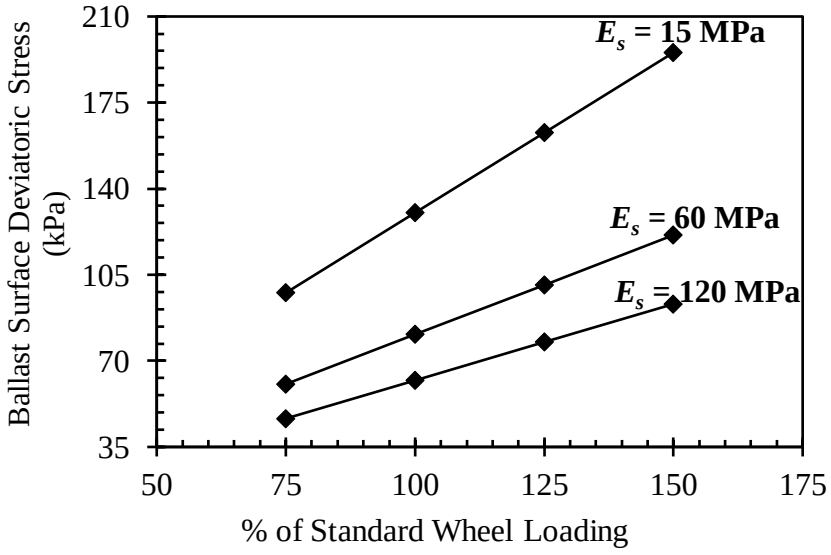

Figure 5.15: Relationship between the deviatoric stress at ballast surface and loading amplitude for the nominal model except those specified.

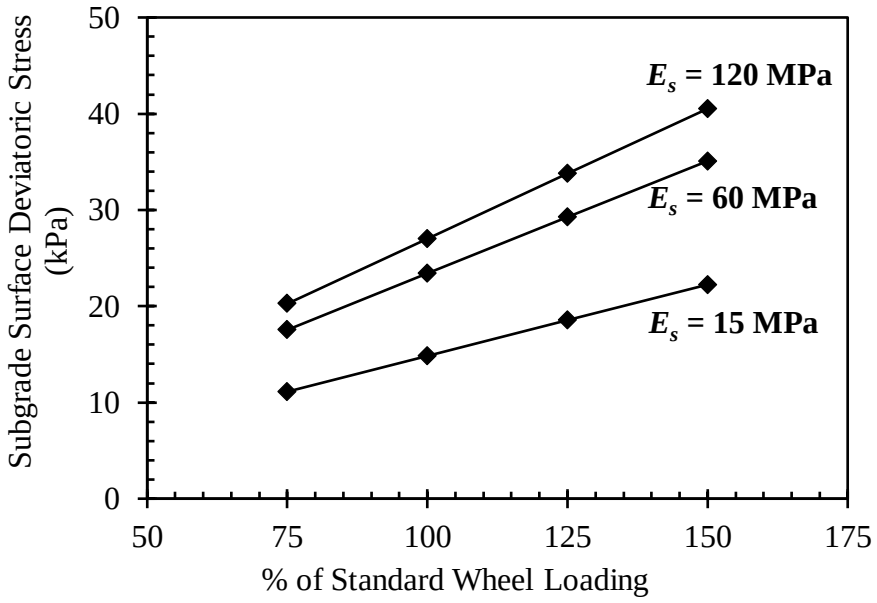

Figure 5.16: Relationship between the deviatoric stress at the subgrade surface and loading amplitude for the nominal model except those specified.

5.5 DEVELOPMENT OF DESIGN CHARTS

To facilitate the use of the proposed method by practitioners, the outcomes of the 3D FE analyses and improved empirical models are employed to develop a set of design charts that form the core of the proposed design method. This section presents the process leading to the development of the design charts, which are based on estimating the granular layer thickness needed to both prevent the progressive shear failure at the top subgrade surface and limit the excessive plastic deformation of the track under repeated train dynamic loading. The two design criteria adopted to achieve these requirements are: (1) limiting the cumulative plastic strain at the subgrade surface; and (2) limiting the total plastic deformation of the track layers below a tolerable level, as represented by Equations (5.1) and (5.2), respectively. For convenience, the distinction between the ballast and sub-ballast is ignored by presenting the granular ballast layer simply as a granular layer in the proposed design method.

For particular loading conditions and characteristics of the granular ballast and subgrade layers, the design of a ballasted railway track is relevant to selecting an adequate granular layer thickness so that the deviatoric stress experienced by the substructure layers is adequately low. Thus, the possibility of occurrence of the

progressive shear failure at the subgrade surface or excessive plastic deformation of the track can be prevented. Based on these principles, the first phase of developing the railway track design charts involves determining the deviatoric stresses in the ballast and subgrade layers for a range of granular ballast and subgrade conditions. The calculation of the deviatoric stresses is performed using 3D FE modelling subjected to train moving loads for a total of 105 cases with various combinations of ballast and subgrade characteristics. The parameters assumed include the ballast modulus (i.e. E_b = 135 MPa, 270 MPa and 540 MPa), subgrade soil modulus (i.e. E_s = 15 MPa, 30 MPa, 60 MPa, 90 MPa and 120 MPa) and granular ballast layer thickness (i.e. H_b = 0.15 m, 0.30 m, 0.45 m, 0.60 m, 0.75 m, 1.05 m and 1.35 m). The other track parameters are fixed at their nominal values given earlier in Table 4.5. The ranges selected above plus those in Table 4.5 for all material parameters are selected carefully to reflect the practical range expected in major railway tracks (Li, 1994; Li and Selig, 1994b).

5.5.1 Preventing Progressive Shear Failure

The design criterion for preventing the progressive subgrade failure is to limit the cumulative plastic strain at the subgrade surface below the allowable value. As indicated in Equation (5.4), the principle of keeping the cumulative plastic strain below a certain tolerable level means limiting the deviatoric stress. The deviatoric stress at the subgrade surface for different substructure conditions is readily calculated using 3D FE modelling. Since the calculation of the deviatoric stress assumes the ballast layer to be linear elastic-plastic and the subgrade layer to be linearly elastic, the ratio of the deviatoric stress to the design dynamic wheel load are set to be constant for a given track-ground condition. This allows development of the following dimensionless strain influence factor:

$$I_\varepsilon = \frac{\sigma_d \times A}{P_d} \tag{5.13}$$

where, I_ε is the strain influence factor; σ_d is the deviatoric stress; P_d is the design dynamic wheel load; A is an area coefficient assumed to be 1 m^2 to make the strain influence factor dimensionless.

The strain influence factor generated at the subgrade surface, I_{ε_s}, from the FE analyses for various substructure conditions can be now readily synthesised into simple design charts similar to those presented in Figure 5.17. This design charts built to calculate the granular layer thickness needed to prevent the progressive shear failure. As shown in the figure, each curve corresponds to a particular ballast and subgrade moduli. Other sets of design charts encompassing other design parameters are given in *Appendix B*.

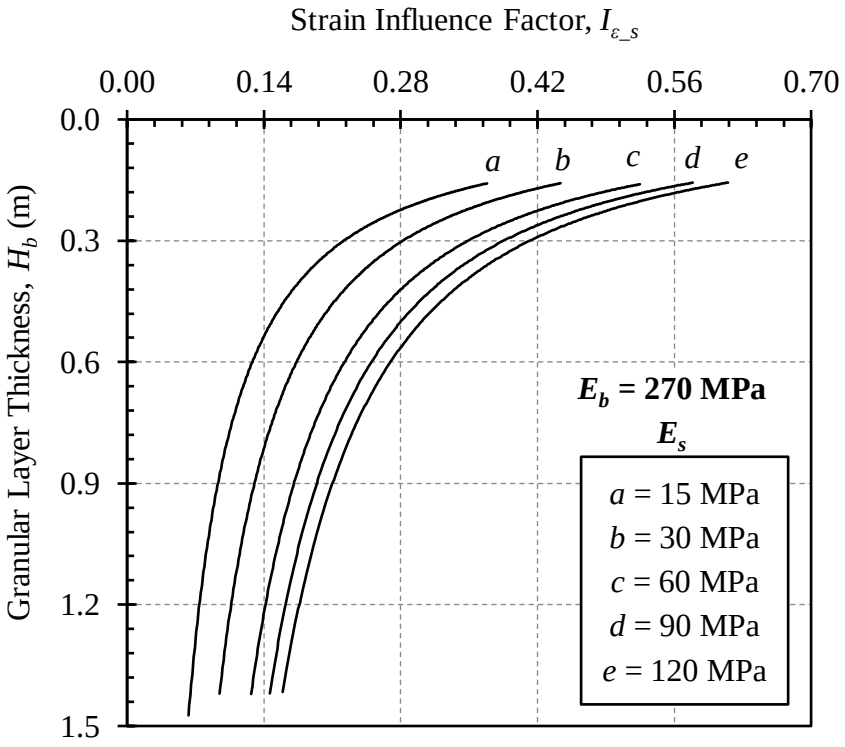

Figure 5.17: An example of design charts to calculate the granular layer thickness (for preventing progressive shear failure).

The development process of the relationship between the granular layer thickness, H_b, and strain influence factor, I_{ε_s}, is illustrated in Figure 5.18. As the process is identical for a certain combination of E_b and E_s, only the establishment of curve 'a' of Figure 5.17 for the substructure with a specific modulus of ballast and subgrade (i.e. E_b = 270 MPa and E_s = 15 MPa) is shown in Figure 5.18. For this purpose, Figure 5.18(a) is first regenerated from Figure 5.10 by simply replacing the deviatoric stress with the strain influence factor using Equation (5.13). It can be seen from Figure 5.18(a) that the strain influence factor at the subgrade surface, I_{ε_s}, decreases with the increase of the granular layer thickness. In order to develop the

design charts, the resulting I_{ε_s} are plotted against H_b for a particular set of granular ballast and subgrade moduli, as shown in Figure 5.18(b).

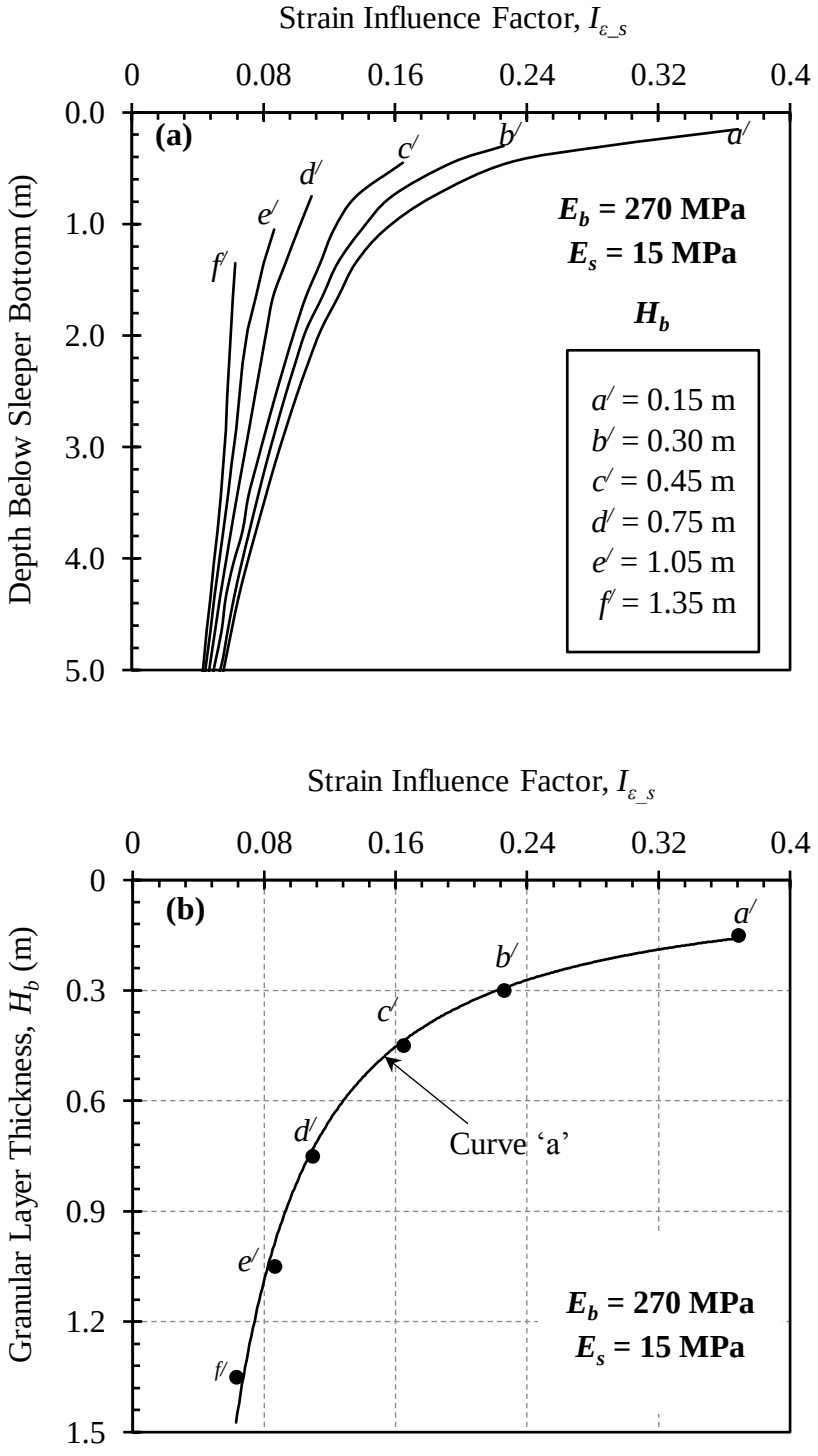

Figure 5.18: Development of curve 'a' of Figure 5.17 from Figure 5.10.

Using the design charts (e.g. Figure 5.17), the minimum required thickness of the granular layer can be determined for an acceptable value of the strain influence factor

at the subgrade surface, I_{ε_s}. Therefore, the value of the allowable I_{ε_s} needs to be determined based on the allowable deviatoric stress at the subgrade surface, $\sigma_{(d\_s)a}$, and the design dynamic wheel load, P_d, using Equation (5.13). In addition, the $\sigma_{(d\_s)a}$ can be calculated based on the soil compressive strength, σ_{s_s}, number of load repetitions on the subgrade, N_s, and allowable cumulative plastic strain, $\varepsilon_{(p\_s)a}$, and the type of the subgrade soil of interest using Equation (5.4).

5.5.2 Preventing Excessive Plastic Deformation

The key principle of preventing the excessive plastic deformation in the track means limiting the track deformation below a tolerable level. Therefore, the total cumulative plastic deformation due to repeated loading in the substructure layers (i.e. granular ballast layer of H_b thickness and subgrade layer of H_s thickness) need to be determined by integrating the cumulative plastic strain of ballast (i.e. Equation 5.3) and subgrade (i.e. Equation 5.4), as follows:

$$\rho_t = \rho_b + \rho_s = \int_0^{H_b} \frac{x\left[1+\ln(N_b)\right]^z}{100}\left(\frac{\sigma_{d\_b}}{\sigma_{s\_b}}\right)^y dh + \int_0^{H_s} \frac{aN_s{}^b}{100}\left(\frac{\sigma_{d\_s}}{\sigma_{s\_s}}\right)^m dh \tag{5.14}$$

Rearranging Equation (5.14) yields:

$$\rho_t = \frac{x\left[1+\ln(N_b)\right]^z}{100}\left(\frac{P_d}{A\sigma_{s\_b}}\right)^y \int_0^{H_b}\left(\frac{A\sigma_{d\_b}}{P_d}\right)^y dh + \frac{aLN_s{}^b}{100}\left(\frac{P_d}{A\sigma_{s\_s}}\right)^m \int_0^{H_s}\left(\frac{A\sigma_{d\_s}}{P_d}\right)^m \frac{dh}{L} \tag{5.15}$$

Using the definition of the strain influence factor (i.e. Equation 5.13), Equation (5.15) can be expressed as follows:

$$\rho_t = \frac{x\left[1+\ln(N_b)\right]^z}{100}\left(\frac{P_d}{A\sigma_{s\_b}}\right)^y \int_0^{H_b}\left(I_{\varepsilon\_b}\right)^y dh + \frac{aLN_s{}^b}{100}\left(\frac{P_d}{A\sigma_{s\_s}}\right)^m \int_0^{H_s}\left(I_{\varepsilon\_s}\right)^m \frac{dh}{L} \tag{5.16}$$

As indicated by Equation (5.16), the deformation of track substructure layers is a function of the strain influence factor, which is a function of the deviatoric stress in the ballast and subgrade soil. Therefore, again, the 3D FE modelling subjected to the X-2000 HST moving loads is used to determine the deviatoric stress distribution with depth within the ballast and subgrade layers for different substructure conditions. Afterwards, the results are presented in terms of the distribution of strain influence factor with depth using Equation (5.13). Figure 5.19 shows an example of the distribution of the dimensionless strain influence factor, I_{ε_b}, with depth in the ballast layer for a particular granular ballast modulus (i.e. E_b =270 MPa) and thickness (H_b = 0.45 m) but different values of the subgrade modulus. This figure is simply a reproduction of Figure 5.6, in which the axis of the deviatoric stress is replaced by the strain influence factor using Equation (5.13). Similarly, the distribution of I_{ε_b} with depth in the ballast layer for different substructure conditions (modulus and thicknesses of ballast, and modulus and thicknesses of subgrade) are presented in *Appendix C*.

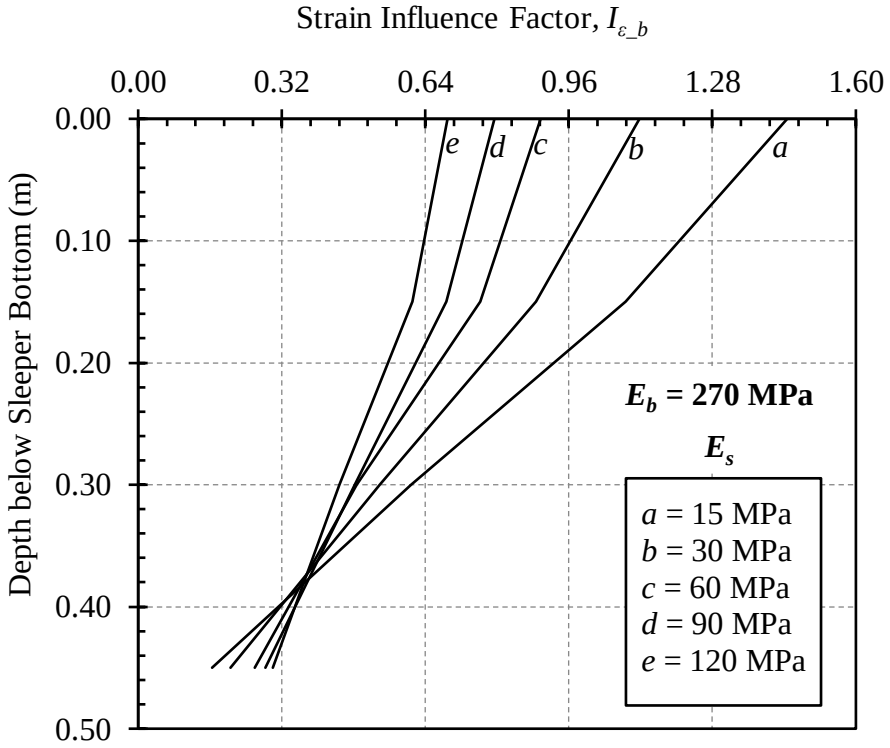

Figure 5.19: Example of distribution of strain influence factor with depth in the ballast layer.

The deformation generated in the ballast layer for the associated track substructure conditions can be determined using the results from *Appendix C* (e.g. Figure 5.19) and the following equation, which is the first part of Equation (5.16):

$$\rho_b = \frac{x\left[1+\ln(N_b)\right]^z}{100}\left(\frac{P_d}{A\sigma_{s\_b}}\right)^y \int_0^{H_b}\left(I_{\varepsilon\_b}\right)^y dh \tag{5.17}$$

The integration in Equation (5.17) can be solved by dividing the granular ballast layer into sublayers of thickness 0.1-0.15 m, then the integration is obtained by summing the multiplication of the strain influence factor at the middle of each sublayer by the corresponding sublayer thickness.

In order to develop design charts for preventing the excessive plastic deformation of track, the second part of Equation (5.16), which quantifies the cumulative plastic deformation of the subgrade layer can be rearranged as follows:

$$\rho_s = \frac{aLN_s^{\,b}}{100}\left(\frac{P_d}{A\sigma_{s\_s}}\right)^m \int_0^{H_s}\left(I_{\varepsilon\_s}\right)^m \frac{dh}{L} = \left[\frac{aLN_s^{\,b}}{100}\left(\frac{P_d}{A\sigma_{s\_s}}\right)^m\right] I_{\rho\_s} \tag{5.18}$$

so,

$$I_{\rho\_s} = \int_0^{H_s}\left(I_{\varepsilon\_s}\right)^m \frac{dh}{L} \tag{5.19}$$

where, I_{ρ_s} is a dimensionless deformation influence factor.

It should be noted that both the area coefficient (A) and length coefficient (L) are used in Equations (5.15-5.19) to non-dimensionalise the strain and deformation influence factors. Similar to the area coefficient, a unit value is assumed for the length coefficient (i.e. L = 1 m) for the ease of calculation.

As indicated in Equation (5.19) that the subgrade deformation influence factor, I_{ρ_s}, is a function of the distribution of the strain influence factor, I_{ε_s}, with depth in the subgrade and thickness of subgrade, H_s. It should also be noted that the distribution of I_{ε_s} with depth in the subgrade is governed by the different combinations of E_b,

E_s and H_b. Accordingly, the values of I_{ρ_s} are calculated using Equation (5.19) for different combinations of E_b, E_s, H_b and H_s, and parameter m depend on subgrade soil type. In order to produce the design charts, the values of resulting I_{ρ_s} are plotted against H_b for particular granular ballast and subgrade layer conditions. Figure 5.20 shows four samples of the design charts that can be used to calculate the granular layer thickness needed to prevent the excessive plastic deformation. Each chart corresponds to one subgrade soil type and one modulus combination for the granular and subgrade layers, and each curve corresponds to one deformable subgrade layer thickness. Following the same process, a total of 60 design charts are developed, which are presented in *Appendix D.*

To apply the proposed design charts for estimating the granular layer thickness, the first step is to determine the cumulative plastic deformation in the initially assumed thickness of the granular ballast layer, ρ_b, as explained above. Then, the allowable subgrade deformation influence factor, $I_{(\rho\_s)a}$ need to be calculated using the following equation, obtained by rearranging Equation (5.18) and substituting $(\rho_t - \rho_b)$ for ρ_s and ρ_{ta} for ρ_t :

$$I_{(\rho\_s)a} = \frac{\rho_{ta} - \rho_b}{\frac{aLN_s^{\,b}}{100}\left(\frac{P_d}{A\sigma_{s\_s}}\right)^m} \tag{5.20}$$

where, ρ_{ta} is the allowable track deformation; ρ_b is the cumulative plastic deformation occurs in the ballast lyer; N_s is the total equivalent number of load repetitions in the subgrade for the design traffic tonnage; P_d is the design dynamic wheel load; σ_{s_s} is the unconfined compressive strength of the soil; *a, m* and *b* are material parameters dependent on the subgrade soil type (see Table 3.2); *A* is the area coefficient (= 1 m^2); and *L* is the length coefficient (= 1 m).

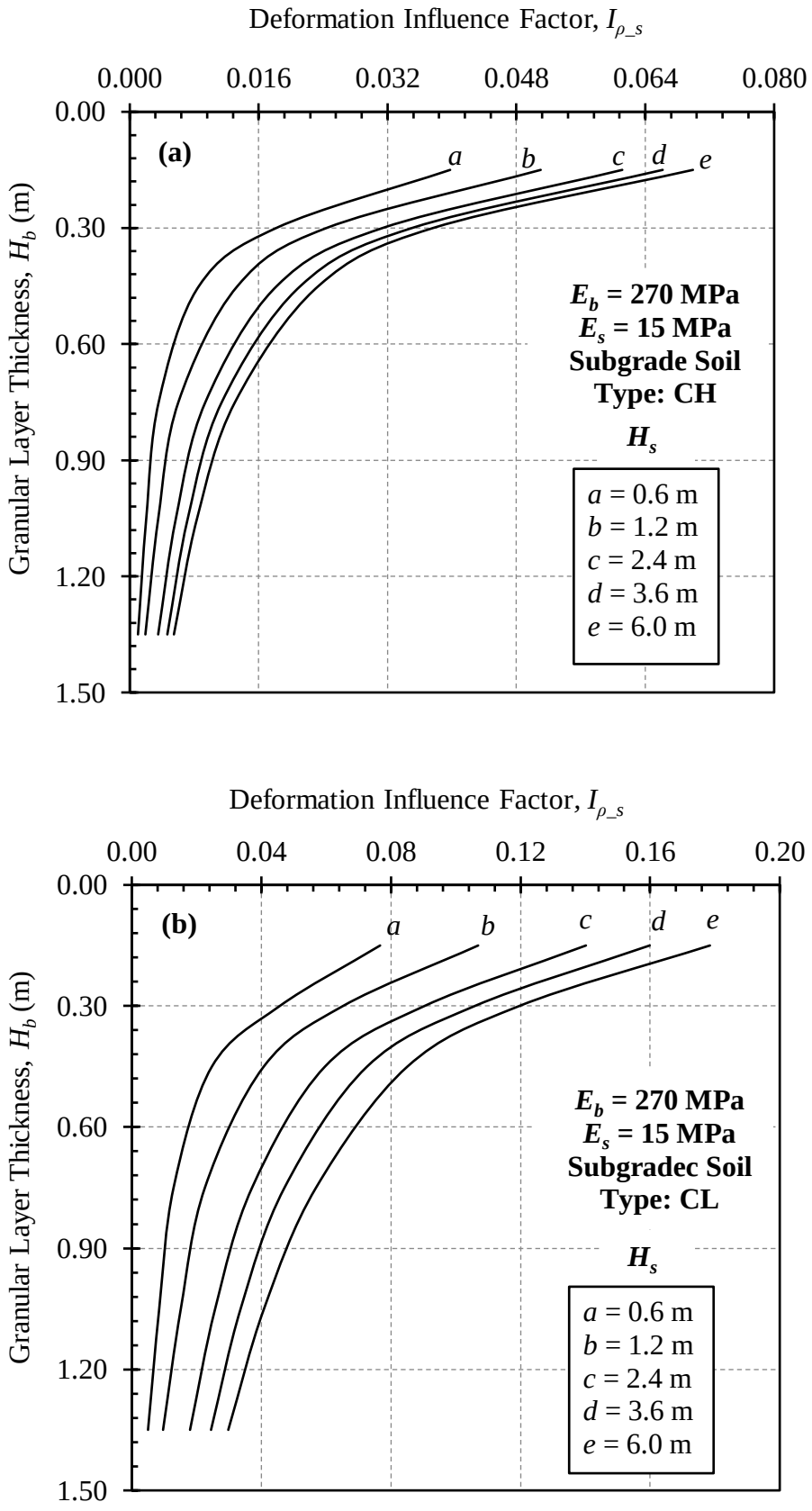

Figure 5.20 (a-b): Design charts to calculate granular layer thickness (for preventing excessive plastic deformation).

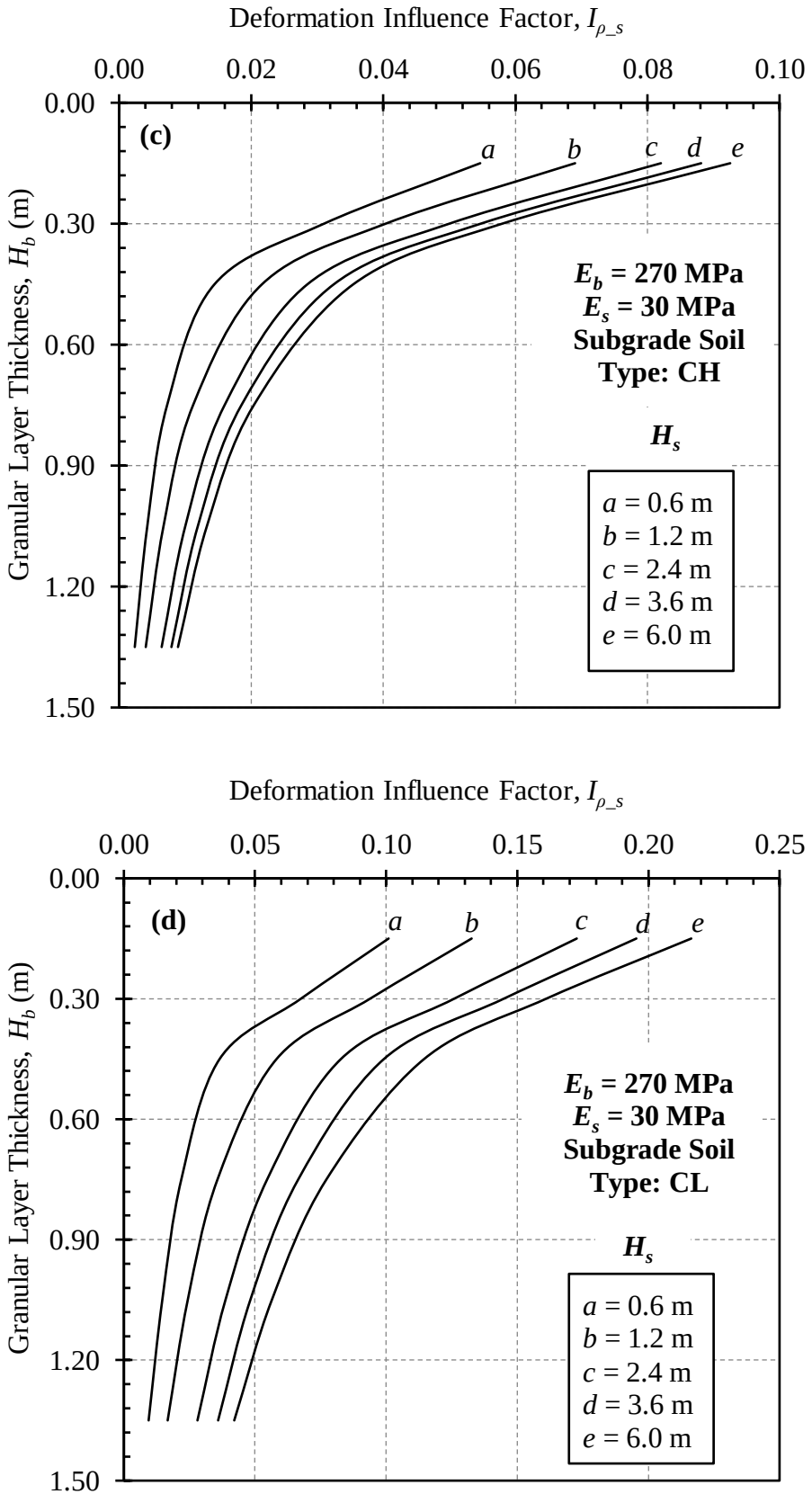

Figure 5.20 (c-d): Design charts to calculate granular layer thickness (for preventing excessive plastic deformation).

After determining $I_{(\rho\_s)a}$, the required granular layer thickness, H_b, can be obtained using the relevant design chart (e.g. Figure 5.20a), based on the specific data of ballast modulus, subgrade modulus, subgrade layer thickness and subgrade soil type. If the thickness obtained from the design chart is not equal to the initially assumed granular layer thickness, the steps of calculating ρ_b for the obtained thickness, $I_{(\rho\_s)a}$ and H_b should be repeated until the granular layer thickness considered in the calculation of ρ_b converges with the thickness obtained from the chart. The design procedures for calculating the H_b using these charts are described in detail below.

5.6 NEW DESIGN METHOD FOR RAILWAY TRACK FOUNDATIONS

This section presents the procedures of the new design method for selecting a granular layer thickness using the design charts developed in the previous section. Based on preventing failure criteria, the design method has two procedures. Out of the two design procedures, one is meant for preventing the progressive shear failure at the top subgrade surface, while the other is for preventing the excessive plastic deformation of the track. The design thickness of the granular layer is the maximum thickness obtained out of the two procedures. When the subgrade is very stiff and dynamic wheel load is low, the obtained design thickness might be very low and in such a case it is suggested to use a minimum thickness of granular layer of 0.45 m, including 0.15 m thick of sub-ballast.

5.6.1 Design Procedure for Preventing Progressive Shear Failure

The design procedure for preventing the progressive shear failure is based on limiting the cumulative plastic strain at the subgrade surface below a threshold value. As discussed previously, limiting the cumulative plastic strain is achieved automatically by limiting the deviatoric stress induced by the dynamic train moving loads. Earlier, Li and Selig (1998a, b) developed a design procedure for preventing this mode of track failure based on the above-mentioned principle; however, their method has several limitations which are discussed in detail in Chapter 2. The intention of the proposed design method is to overcome most of the current limitations of the Li-Selig method as well as other available design methods so as to provide a methodology that suits modern railway traffic.

Figure 5.21 demonstrates a flowchart for calculating the granular layer thickness needed to prevent the progressive shear failure. The flowchart has mainly four steps: (1) data collection and preparation; (2) determination of the allowable deviatoric stress; (3) determination of the allowable strain influence factor; and (4) selection of the granular layer thickness using the design charts. These steps are described below.

Step 1: In this step, the designer should collect and prepare the following information:

- **Loading condition**: This requires calculation of the design dynamic wheel load, P_d, and number of equivalent repeated application of design wheel load in the subgrade layer (N_s) for a design traffic tonnage. In order to establish the design dynamic wheel load, P_d, it is required to determine the dynamic amplification factor (DAF) corresponding to the train speed using a chart from *Appendix A* that best corresponds to the track-ground condition under consideration. It is also required to determine the wheel spacing factor (WSF) corresponding to the wheel spacing from Figure 4.13. The design dynamic wheel load, P_d, can then be estimated using Equation (5.6), and the number of load repetitions in the subgrade layer can be calculated using Equation (5.8). If there are some major groups of wheel loads, the corresponding groups of the dynamic wheel loads and numbers of repeated loads should be determined separately. Then Equations (5.9) and (5.12) have to be employed to determine the total number of equivalent load applications of the design wheel load.
- **Design criterion**: The design proceeds by selecting an acceptable level of the cumulative plastic strain at the subgrade surface, $\varepsilon_{(p\_s)a}$, for a certain number of repeated loads (i.e. for the design traffic tonnage).
- **Subgrade characteristics**: This requires selection of the subgrade soil type and determination of the monotonic strength of soil, σ_{s_s}, from the unconfined compressive strength (UCS) test and subgrade soil modulus, E_s, obtained from the cyclic triaxial compression test under 100 kPa confining pressure.

- **Granular material**: The mechanical properties of the granular materials in terms of ballast modulus, E_b, need to be determined from the cyclic triaxial compression test under 100 kPa confining pressure.

Step 2: The allowable deviatoric stress at the subgrade surface is determined in this step using the following equation, which is derived by rearranging Equations (5.4) and substituting $\sigma_{(d\_s)a}$ and $\varepsilon_{(p\_s)a}$ for $\sigma_{(d\_s)}$ and $\varepsilon_{(p\_s)}$, respectively:

$$\sigma_{(d\_s)a} = \left(\frac{\varepsilon_{(p\_s)a}}{aN_s^{\,b}} \right)^{\frac{1}{m}} \sigma_{s\_s} \times 100 \tag{5.21}$$

where, $\sigma_{(d\_s)a}$ is the allowable deviatoric stress at the subgrade surface; $\varepsilon_{(p\_s)a}$ is the allowable cumulative plastic strain at the subgrade surface needed to prevent the progressive shear failure; σ_{s_s} is the subgrade soil compressive strength; *a*, *m* and *b* are the material parameters pertinent to the subgrade soil type (Table 3.2); N_s is the total equivalent number of repeated applications of the design load obtained from Step 1.

Step 3: This step is needed to determine the allowable strain influence factor at the subgrade surface, using the following equation:

$$I_{(\varepsilon\_s)a} = \frac{\sigma_{(d\_s)a} \times A}{P_d} \tag{5.22}$$

where, $I_{(\varepsilon\_s)a}$ is the allowable strain influence factor based on the allowable deviatoric stress, $\sigma_{(d\_s)a}$, obtained from Step 2, and the design dynamic wheel load, P_d; and the area coefficient, A = 1 m^2.

Step 4: This step involves determination of the required granular layer thickness needed to prevent the progressive shear failure at the subgrade surface, as follows:

- Select a design chart from *Appendix B* (e.g. Figure 5.17) that best corresponds to the ballast modulus.
- Using the design chart, calculate the granular layer thickness corresponding to the allowable strain influence factor and modulus of subgrade soil.

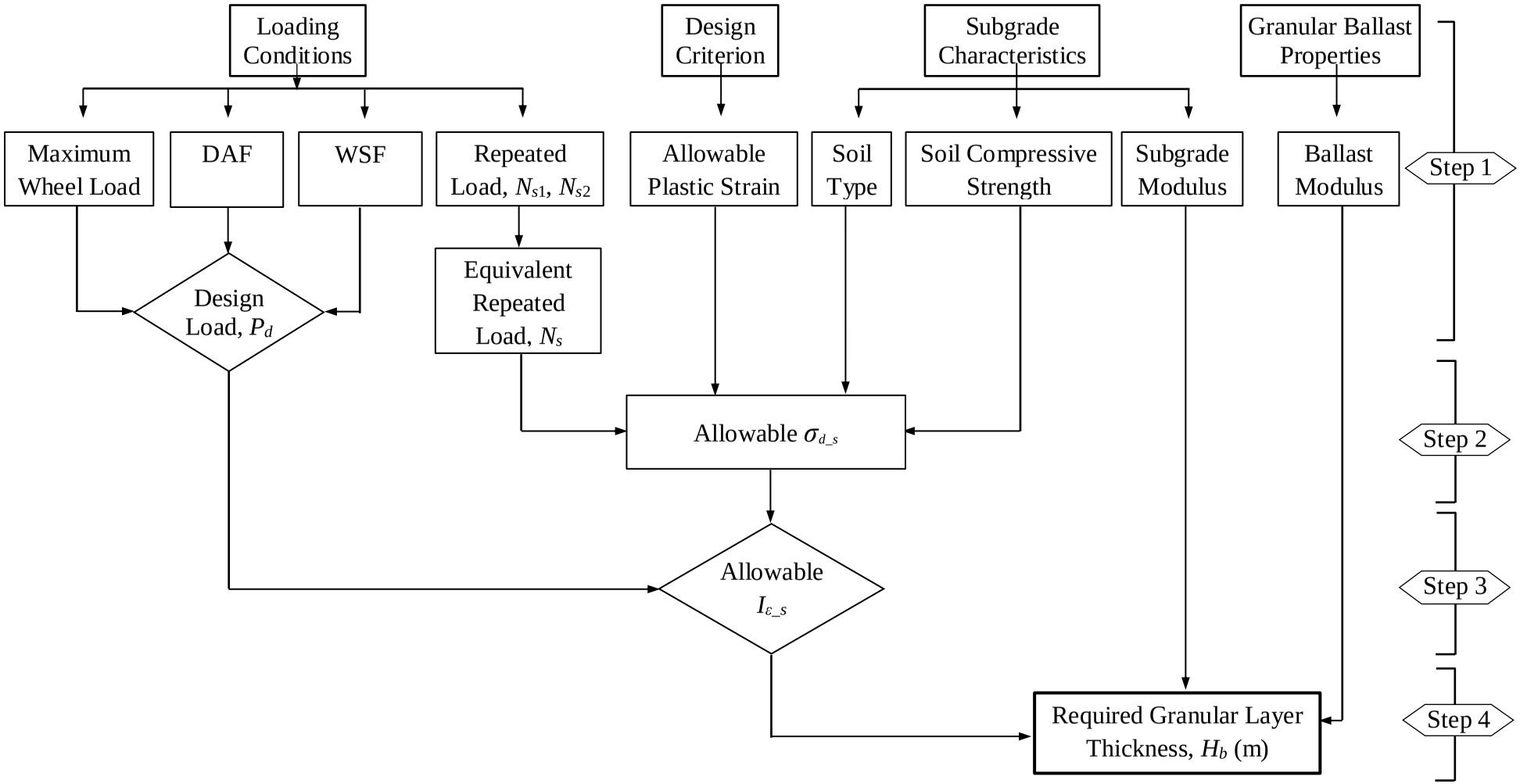

Figure 5.21: Flowchart for design procedure for preventing progressive failure.

5.6.2 Design Procedure for Preventing Excessive Plastic Deformation

A design procedure for preventing the excessive plastic deformation was also developed by Li and Selig (1998a, b). However, the design criterion of their method was limiting only the subgrade deformation, although about 40% of the total track deformation may come from the granular layer (Li et al., 2002; Stewart, 1982). In fact, Li-Selig design method has some other limitations, which are discussed in detail in Chapter 2.

The advantage of the current design method is that the design procedure proposed for preventing the excessive plastic deformation is based on the criterion of limiting the total plastic deformation that occurs in both the ballast and subgrade layers. According to this design procedure, a flowchart for calculating the granular layer thickness is presented in Figure 5.22. As it is difficult to assume the exact value of the granular layer thickness initially, this procedure provides an optimum granular layer thickness after several repetitions of Steps 2 to 4 as given below. The steps of the design procedure for preventing the excessive plastic deformation are as follows:

Step 1: Initially, the designer should collect and prepare the information required for design, including the information needed for the design procedure that prevent progressive shear failure, as presented in Section 5.6.1, and some other information such as the thickness of the deformable subgrade layer, H_s, ballast type, compressive strength of ballast at 50 kPa confining pressure, σ_{s_b}, and number of load repetitions in the ballast layer, N_b. The number of load repetitions in the ballast layer can be calculated using Equation (5.7). Similar to the load repetitions in the subgrade soil, if there are some major groups of wheel loads, the corresponding groups of the dynamic wheel loads and numbers of repeated loads should be determined separately. Equations (5.10) and (5.11) can be employed to determine the total number of equivalent repeated load applications of the design wheel load on the ballast layer. The design criterion for preventing the progressive shear failure (i.e. allowable plastic strain at the subgrade surface, $\varepsilon_{(p\_s)a}$) is substituted by enforcing the allowable total plastic deformation of the track substructure layers, ρ_{ta}, for this design procedure.

Step 2: This step is to determine the deformation of granular ballast layer as follows:

- Assume a granular layer thickness, H_b, equal to the granular layer thickness obtained from the design procedure used to prevent the progressive shear failure.
- Select a chart from *Appendix C* for estimating the distribution of dimensionless strain influence factor, I_{ε_b}, with depth in the granular ballast layer (e.g. Figure 5.19) that best corresponds to the modulus of ballast and subgrade, and the granular layer thickness.
- Determine the deformation of granular ballast layer, ρ_b, using Equation (5.17) based on the information obtained from Step 1, including the design dynamic wheel load, P_d, the total number of equivalent repeated load applications of the design wheel load in the ballast layer, N_b, material parameters of particular ballast type (x, y and z), granular ballast thickness, H_b, and distribution of the I_{ε_b} with ballast depth.

Step 3: This step is to determine the allowable subgrade deformation influence factor, $I_{(\rho\_s)a}$, using Equation (5.20) based on the information obtained from Steps 1 and 2.

Step 4: Finally, determine the required granular layer thickness, H_b, needed to prevent the excessive plastic deformation of the track as follows:

- Select the design chart from *Appendix D* (e.g. Figure 5.20a) that best corresponds to the ballast modulus, existing soil type and soil modulus.
- Calculate the granular layer thickness, H_b, corresponding to the allowable subgrade deformation influence factor and thickness of the deformable subgrade layer using the selected design charts.
- Compare the design thickness obtained in this step with the thickness assumed in the calculation of the granular layer deformation in Step 2. If the obtained thickness from Step 4 is not equal to the assumed thickness, then repeat Steps 2-4 until the assumed H_b converges with the design thickness obtained in Step 4. In each iteration, the calculated thickness can be assumed for the next iteration to achieve faster convergence.

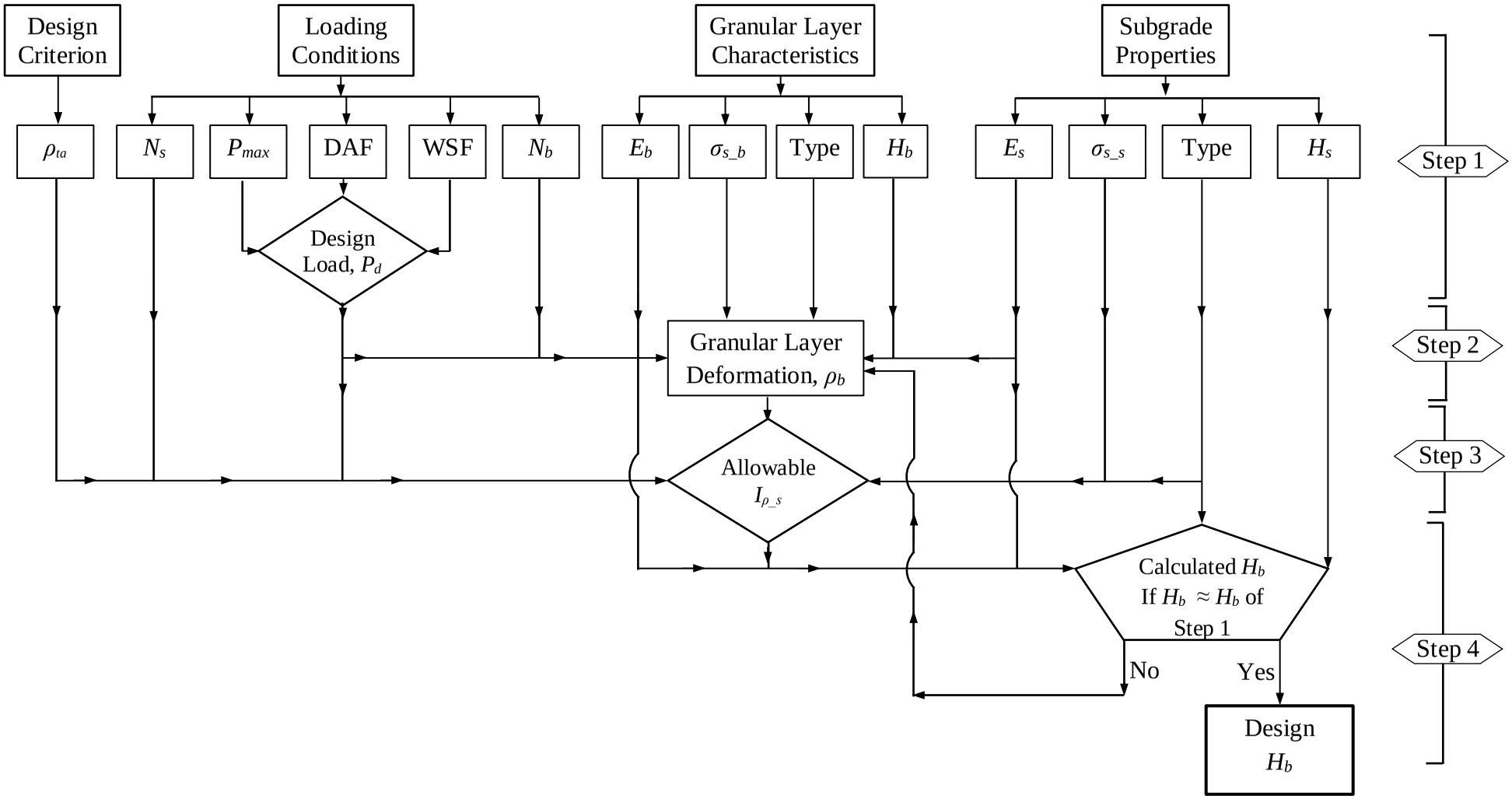

Figure 5.22: Flowchart of design procedure for preventing excessive track deformation.

5.7 DESIGN EXAMPLES

In this section, the new design method for ballasted railway track foundations is applied to two case studies of test tracks constructed on fat clay type subgrade. The test tracks are the Association of American Railroads (AAR) low track modulus (LTM) and trial low track modulus (LTLM) (Li and Selig, 1998b). Detailed description of these two case studies will be presented later in Section 5.8, and the information needed for design of their ballasted tracks are compiled in Table 5.1.

Table 5.1: Design parameters for the LTM and TLTM test tracks (Li et al., 1996).

Design Parameters	**LTM**	**TLTM**
Loading Condition		
Static Wheel Load, P_s	173 kN	173 kN
Wheel Spacing	1.8 m	1.8 m
Train Speed, C	18 m/s	18 m/s
Design Tonnage	60 MGT	60 MGT
Design Criteria		
Cumulative Plastic Strain, $\varepsilon_{(p\_s)a}$	2%	2%
Cumulative Plastic Deformation, ρ_{ta}	25 mm	25 mm
Subgrade Characteristics		
Soil Type	Fat clay (CH)	Fat clay (CH)
Thickness, H_s	1.5 m	1.5 m
Subgrade Modulus, E_s	15 MPa	41 MPa
Unconfined Compressive Strength, σ_{s_s}	90 kPa	165 kPa
Ballast Characteristics		
Ballast Type (assumed)	Granite (G)	Granite (G)
Ballast Modulus, E_b	270 MPa	270 MPa
Compressive Strength, σ_{s_b}	307 kPa	307 kPa

5.7.1 Design Procedure for Preventing Progressive Shear Failure

Step 1: At first, the information needed for design of ballasted railway track foundations (i.e. loading condition, design criteria, ballast and subgrade material characteristics) are obtained and listed in Table 5.1.

For a track-ground condition particular to this case study, Chart A4 (from *Appendix A*) is selected, which yields a value of 1.04 for DAF corresponding to the train speed. The value of WSF corresponding to a wheel spacing of 1.8 m is found to be 1.38 obtained from Figure 4.13. From Equation (5.6), the design dynamic wheel load, P_d, is calculated to be 250 kN. The equivalent number of load repetitions in the subgrade layer is determined using Equation (5.8) to be N_s = 386,000.

Step 2: Considering the appropriate respective design parameters and number of load repetitions, N_s, obtained in Step 1, the allowable deviatoric stress at the subgrade surface, $\sigma_{(d\_s)a}$, is calculated using Equation (5.21) to be 41 kPa and 76 kPa for the LTM and TLTM tracks, respectively.

Step 3: For the LTM and TLTM tracks, the allowable strain influence factors corresponding to the allowable deviatoric stresses, $\sigma_{(d\_s)a}$, and design dynamic wheel load, P_d, are determined using Equation (5.22) to be I_{ε_s} = 0.16 and 0.31, respectively.

Step 4: The design chart B2 from *Appendix B* is selected as it corresponds to ballast modulus E_b = 270 MPa, for both the LTM and TLTM tracks (see Figure 5.23). The required granular layer thickness for the LTM track needed to prevent the progressive shear failure is determined for I_{ε_s} = 0.16 and E_s = 15 MPa, and is found to be H_b = 0.53 m. Similarly, using the same design chart, the required granular layer thickness for the TLTM track (I_{ε_s} = 0.31, E_s = 41 MPa and E_b = 270 MPa) is found to be H_b = 0.40 m.

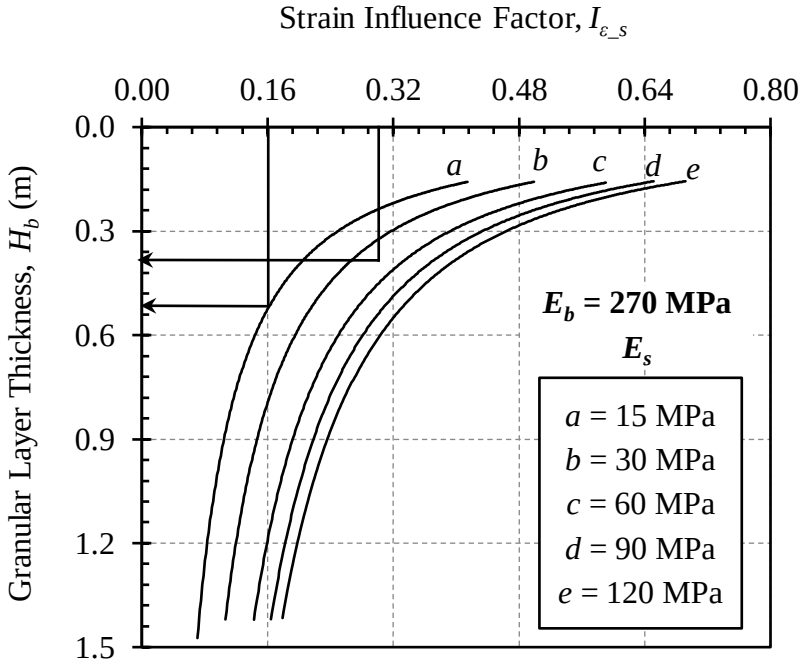

Figure 5.23: Design chart to calculate the granular layer thickness (for preventing progressive shear failure -Chart B2 from *Appendix B*).

5.7.2 Design Procedure for Preventing Excessive Plastic deformation

Step 1: This step is similar to Step 1 of the design procedure for preventing the progressive shear failure. Therefore, the design dynamic wheel load is obtained to be P_d = 250 kN; and equivalent number of load repetitions in the subgrade is considered to be N_s = 386,000. Moreover, the number of load repetitions in the ballast layer is determined using Equation (5.7) to be N_b = 772000.

Step 2: At first, the granular layer thickness is assumed to be equal to the thickness obtained from the design procedure for preventing the progressive shear failure (i.e. H_b = 0.53 m for the LTM track and H_b = 0.40 m for the TLTM track).

For the LTM track (E_b = 270 MPa, H_b = 0.53 m and E_s = 15 MPa), the distribution of the dimensionless strain influence factor, I_{ε_b}, with the ballast depth is obtained from charts C7 and C8 from *Appendix C*. Afterwards, for the granite ballast (assumed), σ_{s_b} = 307 kPa, P_d = 250 kN and N_b = 772,000, the deformation of the granular ballast layer, ρ_b, is determined using Equation (5.17) to be 0.011 m. Similarly, for the TLTM track (E_b = 270 MPa, H_b = 0.40 m and E_s = 41 MPa), the

dimensionless strain influence factor, I_{ε_b}, with ballast depth is obtained from charts C6 and C7 of *Appendix C*. Afterwards, the deformation of the ballast layer is determined using Equation (5.17) to be 0.006 m.

Step 3: For the LTM track loading and subgrade conditions (P_d = 250 kN, N_s = 386000, CH type subgrade and σ_{s_s} = 90 kPa) and design criterion ρ_{ta} = 0.025 m, the allowable subgrade deformation influence factor, $I_{(\rho\_s)a}$, is obtained to be 0.01 from Equation (5.20). Likewise, for the TLTM track, the allowable subgrade deformation influence factor is obtained by Equation (5.20) to be $I_{(\rho\_s)a}$ = 0.06 for P_d = 250 kN, N_s = 386000, CH type subgrade and σ_{s_s} = 165 kPa.

Step 4: To determine the design thickness, the chart D21 from *Appendix D* (see Figure 5.24) is selected which best corresponds to the LTM track substructure conditions (E_b = 270 MPa, E_s = 15 MPa and CH soil). From this chart, the required granular layer thickness corresponding to the deformable subgrade layer, H_s = 1.5 m and $I_{(\rho\_s)a}$ = 0.01 obtained in Step 3, is found to be H_b = 0.66 m. As the obtained thickness is not equal to the assumed thickness (i.e. $H_b \neq H_b$ of Step 1), Step 2 (i.e. calculation of granular ballast deformation, ρ_b) is repeated considering the granular ballast thickness obtained in Step 4 (H_b = 0.66 m). Following several repetitions of Steps 2-4, the granular layer thickness for the LTM track is obtained to be H_b = 0.70 m.

Similarly, for the TLTM track (E_b = 270 MPa, E_s = 41 MPa and CH soil), Figure 5.25 is selected from *Appendix D*. Employing the selected design chart, the required granular layer thickness is determined corresponding to the deformable subgrade layer, H_s = 1.5 m and $I_{(\rho\_s)a}$ = 0.06 to be H_b = 0.25 m. Again, as the obtained $H_b \neq H_b$ of Step 1, Steps 2-4 are repeated. Finally, the required granular layer thickness needed to prevent the excessive plastic deformation is obtained to be H_b = 0.30 m.

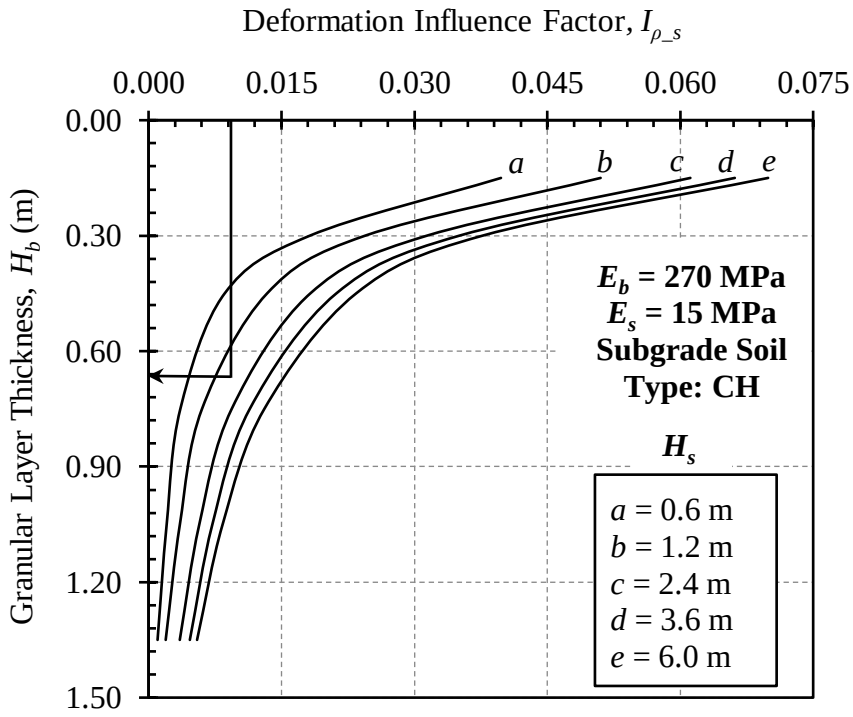

Figure 5.24: Design chart to calculate the granular layer thickness (for preventing excessive plastic deformation -Chart D21 from *Appendix D*).

5.7.3 Design Thickness for LTM and TLTM Tracks

For the LTM track, the granular layer thickness required to prevent the excessive plastic deformation (H_b = 0.70 m) is higher than that needed to prevent the progressive shear failure (H_b = 0.53 m). Thus, the design thickness is the maximum of the two obtained results, i.e. H_b = 0.70 m. On the other hand, for the TLTM track, the granular layer thickness required to prevent the excessive plastic deformation (H_b = 0.30 m) is less than that needed to prevent the progressive shear failure (i.e. H_b = 0.40 m). Hence, the design thickness is H_b = 0.40 m.

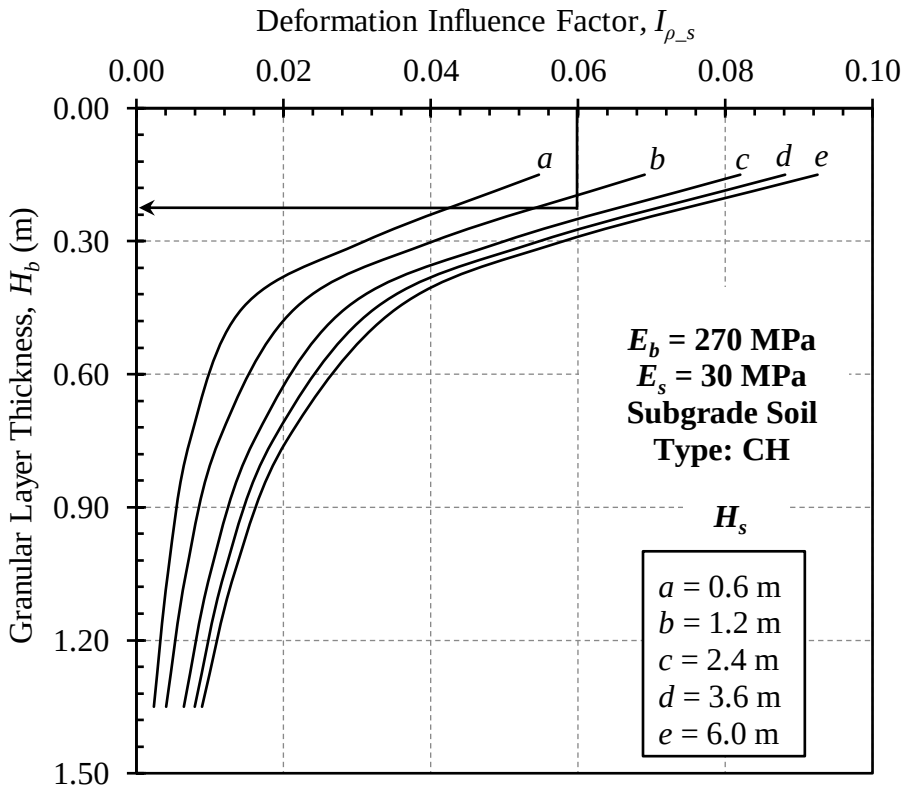

Figure 5.25: Design chart to calculate the granular layer thickness (for preventing excessive plastic deformation -Chart D25 from *Appendix D*).

5.8 COMPARISONS BETWEEN PROPOSED DESIGN METHOD AND FIELD RESULTS

To validate the proposed design method, comparisons between the results of the design method and field results for some well documented case studies found in the literature are presented below.

5.8.1 LTM and TLTM Tracks

In 1991, a 183 m long low track modulus (LTM) test track was built on a fat clay type subgrade at the Association of American Railroads (AAR) Heavy Tonnage Loop (HTL) in Pueblo, Colorado. Prior to the construction of the LTM, a 30 m long trial low track modulus (TLTM) track was constructed to examine the practicality of building a longer LTM track. The key objective of constructing the LTM test track was to investigate the impact of the soft subgrade on the track performance under repeated heavy axle train (HAT) moving loads (Li and Selig, 1996).

The subgrade soil at the Pueblo test track site was originally silty sand, which does not represent a soft subgrade soil. To construct a track on soft subgrade soil, a 3.66 m wide and 1.5 m deep trench was dug in the natural subgrade and filled with the Mississippi buckshot clay (*LL* = 60-70, *PI* = 40-45). The cross-section of the test track and subgrade is shown in Figure 5.26.

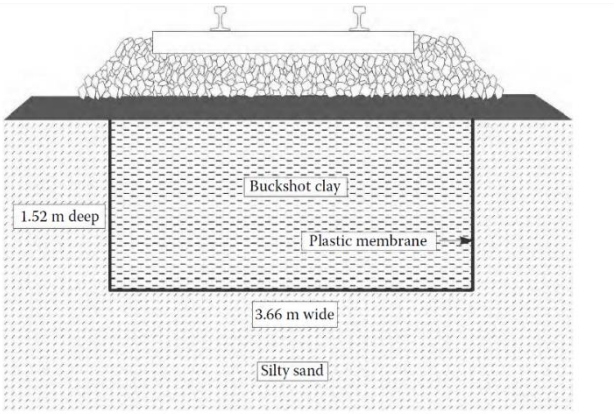

Figure 5.26: Cross-section of the LTM and TLTM test track (Li and Selig, 1996).

To achieve a subgrade of low stiffness, the filled material within the trench was compacted at a particularly high water content (30%) and a specific dry density (90% of its maximum dry density, whereas according to ASTM D698 the maximum dry density was 14.91 kN/m^3). Although the water content for both the LTM and TLTM subgrades was targeted to be 30%, the average water content in the LTM and TLTM subgrades were actually 33% and 29%, respectively (Li and Selig, 1996). Hence, the corresponding unconfined compressive strength of subgrade soil was about 90 kPa for the LTM track subgrade and 166 kPa for the TLTM track subgrade. The relevant soil modulus of the LTM track subgrade was varied from 14 MPa to 21 MPa, while it was in the range of 41-55 MPa for the TLTM track subgrade. The differences between these two track sites were their subgrade modulus and unconfined compressive strength (see Table 5.1). Accordingly, it is expected that the design thickness for the LTM and TLTM tracks will be different. Based on the proposed design method for preventing the progressive shear failure (i.e. $\varepsilon_{(p\_s)a} \leq$ 2%) and for preventing the excessive plastic deformation (i.e. $\rho_{ta} \leq$ 0.025 m), the required granular layer thickness for the LTM and TLTM tracks are determined to be H_b = 0.70 m and 0.40 m, respectively, as calculated earlier in Section 5.7.

In reality, during the construction of both the LTM and TLTM tracks, a granular layer of 0.45 m thickness (0.30 m ballast and 0.15 m sub-ballast) was adopted based on an assumption of a 30% water content in the subgrade soil and a minimum density of 90% of the standard maximum dry density. Afterwards, the track responses in these sites were measured and the subgrade conditions were evaluated experimentally, which now provide an excellent opportunity to assess the proposed design method.

From the field measurement of track performance, it was found that the LTM track with the adopted granular layer thickness of 0.45 m was unable to bear the HAL for the design traffic of 60 MGT, and thus had more difficulty in sustaining the required track surface geometry. The LTM track subgrade suffered rapid progressive shear failure and excessive plastic deformation. Therefore, the test track needed frequent rail lifting by ballast tamping. Figure 5.27 shows the cumulative track settlement with traffic load for the LTM track. It can be seen that the track actually required frequent ballast tamping and surfacing (rail lift up) following 12.4 MGT, and finally, the traffic along the track had to be stopped after approximately 62.3 MGT and the test track was then rebuilt. On the other hand, the TLTM track with the same granular layer thickness of 0.45 m was able to carry the HAL for the design traffic of 60 MGT without any track failure. Consequently, no track maintenance was invoked during the design life of this track.

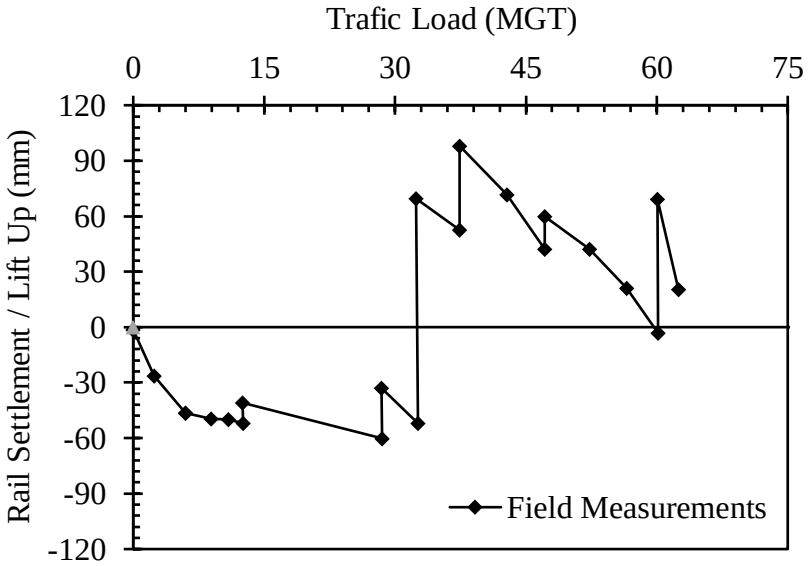

Figure 5.27: Average settlement / lift up of rail with traffic in the LTM test track (Li, 1994).

A comparison between the originally adopted H_b and obtained design H_b (see Table 5.2) indicates that the adopted thickness for the LTM track (0.45 m) was much lesser than the required 0.70 m thickness, but the adopted thickness for the TLTM track (0.45 m) was higher than the required thickness (0.40 m). Therefore, the LTM track was unable to maintain the track geometry and invoked maintenance, whereas the TLTM track was able to sustain the required track geometry without any maintenance. In other words, the proposed design method has successfully predicted the failure of the LTM track and success of the TLTM track. These are extremely encouraging results for the proposed design method.

Table 5.2: Design results and track conditions for the LTM and TLTM test tracks.

Comparison Parameters	**LTM**	**TLTM**
Unconfined Compressive Strength, σ_{s_s} (kPa)	90	165
Subgrade Modulus, E_s (MPa)	14	41
Adopted Granular Layer Thickness, H_b (m)	0.45	0.45
Required Granular Layer Thickness, H_b (m)	0.70	0.40
Track Condition with the Adopted Granular Layer Thickness	Track excessive plastic deformation and progressive shear failure	No track failures

As an additional validation tool, the actual LTM track-subgrade condition shown in Figure 5.26 with 0.45 m granular layer thickness is simulated using the 3D FE modelling and the distribution of strain influence factor with depth in the ballast and subgrade layers is obtained. Then, the cumulative vertical track deflection for the ballast and subgrade layers at different traffic loads is computed using Equation (5.16) and the results obtained from the 3D FE modelling. The cumulative track deflection is plotted against the traffic load in MGT and compared with the field results available in the literature (Li and Selig 1996), as shown in Figure 5.28. It can be clearly seen that good agreement exists between the FE predictions and field measurements, which confirms that the FE modelling process and improved empirical models for predicting the cumulative plastic deformation of ballast and subgrade adopted in this study are reliable and can be used with confidence to predict the railway track behaviour. In other words, it can be stated that the design

method developed in this study based on the combined FE modelling and improved empirical models is reliable.

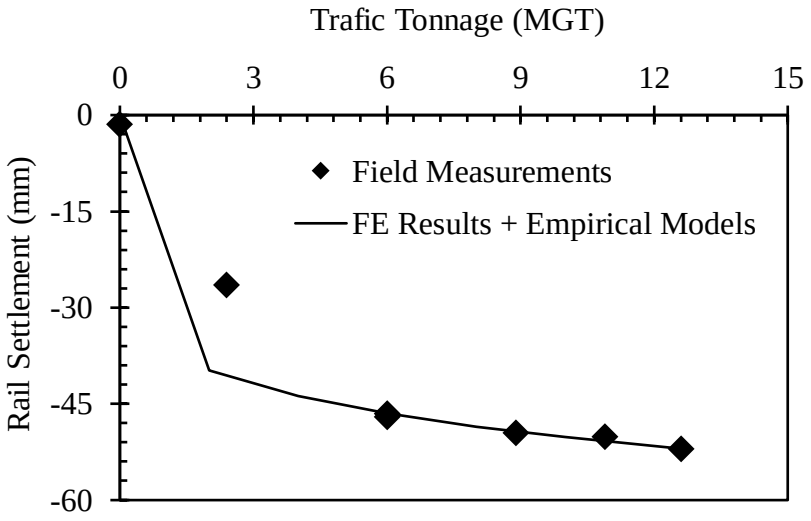

Figure 5.28: Comparison between the combined use of FE model together with extensive laboratory experiment and field measurements.

5.8.2 Edgewood and Aberdeen Sites

Another two case studies of real track sites on the Northeast Corridor (NC) between Baltimore and Philadelphia are studied herein to compare the results of the proposed design method and field results. One of the two sites is located in Edgewood, Maryland, and the other site is in Aberdeen, Maryland, some 16 km apart from the Edgewood site. The track in Edgewood site suffered frequent bouts of differential settlements over a distance of approximately 10 km. This track site needed frequent maintenance by ballast tamping at least twice a year. Moreover, remedy measures such as application of geotextiles and lime slurry injection were taken since 1984; however, such remedies were not fruitful. For the other site in Aberdeen, only a small portion of the track (about 60 m long) suffered a problem of mud pumping; however, the geometry deterioration was not a concern (Li and Selig, 1998b).

To investigate the key reasons for the track failures at both sites, the loading characteristics and material properties were studied in 1994 by Li and Selig (1994a). Based on the information available in the literature, the minimum required granular layer thickness for both sites are determined using the current proposed design method. At the Edgewood site, the subgrade soil was lean clay (LC) with unconfined

compressive strength of approximately 48-83 kPa. On the other hand, the subgrade soil at the Aberdeen site was also lean clay but its unconfined compressive strength was in the range of 97-290 kPa. The subgrade soil properties and other information required for design of both sites are given in Table 5.3.

Table 5.3: Design parameters for the tracks in Edgewood site and Aberdeen site (Li and Selig, 1998b).

Design Parameters	**Edgewood Site**	**Aberdeen Site**
Subgrade Characteristics		
Soil type	Lean clay (CL)	Lean clay (CL)
Thickness, H_s	1.5 m	1.5 m
Subgrade Modulus, E_s	15 MPa	30 MPa
Unconfined Compressive Strength, σ_{s_s}	48-83 kPa	97-290 kPa
Ballast Characteristics		
Ballast Type	Granite (G)	Granite (G)
Ballast Modulus, E_b	270 MPa	270 MPa
Compressive Strength, σ_{s_b}	307 kPa	307 kPa
Design Criteria		
Cumulative Plastic Strain, $\varepsilon_{(p\_s)a}$	2%	2%
Cumulative Plastic Deformation, ρ_{ta}	25 mm	25 mm

As both sites were parts of the NC and not far away from each other, the traffic was the same. The traffic along the NC track was mixed (50% passenger trains and 50% freight trains). Table 5.4 gives the loading characteristics used for design of these two tracks. As the traffic was mixed, the number of equivalent load applications in the ballast and subgrade layers is determined using Equations (5.7-5.12).

Table 5.4: Traffic characteristics along the NC (Li and Selig, 1998b).

Loading Condition	**Static Wheel Load (kN)**	**Design Tonnage (MGT)**	**Speed (km/h)**	**Wheel Spacing**
Freight Train				
Wheel 1	156	150	60	2.2
Wheel 2	44	270	60	2.2
Passenger Train				
Wheel 1	70	150	190	2.9

Based on the design criteria of preventing the progressive shear failure (i.e. $\varepsilon_{pa} \leq$ 2%) and for preventing the excessive plastic deformation (i.e. $\rho_{ta} \leq 0.025$ m), the required granular layer thickness for the Edgewood site is determined to be H_b = 1.08 m and 1.16 m, respectively. So the design thickness for this site should be $H_b \approx$ 1.2 m. However, the actual granular layer thickness at the Edgewood site was varied from 0.30 to 0.50 m (from the cone penetration tests and cross trench measurements of the track site) (Li and Selig, 1994a). This thickness is significantly less than the design thickness of 1.2 m required to reduce the dynamic train induced stresses transmitted to the subgrade below the allowable value needed to prevent the progressive shear failure and excessive plastic deformation. As a result, it is not surprising that the track of this site suffered a significant progressive shear failure at the subgrade surface and also deep ballast pockets occurred expectedly. Moreover, the non-uniform compressive strength of the subgrade (48 kPa to 83 kPa) caused excessive differential track settlement.

For the Aberdeen site, the required granular layer thickness calculated from the proposed design method should be H_b = 0.66 m for preventing the progressive shear failure and H_b = 0.60 m for preventing the excessive plastic deformation. Therefore, the design thickness of this site should be $H_b \approx$ 0.70 m. From the field measurement, the actual granular layer thickness at this site was varied between 0.70 and 1.0 m, which is equal or larger than the required design thickness needed to prevent the progressive shear failure and excessive plastic deformation. As the dynamic train induced stresses in the subgrade were lower than the allowable value, this track was able to carry the design load without any geometry deterioration. Comparison of the design thickness obtained from the proposed design method with the actual thickness at both the Edgewood and Aberdeen sites is summarised in Table 5.5, which also includes the track conditions for both sites. Evidently, the design results are again consistent with the field observations and test results performed by Li and Selig (1994a).

Table 5.5: Comparison of design thickness with the existing thickness and the track conditions.

Comparison Parameters	Edgewood Site	Aberdeen Site
Design Thickness, H_b (m)	1.20	0.70
Existing Thickness, H_b (m)	0.3-0.5	0.70-1.0
Remark	Existing thickness is less than design thickness.	Existing thickness is more than design thickness.
Track Condition with the Adopted Thickness	Subgrade progressive shear failure, deep ballast pocket and differential settlement	No track failures

5.9 SUMMARY AND CONCLUSIONS

Determination of the granular layer thickness of railway tracks is required to prevent both the progressive shear failure at the subgrade surface and excessive plastic deformation of the track. The design criterion to prevent the progressive shear failure at the top surface of subgrade is to limit the excessive cumulative plastic strain. On the other hand, the design criterion to avoid the excessive plastic deformation in the track is to limit the total plastic deformation accumulated by all the ballast and subgrade sublayers. The basis of limiting the cumulative plastic strain or deformation below a tolerable level is placing an adequate granular thickness to limit the deviatoric stress transmitted to the subgrade below a tolerable level. Therefore, transmission and distribution of the deviatoric stresses in the granular layer and subgrade layer were investigated in the current study using sophisticated 3D FE modelling subjected to train moving loads under various track-ground conditions. The parameters considered included the modulus and thicknesses of ballast and subgrade as well as train loadings. From the deviatoric stress analyses, the following conclusions are drawn:

- Along the rail, the maximum deviatoric stress in the ballast surface and subgrade surface occur below the sleeper rather than the crib. Besides, the maximum deviatoric stress at any depth below the sleeper bottom occurs at the sleeper end. Therefore, for design purposes, the deviatoric stress in the ballast and subgrade layers should be measured below the sleeper end.

- The deviatoric stress distribution in the ballast layer is affected significantly by the modulus of the ballast and subgrade. The maximum deviatoric stress occurs in the ballast surface, both for stiffer ballast and soft subgrade condition. Moreover, with the increase of ballast modulus and decrease of the subgrade modulus, the effect of stress spreading in the ballast layer increases, and vice versa.
- The deviatoric stress distribution in the subgrade layer is also influenced by the modulus of the ballast and subgrade. Increasing the ballast modulus decreases the deviatoric stress at the subgrade surface regardless of subgrade condition; however, the difference in the deviatoric stress at any depth below the sleeper bottom decreases with depth and becomes almost negligible at 6 m depth for the soft subgrade condition. In contrast, the difference in the deviatoric stress at each depth of the subgrade layer (due to different ballast modulus) does not decrease significantly with depth in the stiff subgrade. Besides, the higher deviatoric stress occurring at the subgrade surface increases with the increase of the subgrade stiffness; however, the difference in the deviatoric stress at any depth below the sleeper bottom reduces with depth.
- Increasing the granular layer thickness decreases the distribution of deviatoric stress in the subgrade layer by two ways. Firstly, with the increase in the granular layer thickness, the distance of the subgrade surface below the sleeper bottom increases. This causes an automatic reduction in the deviatoric stress at the subgrade surface. Secondly, an increase in the granular thickness increases the stress spreading effect due to its higher stiffness, which results in a reduction in the deviatoric stress at any depth in the subgrade.
- The distribution of deviatoric stress in the subgrade layer is not influenced by the thickness of the subgrade layer.
- The deviatoric stress at any depth below the sleeper (in both the ballast and subgrade layers) increases proportionally with the increase of the wheel load regardless of the subgrade condition. This allows representation of the results by a normalised stress or strain influence factor.

The development process followed for the new design method and associated design charts are discussed in detail in Sections 5.5 and 5.6, respectively. The main design parameters considered in the design method included the dynamic amplification factor, wheel spacing factor, traffic tonnage in million gross tonnes (MGT), modulus of granular materials and subgrade soil, types of ballast and subgrade soil, and compressive strength of ballast and subgrade. The design method developed in this study was examined against four track sites that contain detailed field measurements reported in the literature. The design results were found to be consistent with the field observations. The design methodology presented in this thesis was able to overcome most shortcomings of the available design methods and it is thus believed to provide excellent outcomes. However, further verification through more field practices is still highly desirable. To facilitate the use of the developed design method by practitioners, a user friendly computer program will be developed in the near future and will be made available upon request.

CHAPTER 6

SUMMARY, CONCLUSIONS AND RECOMMENDATIONS

6.1. SUMMARY

This thesis proposed improvements to the existing empirical models for better estimation of cumulative plastic strain or deformation of granular materials, and investigated and quantified the dynamic response of railway track under various train-track-ground conditions using sophisticated three-dimensional (3D) finite element (FE) modelling. The research results provide a better understanding of the impact of several parameters pertinent to the train-track-ground system on the track performance. Based on combined use of the improved empirical models and results obtained from the numerical modelling, a new design method for railway track foundations was developed. The merit of the design method is that the design thickness can prevent both the subgrade progressive shear failure and excessive plastic deformation of tracks, and it has overcome most limitations of the existing design methods. The outcomes of the investigations were synthesised into a set of design charts, which facilitate the use of the design method by railway engineers for routine design practice. In the section that follows the key observations from each chapter are summarised in a sequential order.

Chapter 2 presented a brief overview of the different components of ballasted railway track structure, reasons of various types of track substructure failure and possible remedial measures. Various methods of loading and stress analysis of railway track, including empirical, analytical and numerical methods were also included in this chapter. It was identified that among the different analysis methods available in the literature, numerical FE modelling can accurately simulate the boundary value problems associated with railway tracks under dynamic loading of moving trains. The basis of some of the most commonly used design methods of railway track foundations and their applicability in some real sites were also described. It was established that existing design methods are not suitable for tracks with modern train traffics and new methods are urgently needed. In the final part of this chapter, the limitations of existing design methods and missing critical factors

were discussed. The most important factors that were defined to develop an advanced design method include: (1) deformation of both the granular ballast and subgrade layers; (2) stress analysis that can accurately simulate the true train moving loads; (3) determination of the dynamic amplification factor (DAF) and critical speed corresponding to the train-track-ground condition; and (4) effect of the wheel spacing.

In Chapter 3, an improved empirical model was proposed for better estimation of the cumulative plastic strain of granular ballast materials. The model was based on extensive test results reported in the literature. The effect of the most important influence factor (i.e. deviatoric stress) on the relationship between the cumulative plastic strain and number of load applications was explicitly considered in the model. In addition, the ballast physical state as defined by the void ratio, gradation, moisture content and ballast structure was introduced implicitly by translating all these parameters into the ballast monotonic strength in triaxial compression test. The proposed empirical model requires certain material parameters according to the type of ballast used. Default values were suggested for three types of ballast, namely basalt, granite and dolomite in the absence of test results, which were determined by regression analysis of test results available in the literature. Comparison between the predicted and available test results from the literature indicated that the proposed model is valid in accounting for the influence of the defined major factors. In the proposed model, the deviatoric stress was found to be the most significant factor that affects the straining actions within the railway track system. Therefore, it was decided to obtain the stress behaviour of ballast and subgrade from a sophisticated 3D FE numerical modelling for the development of an advanced design method for ballasted railway track foundations.

In Chapter 4, a sophisticated 3D FE numerical modelling was developed to simulate the dynamic response of ballasted railway tracks subjected to train moving loads. It was shown that the developed FE modelling process successfully predicts the field measurements documented in two credible case studies available in the literature. The obtained results confirmed that the FE modelling were indeed reliable and can be applied with confidence to simulate the behaviour of ballasted railway track foundations, for both the quasi-static and dynamic loading conditions. This chapter

also presented results of a comprehensive parametric study that was carried out to investigate the track responses over a wide range of track parameters, including the modulus and thickness of ballast, sub-ballast and subgrade materials. Additional FE analyses were also performed to investigate the impact of the train speed on the behaviour of ballasted railway track foundations and to evaluate the critical speed under various conditions of the train-track-ground system. Chapter 4 yielded the following specific findings:

- The subgrade modulus is the most dominant factor that influences the overall track performance. A decrease in the subgrade modulus significantly affects the track responses in terms of the rail deflection, ballast and sub-ballast surface vertical stresses, subgrade surface strain and track stiffness. This clearly indicates why regular maintenance remains a critical issue for tracks built on soft subgrades.
- In general, the dynamic response of tracks in term of sleeper deflection increases with the increase in train speed; it reaches its maximum value at the critical speed before it decreases with further increase in the train speed.
- As the stiffness of underlying hard rock can be significantly greater than that of the subgrade soil, the critical speed is higher than both the Rayleigh wave and shear wave velocities of the top subgrade soil.
- The evolution of sleeper deflection with train speed indicates that when the train speed exceeds 75% of the critical speed, the amplitude of the track dynamic response increases dramatically. Therefore, 75% of the critical speed may be conservatively assumed as the practical speed limit of ballasted railway tracks.
- The train speed induces significant vibrations at the track centre, which extends with less magnitude in the transverse direction from the track centre to a distance equal to about 8 m. This phenomenon can cause detrimental impact on the train-track-ground system and nearby structures, which is especially true in the case of critical speed.
- Due to the stress-strain nonlinearity of substructure materials, slightly greater downward deflections occur in the nonlinear subgrade track than those of a linear subgrade track. However, the impact of nonlinearity of the substructure materials on the critical speed is almost negligible.

- The subgrade stiffness and thickness have a significant influence on both the DAF and critical speed of the train-track-ground system. The DAF is a decreasing function of both the subgrade stiffness and thickness. On the other hand, the magnitude of the critical speed increases with the increase in the subgrade stiffness and decrease with the increase in the subgrade thickness.
- The ballast stiffness and thickness have little or no influence either on the DAF or the critical speed of the train-track-ground system.
- The critical speed of the train-track-ground system is independent of the train loading amplitude; conversely, the critical speed is significantly influenced by the train loading geometry.
- At the critical speed condition, the carriage passing frequency of any particular train is equal to the natural frequency of the train-track-ground system.

In Chapter 5, a new method for design of railway track foundations was developed in the form of easy-to-use design charts. The two most common track failures, namely the subgrade surface progressive shear failure and excessive plastic deformation of the track were taken into account in the proposed design method. Specifically, two design criteria were set to prevent these track failures. The design criterion for preventing the progressive shear failure aims at limiting the cumulative plastic strain below a tolerable level while the criterion for preventing the excessive track deformation aims at limiting the total plastic deformation of the track substructure layers below another tolerable level. The basis of limiting the cumulative plastic strain or deformation below a tolerable level is placing an adequate granular thickness to limit the deviatoric stress transmitted to the subgrade below a tolerable level. Therefore, the transmission and distribution of the deviatoric stresses with depth in the track substructure layers were investigated in detail using a sophisticated 3D FE modelling subjected to realistic train moving loads under various train-track-ground conditions. The parameters considered include the modulus and thicknesses of ballast and subgrade, as well as train loadings. The deviatoric stress analyses led to the following findings:

- The maximum deviatoric stress along the rail in the ballast surface and subgrade surface occurs bellow the sleeper rather than the crib. Besides, the maximum deviatoric stress at any depth below the sleeper bottom occurs at the sleeper end.

Therefore, for all design purposes, the deviatoric stress in the ballast and subgrade layer need to be measured below the sleeper end.

- The deviatoric stress distribution in the ballast layer is affected significantly by the modulus of the ballast and subgrade. The maximum deviatoric stress develops in the ballast surface for the combined conditions of stiffer ballast and soft subgrade. Moreover, with the combined increase of the ballast modulus and decrease of the subgrade modulus, the stress spreading effect in the ballast layer increases, and vice versa.
- The deviatoric stress distribution in the subgrade layer is also influenced by the modulus of the ballast and subgrade. An increase of the ballast modulus decreases the deviatoric stress at the subgrade surface regardless of the subgrade condition; however, the difference in the deviatoric stress (due to different stiffness of ballast) at any depth below the sleeper bottom decreases with depth and becomes negligible after about 6 m depth for the soft subgrade condition. In contrast, the variation of deviatoric stress at each depth in the subgrade layer does not decrease significantly with depth in the stiff subgrades. Besides, the deviatoric stress developed at the subgrade surface increases with the increase of the subgrade stiffness; however, the difference of the deviatoric stress at any depth below the sleeper bottom reduces with depth.
- An increase in the granular layer thickness has two significant effects on the distribution of the deviatoric stress in the subgrade layer. Firstly, with the increase in the granular layer thickness, the distance of the subgrade surface below the sleeper bottom increases. This causes an automatic reduction of the deviatoric stress at the subgrade surface. Secondly, an increase in the granular layer thickness increases the stress spreading effect due to its higher stiffness, which results in a reduction of the deviatoric stress at any depth in the subgrade.
- The distribution of the deviatoric stress in the subgrade layer is not influenced by the thickness of the subgrade layer.
- The deviatoric stress at any depth below the sleeper (in both the ballast and subgrade layer) increases proportionally with the increase of the wheel loading, regardless of the subgrade condition. This allows the results to be presented using a normalised stress or strain influence factor.

The process followed towards the development of a new design method via design charts were discussed in detail in Chapter 5. The proposed design method was

developed based on improved empirical models for predicting the cumulative plastic deformation of the track substructure materials and stress obtained from sophisticated 3D FE numerical modelling. The main design parameters considered in the design method were comprehensive, including DAF, WSF, traffic tonnage, ballast modulus, ballast type, ballast static strength, subgrade modulus, subgrade type, subgrade static strength and subgrade thickness. The design method was examined against four track sites that have detailed field measurements, and the results were found to be consistent with field observations. The design methodology presented in this thesis has overcome most shortcomings of the existing design methods and it is thus believed to provide the most promising approach currently available.

6.2. CONCLUSIONS

In this study, the deformation behaviours of ballast under repeated loading were analysed, and an improved empirical model was proposed to incorporate the deformation of granular ballast materials in design of ballasted railway track foundations. Comparisons between predicted and available test results indicated that the proposed empirical model can indeed account for the major factors affecting the cumulative plastic deformation of ballast. In addition, a sophisticated 3D FE numerical modelling was developed to accurately simulate the dynamic response of railway tracks subjected to true train moving loads. A comprehensive parametric study was performed to investigate the track response for a broad range of track parameters, including the modulus and thickness of ballast, sub-ballast and subgrade plus loading characteristics. The developed FE model was used to carry out further analysis to investigate the influence of train speed on the behaviour of ballasted railway track foundations and to evaluate the critical speed under various conditions of the train-track-ground system. The research results provide a better understanding of the impact of the different parameters of the train-track-ground system on track performance.

In the final phase of this thesis, an advanced design method for ballasted railway track foundation was developed to prevent the progressive shear failure and to limit the excessive plastic deformation. The method was based on combined use of the

improved empirical models for predicting the cumulative strain or deformation of ballast and subgrade under repeated load applications and the results of the stress in the track layers obtained from the sophisticated 3D FE numerical modelling. The proposed design method has significant advantages over the existing design methods. The new design method accounted for all governing parameters that significantly affect the selection of the granular layer thickness needed to prevent track failures. The proposed design method was studied further against several track sites with their associated field measurements and the results obtained were found to be consistent with the field observations. The proposed design method is expected to provide a significant contribution to the current railway track code of practice.

6.3. RECOMMENDATIONS FOR FUTURE WORK

Although the proposed design method is believed to provide excellent approach for modern railway traffic, further studies on the following aspects are recommended:

- The developed design method uses results from traditional cyclic triaxial tests for behaviour of ballast and subgrade soils in which the rotation of principal stresses are not captured. However, in reality, when a train passes along the track, the particles within the substructure are subjected to a complex loading regime that involves principal stress rotation. Therefore, it is worthwhile to investigate the deformation behaviour of ballast and subgrade soils under actual loading condition considering principal stress rotation so as to incorporate this effect into the design method.
- The developed design method is based on an empirical model for predicting the cumulative plastic strain of ballast and subgrade layers and the stresses developed in these layers. Thus, the method gives only the thickness of ballast layer. However, the sub-ballast layer is also necessary to be considered for economical design and better drainage in the track.
- The design period (traffic tonnage) has a significant impact on the estimation of the granular layer thickness. However, no proper guidelines for the selection of the design period for various types of railway tracks are currently available. Therefore, considerations can be given to relate the design period to a usual ballast tamping period.

- The selection of design criteria for preventing the progressive shear failure (i.e. cumulative plastic strain) needs an extended study with respect to various types of ballasted railway tracks. Attention can be given to connecting the allowable cumulative plastic strain to the change in track geometry for different types of track. Similarly, further study on the selection of design criteria for preventing the excessive plastic deformation (i.e. allowable track settlement) is also recommended.
- Although the results obtained from the proposed design method are consistent with the limited field measurements investigated, further verifications of the proposed design method are desirable for more field measurements.

REFERENCES

Achenbach, J. D. (1973). *Wave Propagation in Elastic Solids*, North Holland Publishing Co., New York, USA.

Adam, M., Pflanz, G., and Schmid, G. (2000). "Two- and three-dimensional modelling of half-space and train-track embankment under dynamic loading." *Soil Dynamics and Earthquake Engineering*, 19(8), 559-573.

Al-Shayea, N., Abduljauwad, S., Bashir, R., Al-Ghamedy, H., and Asi, I. (2003). "Determination of parameters for a hyperbolic model of soils." *Proceedings of the Institution of Civil Engineers: Geotechnical Engineering*, 105-117.

Alva-Hurtado, J. E. D. (1980). "A methodology to predict the elastic and inelastic behavior of railroad ballast." PhD Thesis, University of Massachusetts, Amherst, Massachusetts, USA.

Alves Costa, P., Calçada, R., and Silva Cardoso, A. (2012). "Track-ground vibrations induced by railway traffic: In-situ measurements and validation of a 2.5D FEM-BEM model." *Soil Dynamics and Earthquake Engineering*, 32(1), 111-128.

Alves Costa, P., Colaço, A., Calçada, R., and Cardoso, A. S. (2015). "Critical speed of railway tracks. Detailed and simplified approaches." *Transportation Geotechnics*, 2, 30-46.

Andersen, L., and Nielsen, S. R. (2003). "Boundary element analysis of the steady-state response of an elastic half-space to a moving force on its surface." *Engineering Analysis with Boundary Elements*, 27(1), 23-38.

Anderson, W. F., and Key, A. J. (1999). "Two layer ballast beds as railway track foundations." *Geotechnical Engineering for Transportation Infrastructure: Theory and Practice, Planning and Design, Construction and Maintenance*, Taylor & Francis Group, USA, 1725-1731.

Anderson, W. F., and Key, A. J. (2000). "Model testing of two-layer railway track ballast." *Journal of Geotechnical and Geoenvironmental Engineering*, 126(4), 317-323.

Araújo, N. M. F. (2011). "High-speed trains on ballasted railway track: Dynamic stress field analysis." PhD Thesis, Universidade do Minho, Portugal.

AREA. (1996). *Manual for Railway Engineering*, Vol 1, American Railway Engineering Association (AREA), Washington, D.C.

AREMA. (2003). *Practical Guide to Railway Engineering*, American Railway Engineering and Maintenance of Way Association, Simmons-Boardman Publishing Corporation, Maryland.

Atalar, C., Das, B. M., Shin, E. C., and Kim, D. H. (2001). "Settlement of geogrid-reinforced railroad bed due to cyclic load." *Proceedings of the International Conference on Soil Mechanics and Geotechnical Engineering*, Istanbul, 2045-2048.

Banimahd, M., Woodward, P., Kennedy, K. J., and Medero, M. G. (2013). "Three-dimensional modelling of high speed ballasted railway tracks." *Proceedings of the ICE - Transport*, 166(2), 113-123.

Bettess, P. (1977). "Infinite elements." *International Journal for Numerical Methods in Engineering*, 11, 53-64.

Bian, X., Cheng, C., Jiang, J., Chen, R., and Chen, Y. (2014). "Numerical analysis of soil vibrations due to trains moving at critical speed." *Acta Geotechnica*, 1-14.

Bonnett, F. B. (2005). *Practical Railway Engineering*, Imperial College Press, London. UK.

Bortfeld, R. (1967). "Elastic Waves in Layered Media*." *Geophysical Prospecting*, 15(4), 644-650.

Brown, S. F. (1996). "Soil mechanics in pavement engineering." *Géotechnique*, 46(3), 383-426.

Burrow, M. P. N., Bowness, D., and Ghataora, G. S. (2007). "A comparison of railway track foundation design methods." *Proceedings of the Institution of Mechanical Engineers, Part F: Journal of Rail and Rapid Transit*, 221(1), 1-12.

Burrow, M. P. N., Evdorides, H. T., and Ghataora, G. S. (2006). "A comparative analysis of railway foundation design principles: A case study." *Proceedings of the Railfound 06 - International Conference on Railway Track Foundations*, 316-327.

Burrow, M. P. N., Ghataora, G. S., and Evdorides, H. (2011). "Railway foundation design principles." *Journal of Civil Engineering and Architecture*, 5(3), 224-232.

Chatterjee, P., Degrande, G., Clouteau, D., Al-Hussaini, T., Arnst, M., and Othman, R. (2003). "Numerical modelling of ground borne vibrations from underground railway traffic." *Proceedings of the 6th National Congress on Theoretical and Applied Mechanics*, Ghent, Belgium.

Chebli, H., Clouteau, D., and Schmitt, L. (2008). "Dynamic response of high-speed ballasted railway tracks: 3D periodic model and in situ measurements." *Soil Dynamics and Earthquake Engineering*, 28(2), 118-131.

Chowdhury, I., and Dasgupta, S. P. (2003). "Computation of Rayleigh damping coefficients for large systems." *The Electronic Journal of Geotechnical Engineering*, 8, 1-11.

Chrismer, S., and Selig, E. T. (1993). "Computer model for ballast maintenance planning." *Proceedings of the 5th International Heavy Haul Railway Conference*, 223-227.

Clouteau, D., Elhabre, M. L., and Aubry, D. (2000). "Periodic BEM and FEM-BEM coupling." *Computational Mechanics*, 25(6), 567-577.

Clouteau, D., Othman, R., Arnst, M., Chebli, H., Degrande, G., Chatterjee, P., and Janssens, B. (2004). "A numerical model for ground-borne vibrations from underground railway traffic based on a periodic FE-BE formulation." *Proceedings of the Eighth International Workshop on Railway Noise*, No. 1, Buxton, UK, 167-178.

Correia, A. G., Cunha, J., Marcelino, J., Caldeira, L., Varandas, J., Dimitrovová, Z., Antão, A., and Silva, M. (2007). "Dynamic analysis of rail track for high speed trains. 2D approach." *Proceedings of the 5th International Workshop on Applications of Computational Mechanics in Geotechnical Engineering*, Guimarães, 461-472.

Cunha, J., and Correia, A. G. (2012). "Evaluation of a linear elastic 3D FEM to simulate rail track response under a high-speed train." *ICTG - Advances in Transportation Geotechnics II*, Miura et al., eds., Taylor & Francis - Balkema, London, 196-201.

Cunha, J. P. F. (2013). "Modelling of ballasted railway tracks for high-speed trains." PhD Thesis, University of Minho, Guimaraes, Portugal.

Dahlberg, T. (2003). *Railway track dynamics: A survey*, Technical Report, Solid Mechanics/IKP, Linkping University.

Das, B. M. (2005). *Fundamentals of Geotechnical Engineering*, Chris Carson, United States.

Das, B. M. (2006). *Principles of Geotechnical Engineering*, Chris Carson, United States.

Degrande, G., Chatterjee, P., Clouteau, D., Al-Hussaini, T., Arnst, M., and Othman, R. (2003). "A numerical prediction model for ground-borne vibrations from underground railway traffic using a coupled periodic FEM-BEM approach." *In: 10th International Congress on Sound and Vibration*, Stockholm, Sweden.

Degrande, G., and Schillemans, L. (2001). "Free field vibrations during the passage of a Thalys high-speed train at variable speed." *Journal of Sound and Vibration*, 247(1), 131-144.

Dieterman, H. A., and Metrikine, A. V. (1996). "The equivalent stiffness of a half-space interacting with a beam. Critical velocities of a moving load along the beam." *European Journal of Mechanics, A/Solids*, 15(1), 67-90.

Dieterman, H. A., and Metrikine, A. V. (1997). "Steady-state displacements of a beam on an elastic half-space due to a uniformly moving constant load." *European Journal of Mechanics, A/Solids*, 16(2), 295-306.

Diyaljee, V. A. (1987). "Effects of stress history on ballast deformation." *Journal of Geotechnical Engineering, ASCE*, 113(8), 909-914.

Duncan, J. M., Byrne, P., Wong, K. S., and Mabry, P. (1980). *Strength, stress-strain and bulk modulus parameters for finite element analyses of stresses and movements in soil masses, Report No. UCB/GT/80-01*, University of California, Berkeley, California.

Duncan, J. M., and Chang, C. Y. (1970). "Nonlinear analysis of stress and strain in soils." *Journal of the Soil Mechanics and Foundations Division*, 96(5), 1629-1653.

Eisenmann, J. (1972). "Germans gain a better understanding of track structure." *Railway Gazette International*, 128(8).

Ekevid, T., and Wiberg, N. E. (2002). "Wave propagation related to high-speed train a scaled boundary FE-approach for unbounded domains." *Computer Methods in Applied Mechanics and Engineering*, 191(36), 3947-3964.

El Kacimi, A., Woodward, P. K., Laghrouche, O., and Medero, G. (2013). "Time domain 3D finite element modelling of train-induced vibration at high speed." *Computers and Structures*, 118, 66-73.

Esveld, C. (2001). *Modern Railway Track*, MRT-Productions, Delft University of Technology, The Netherlands.

Fair, P. (2004). "The geotechnical behaviour of ballast materials for railway track maintenance." PhD Thesis, University of Sheffield, England.

Feldman, F., and Nissen, D. (2002). "Alternative testing method for the measurement of ballast fouling : Percentage void contamination." *Proceedings of the Conference on Railway Engineering*, Wollongong, Australia, 101-111.

Feng, H. (2011). "3D-models of railway track for dynamic analysis." Master of Science Thesis, Royal Institute of Technology (KTH), Stockholm, Sweden.

Fiala, P., Degrande, G., and Augusztinovicz, F. (2007). "Numerical modelling of ground-borne noise and vibration in buildings due to surface rail traffic." *Journal of Sound and Vibration*, 301(3-5), 718-738.

Galavi, V., and Brinkgreve, R. B. J. (2014). "Finite element modelling of geotechnical structures subjected to moving loads." *VIII ECNUMGE - Numerical Methods in Geotechnical Engineering*, Hicks et al., eds., Taylor and Francis - Balkema, Delft, Netherlands, 235-240.

Galvín, P., Romero, A., and Domínguez, J. (2010). "Fully three-dimensional analysis of high-speed train-track-soil-structure dynamic interaction." *Journal of Sound and Vibration*, 329(24), 5147-5163.

Gardien, W., and Stuit, H. G. (2003). "Modelling of soil vibrations from railway tunnels." *Journal of Sound and Vibration*, 267(3), 605-619.

Gibb, R. A., Knowles, R. D., and Farrington, J. H. (1992). "The Channel Tunnel Rail Link and regional development: An evaluation of British Rail's procedures and policies." *Geographical Journal*, 273-285.

Gräbe, P. J. (2002). "Resilient and permanent deformation of railway foundations under principal stress rotation." PhD Thesis, University of Southampton, Southampton, England.

Gupta, S., Degrande, G., Chebli, H., Clouteau, D., Hussein, M. F. M., and Hunt, H. E. M. (2006a). "A numerical model for prediction of vibration from underground railways." *In: Euromech Colloquium 484, Wave mechanics and stability of*

long flexible structures subject to moving loads and flows, Delft University of Technology, the Netherlands.

Gupta, S., Fiala, P., Hussein, M. F. M., Chebli, H., Degrande, G., Auguszinovicz, F., Hunt, H. E. M., and Clouteau, D. (2006b). "A numerical model for ground-borne vibrations and reradiated noise in buildings from underground railways." *In: International Conference on Modal Analysis Noise and Vibration Engineering*, Katholieke Univ. Leuven, Dep. Werktuigkunde.

Hall, L. (2000). "Simulations and analyses of train-induced ground vibrations: A comparative study of two- and three-dimensional calculations with actual measurements." PhD Thesis, Royal Institute of Technology.

Hall, L. (2003). "Simulations and analyses of train-induced ground vibrations in finite element models." *Soil Dynamics and Earthquake Engineering*, 23(5), 403-413.

Hay, W. W. (1982). *Railroad Engineering*, John Wiley & Sons, Inc, New York City, New York.

Heath, D. L., Shenton, M. J., Sparrow, R. W., and Waters, J. M. (1972). "Design of conventional rail track foundations." *Proceedings of the Institution of Civil Engineers*, 51, 251-267.

Hossain, Z., Indraratna, B., Darve, F., and Thakur, P. K. (2007). "DEM analysis of angular ballast breakage under cyclic loading." *Geomechanics and Geoengineering: An International Journal*, 2(3), 175-181.

Huang, Y. H., Rose, J. G., and Khoury, C. J. (1987). "Thickness design for hot-mix asphalt railroad trackbeds." *Annual Journal AAPT, Miscellaneous*, 56(87), 427-453.

Inam, A., Ishikawa, T., and Miura, S. (2012). "Effect of principal stress axis rotation on cyclic plastic deformation characteristics of unsaturated base course material." *Soils and Foundations*, 52(3), 465-480.

Indraratna, B., and Ionescu, D. (2000). "State of the art large scale testing of ballast." *Proceedings of the CORE2000, Railway Technology for the 21st Century*, Adelaide, Australia, 24, 1-13.

Indraratna, B., Ionescu, D., and Christie, H. D. (1998). "Shear behavior of railway ballast based on large-scale triaxial tests." *Journal of Geotechnical and Geoenvironmental Engineering*, 124(5), 439-449.

Indraratna, B., Salim, M. W., and Rujikiatkamjorn, C. (2011a). *Advanced Rail Geotechnology - Ballasted Track*, Taylor & Francis Group, London, UK.

Indraratna, B., and Salim, W. (2003). "Deformation and degradation mechanics of recycled ballast stabilised with geosynthetics." *Soils and Foundations*, 43()(4), 35-46.

Indraratna, B., Salim, W., Ionescu, D., and Christie, D. (2001). "Stress-strain and degradation behaviour of railway ballast under static and dynamic loading, based on large-scale triaxial testing." *Proceedings of the 15th International Conference on Soil Mechanics and Geotechnical Engineering*, Istanbul, 2093-2096.

Indraratna, B., Shahin, M. A., and Salim, W. (2005). "Use of geosynthetics for stabilizing recycled ballast in railway track substructures." *Proceedings of the NAGS2005/GRI 19 Cooperative Conference*, 1-15.

Indraratna, B., Shahin, M. A., and Salim, W. (2007). "Stabilisation of granular media and formation soil using geosynthetics with special reference to railway engineering." *Journal of Ground Improvement* 11(1), 27-44.

Indraratna, B., Su, L. J., and Rujikiatkamjorn, C. (2011b). "A new parameter for classification and evaluation of railway ballast fouling." *Canadian Geotechnical Journal*, 48(2), 322-326.

Indraratna, B., Thakur, P. K., and Vinod, J. S. (2010). "Experimental and numerical study of railway ballast behavior under cyclic loading." *International Journal of Geomechanics*, 10(4), 136-144.

Jain, S. V. K., Kumar, S. P., Raina, S. S. K., and Mishra, S. A. K. (2003). *Guidelines for earthwork in railway projects, Guideline No. GE: G-1*, Geo-technical Engineering Directorate, RDSO, Manak Nagar, Lucknow - 11.

Jeffs, T., and Marich, S. (1987). "Ballast characteristics in the laboratory." *Proceedings of the Conference on Railway Engineering*, Institution of Engineers, Perth, Australia, 141-147.

Jeffs, T., and Tew, G. P. (1991). *A review of track design procedures, Vol. 2, Sleepers and Ballast*, BHP Research - Melbourne Laboratories, Railways of Australia, Victoria, Australia.

Kaewunruen, S., and Remennikov, A. M. (2008). "Dynamic properties of railway track and its components : A state-of-the-art review." *New Research on Acoustics*, B. Weiss, eds., Nova Science Publishers, Hauppauge, New York, 197-220.

Kaynia, A. M., Madshus, C., and Zackrisson, P. (2000). "Ground vibration from high-speed trains: prediction and countermeasure." *Journal of Geotechnical and Geoenvironmental Engineering*, 126(6), 531-537.

Kennedy Jr, J. C., and Prause, R. (1979). "Parametric study of track response." *Transportation Research Record*, 721.

Knothe, K. L., and Grassie, S. L. (1993). "Modelling of railway track and vehicle/track interaction at high frequencies." *Vehicle System Dynamics: International Journal of Vehicle Mechanics and Mobility*, 22(3-4), 209-262.

Kouroussis, G., Verlinden, O., and Conti, C. (2009). "Ground propagation of vibrations from railway vehicles using a finite/infinite-element model of the soil." *Journal of Rail and Rapid Transit*, 223(4), 405-413.

Kouroussis, G., Verlinden, O., and Conti, C. (2011a). "Finite-dynamic model for infinite media: corrected solution of viscous boundary efficiency." *Journal of Engineering Mechanics*, 137(7), 509-511.

Kouroussis, G., Verlinden, O., and Conti, C. (2011b). "Free field vibrations caused by high-speed lines: measurement and time domain simulation." *Soil Dynamics and Earthquake Engineering*, 31(4), 692-707.

Kozickia, J., and Donzéb, F. V. (2008). "A new open-source software developed for numerical simulations using discrete modeling methods." *Computer Methods in Applied Mechanics and Engineering*, 197(49-50), 4429-4443.

Krylov, V. V. (1994). "On the theory of railway-induced ground vibrations." *Journal De Physique*, 4(C5), 769-772.

Krylov, V. V. (1995). "Generation of ground vibrations by superfast trains." *Applied Acoustics*, 44(2), 149-164.

Krylov, V. V. (2001). *Noise and Vibration from High-speed Trains*, Thomas Telford, London.

Lackenby, J., Christie, D., Indraratna, B., and McDowell, G. (2007). "Effect of confining pressure on ballast degradation and deformation under cyclic triaxial loading." *Géotechnique*, 57(6), 527-536.

Lamb, H. (1904). "On the propagation of tremors over the surface of an elastic solid." *Philosophical Transactions of the Royal Society of London*, 203(Series A), 1-42.

Lekarp, F., Isacsson, U., and Dawson, A. (2000a). "State of the art. I: Resilient response of unbound aggregates." *Journal of Transportation Engineering*, 126(1), 66-75.

Lekarp, F., Isacsson, U., and Dawson, A. R. (2000b). "State of the art. II: Permanent strain response of unbound aggregates." *Journal of Transportation Engineering*, 126(1), 76-83.

Li, D. (1994). "Railway track granular layer thickness design based on subgrade performance under repeated loading." PhD Thesis, University of Massachusetts, Amherst, Massachusetts, USA.

Li, D., Hyslip, J., Sussmann, T., and Chrismer, S. (2002). *Railway Geotechnics*, CRC Press, Tailor & Francis Group, Broken Sound Parkway NW, USA.

Li, D., and Selig, E. T. (1994a). *Investigation of AMTRAK track foundation problems in Edgewood and Aberdeen, MD.*, Internal Rep. to the Assoc. of Am. Railroads and Amtrak, Amherst, Mass.

Li, D., and Selig, E. T. (1994b). "Resilient modulus for fine-grained subgrade soils." *Journal of Geotechnical Engineering*, 120(6), 939-957.

Li, D., and Selig, E. T. (1995). "Evaluation of railway subgrade problems." *Transportation Research Record*, 1489, 17-25.

Li, D., and Selig, E. T. (1996). "Cumulative plastic deformation for fine-grained subgrade soils." *Journal of Geotechnical Engineering*, 122(12), 1006-1013.

Li, D., and Selig, E. T. (1998a). "Method for railroad track foundation design. I: Development." *Journal of Geotechnical and Geoenvironmental Engineering*, 124(4), 316.

Li, D., and Selig, E. T. (1998b). "Method for railroad track foundation design. II: Applications." *Journal of Geotechnical and Geoenvironmental Engineering*, 124(4), 323.

Li, D., Sussmann, T. R., and Selig, E. T. (1996). *Procedure for railway track granular layer thickness determination, Report No. R-898*, Association of American Railroads, Transportation Technology Center, Pueblo, Colorado, USA.

Liang, B., Zhu, D., and Cai, Y. (2001). "Dynamic analysis of the vehicle–subgrade model of a vertical coupled system." *Journal of Sound and Vibration*, 245(1), 79-92.

Lim, W. L., and McDowell, G. R. (2005). "Discrete element modelling of railway ballast." *Granular Matter*, 7, 19-29.

Lobo-Guerrero, S., and Vallejo, L. E. (2006). "Discrete element method analysis of railtrack ballast degradation during cyclic loading." *Granular Matter*, 8(3-4), 195-204.

Lu, M. (2008). "Discrete element modelling of railway ballast." PhD Thesis, University of Nottingham, England.

Lu, M., and McDowell, G. (2007). "The importance of modelling ballast particle shape in the discrete element method." *Granular Matter*, 9, 69-80.

Lu, M., and McDowell, G. R. (2008). "Discrete element modelling of railway ballast under triaxial conditions." *Geomechanics and Geoengineering*, 3(4), 257-270.

Lysmer, J., and Kuhlemeyer, R. L. (1969). "Finite dynamic model for infinite media." *Journal of the Engineering Mechanics Division, ASCE*, 95(EM4), 859-877.

Madshus, C., and Kaynia, A. M. (1999). "Dynamic ground interaction; a critical issue for high speed train lines on soft soil." *Geotechnical engineering for transportation infrastructure*, Barends et al., eds., Balkema, Amsterdam, Netherlands, 1-8.

Madshus, C., and Kaynia, A. M. (2000). "High-speed railway lines on soft ground: Dynamic behaviour at critical train speed." *Journal of Sound and Vibration*, 231(3), 689-701.

MIDAS IT. Co. Ltd. (2013). *Manual of GTS-NX 2013 v1.2: new experience of geotechnical analysis system*, MIDAS Company Limited, South Korea.

Network Rail. (2005). *Company Code of Practice, Formation Treatments, NR/SB/TRK/9039*, Network Rail, 40 Melton Street, London W1 2EE, Dec. 2005.

O'Brien, J., and Rizos, D. C. (2005). "A 3D BEM-FEM methodology for simulation of high speed train induced vibrations." *Soil Dynamics and Earthquake Engineering*, 25(4), 289-301.

O'Riordan, N., and Phear, A. (2001). "Design and construction control of ballasted track formation and subgrade for high speed lines." *Proceedings of the International Conference Railway Engineering*, London, UK.

Odemark, N. (1949). *Investigations as to the Elastic Properties of Soils and Design of Pavements According to the Theory of Elasticity*, Statens Vagistitute, Meddeland, 77, Stockholm, Sweden.

Okabe, Z. (1961). "Laboratory investigation of railroad ballasts." *Bulletin of the Permanent Way Society of Japan*, 4(4), 1-19

Powrie, W., Yang, L. A., and Clayton, C. R. I. (2007). "Stress changes in the ground below ballasted railway track during train passage." *Proceedings of the Institution of Mechanical Engineers. Part F, Journal of rail and rapid transit*, 221(2), 247-261.

Priest, J. A., and Powrie, W. (2009). "Determination of dynamic track modulus from measurement of track velocity during train passage." *Journal of geotechnical and geoenvironmental engineering*, 135(11), 1732-1740.

Raymond, G. P. (1978). "Design for railroad ballast and subgrade support." *Journal of the Geotechnical Engineering Division*, 104(1), 45-60.

Raymond, G. P., and Bathurst, R. J. (1994). "Repeated-load response of aggregates in relation to track quality index." *Canadian Geotechnical Journal*, 31, 547-554.

Raymond, G. P., and Diyaljee, V. A. (1979). "Railroad ballast sizing and grading." *Journal of the Geotechnical Engineering Division, ASCE*, 105(GT5), 676-681.

Raymond, G. P., and Williams, D. R. (1978). "Repeated Load Triaxial Tests on a Dolomite Ballast." *Journal of the Geotechnical Engineering Division*, 104(7), 1013-1029.

Salim, M. W. (2004). "Deformation and degradation aspects of ballast and constitutive modelling under cyclic loading." PhD Thesis, University of Wollongong, Wollongong NSW, Australia.

Saussine, G., Cholet, C., Gautier, P. E., Dubois, F., Bohatier, C., and Moreau, J. J. (2004). *Modelling ballast under cyclic loading using Discrete Element Method*, Taylor & Francis Group, London.

Sayeed, M. A., and Shahin, M. A. (2015). "Modelling of ballasted railway track under train moving loads." *Proceedings of the 12th Australia New Zealand Conference on Geomechanics*, Wellington, New Zealand, Paper No. 132: 1-8.

Sayeed, M. A., and Shahin, M. A. (2016a). "Investigation into impact of train speed for behavior of ballasted railway track foundations." *Proceedings of the 3rd International Conference on Transportation Geotechnics*, Procedia Engineering, 143, 1152-1159.

Sayeed, M. A., and Shahin, M. A. (2016b). "Three-dimensional numerical modelling of ballasted railway track foundations for high-speed trains with special reference to critical speed." *Transportation Geotechnics*, 6, 55-65.

Selig, E. (1998). "Ballast's part: Its key roles and qualities." *Railway Track and Structures*, 94(3).

Selig, E. T., and Cantrell, D. D. (2001). "Track Substructure Maintenance--From Theory to Practice." *In: American Railway Engineering and Maintenance of Way Association Annual Conference*, Chicago, Illinois.

Selig, E. T., and Li, D. (1994). *Track modulus: Its meaning and factor influencing it*.

Selig, E. T., and Waters, J. M. (1994). *Track Geotechnology and Substructure Management*, Thomas Telford, London, UK.

Selig, E. T., Yoo, T. S., Adegoke, C. W., and Stewart, H. E. (1981). *Status Report-Ballast Experiments, Intermediate (175 MGT), Substructure Stress and Strain Data, FAST/TTC/TM-81/03 by University of Massachusetts*, for US DOT Transportation Systems Center, Cambridge, MA, USA.

Shahin, M. A. (2009). "Design of ballasted railway track foundations under cyclic loading." *Proceedings of the 2009 GeoHunan International Conference - Slope Stability, Retaining Walls, and Foundations*, Changsha, Hunan, China, 68-73.

Shahin, M. A., and Indraratna, B. (2006). "Parametric study on the resilient response of ballasted railway track substructure using numerical modeling." *Proceedings of the GeoCongress 2006: Geotechnical Engineering in the Information Technology Age*, 1-6.

Shahu, J. T., Kameswara Rao, N. S. V., and Yudhbir. (1999). "Parametric study of resilient response of tracks with a sub-ballast layer." *Canadian Geotechnical Journal*, 36(6), 1137-1150.

Shahu, J. T., Yudhbir, and Kameswara Rao, N. S. V. (2000). "A rational method for design of railroad track foundation." *Soils and Foundations*, 40(6), 1-10.

Sheng, X., Jones, C. J. C., and Thompson, D. J. (2004). "A theoretical study on the influence of the track on train-induced ground vibration." *Journal of Sound and Vibration*, 272(3), 909-36.

Sheng, X., Jones, C. J. C., and Thompson, D. J. (2006). "Prediction of ground vibration from trains using the wavenumber finite and boundary element methods." *Journal of Sound and Vibration*, 293(3–5), 575-586.

Shenton, M. J. (1975). "Deformation of railway ballast under repeated loading conditions." *Proceedings of the Symposium on Railroad Track Mechanics*, Princton University, 387-404.

Shenton, M. J. (1985). "Ballast deformation and track deterioration." *Track technology*, Thomas Telford Ltd, London, 253-265.

Stewart, H. E. (1982). "The prediction of track performance under dynamic traffic loading." PhD Thesis, University of Massachusetts, Amherst, Massachusetts, USA.

Stewart, H. E. (1986). "Permanent strains from cyclic variable amplitude loadings." *Journal of Geotechnical Engineering, ASCE*, 112(6), 646-660.

Suiker, A. S. (2002). "The mechanical behaviour of ballasted railway tracks." PhD Thesis, Delft University of Technology, Delft, Netherlands.

Takemiya, H. (2003). "Simulation of track-ground vibrations due to a high-speed train: the case of X-2000 at Ledsgard." *Journal of Sound and Vibration*, 261(3), 503-26.

Tennakoon, N., Indraratna, B., and Nimbalkar, S. (2014). "Impact of ballast fouling on rail tracks." *In: Second International Conference on Railway Technology: Research, Development and Maintenance*, Ajaccio, Corsica, France, 1-11.

Transportation Officials. (1993). *AASHTO Guide for design of pavement structures*, AASHTO, Washington D.C., USA.

Tutumluer, E., Huang, H., and Hashash, Y. M. A. (2007). "Discrete element modeling of railroad ballast settlement." *In: AREMA 2007 Annual Conferences*, Chicago, Illinois, USA.

UIC. (1994). *Earthworks And Trackbed Construction For Railway Lines*, UIC Code 719 R, The international Union of Railways, Parish, France.

Wanming, Z., Zhenxing, H., and Xiaolin, S. (2010). "Prediction of high-speed train induced ground vibration based on train-track-ground system model." *Earthquake Engineering and Engineering Vibration*, 9(4), 545-554.

Wener-Fligner, Z. (2015). "A new Japanese train has broken the world speed record twice this week." QUARTZ.

Wolf, J. P., and Song, C. (1996). "Finite-element modelling of unbounded media." *Proceedings of the Eleventh World Conference on Earthquake Engineering*, Paper No. 70: 1-8.

Woodward, P. K., Thompson, D., and Banimahd, M. (2007). "Geocomposite technology: reducing railway maintenance." *Proceedings of the ICE - Transport*, 160(3), 109-115.

Wrobel, L. C. (2002). *The Boundary Element Method; Vol. 2. Applications in Solids and Structures*, Chichester; New York : Wiley.

Yang, L., Powrie, W., and Priest, J. A. (2009). "Dynamic stress analysis of a ballasted railway track bed during train passage." *Journal of Geotechnical and Geoenvironmental Engineering*, 135(5), 680-689.

Appendix A
Charts for Determining the Dynamic Amplification Factor (DAF)

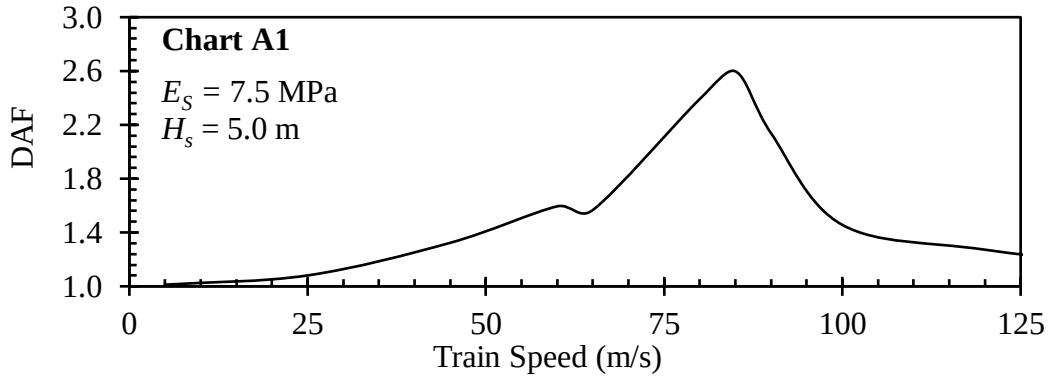

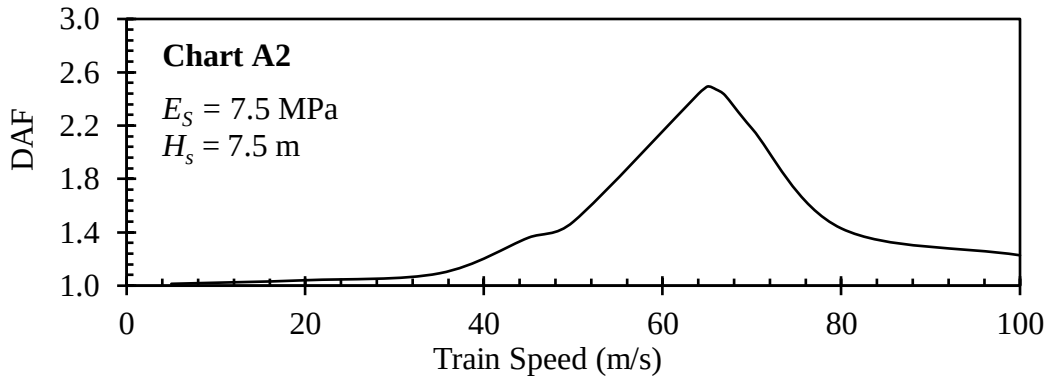

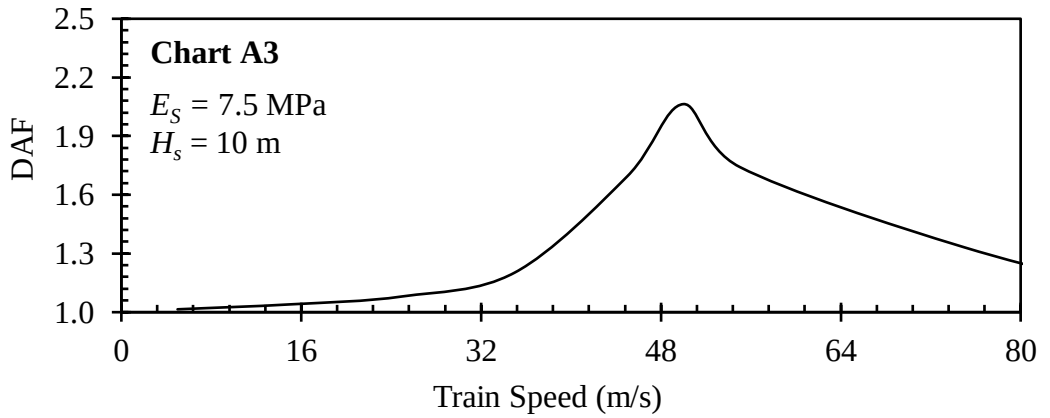

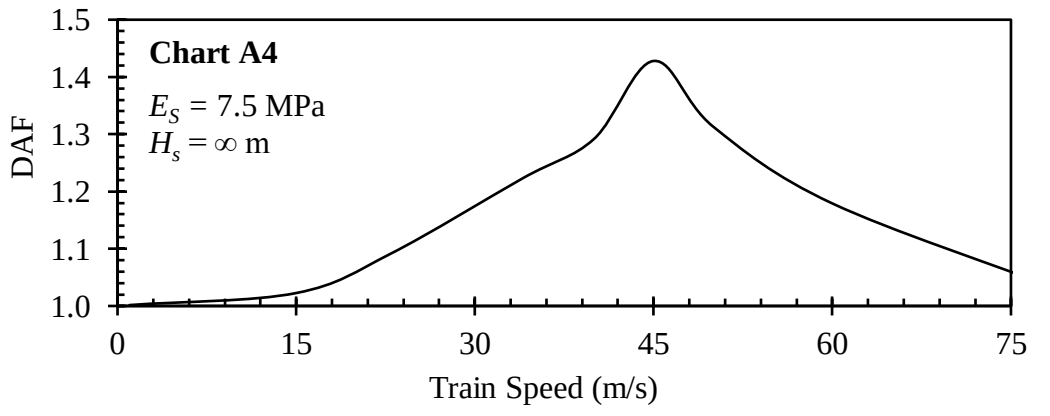

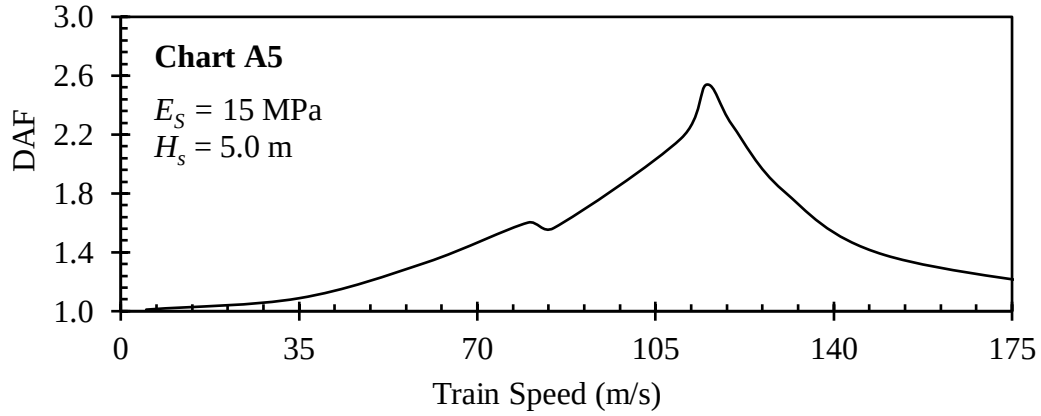
Chart A5
E_S = 15 MPa
H_s = 5.0 m
DAF
3.0
2.6
2.2
1.8
1.4
1.0
0
35
70
105
140
175
Train Speed (m/s)

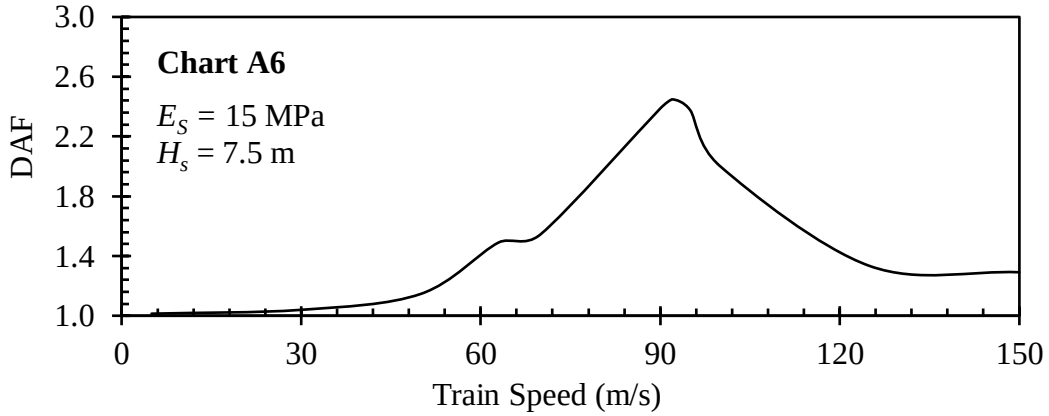
Chart A6
E_S = 15 MPa
H_s = 7.5 m
DAF
3.0
2.6
2.2
1.8
1.4
1.0
0
30
60
90
120
150
Train Speed (m/s)

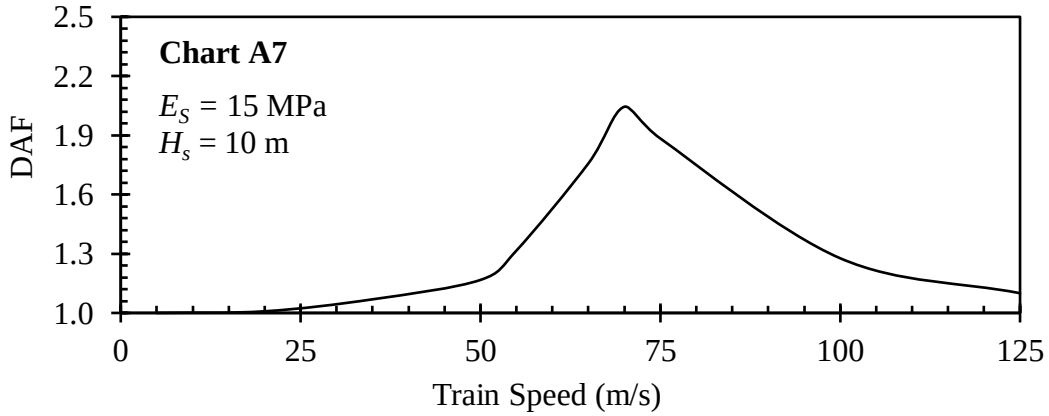
Chart A7
E_S = 15 MPa
H_s = 10 m
DAF
2.5
2.2
1.9
1.6
1.3
1.0
0
25
50
75
100
125
Train Speed (m/s)

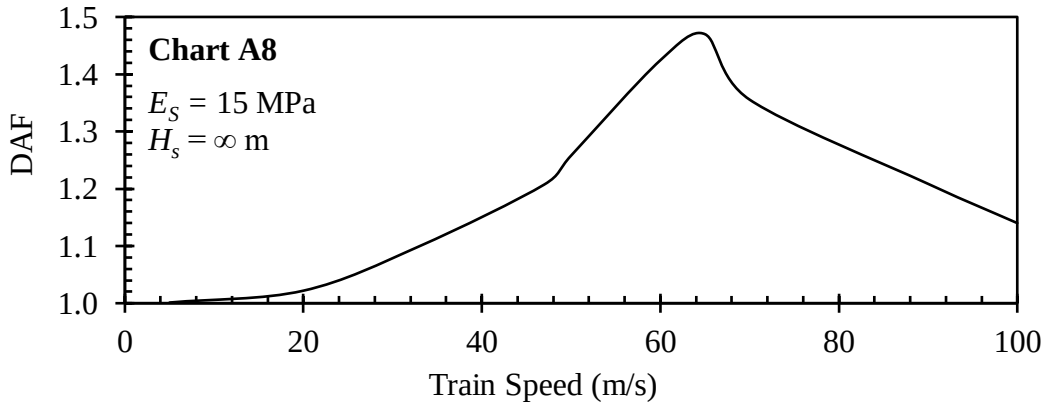
Chart A8
E_S = 15 MPa
H_s = ∞ m
DAF
1.5
1.4
1.3
1.2
1.1
1.0
0
20
40
60
80
100
Train Speed (m/s)

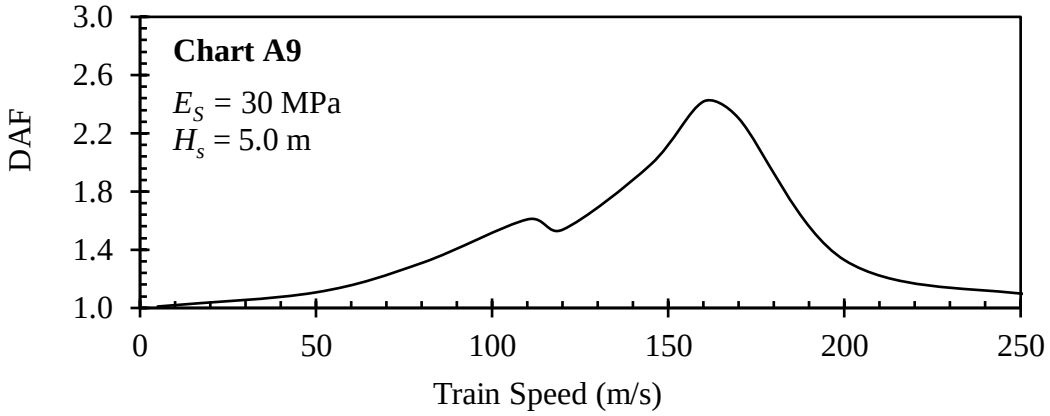
Chart A9
E_S = 30 MPa
H_s = 5.0 m
DAF
3.0
2.6
2.2
1.8
1.4
1.0
0
50
100
150
200
250
Train Speed (m/s)

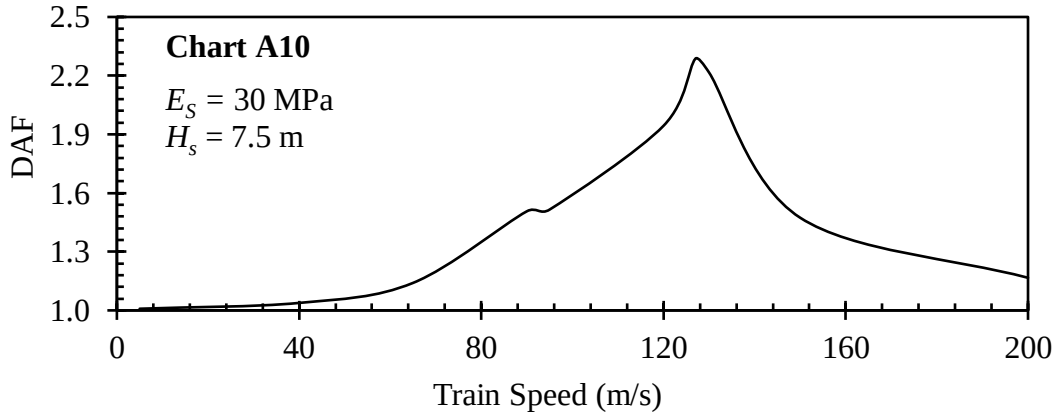
Chart A10
E_S = 30 MPa
H_s = 7.5 m
DAF
2.5
2.2
1.9
1.6
1.3
1.0
0
40
80
120
160
200
Train Speed (m/s)

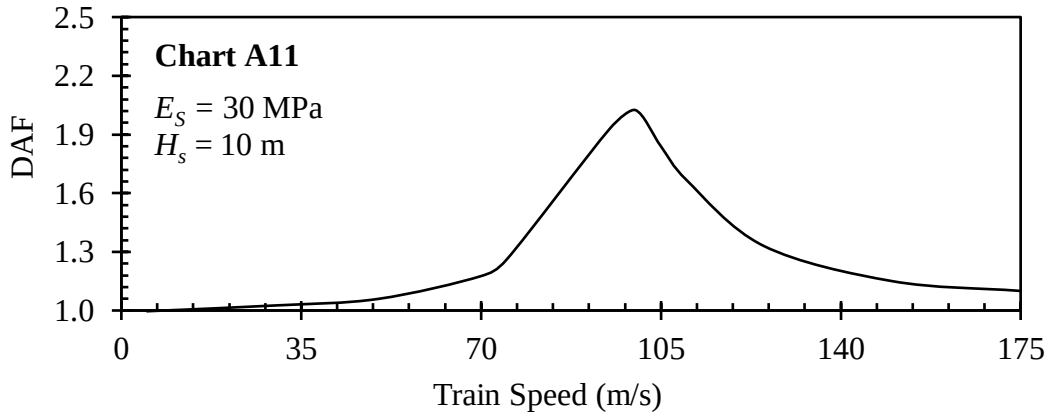
Chart A11
E_S = 30 MPa
H_s = 10 m
DAF
2.5
2.2
1.9
1.6
1.3
1.0
0
35
70
105
140
175
Train Speed (m/s)

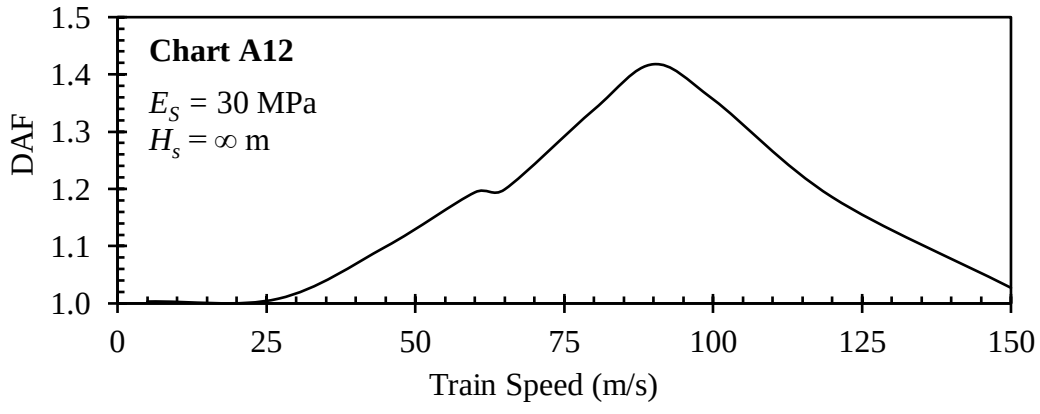
Chart A12
E_S = 30 MPa
H_s = ∞ m
DAF
1.5
1.4
1.3
1.2
1.1
1.0
0
25
50
75
100
125
150
Train Speed (m/s)

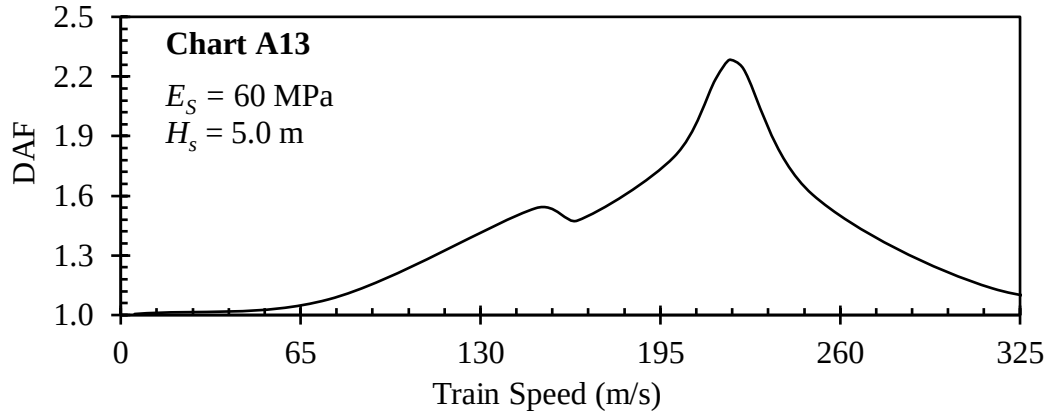
Chart A13
E_S = 60 MPa
H_s = 5.0 m
DAF
2.5
2.2
1.9
1.6
1.3
1.0
0
65
130
195
260
325
Train Speed (m/s)

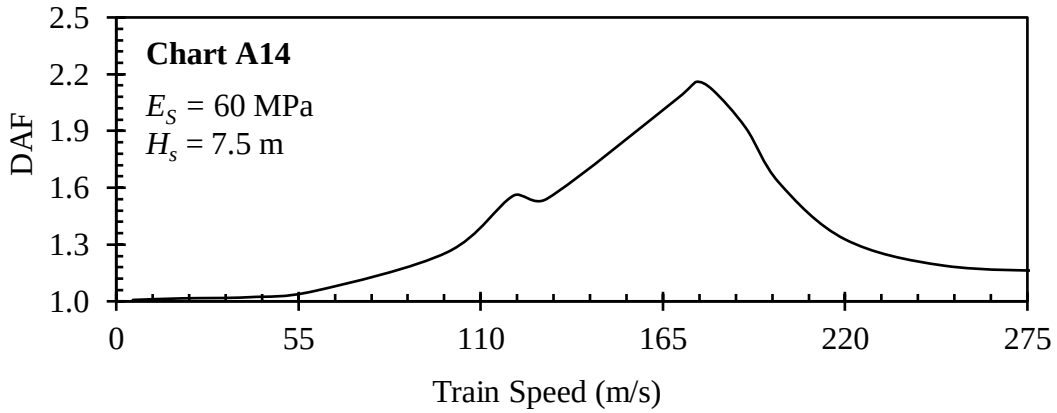
Chart A14
E_S = 60 MPa
H_s = 7.5 m
DAF
2.5
2.2
1.9
1.6
1.3
1.0
0
55
110
165
220
275
Train Speed (m/s)

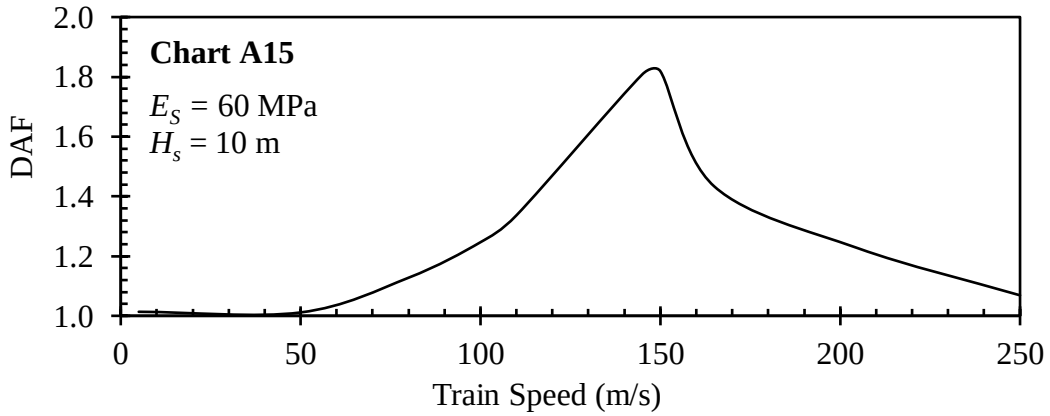
Chart A15
E_S = 60 MPa
H_s = 10 m
DAF
2.0
1.8
1.6
1.4
1.2
1.0
0
50
100
150
200
250
Train Speed (m/s)

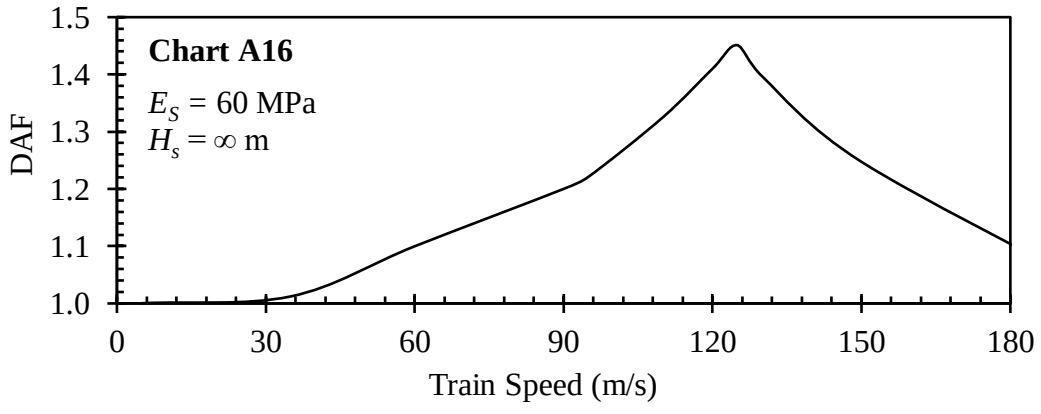
Chart A16
E_S = 60 MPa
H_s = ∞ m
DAF
1.5
1.4
1.3
1.2
1.1
1.0
0
30
60
90
120
150
180
Train Speed (m/s)

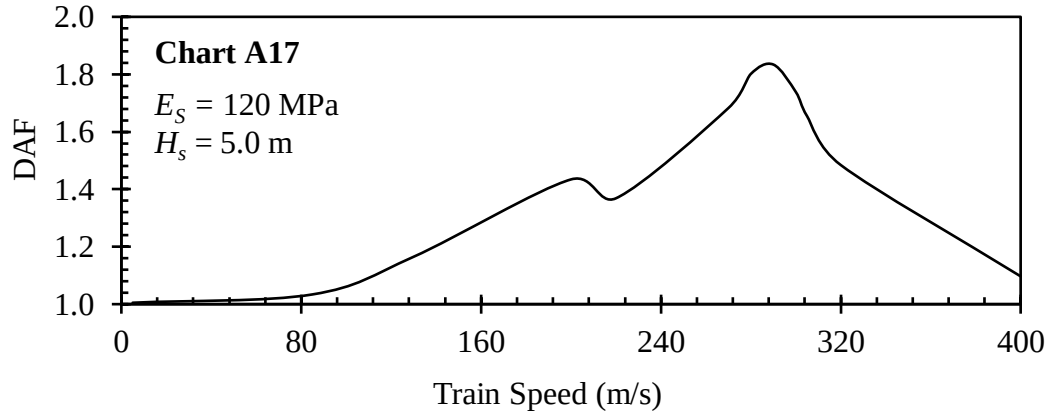
Chart A17
E_S = 120 MPa
H_s = 5.0 m
DAF
2.0
1.8
1.6
1.4
1.2
1.0
0
80
160
240
320
400
Train Speed (m/s)

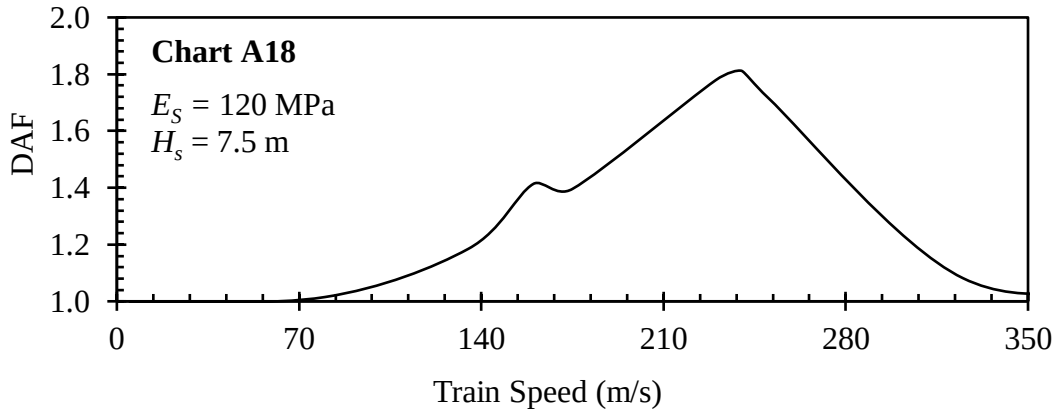
Chart A18
E_S = 120 MPa
H_s = 7.5 m
DAF
2.0
1.8
1.6
1.4
1.2
1.0
0
70
140
210
280
350
Train Speed (m/s)

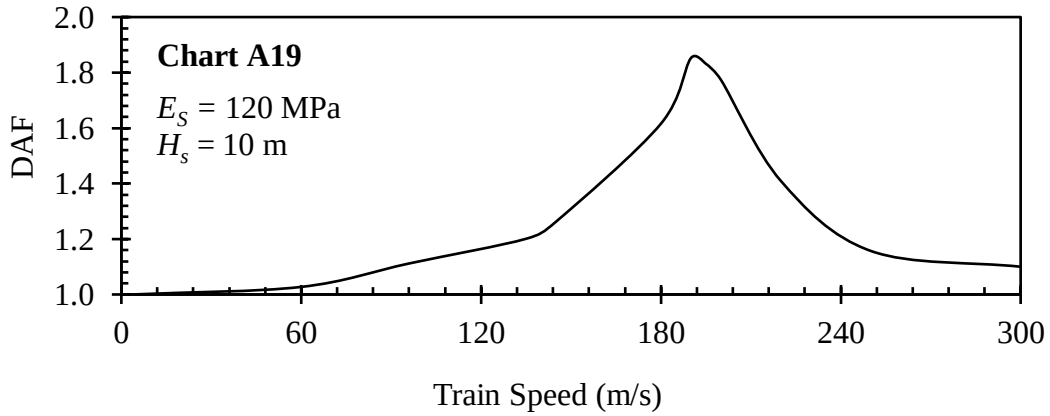
Chart A19
E_S = 120 MPa
H_s = 10 m
DAF
2.0
1.8
1.6
1.4
1.2
1.0
0
60
120
180
240
300
Train Speed (m/s)

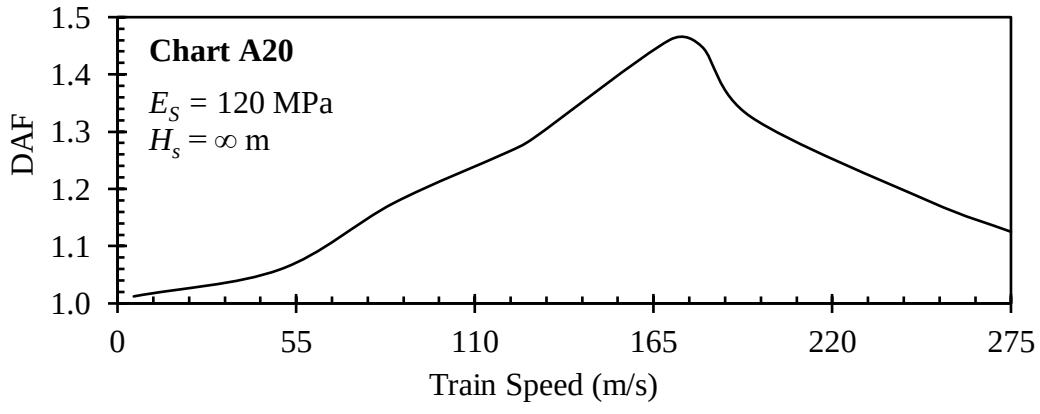
Chart A20
E_S = 120 MPa
H_s = ∞ m
DAF
1.5
1.4
1.3
1.2
1.1
1.0
0
55
110
165
220
275
Train Speed (m/s)

Appendix B

Design Charts to Prevent Progressive Shear Failure

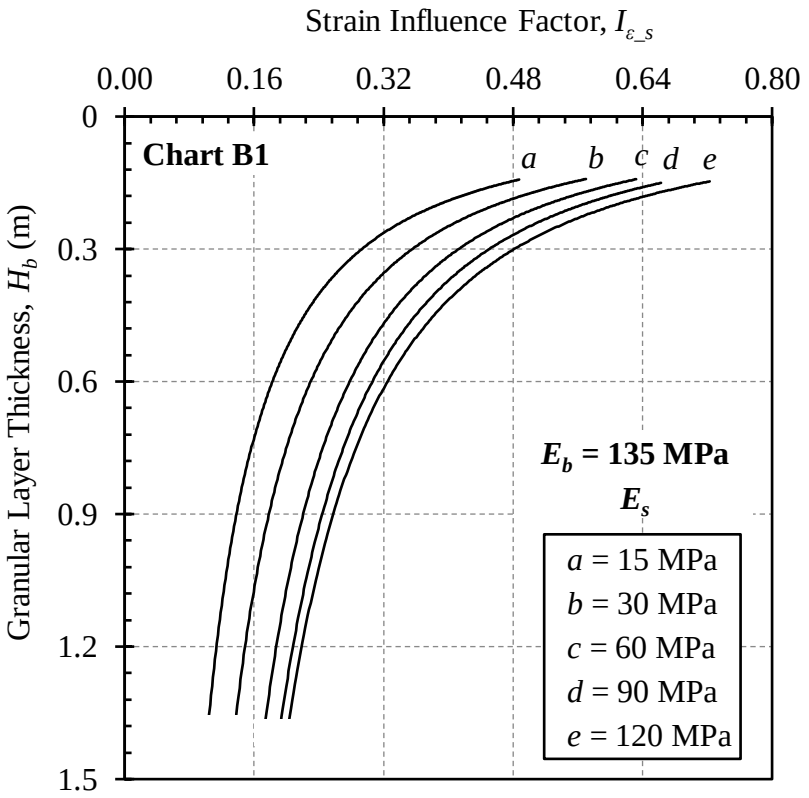

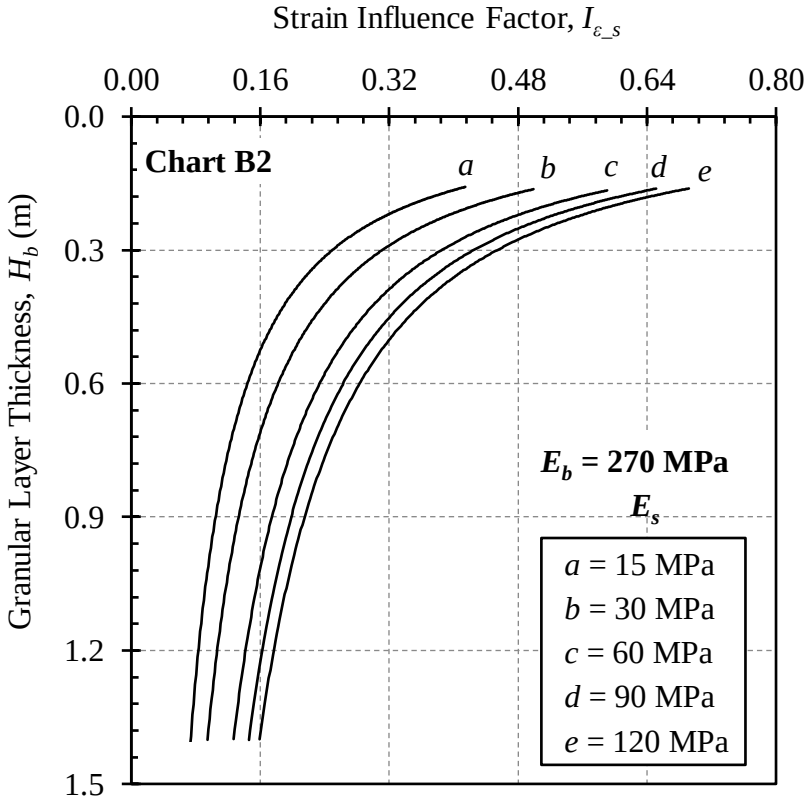

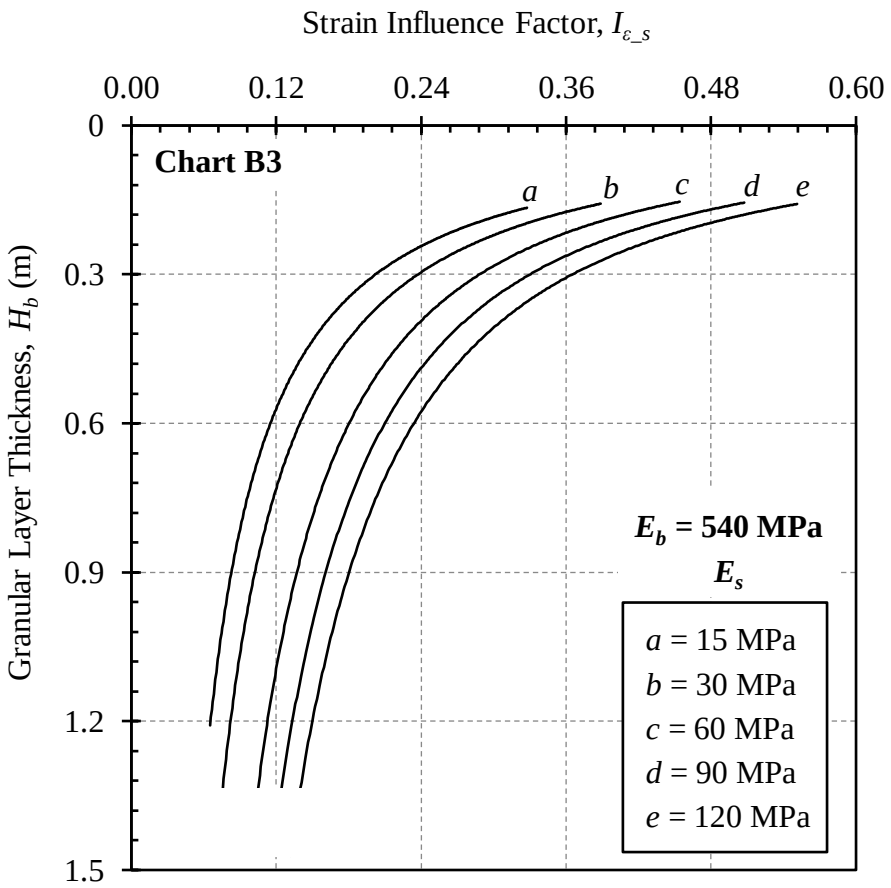
Strain Influence Factor, I_{ε_s}
0.00
0.12
0.24
0.36
0.48
0.60
0
0.3
0.6
0.9
1.2
1.5
Granular Layer Thickness, H_b (m)
Chart B3
a
b
c
d
e
E_b = 540 MPa
E_s
a = 15 MPa
b = 30 MPa
c = 60 MPa
d = 90 MPa
e = 120 MPa

Appendix C

Distribution of Strain Influence Factor with Ballast Depth

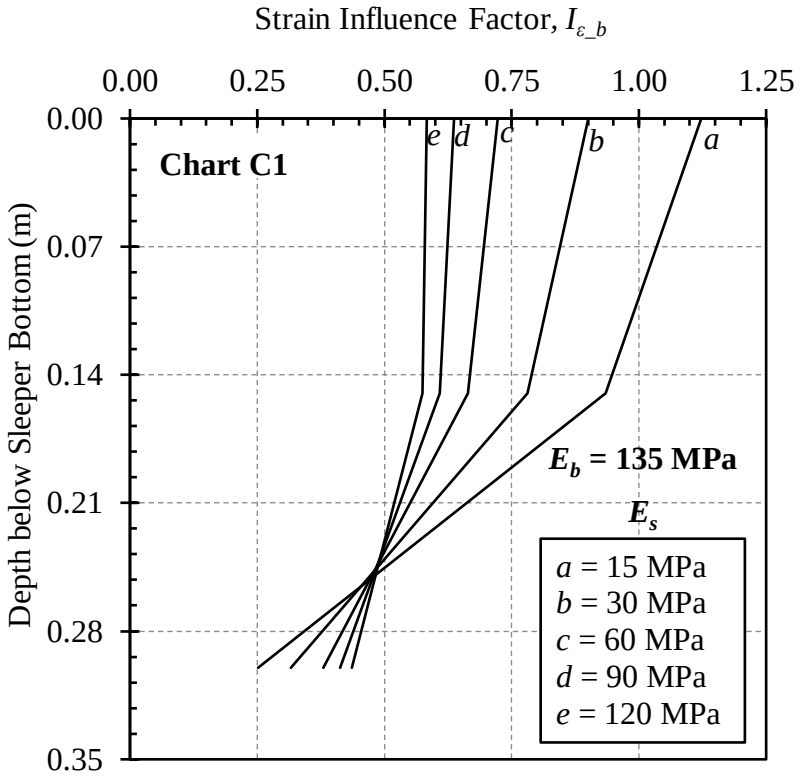

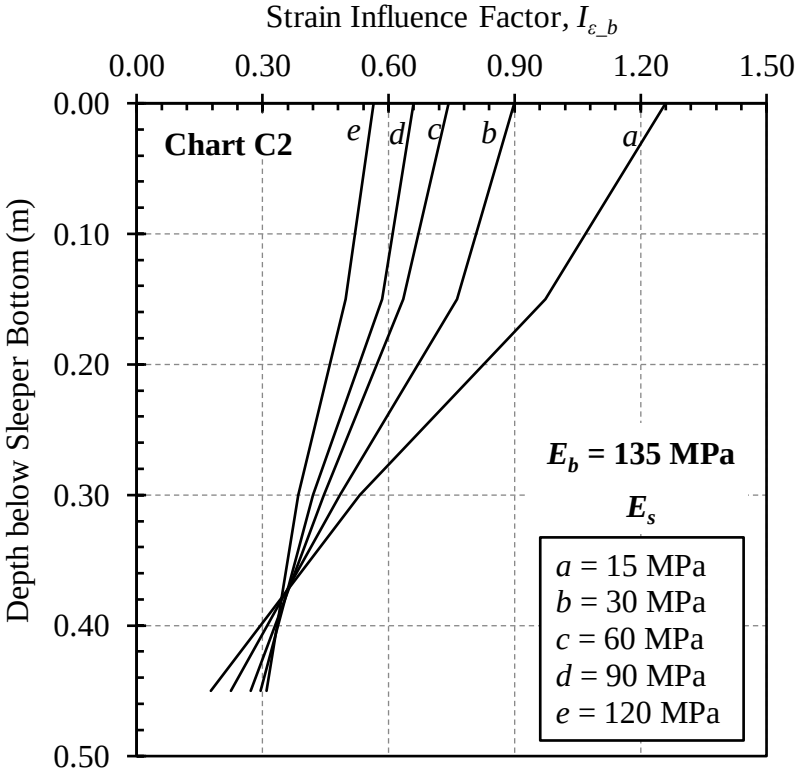

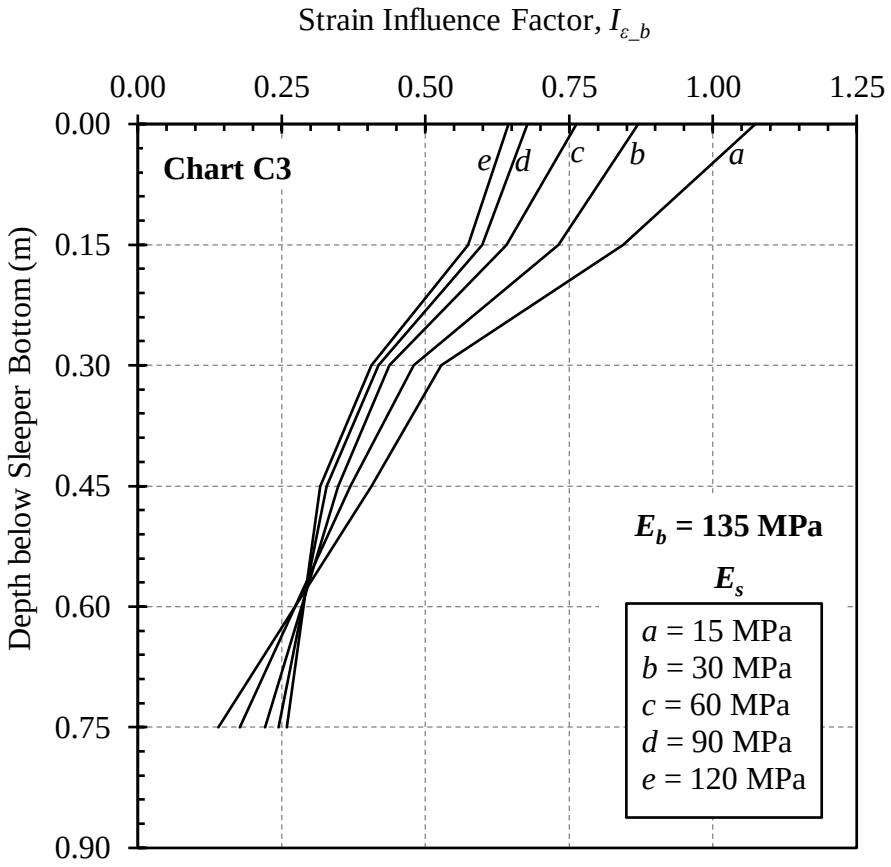
Strain Influence Factor, I_{ε_b}
0.00
0.25
0.50
0.75
1.00
1.25
Chart C3
e
d
c
b
a
Depth below Sleeper Bottom (m)
0.00
0.15
0.30
0.45
0.60
0.75
0.90
E_b = 135 MPa
E_s
a = 15 MPa
b = 30 MPa
c = 60 MPa
d = 90 MPa
e = 120 MPa

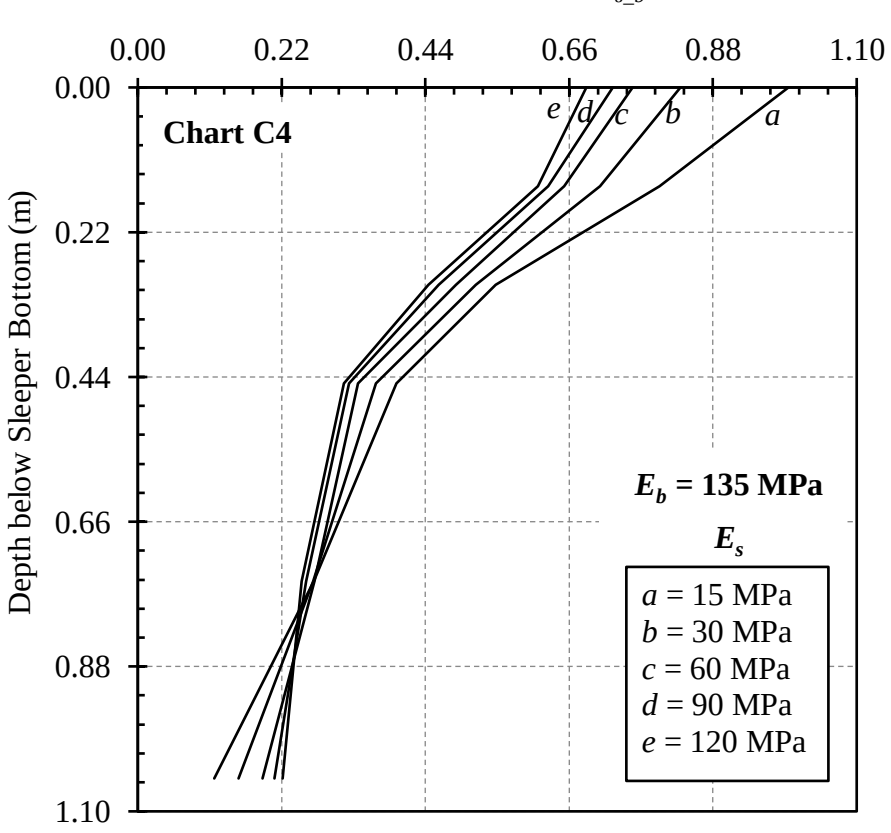
Strain Influence Factor, I_{ε_b}
0.00
0.22
0.44
0.66
0.88
1.10
Chart C4
e
d
c
b
a
Depth below Sleeper Bottom (m)
0.00
0.22
0.44
0.66
0.88
1.10
E_b = 135 MPa
E_s
a = 15 MPa
b = 30 MPa
c = 60 MPa
d = 90 MPa
e = 120 MPa

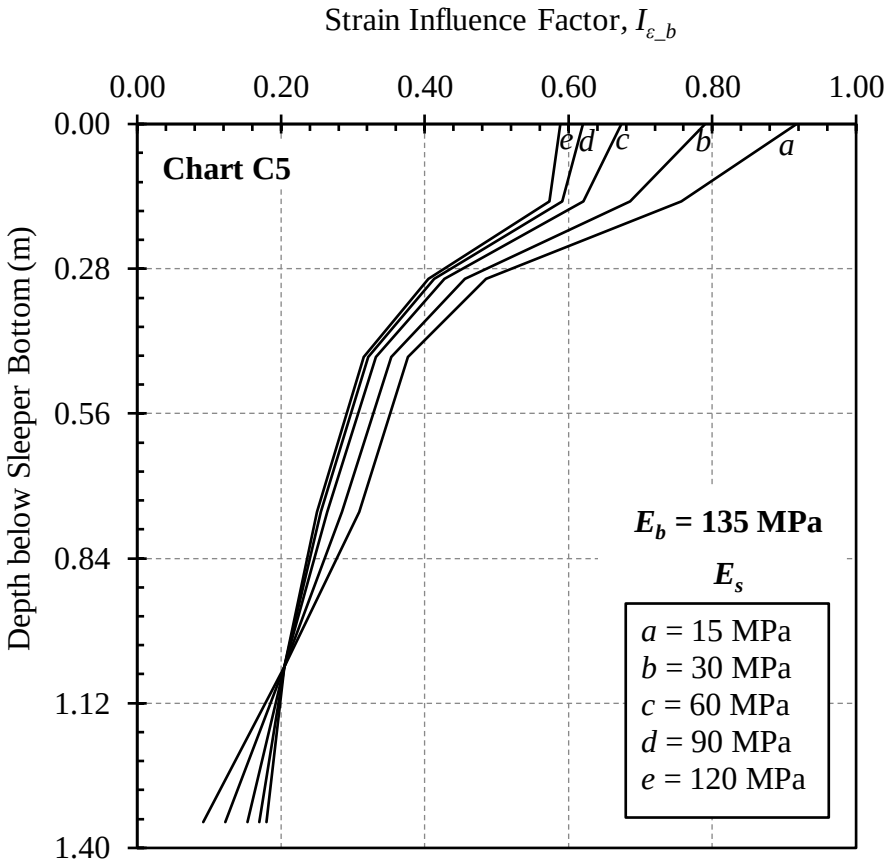
Strain Influence Factor, I_{ε_b}
0.00
0.20
0.40
0.60
0.80
1.00
Depth below Sleeper Bottom (m)
0.00
0.28
0.56
0.84
1.12
1.40
Chart C5
e
d
c
b
a
E_b = 135 MPa
E_s
a = 15 MPa
b = 30 MPa
c = 60 MPa
d = 90 MPa
e = 120 MPa

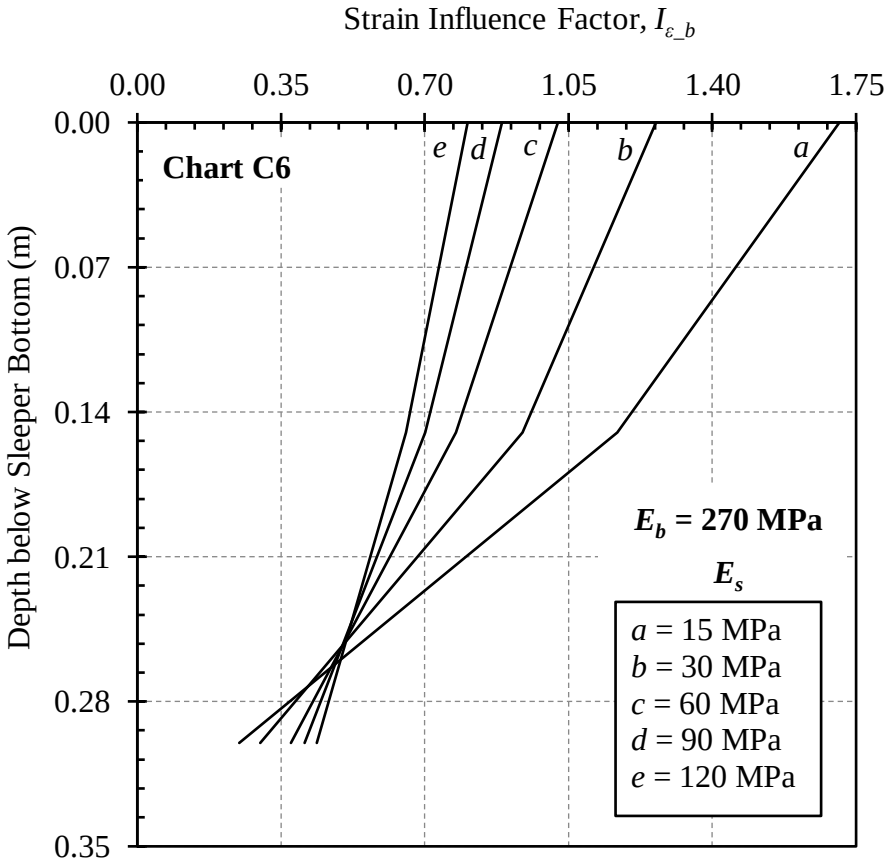
Strain Influence Factor, I_{ε_b}
0.00
0.35
0.70
1.05
1.40
1.75
Depth below Sleeper Bottom (m)
0.00
0.07
0.14
0.21
0.28
0.35
Chart C6
e
d
c
b
a
E_b = 270 MPa
E_s
a = 15 MPa
b = 30 MPa
c = 60 MPa
d = 90 MPa
e = 120 MPa

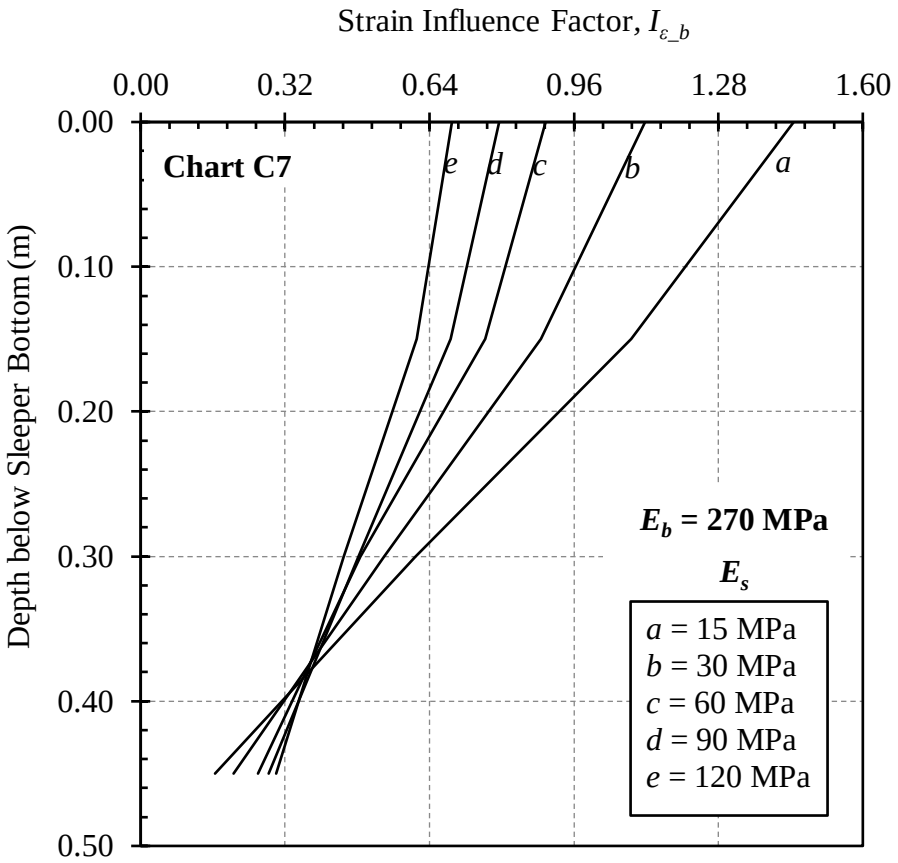
Strain Influence Factor, I_{ε_b}
0.00
0.32
0.64
0.96
1.28
1.60
Chart C7
e
d
c
b
a
Depth below Sleeper Bottom (m)
0.00
0.10
0.20
0.30
0.40
0.50
E_b = 270 MPa
E_s
a = 15 MPa
b = 30 MPa
c = 60 MPa
d = 90 MPa
e = 120 MPa

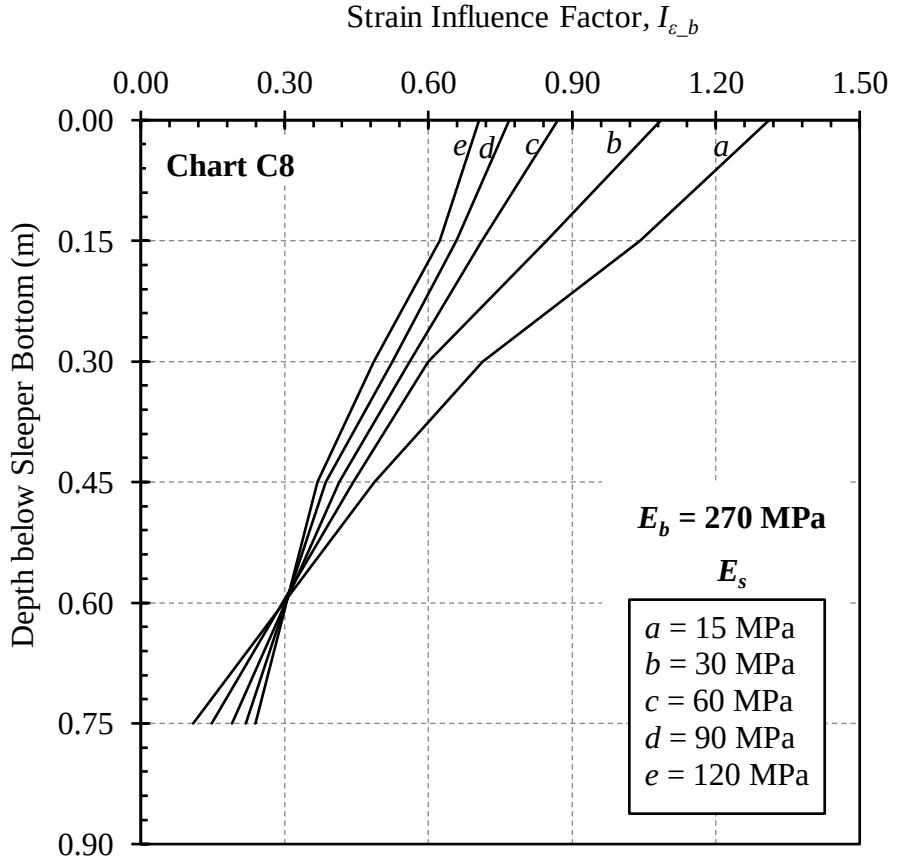
Strain Influence Factor, I_{ε_b}
0.00
0.30
0.60
0.90
1.20
1.50
Chart C8
e
d
c
b
a
Depth below Sleeper Bottom (m)
0.00
0.15
0.30
0.45
0.60
0.75
0.90
E_b = 270 MPa
E_s
a = 15 MPa
b = 30 MPa
c = 60 MPa
d = 90 MPa
e = 120 MPa

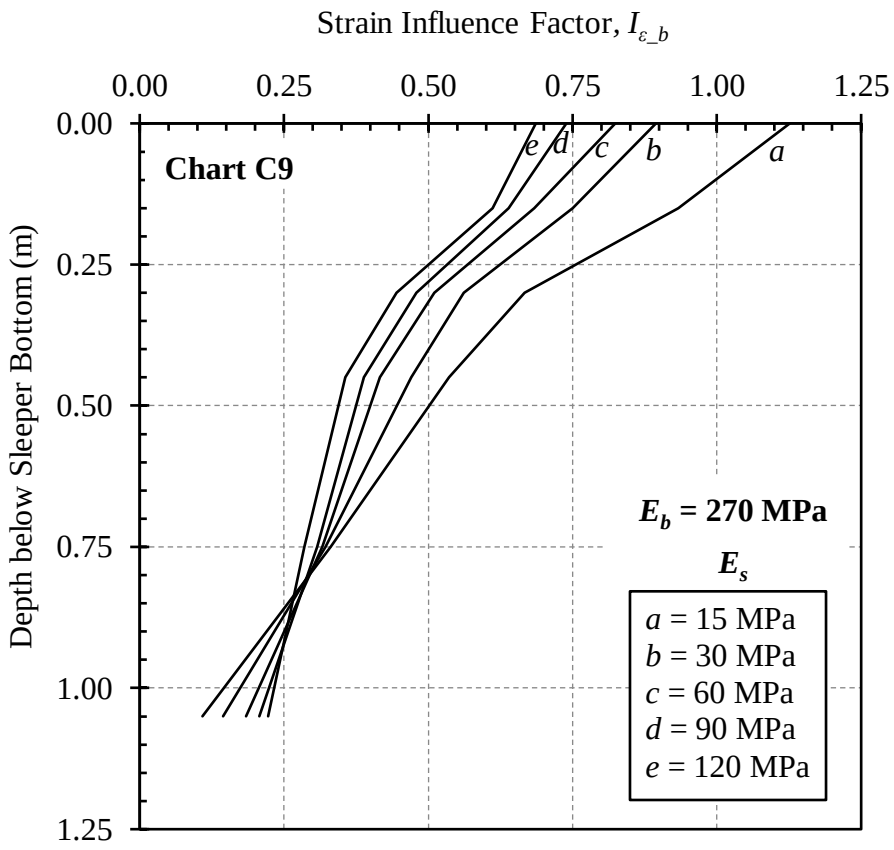
Strain Influence Factor, I_{ε_b}
0.00
0.25
0.50
0.75
1.00
1.25
Depth below Sleeper Bottom (m)
0.00
0.25
0.50
0.75
1.00
1.25
Chart C9
e
d
c
b
a
E_b = 270 MPa
E_s
a = 15 MPa
b = 30 MPa
c = 60 MPa
d = 90 MPa
e = 120 MPa

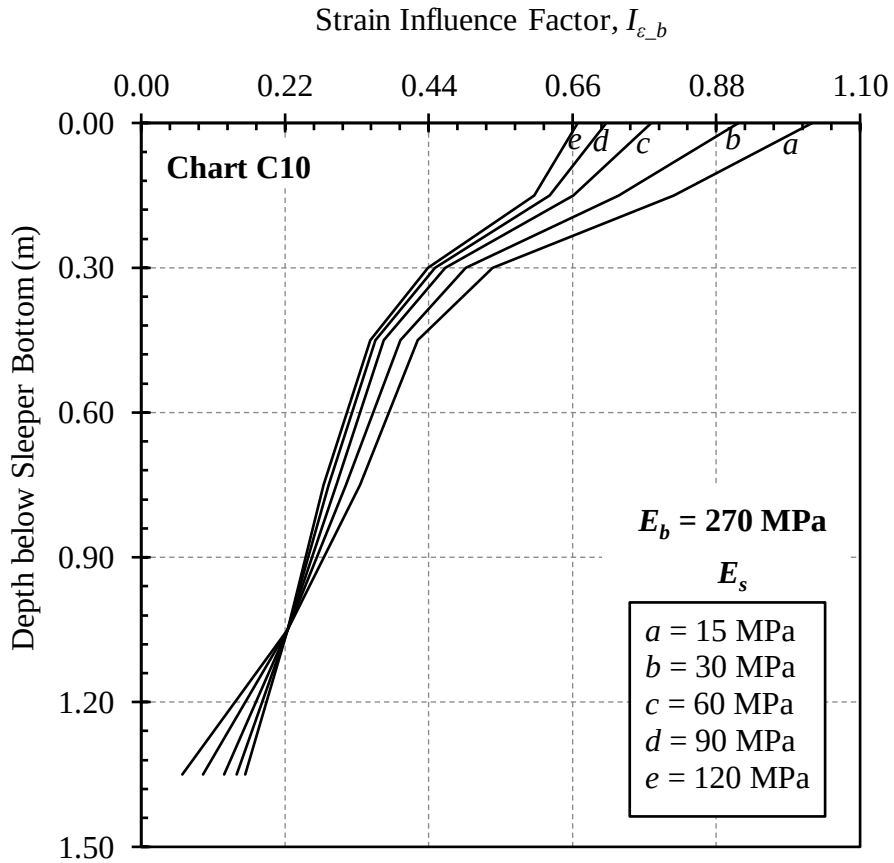
Strain Influence Factor, I_{ε_b}
0.00
0.22
0.44
0.66
0.88
1.10
Depth below Sleeper Bottom (m)
0.00
0.30
0.60
0.90
1.20
1.50
Chart C10
e
d
c
b
a
E_b = 270 MPa
E_s
a = 15 MPa
b = 30 MPa
c = 60 MPa
d = 90 MPa
e = 120 MPa

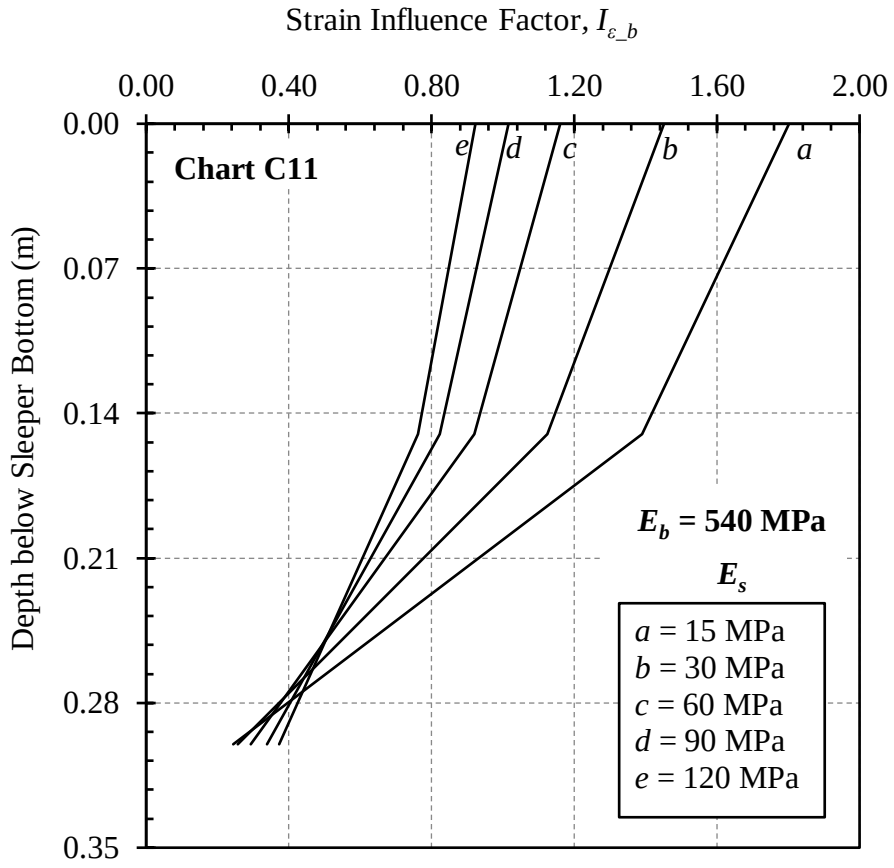
Strain Influence Factor, I_{ε_b}
0.00
0.40
0.80
1.20
1.60
2.00
0.00
0.07
0.14
0.21
0.28
0.35
Depth below Sleeper Bottom (m)
Chart C11
e
d
c
b
a
E_b = 540 MPa
E_s
a = 15 MPa
b = 30 MPa
c = 60 MPa
d = 90 MPa
e = 120 MPa

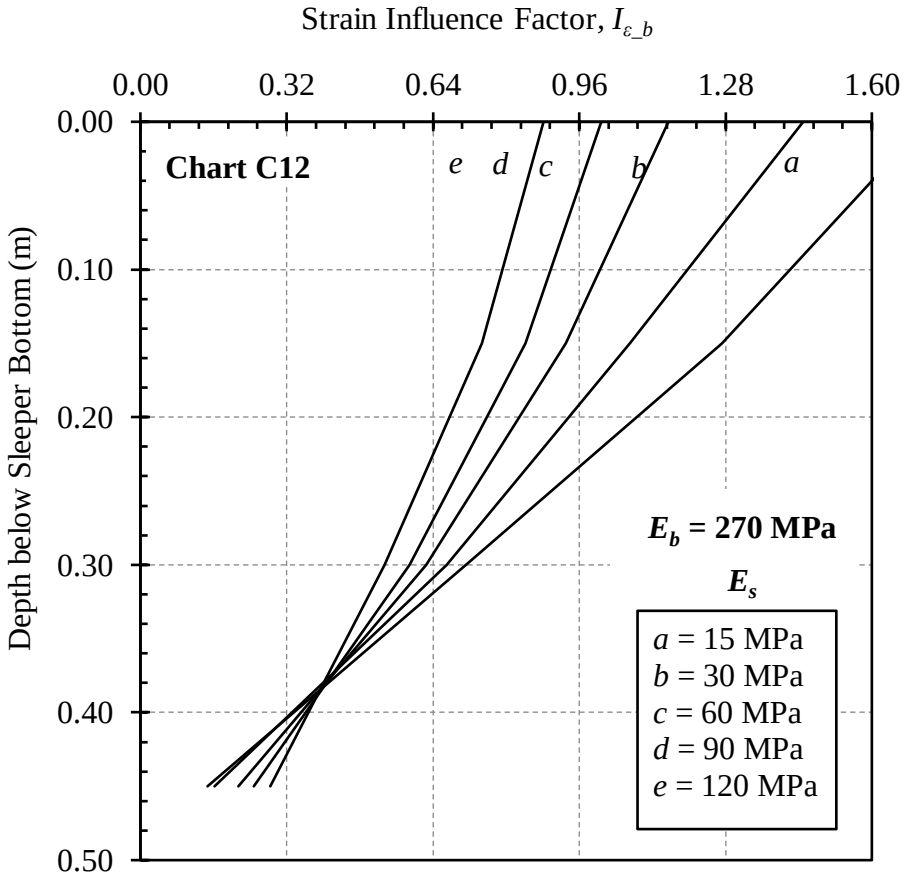
Strain Influence Factor, I_{ε_b}
0.00
0.32
0.64
0.96
1.28
1.60
0.00
0.10
0.20
0.30
0.40
0.50
Depth below Sleeper Bottom (m)
Chart C12
e
d
c
b
a
E_b = 270 MPa
E_s
a = 15 MPa
b = 30 MPa
c = 60 MPa
d = 90 MPa
e = 120 MPa

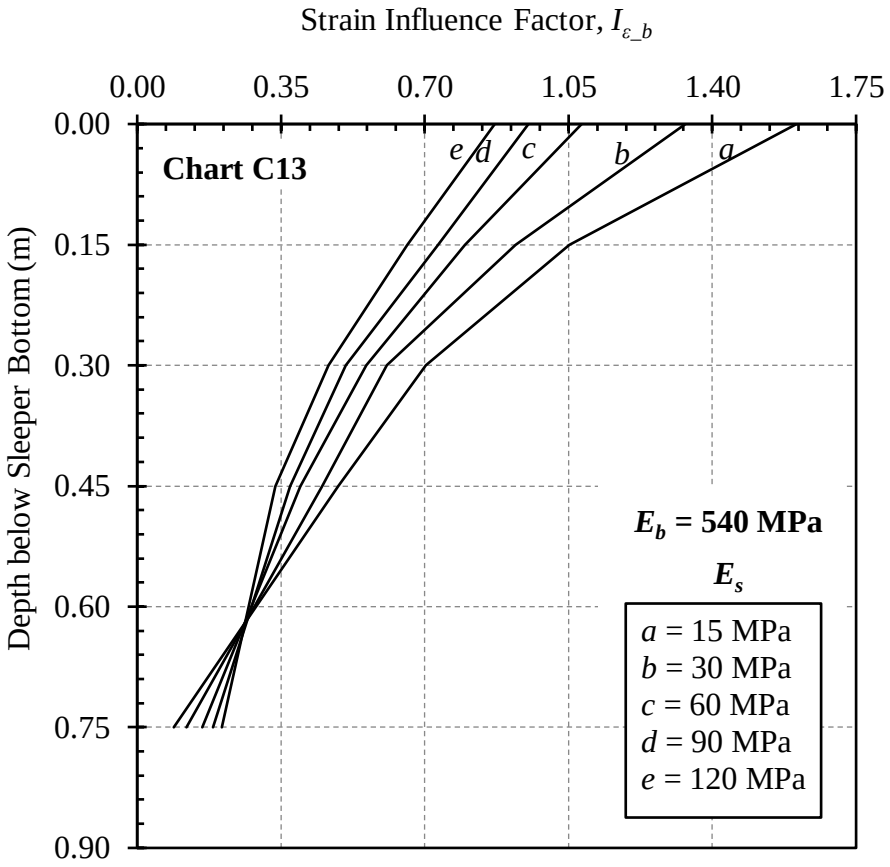
Strain Influence Factor, I_{ε_b}
0.00
0.35
0.70
1.05
1.40
1.75
Depth below Sleeper Bottom (m)
0.00
0.15
0.30
0.45
0.60
0.75
0.90
Chart C13
e
d
c
b
a
E_b = 540 MPa
E_s
a = 15 MPa
b = 30 MPa
c = 60 MPa
d = 90 MPa
e = 120 MPa

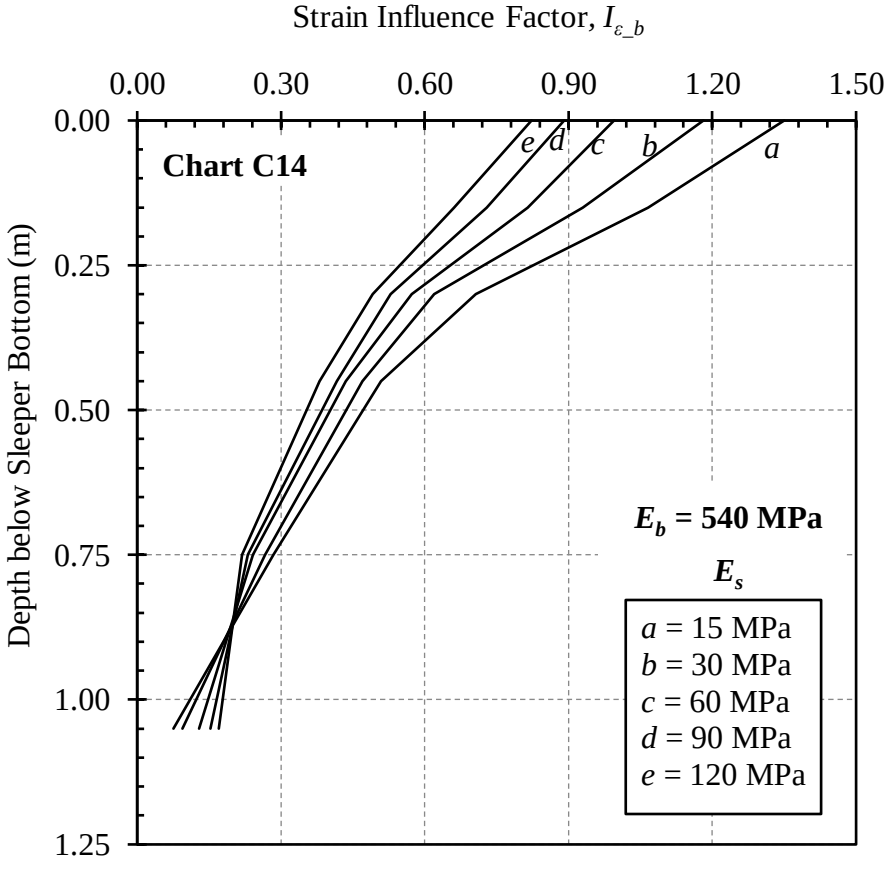
Strain Influence Factor, I_{ε_b}
0.00
0.30
0.60
0.90
1.20
1.50
Depth below Sleeper Bottom (m)
0.00
0.25
0.50
0.75
1.00
1.25
Chart C14
e
d
c
b
a
E_b = 540 MPa
E_s
a = 15 MPa
b = 30 MPa
c = 60 MPa
d = 90 MPa
e = 120 MPa

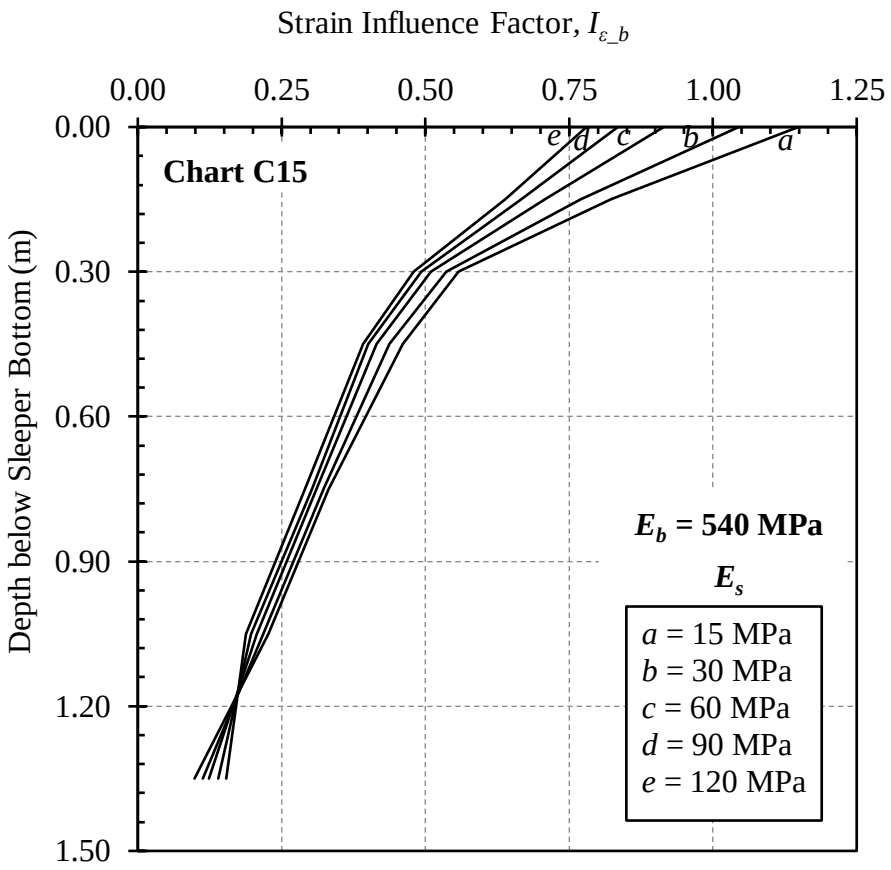
Strain Influence Factor, I_{ε_b}
0.00
0.25
0.50
0.75
1.00
1.25
0.00
0.30
0.60
0.90
1.20
1.50
Depth below Sleeper Bottom (m)
Chart C15
e
d
c
b
a
E_b = 540 MPa
E_s
a = 15 MPa
b = 30 MPa
c = 60 MPa
d = 90 MPa
e = 120 MPa

Appendix D

Design Charts to Prevent Excessive Plastic Deformation

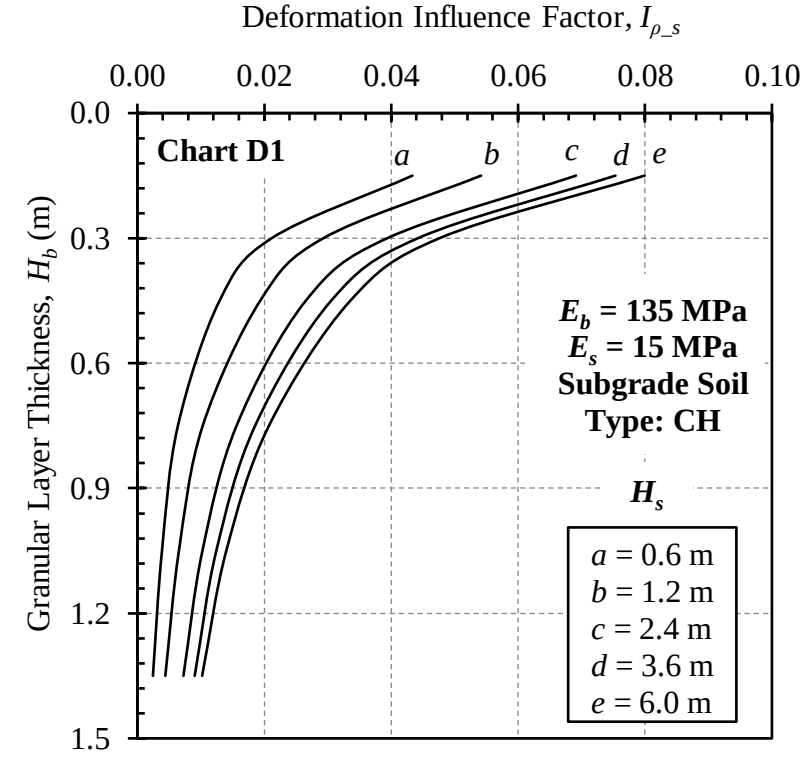

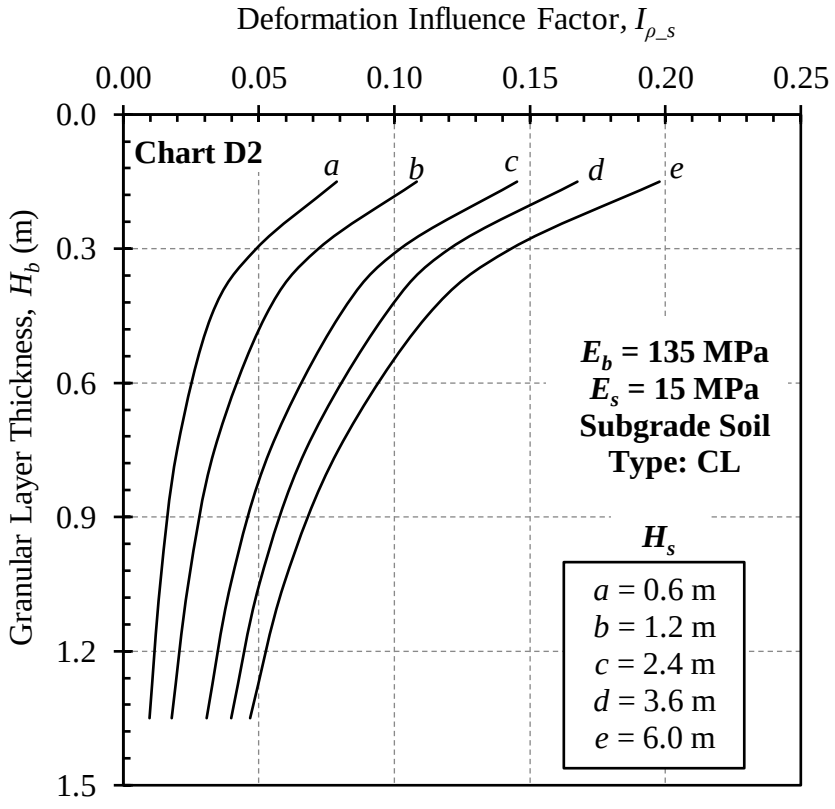

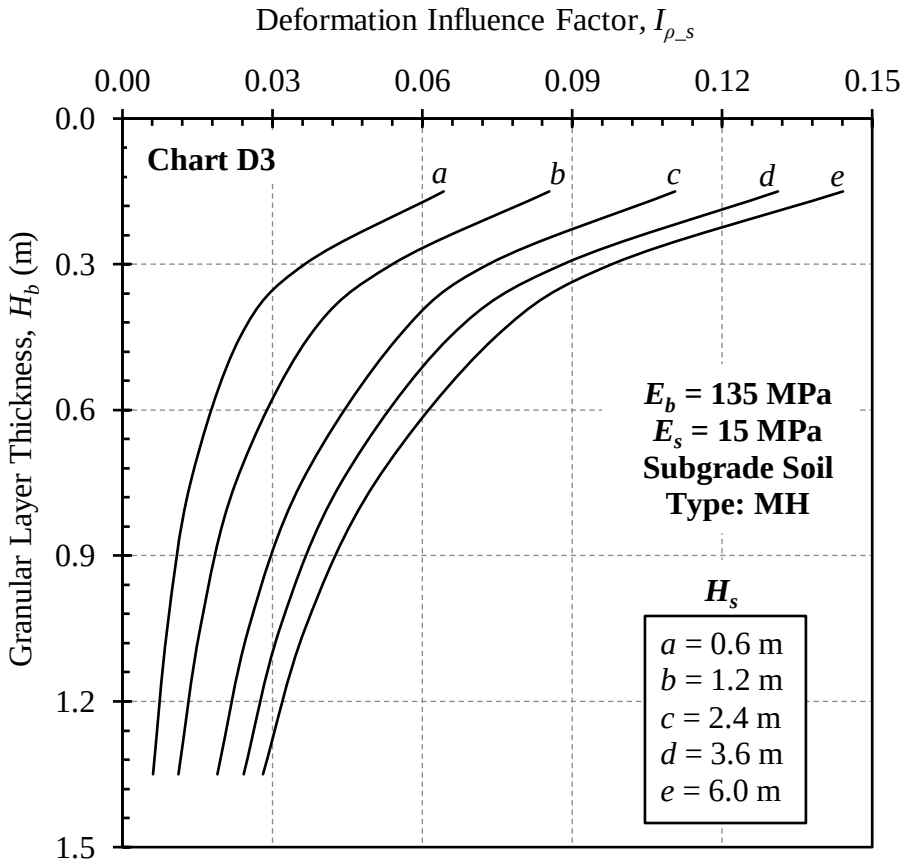
Deformation Influence Factor, I_{ρ_s}
0.00
0.03
0.06
0.09
0.12
0.15
Chart D3
a
b
c
d
e
Granular Layer Thickness, H_b (m)
0.0
0.3
0.6
0.9
1.2
1.5
E_b = 135 MPa
E_s = 15 MPa
Subgrade Soil Type: MH
H_s
a = 0.6 m
b = 1.2 m
c = 2.4 m
d = 3.6 m
e = 6.0 m

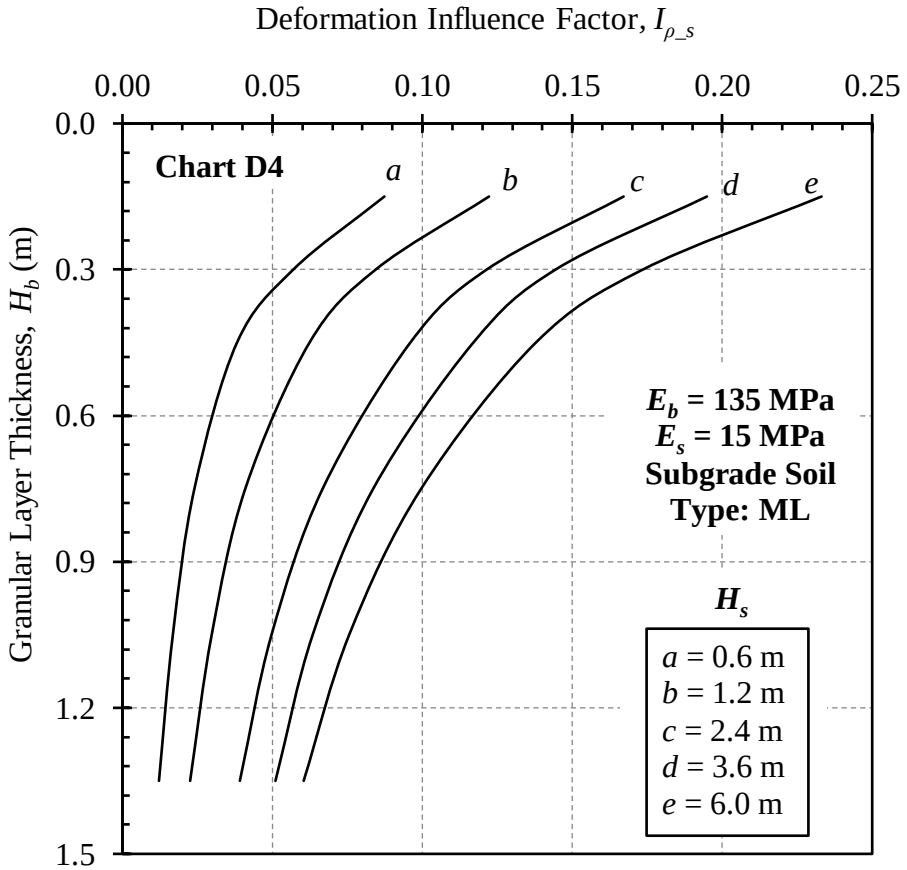
Deformation Influence Factor, I_{ρ_s}
0.00
0.05
0.10
0.15
0.20
0.25
Chart D4
a
b
c
d
e
Granular Layer Thickness, H_b (m)
0.0
0.3
0.6
0.9
1.2
1.5
E_b = 135 MPa
E_s = 15 MPa
Subgrade Soil Type: ML
H_s
a = 0.6 m
b = 1.2 m
c = 2.4 m
d = 3.6 m
e = 6.0 m

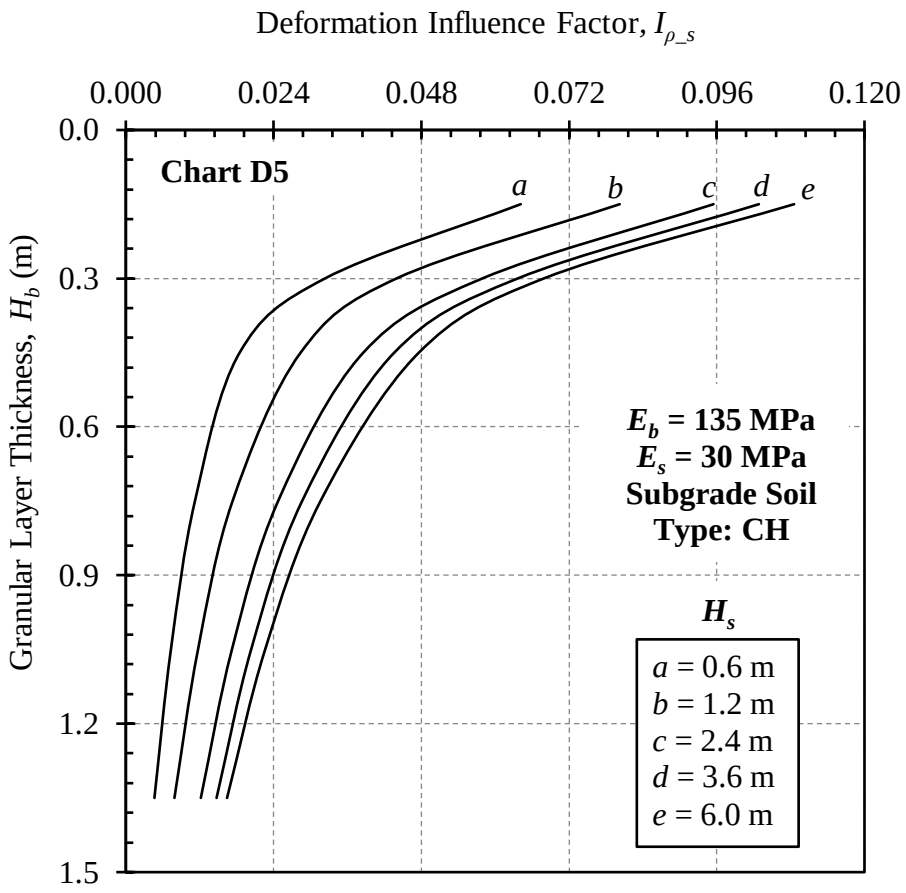
Deformation Influence Factor, I_{ρ_s}
0.000
0.024
0.048
0.072
0.096
0.120
0.0
0.3
0.6
0.9
1.2
1.5
Granular Layer Thickness, H_b (m)
Chart D5
a
b
c
d
e
E_b = 135 MPa
E_s = 30 MPa
Subgrade Soil
Type: CH
H_s
a = 0.6 m
b = 1.2 m
c = 2.4 m
d = 3.6 m
e = 6.0 m

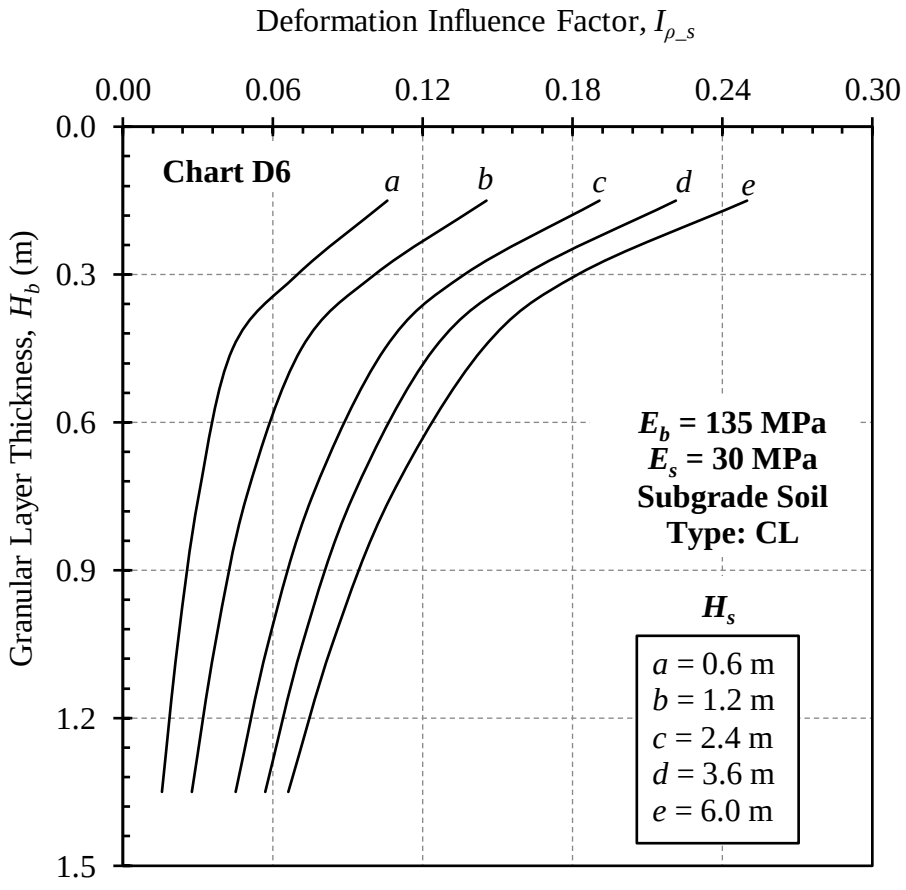
Deformation Influence Factor, I_{ρ_s}
0.00
0.06
0.12
0.18
0.24
0.30
0.0
0.3
0.6
0.9
1.2
1.5
Granular Layer Thickness, H_b (m)
Chart D6
a
b
c
d
e
E_b = 135 MPa
E_s = 30 MPa
Subgrade Soil
Type: CL
H_s
a = 0.6 m
b = 1.2 m
c = 2.4 m
d = 3.6 m
e = 6.0 m

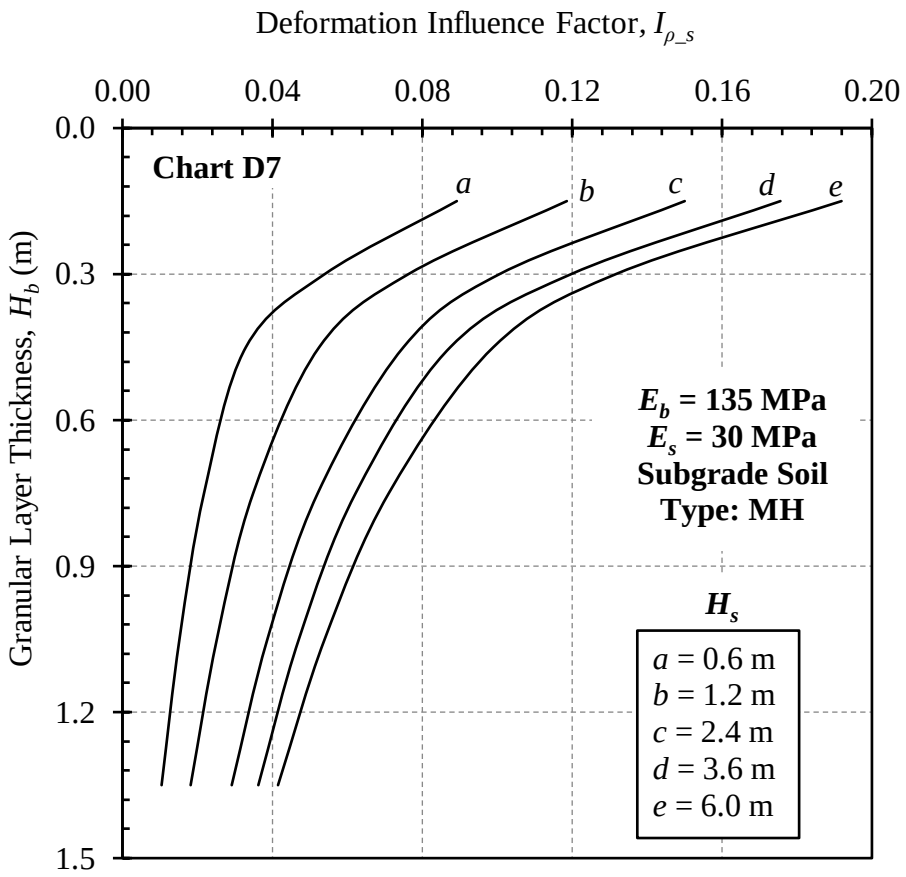
Deformation Influence Factor, I_{ρ_s}
0.00
0.04
0.08
0.12
0.16
0.20
0.0
0.3
0.6
0.9
1.2
1.5
Granular Layer Thickness, H_b (m)
Chart D7
a
b
c
d
e
E_b = 135 MPa
E_s = 30 MPa
Subgrade Soil
Type: MH
H_s
a = 0.6 m
b = 1.2 m
c = 2.4 m
d = 3.6 m
e = 6.0 m

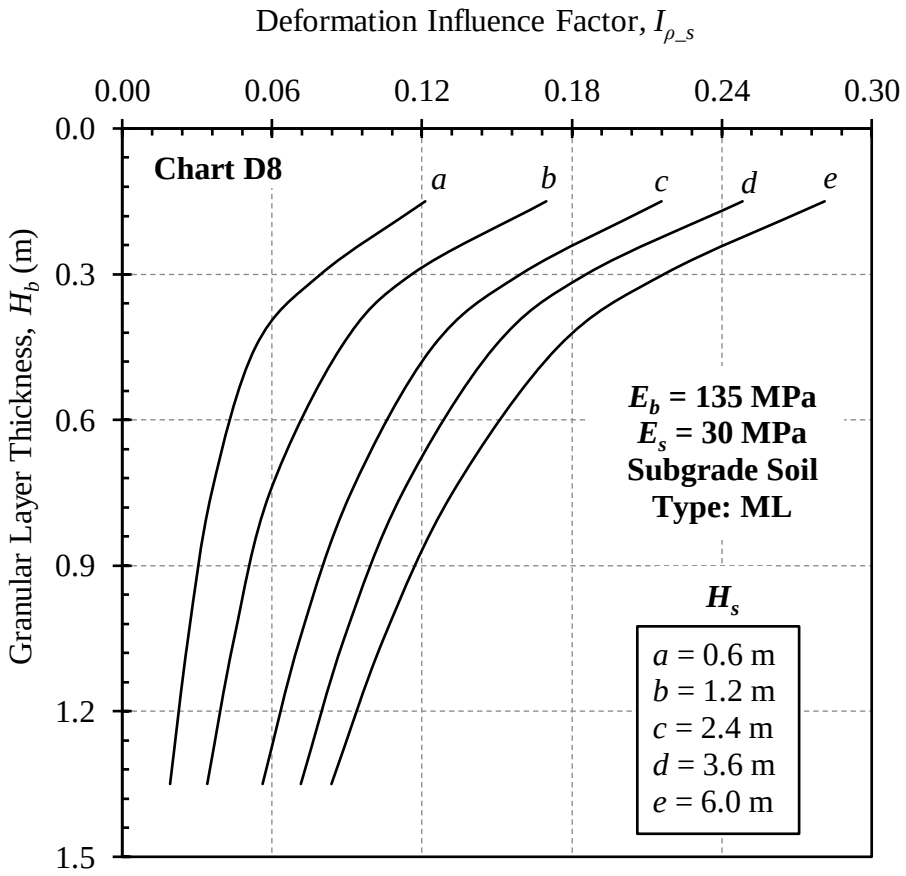
Deformation Influence Factor, I_{ρ_s}
0.00
0.06
0.12
0.18
0.24
0.30
0.0
0.3
0.6
0.9
1.2
1.5
Granular Layer Thickness, H_b (m)
Chart D8
a
b
c
d
e
E_b = 135 MPa
E_s = 30 MPa
Subgrade Soil
Type: ML
H_s
a = 0.6 m
b = 1.2 m
c = 2.4 m
d = 3.6 m
e = 6.0 m

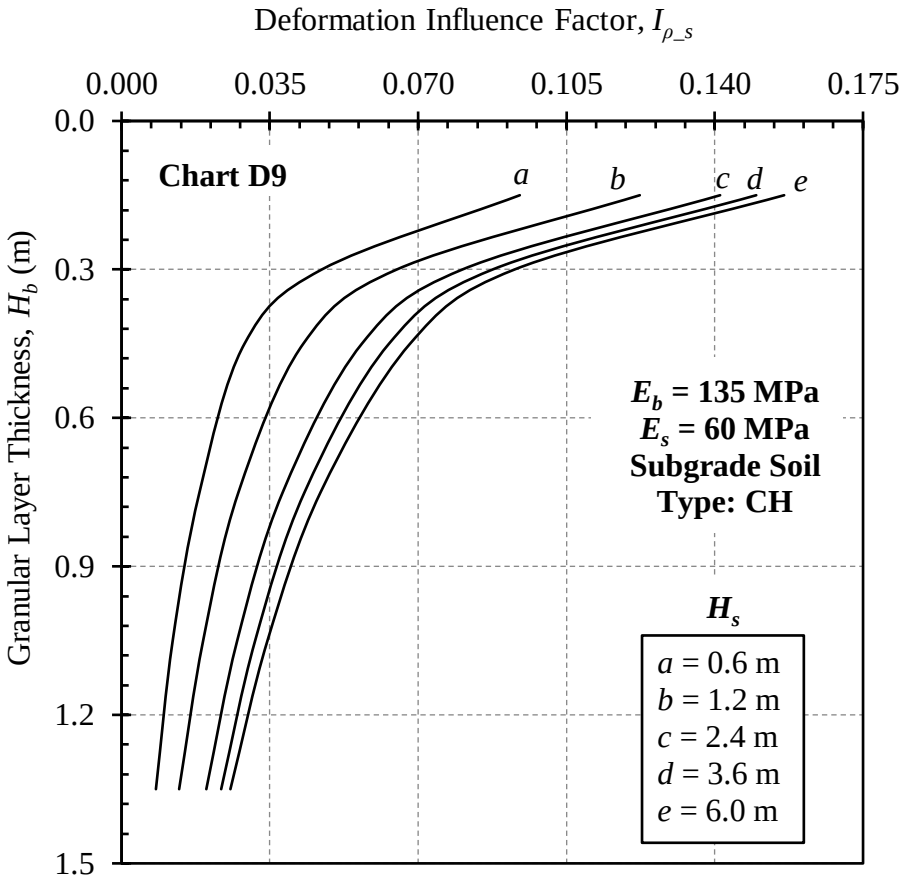
Deformation Influence Factor, I_{ρ_s}
0.000
0.035
0.070
0.105
0.140
0.175
0.0
0.3
0.6
0.9
1.2
1.5
Granular Layer Thickness, H_b (m)
Chart D9
a
b
c
d
e
E_b = 135 MPa
E_s = 60 MPa
Subgrade Soil
Type: CH
H_s
a = 0.6 m
b = 1.2 m
c = 2.4 m
d = 3.6 m
e = 6.0 m

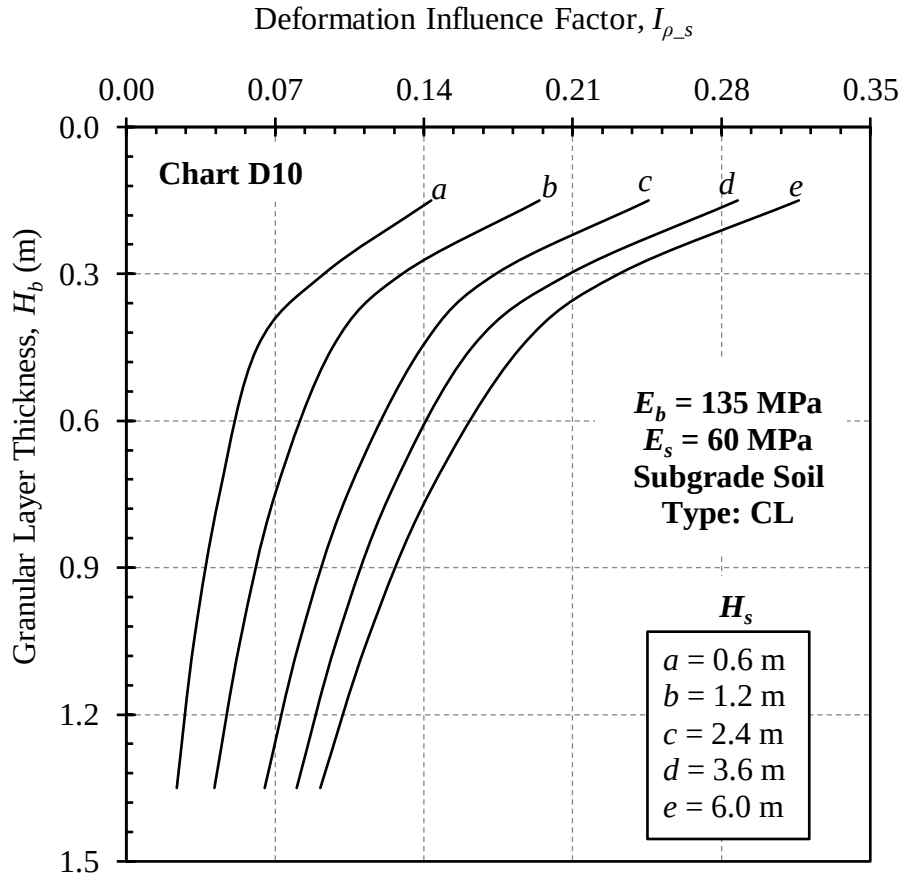
Deformation Influence Factor, I_{ρ_s}
0.00
0.07
0.14
0.21
0.28
0.35
0.0
0.3
0.6
0.9
1.2
1.5
Granular Layer Thickness, H_b (m)
Chart D10
a
b
c
d
e
E_b = 135 MPa
E_s = 60 MPa
Subgrade Soil
Type: CL
H_s
a = 0.6 m
b = 1.2 m
c = 2.4 m
d = 3.6 m
e = 6.0 m

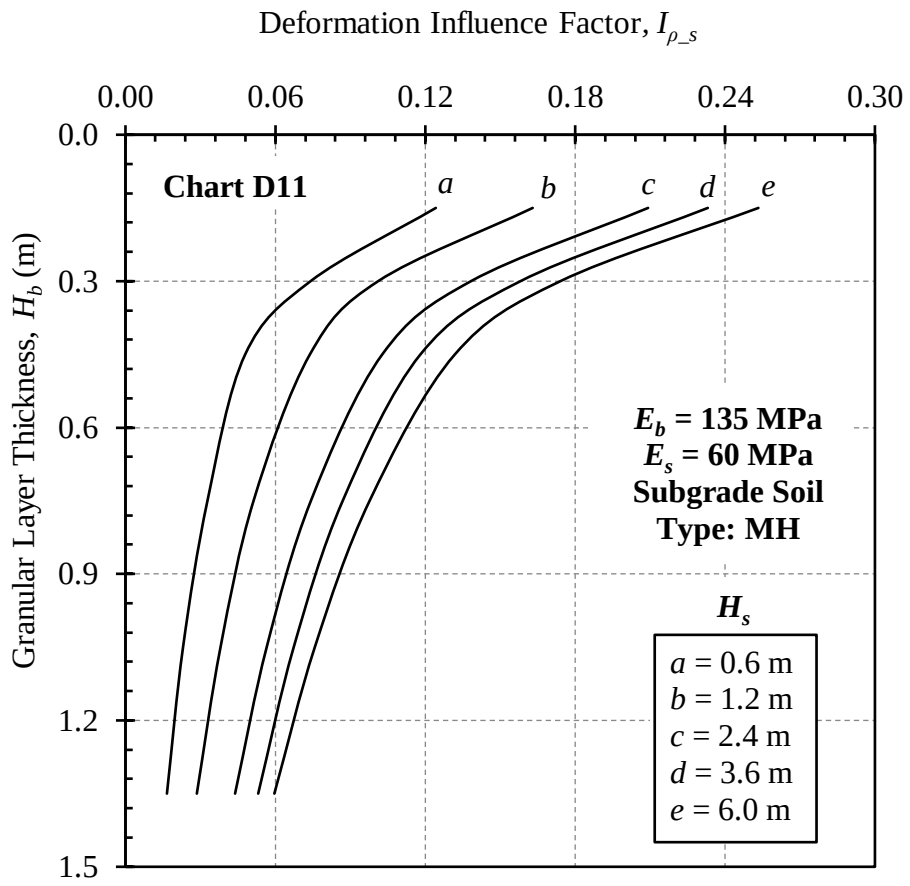
Deformation Influence Factor, I_{ρ_s}
0.00
0.06
0.12
0.18
0.24
0.30
0.0
0.3
0.6
0.9
1.2
1.5
Granular Layer Thickness, H_b (m)
Chart D11
a
b
c
d
e
E_b = 135 MPa
E_s = 60 MPa
Subgrade Soil
Type: MH
H_s
a = 0.6 m
b = 1.2 m
c = 2.4 m
d = 3.6 m
e = 6.0 m

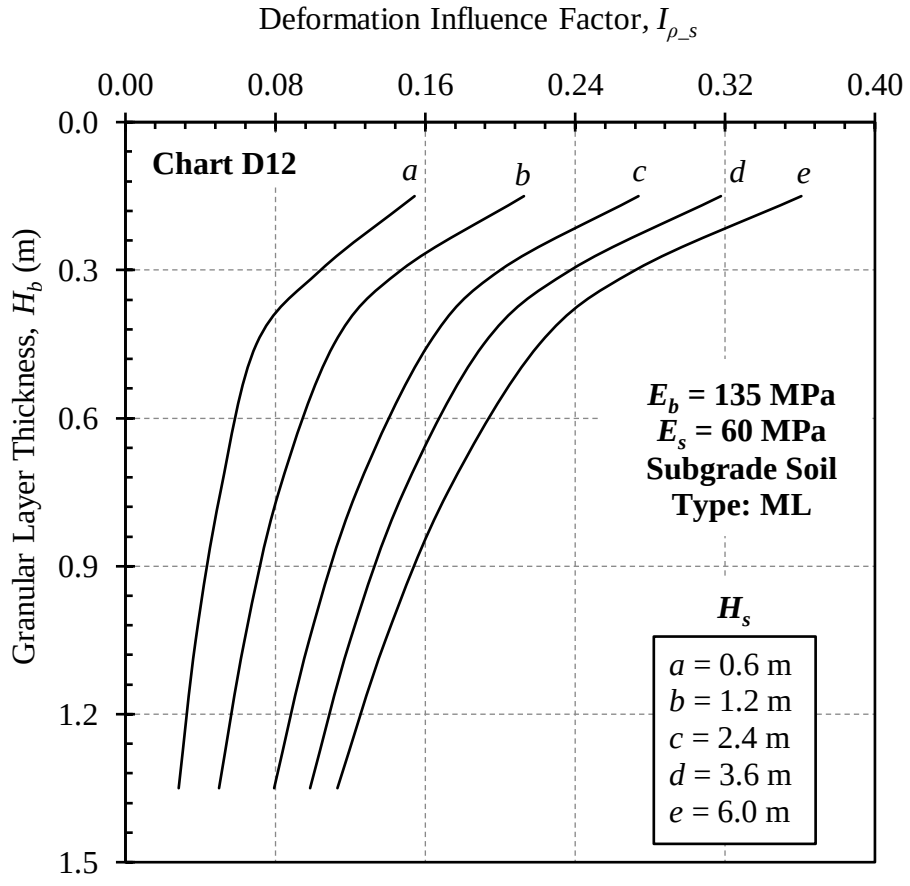
Deformation Influence Factor, I_{ρ_s}
0.00
0.08
0.16
0.24
0.32
0.40
0.0
0.3
0.6
0.9
1.2
1.5
Granular Layer Thickness, H_b (m)
Chart D12
a
b
c
d
e
E_b = 135 MPa
E_s = 60 MPa
Subgrade Soil
Type: ML
H_s
a = 0.6 m
b = 1.2 m
c = 2.4 m
d = 3.6 m
e = 6.0 m

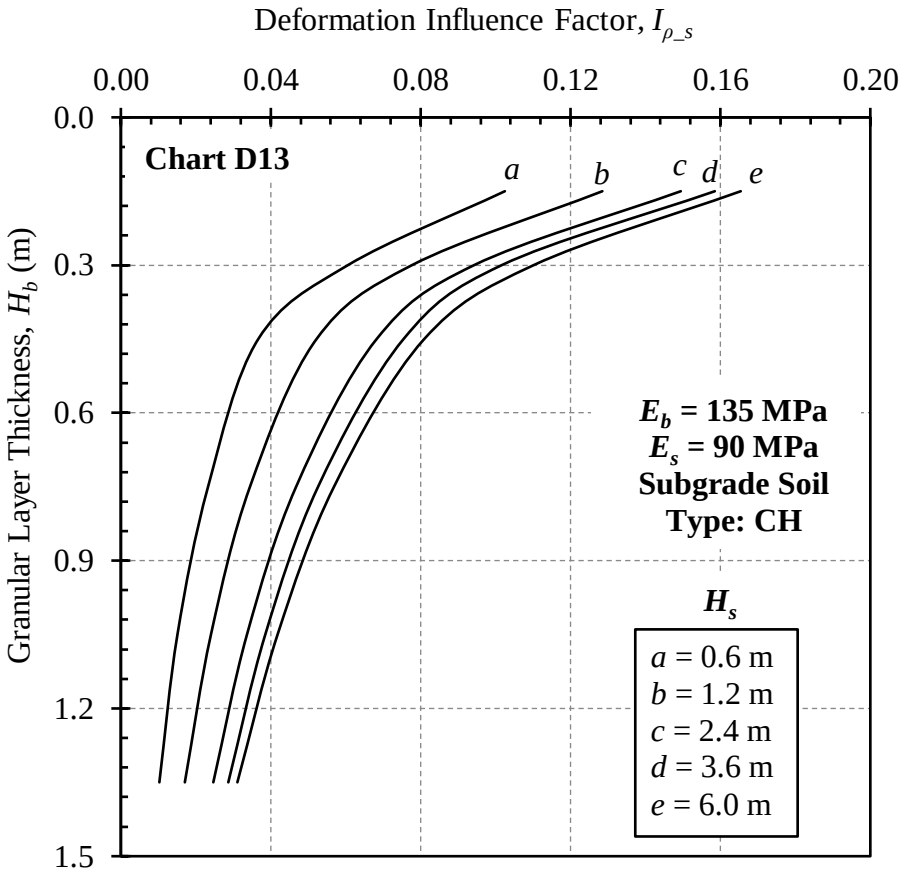
Deformation Influence Factor, I_{ρ_s}
0.00
0.04
0.08
0.12
0.16
0.20
0.0
0.3
0.6
0.9
1.2
1.5
Granular Layer Thickness, H_b (m)
Chart D13
a
b
c
d
e
E_b = 135 MPa
E_s = 90 MPa
Subgrade Soil
Type: CH
H_s
a = 0.6 m
b = 1.2 m
c = 2.4 m
d = 3.6 m
e = 6.0 m

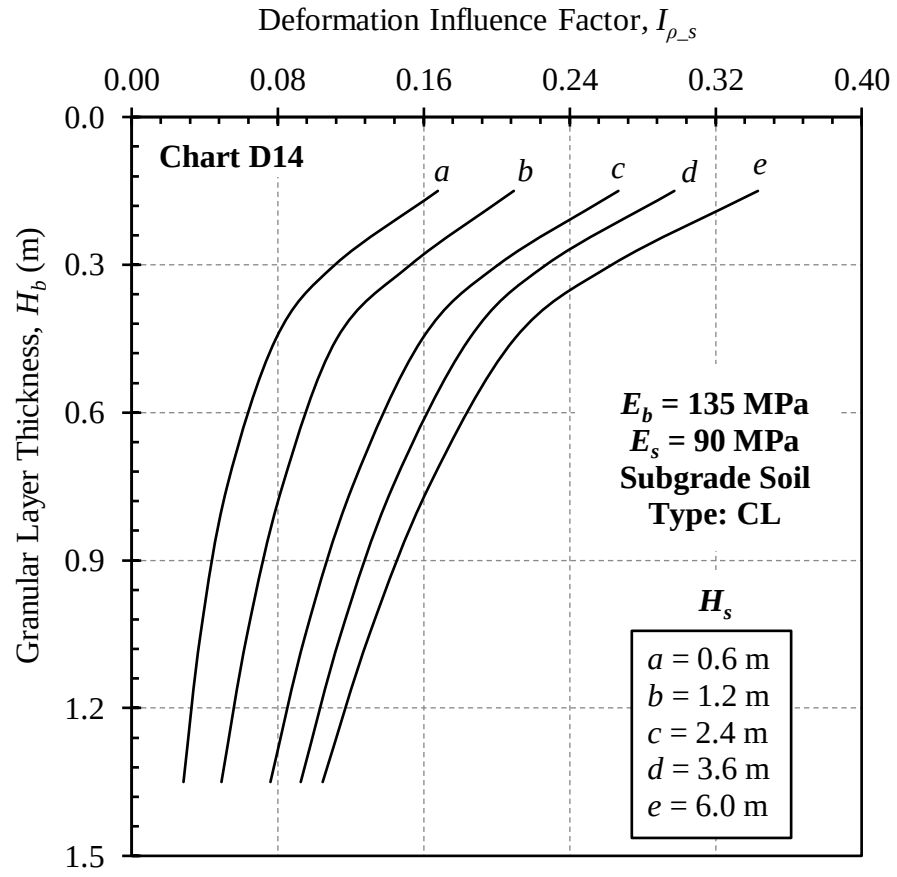
Deformation Influence Factor, I_{ρ_s}
0.00
0.08
0.16
0.24
0.32
0.40
0.0
0.3
0.6
0.9
1.2
1.5
Granular Layer Thickness, H_b (m)
Chart D14
a
b
c
d
e
E_b = 135 MPa
E_s = 90 MPa
Subgrade Soil
Type: CL
H_s
a = 0.6 m
b = 1.2 m
c = 2.4 m
d = 3.6 m
e = 6.0 m

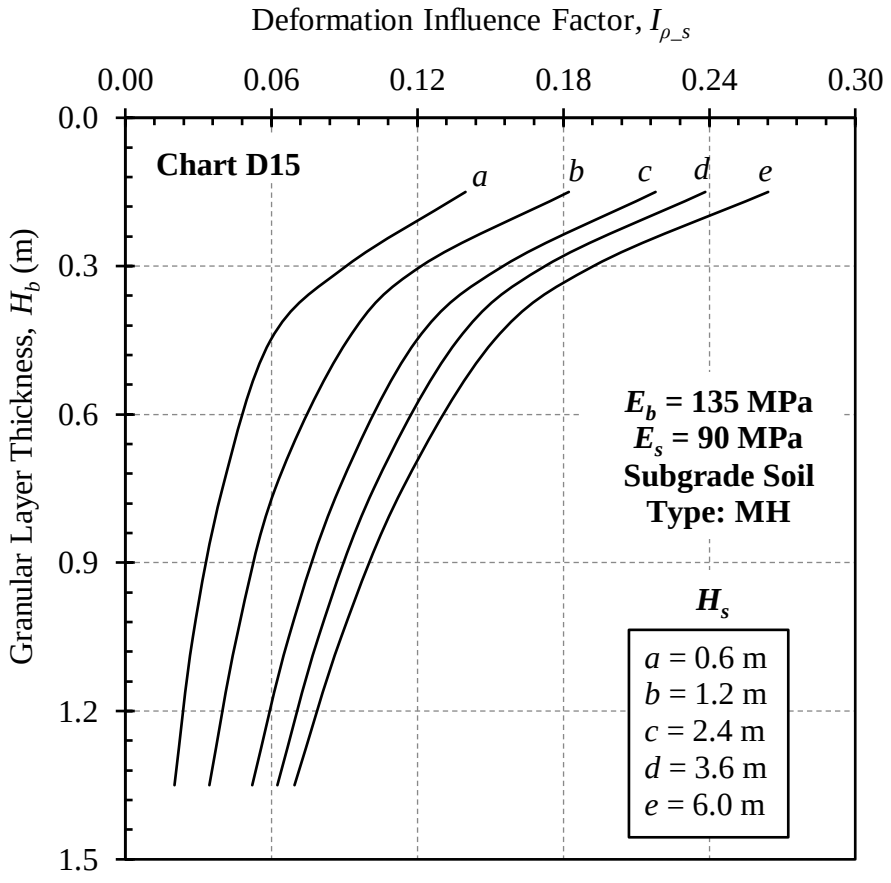
Deformation Influence Factor, I_{ρ_s}
0.00
0.06
0.12
0.18
0.24
0.30
0.0
0.3
0.6
0.9
1.2
1.5
Granular Layer Thickness, H_b (m)
Chart D15
a
b
c
d
e
E_b = 135 MPa
E_s = 90 MPa
Subgrade Soil Type: MH
H_s
a = 0.6 m
b = 1.2 m
c = 2.4 m
d = 3.6 m
e = 6.0 m

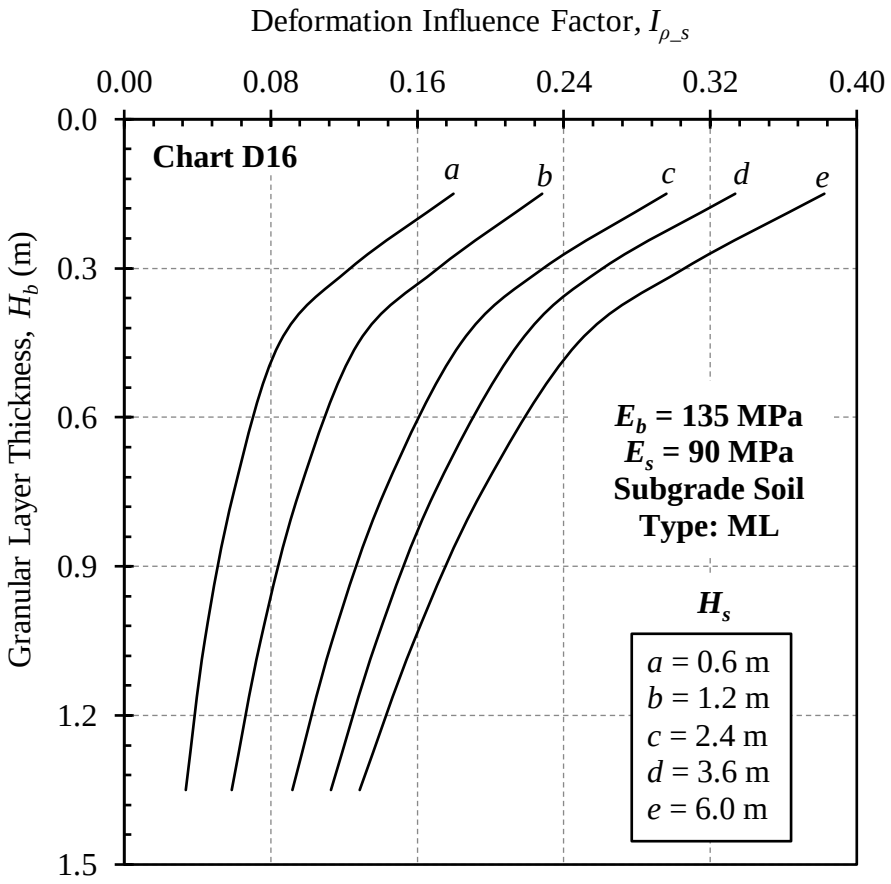
Deformation Influence Factor, I_{ρ_s}
0.00
0.08
0.16
0.24
0.32
0.40
0.0
0.3
0.6
0.9
1.2
1.5
Granular Layer Thickness, H_b (m)
Chart D16
a
b
c
d
e
E_b = 135 MPa
E_s = 90 MPa
Subgrade Soil Type: ML
H_s
a = 0.6 m
b = 1.2 m
c = 2.4 m
d = 3.6 m
e = 6.0 m

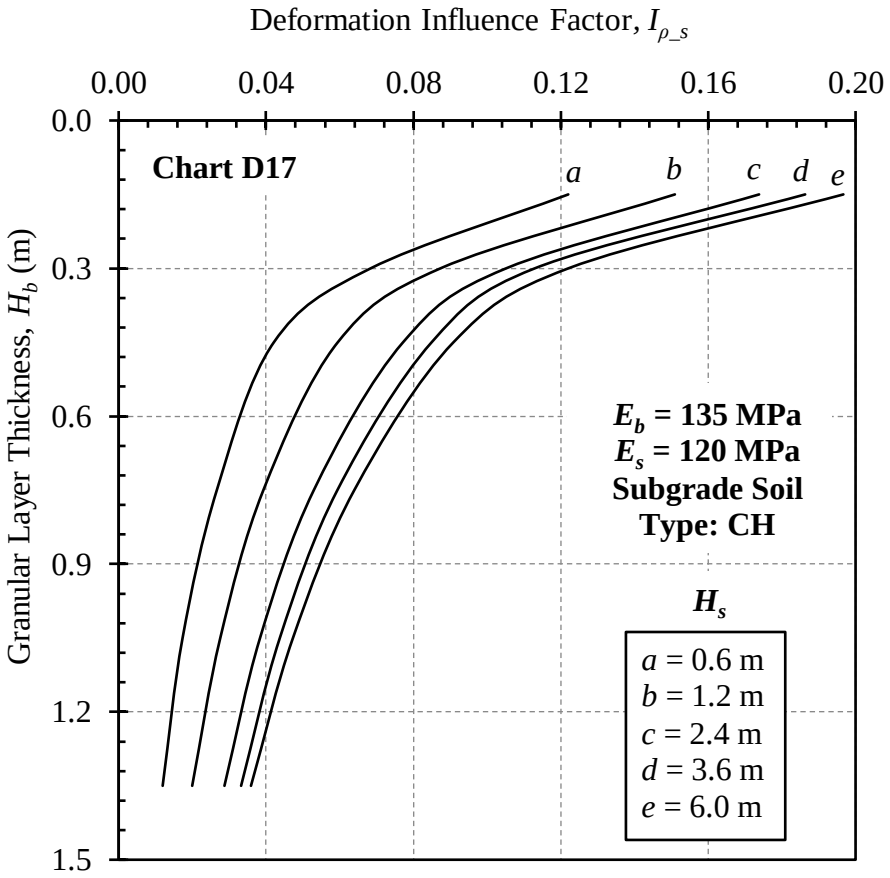
Deformation Influence Factor, I_{ρ_s}
0.00
0.04
0.08
0.12
0.16
0.20
0.0
0.3
0.6
0.9
1.2
1.5
Granular Layer Thickness, H_b (m)
Chart D17
a
b
c
d
e
E_b = 135 MPa
E_s = 120 MPa
Subgrade Soil
Type: CH
H_s
a = 0.6 m
b = 1.2 m
c = 2.4 m
d = 3.6 m
e = 6.0 m

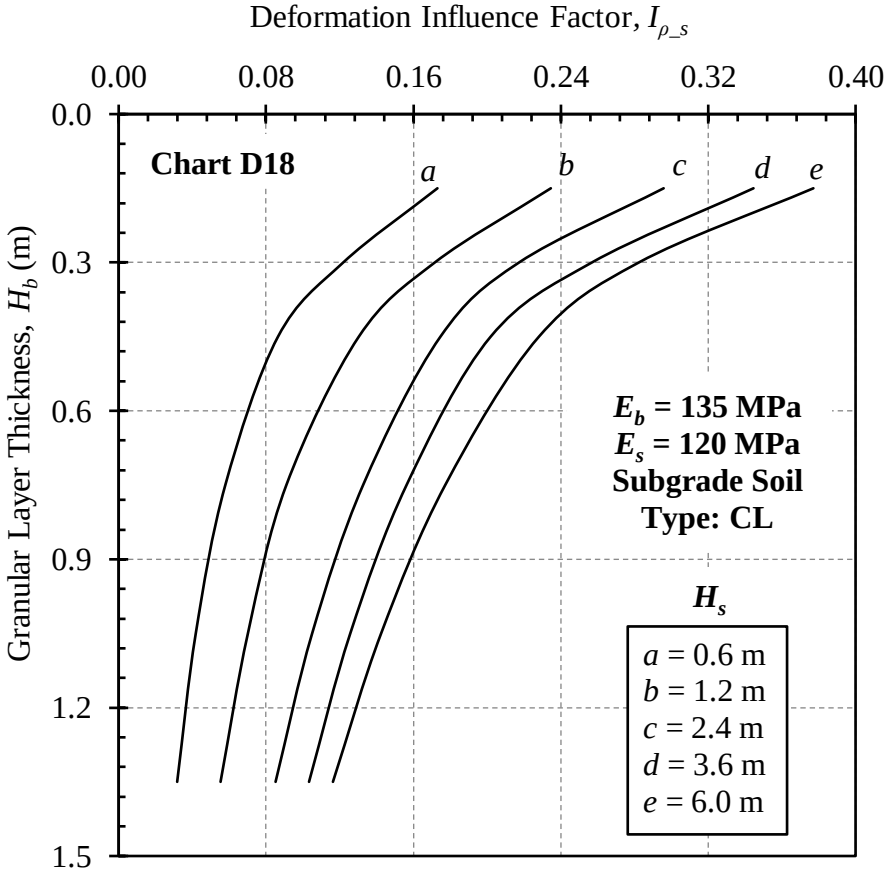
Deformation Influence Factor, I_{ρ_s}
0.00
0.08
0.16
0.24
0.32
0.40
0.0
0.3
0.6
0.9
1.2
1.5
Granular Layer Thickness, H_b (m)
Chart D18
a
b
c
d
e
E_b = 135 MPa
E_s = 120 MPa
Subgrade Soil
Type: CL
H_s
a = 0.6 m
b = 1.2 m
c = 2.4 m
d = 3.6 m
e = 6.0 m

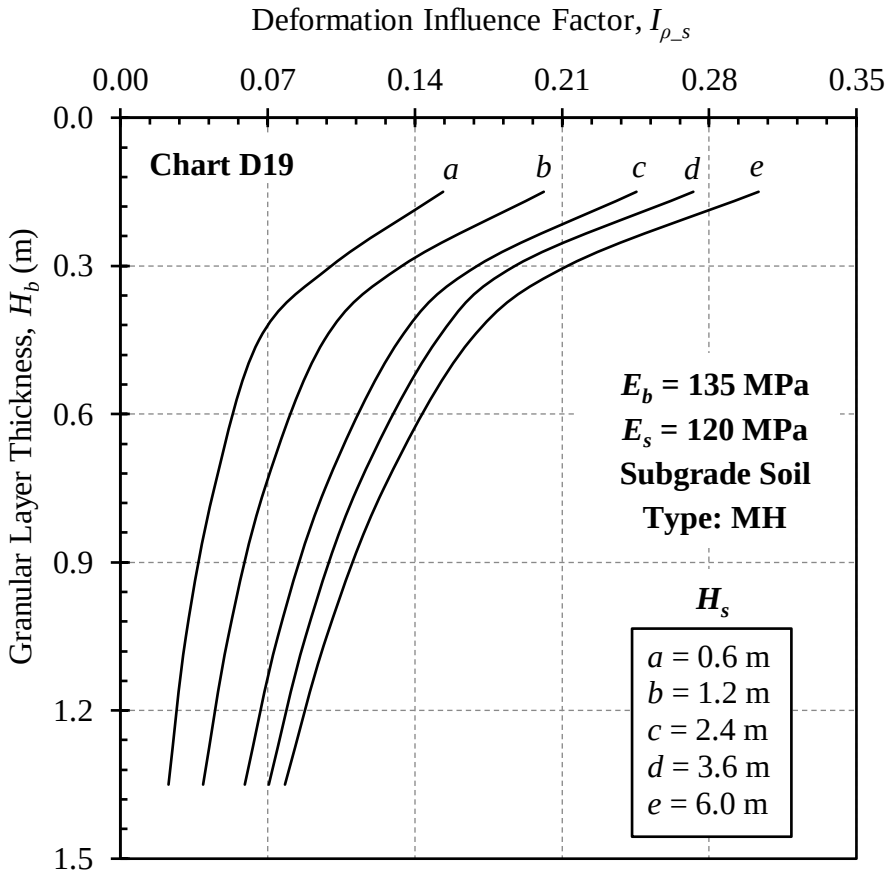
Deformation Influence Factor, I_{ρ_s}
0.00
0.07
0.14
0.21
0.28
0.35
0.0
0.3
0.6
0.9
1.2
1.5
Granular Layer Thickness, H_b (m)
Chart D19
a
b
c
d
e
E_b = 135 MPa
E_s = 120 MPa
Subgrade Soil
Type: MH
H_s
a = 0.6 m
b = 1.2 m
c = 2.4 m
d = 3.6 m
e = 6.0 m

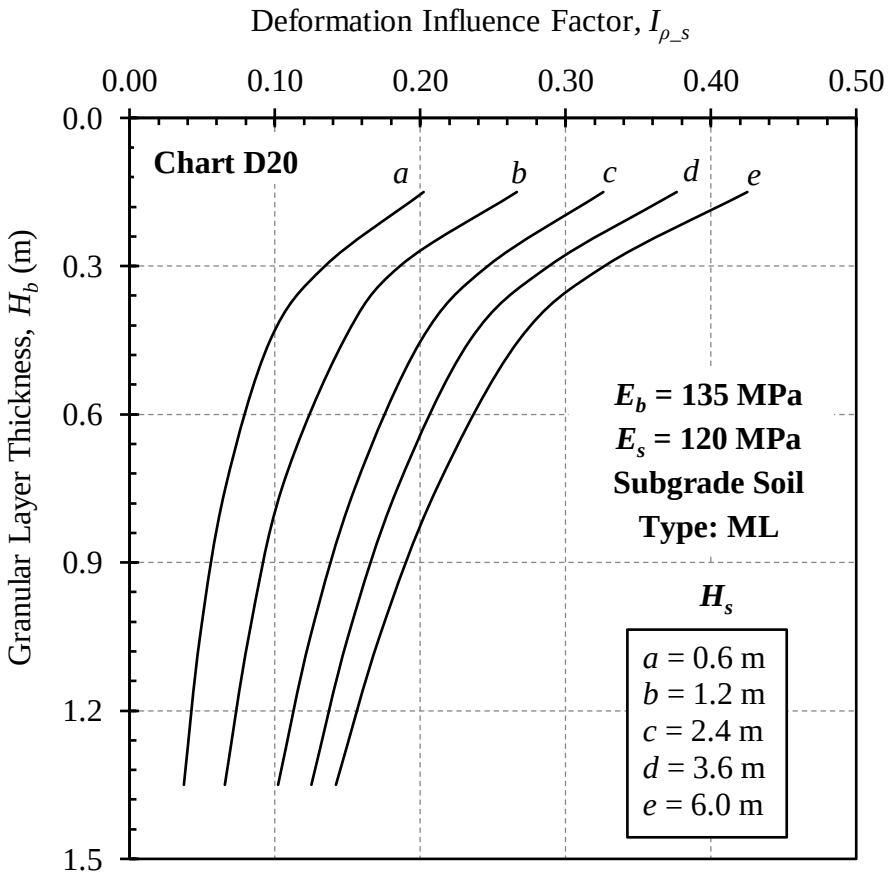
Deformation Influence Factor, I_{ρ_s}
0.00
0.10
0.20
0.30
0.40
0.50
0.0
0.3
0.6
0.9
1.2
1.5
Granular Layer Thickness, H_b (m)
Chart D20
a
b
c
d
e
E_b = 135 MPa
E_s = 120 MPa
Subgrade Soil
Type: ML
H_s
a = 0.6 m
b = 1.2 m
c = 2.4 m
d = 3.6 m
e = 6.0 m

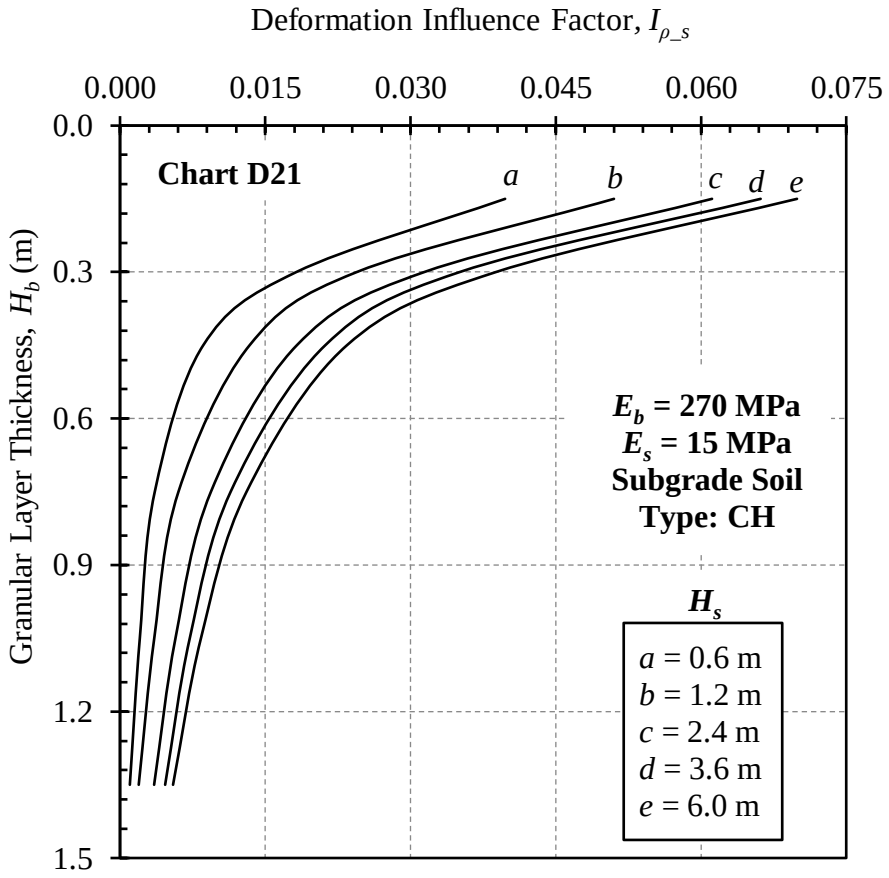
Deformation Influence Factor, I_{ρ_s}
0.000
0.015
0.030
0.045
0.060
0.075
0.0
0.3
0.6
0.9
1.2
1.5
Granular Layer Thickness, H_b (m)
Chart D21
a
b
c
d
e
E_b = 270 MPa
E_s = 15 MPa
Subgrade Soil
Type: CH
H_s
a = 0.6 m
b = 1.2 m
c = 2.4 m
d = 3.6 m
e = 6.0 m

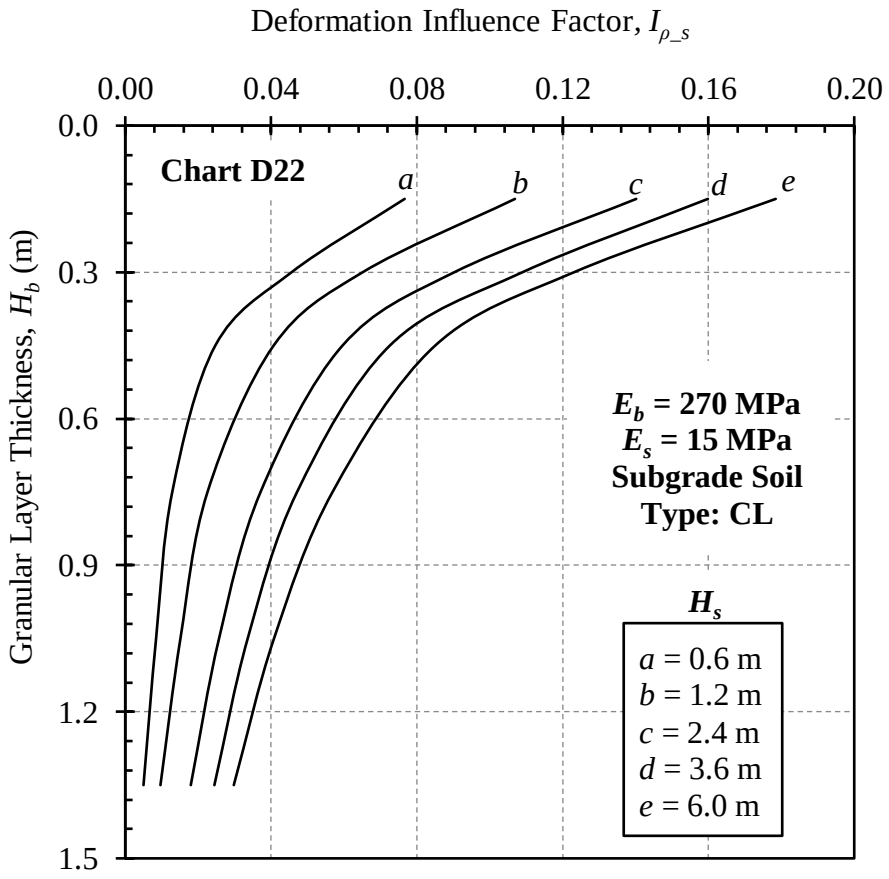
Deformation Influence Factor, I_{ρ_s}
0.00
0.04
0.08
0.12
0.16
0.20
0.0
0.3
0.6
0.9
1.2
1.5
Granular Layer Thickness, H_b (m)
Chart D22
a
b
c
d
e
E_b = 270 MPa
E_s = 15 MPa
Subgrade Soil
Type: CL
H_s
a = 0.6 m
b = 1.2 m
c = 2.4 m
d = 3.6 m
e = 6.0 m

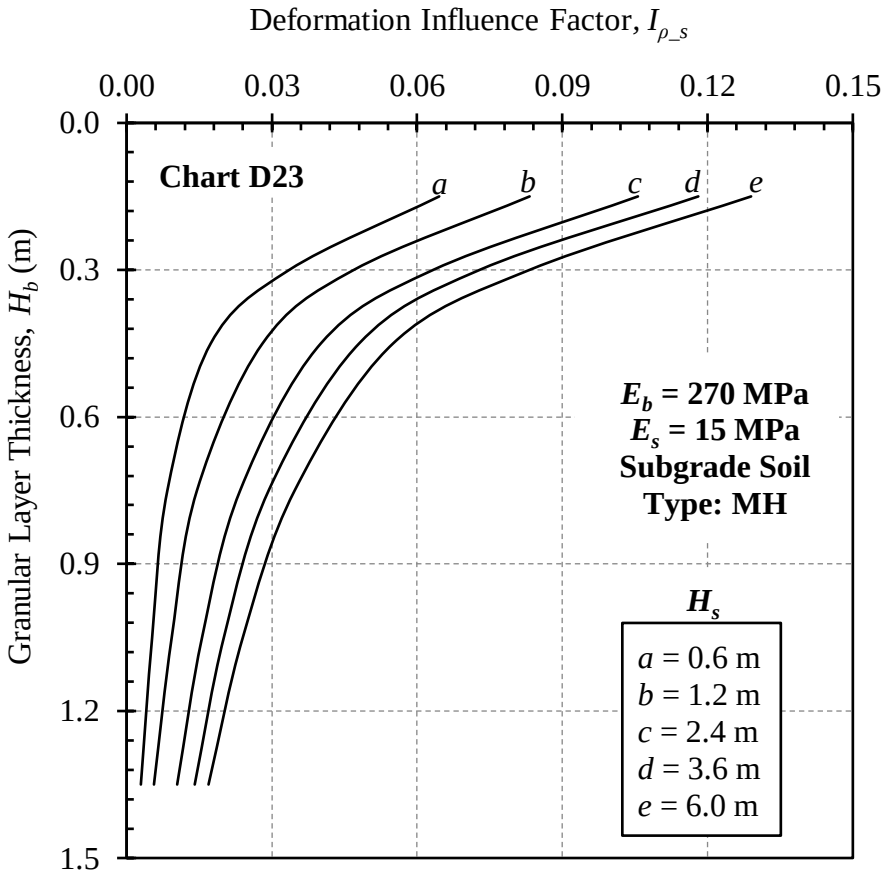
Deformation Influence Factor, I_{ρ_s}
0.00
0.03
0.06
0.09
0.12
0.15
0.0
0.3
0.6
0.9
1.2
1.5
Granular Layer Thickness, H_b (m)
Chart D23
a
b
c
d
e
E_b = 270 MPa
E_s = 15 MPa
Subgrade Soil Type: MH
H_s
a = 0.6 m
b = 1.2 m
c = 2.4 m
d = 3.6 m
e = 6.0 m

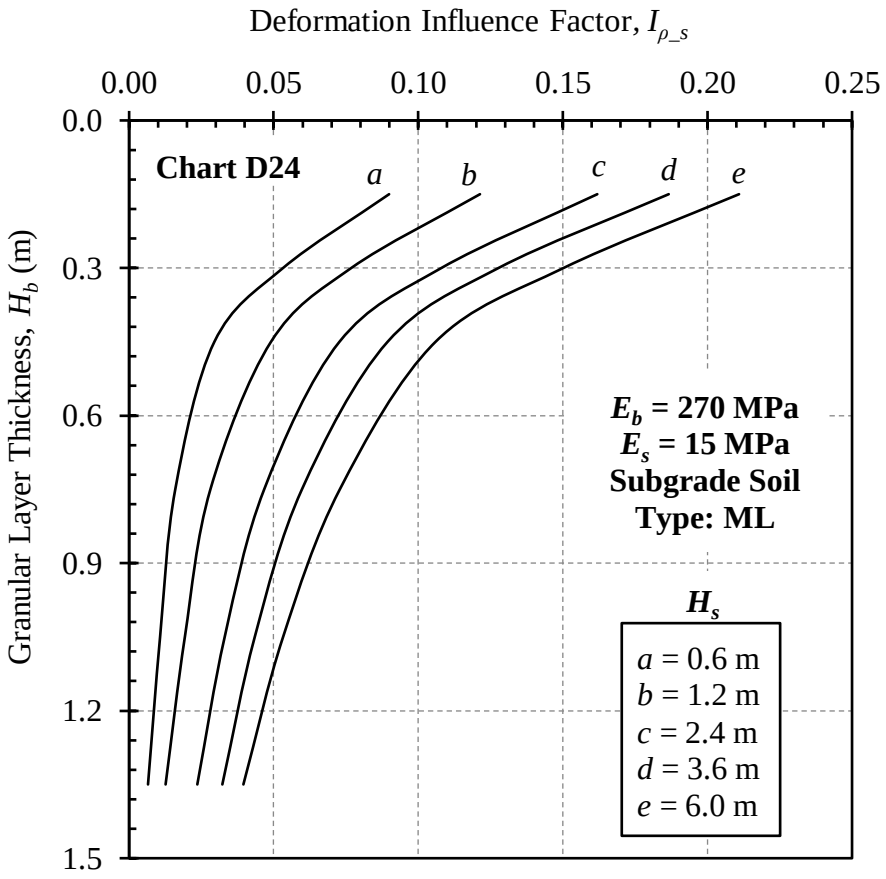
Deformation Influence Factor, I_{ρ_s}
0.00
0.05
0.10
0.15
0.20
0.25
0.0
0.3
0.6
0.9
1.2
1.5
Granular Layer Thickness, H_b (m)
Chart D24
a
b
c
d
e
E_b = 270 MPa
E_s = 15 MPa
Subgrade Soil Type: ML
H_s
a = 0.6 m
b = 1.2 m
c = 2.4 m
d = 3.6 m
e = 6.0 m

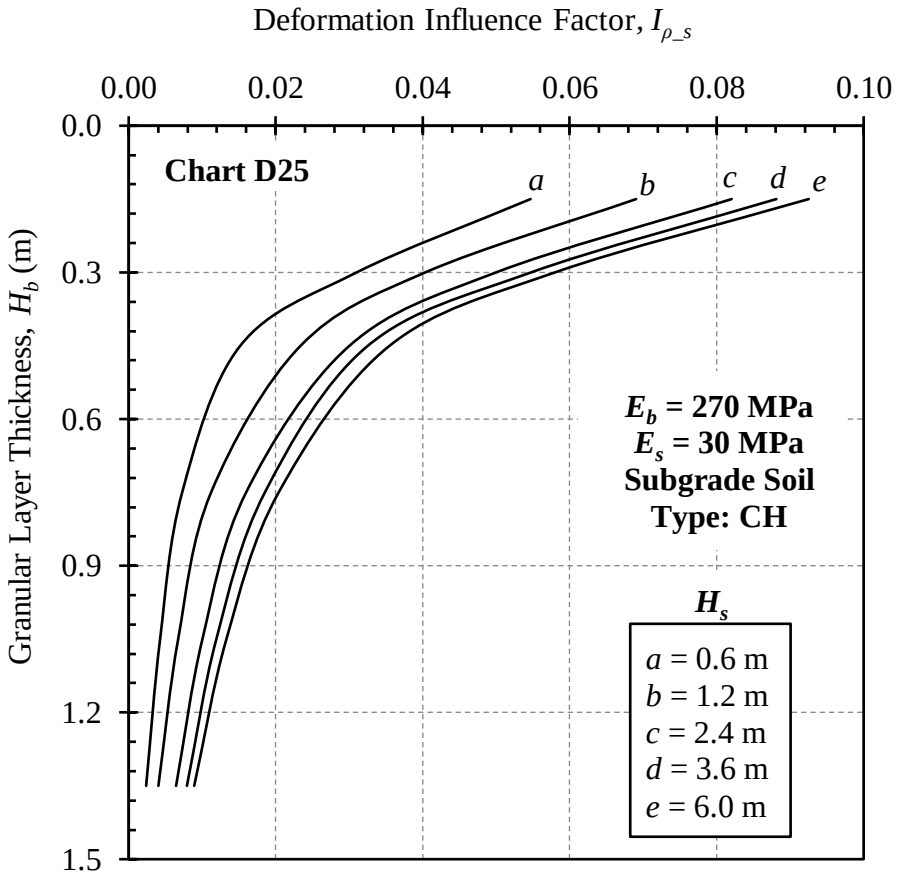
Deformation Influence Factor, I_{ρ_s}
0.00
0.02
0.04
0.06
0.08
0.10
0.0
0.3
0.6
0.9
1.2
1.5
Granular Layer Thickness, H_b (m)
Chart D25
a
b
c
d
e
E_b = 270 MPa
E_s = 30 MPa
Subgrade Soil
Type: CH
H_s
a = 0.6 m
b = 1.2 m
c = 2.4 m
d = 3.6 m
e = 6.0 m

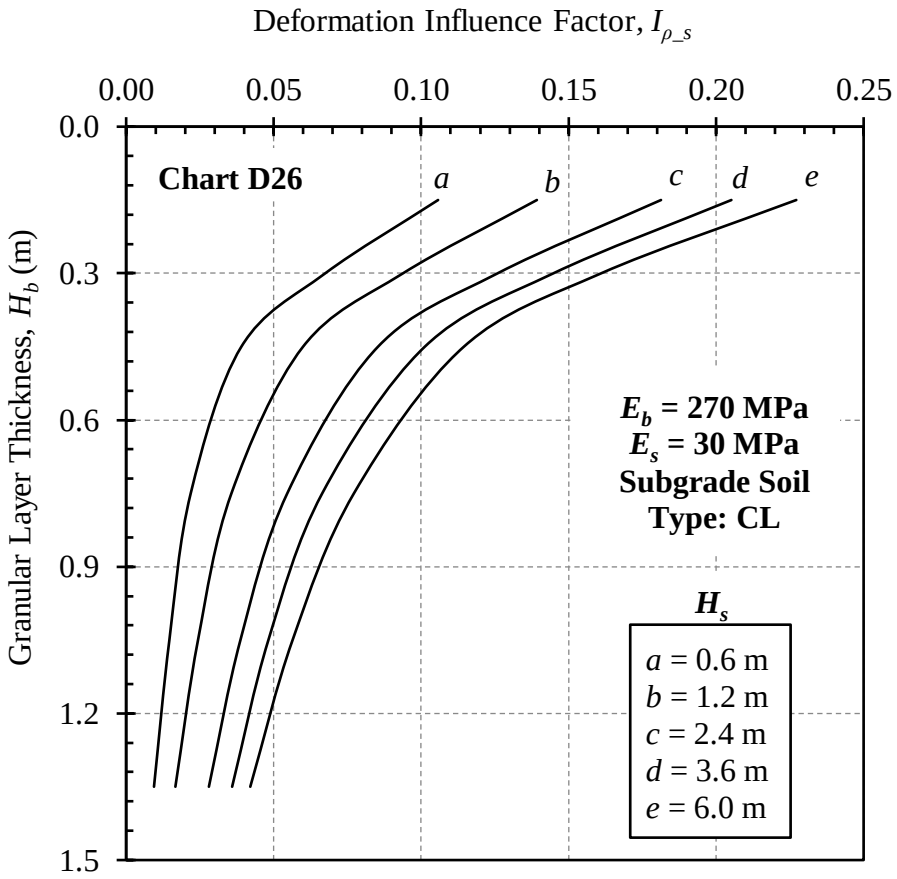
Deformation Influence Factor, I_{ρ_s}
0.00
0.05
0.10
0.15
0.20
0.25
0.0
0.3
0.6
0.9
1.2
1.5
Granular Layer Thickness, H_b (m)
Chart D26
a
b
c
d
e
E_b = 270 MPa
E_s = 30 MPa
Subgrade Soil
Type: CL
H_s
a = 0.6 m
b = 1.2 m
c = 2.4 m
d = 3.6 m
e = 6.0 m

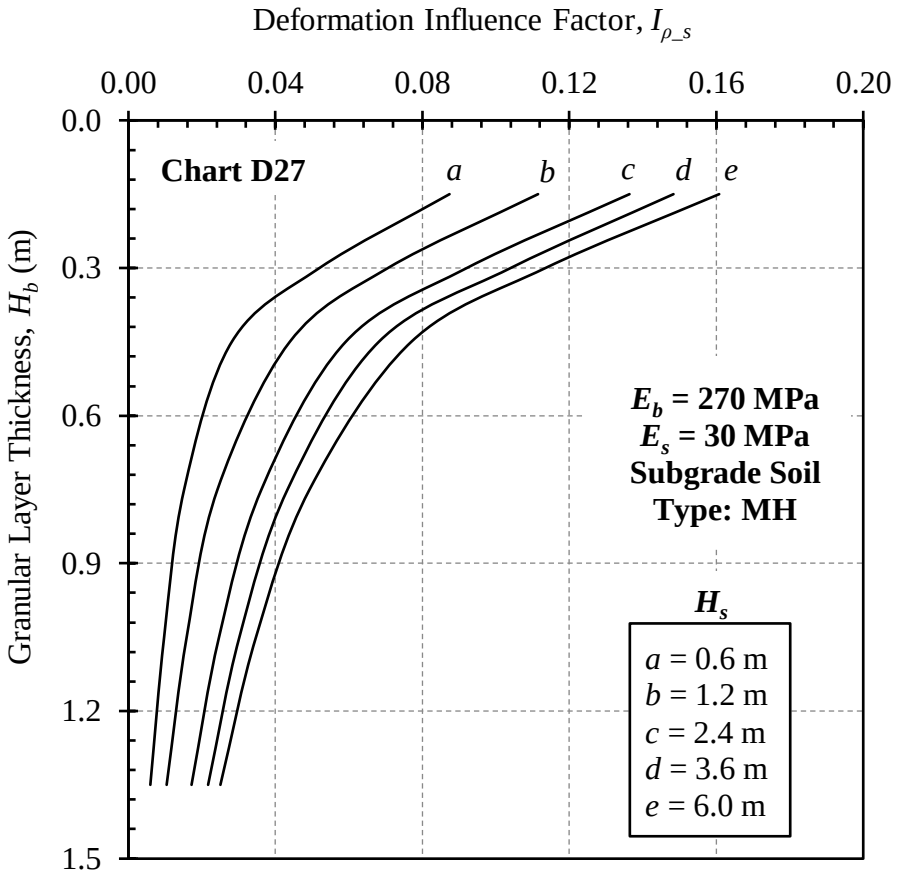
Deformation Influence Factor, I_{ρ_s}
0.00
0.04
0.08
0.12
0.16
0.20
0.0
0.3
0.6
0.9
1.2
1.5
Granular Layer Thickness, H_b (m)
Chart D27
a
b
c
d
e
E_b = 270 MPa
E_s = 30 MPa
Subgrade Soil Type: MH
H_s
a = 0.6 m
b = 1.2 m
c = 2.4 m
d = 3.6 m
e = 6.0 m

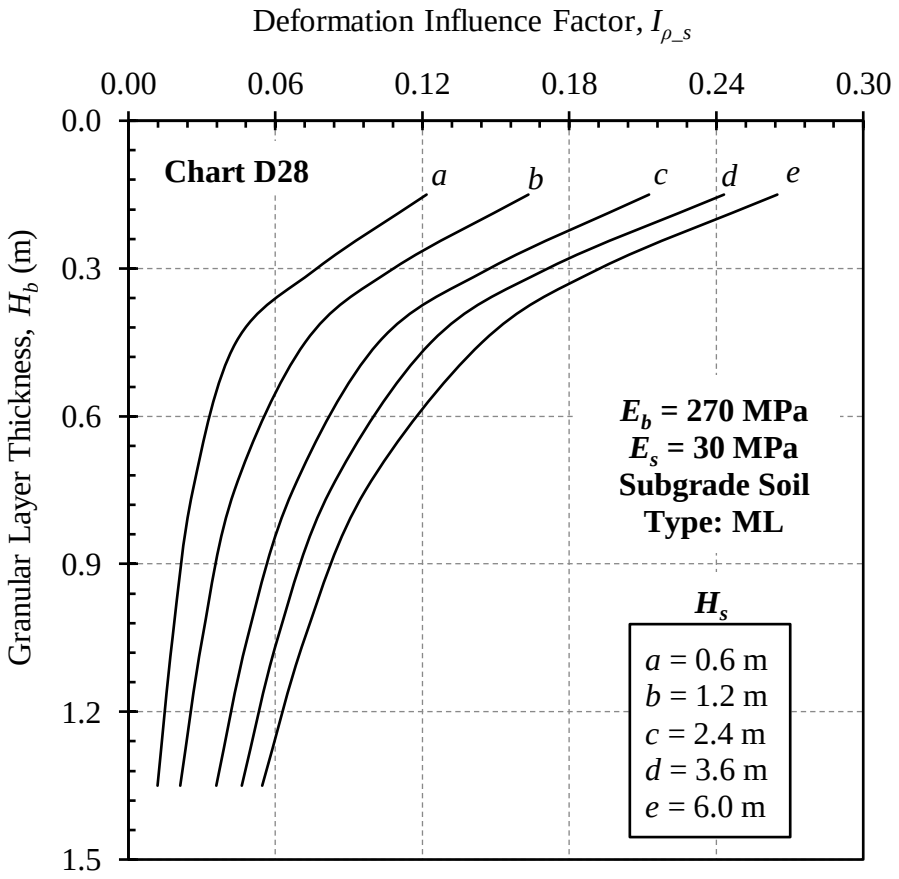
Deformation Influence Factor, I_{ρ_s}
0.00
0.06
0.12
0.18
0.24
0.30
0.0
0.3
0.6
0.9
1.2
1.5
Granular Layer Thickness, H_b (m)
Chart D28
a
b
c
d
e
E_b = 270 MPa
E_s = 30 MPa
Subgrade Soil Type: ML
H_s
a = 0.6 m
b = 1.2 m
c = 2.4 m
d = 3.6 m
e = 6.0 m

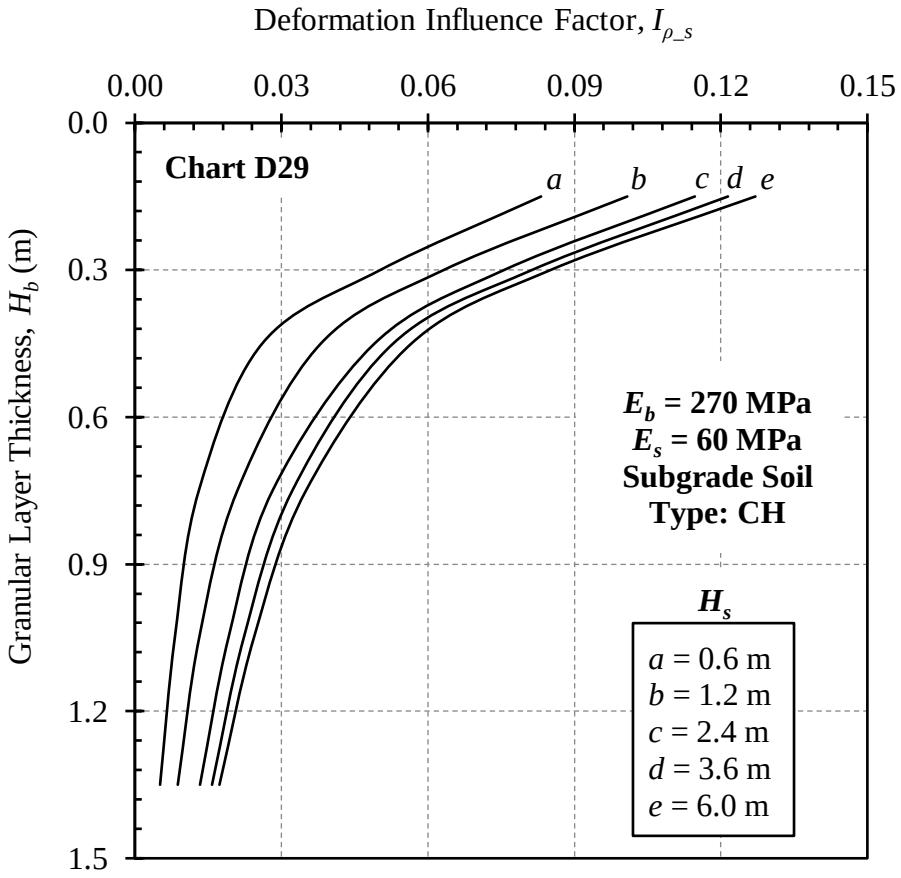
Deformation Influence Factor, I_{ρ_s}
0.00
0.03
0.06
0.09
0.12
0.15
0.0
0.3
0.6
0.9
1.2
1.5
Granular Layer Thickness, H_b (m)
Chart D29
a
b
c
d
e
E_b = 270 MPa
E_s = 60 MPa
Subgrade Soil
Type: CH
H_s
a = 0.6 m
b = 1.2 m
c = 2.4 m
d = 3.6 m
e = 6.0 m

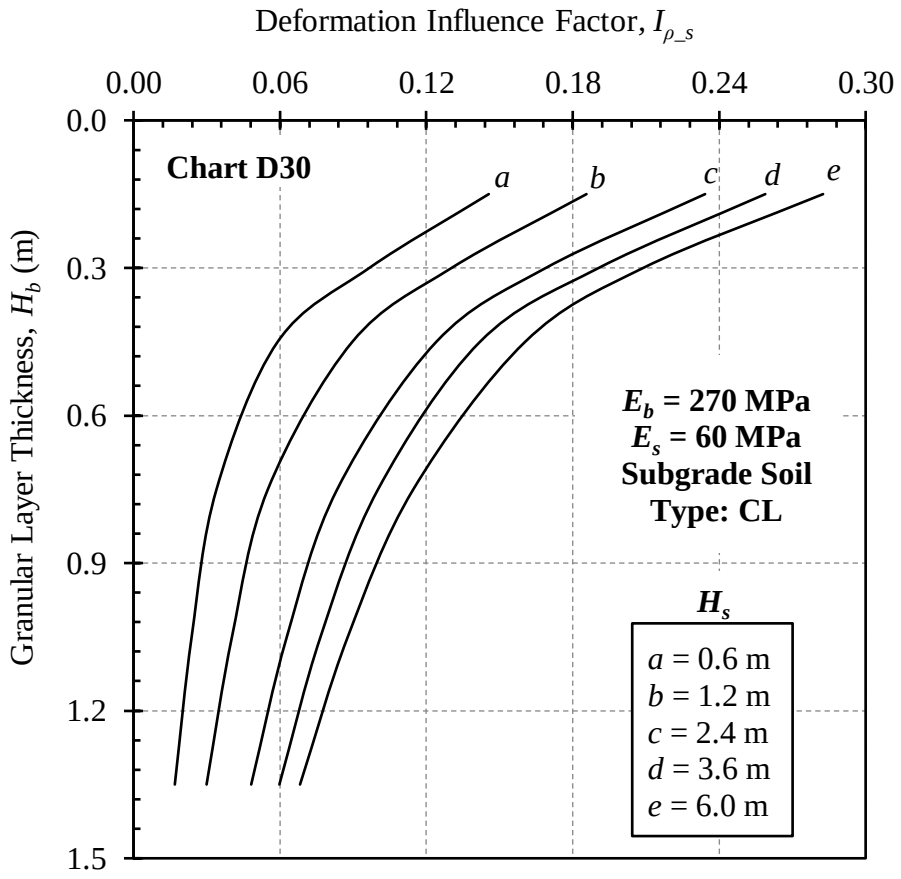
Deformation Influence Factor, I_{ρ_s}
0.00
0.06
0.12
0.18
0.24
0.30
0.0
0.3
0.6
0.9
1.2
1.5
Granular Layer Thickness, H_b (m)
Chart D30
a
b
c
d
e
E_b = 270 MPa
E_s = 60 MPa
Subgrade Soil
Type: CL
H_s
a = 0.6 m
b = 1.2 m
c = 2.4 m
d = 3.6 m
e = 6.0 m

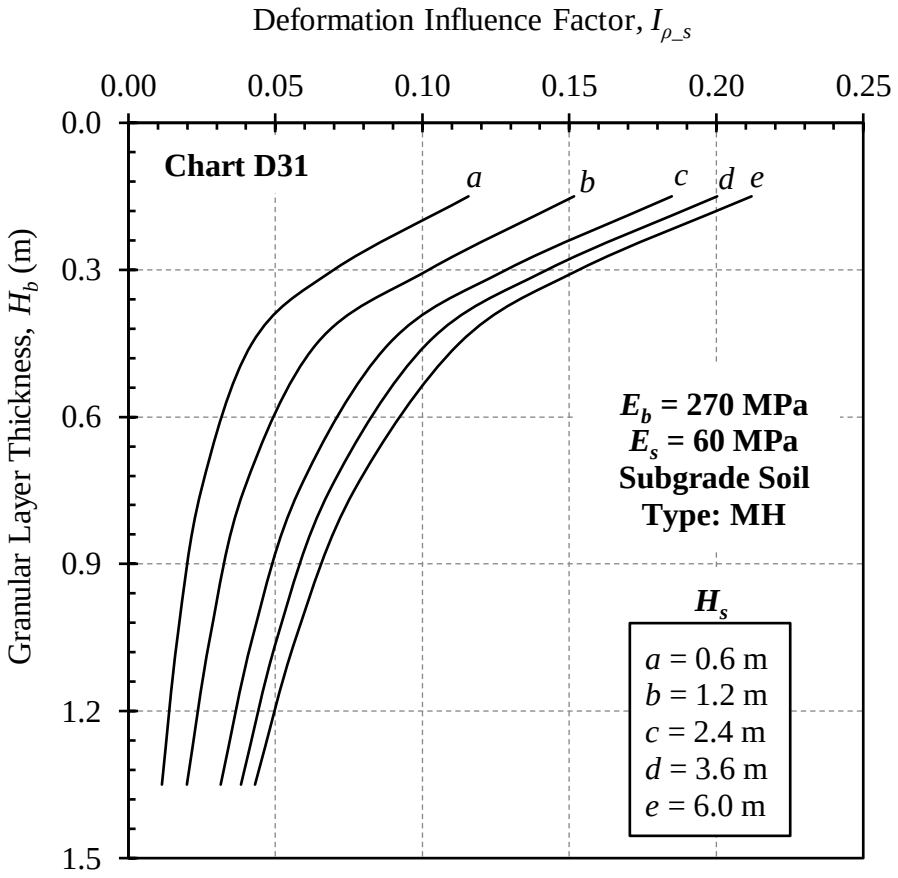
Deformation Influence Factor, I_{ρ_s}
0.00
0.05
0.10
0.15
0.20
0.25
0.0
0.3
0.6
0.9
1.2
1.5
Granular Layer Thickness, H_b (m)
Chart D31
a
b
c
d
e
E_b = 270 MPa
E_s = 60 MPa
Subgrade Soil
Type: MH
H_s
a = 0.6 m
b = 1.2 m
c = 2.4 m
d = 3.6 m
e = 6.0 m

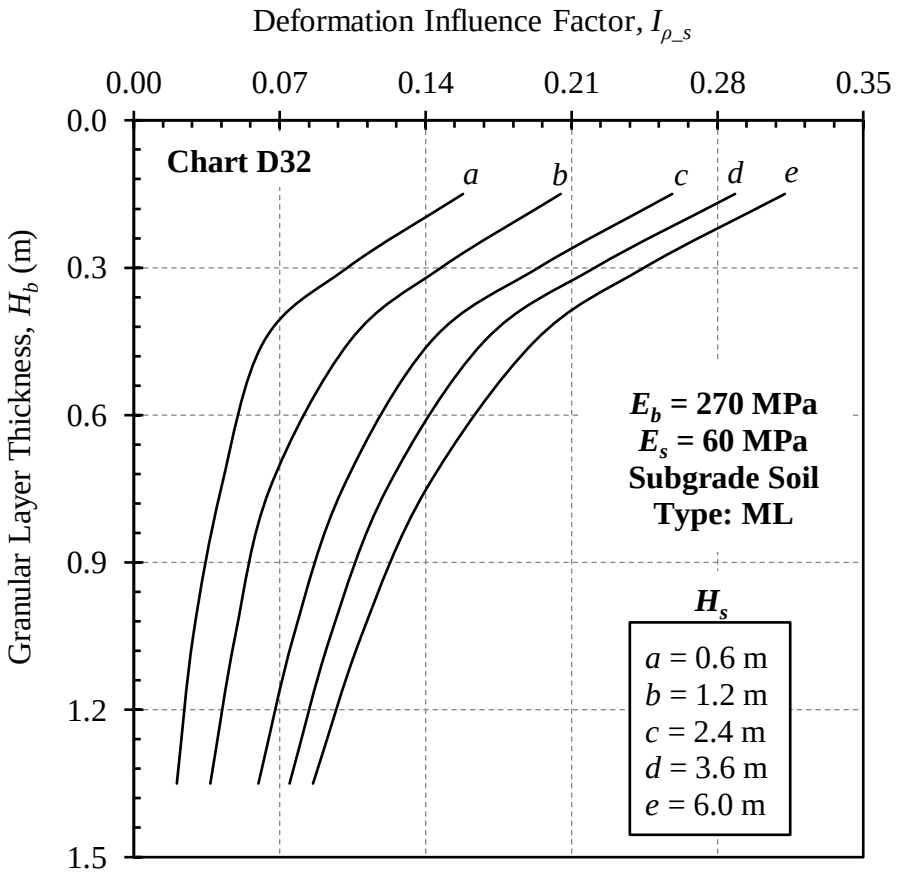
Deformation Influence Factor, I_{ρ_s}
0.00
0.07
0.14
0.21
0.28
0.35
0.0
0.3
0.6
0.9
1.2
1.5
Granular Layer Thickness, H_b (m)
Chart D32
a
b
c
d
e
E_b = 270 MPa
E_s = 60 MPa
Subgrade Soil
Type: ML
H_s
a = 0.6 m
b = 1.2 m
c = 2.4 m
d = 3.6 m
e = 6.0 m

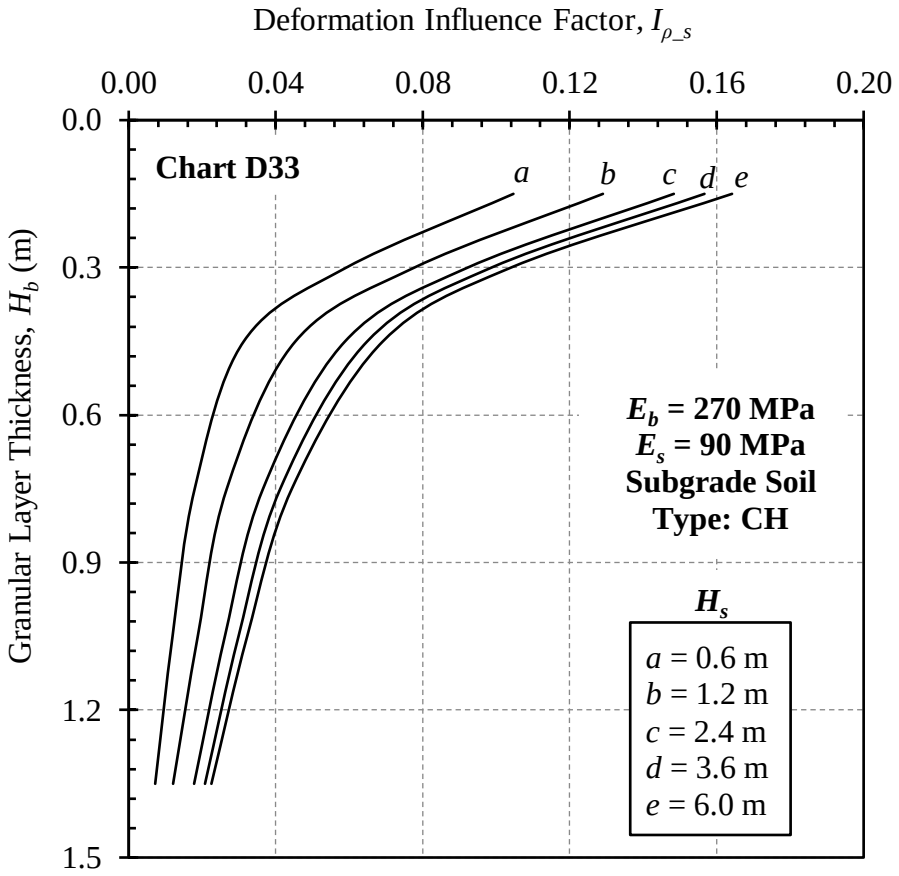
Deformation Influence Factor, I_{ρ_s}
0.00
0.04
0.08
0.12
0.16
0.20
0.0
0.3
0.6
0.9
1.2
1.5
Granular Layer Thickness, H_b (m)
Chart D33
a
b
c
d
e
E_b = 270 MPa
E_s = 90 MPa
Subgrade Soil
Type: CH
H_s
a = 0.6 m
b = 1.2 m
c = 2.4 m
d = 3.6 m
e = 6.0 m

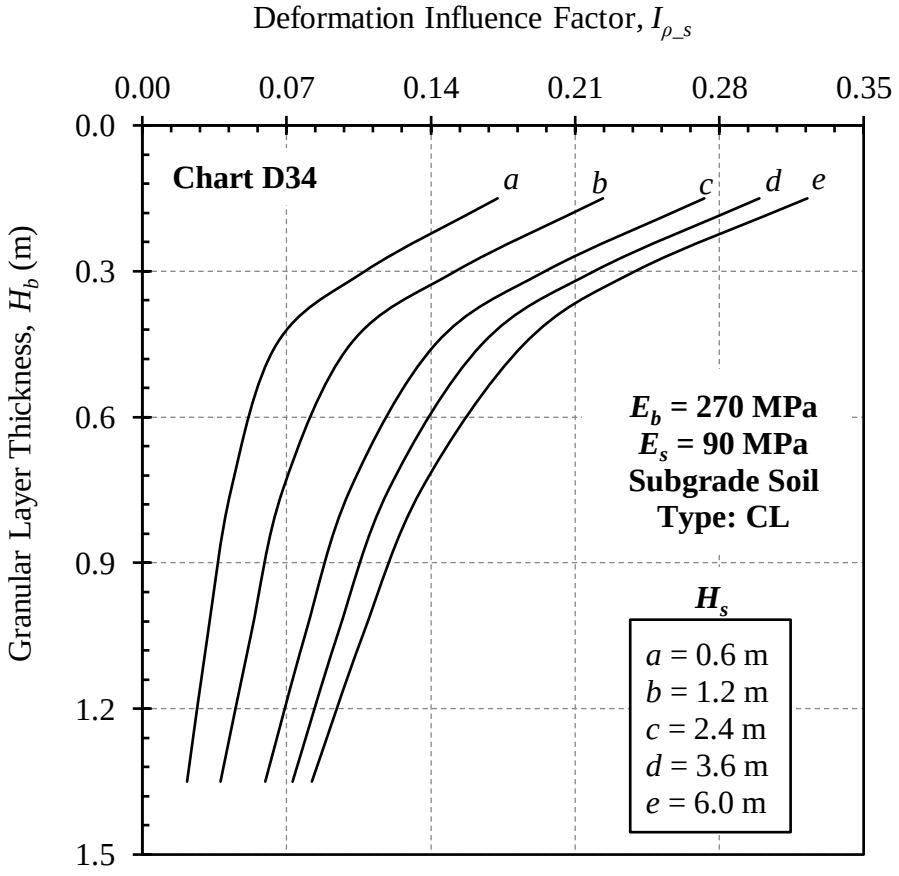
Deformation Influence Factor, I_{ρ_s}
0.00
0.07
0.14
0.21
0.28
0.35
0.0
0.3
0.6
0.9
1.2
1.5
Granular Layer Thickness, H_b (m)
Chart D34
a
b
c
d
e
E_b = 270 MPa
E_s = 90 MPa
Subgrade Soil
Type: CL
H_s
a = 0.6 m
b = 1.2 m
c = 2.4 m
d = 3.6 m
e = 6.0 m

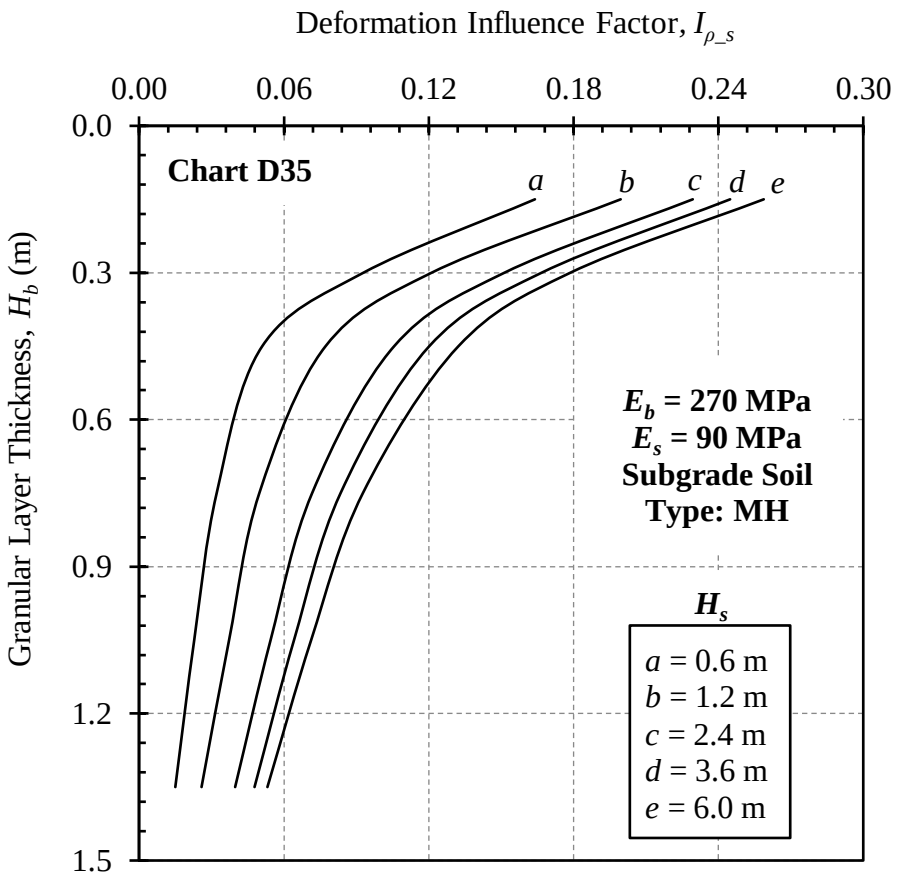
Deformation Influence Factor, I_{ρ_s}
0.00
0.06
0.12
0.18
0.24
0.30
0.0
0.3
0.6
0.9
1.2
1.5
Granular Layer Thickness, H_b (m)
Chart D35
a
b
c
d
e
E_b = 270 MPa
E_s = 90 MPa
Subgrade Soil Type: MH
H_s
a = 0.6 m
b = 1.2 m
c = 2.4 m
d = 3.6 m
e = 6.0 m

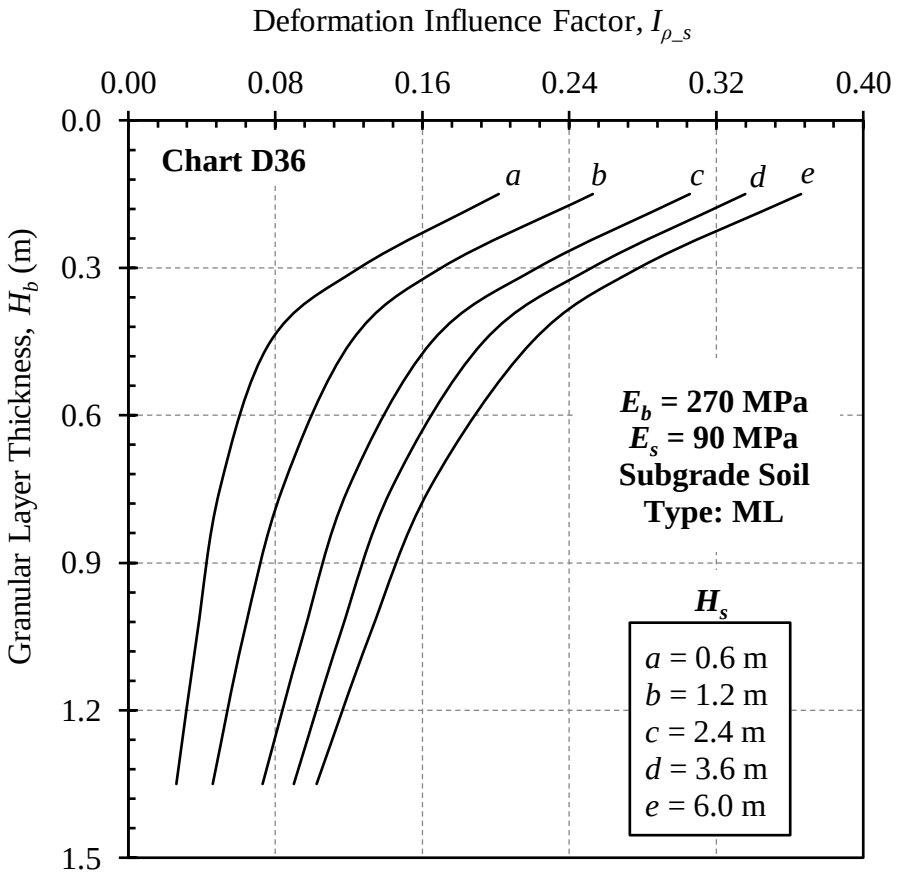
Deformation Influence Factor, I_{ρ_s}
0.00
0.08
0.16
0.24
0.32
0.40
0.0
0.3
0.6
0.9
1.2
1.5
Granular Layer Thickness, H_b (m)
Chart D36
a
b
c
d
e
E_b = 270 MPa
E_s = 90 MPa
Subgrade Soil Type: ML
H_s
a = 0.6 m
b = 1.2 m
c = 2.4 m
d = 3.6 m
e = 6.0 m

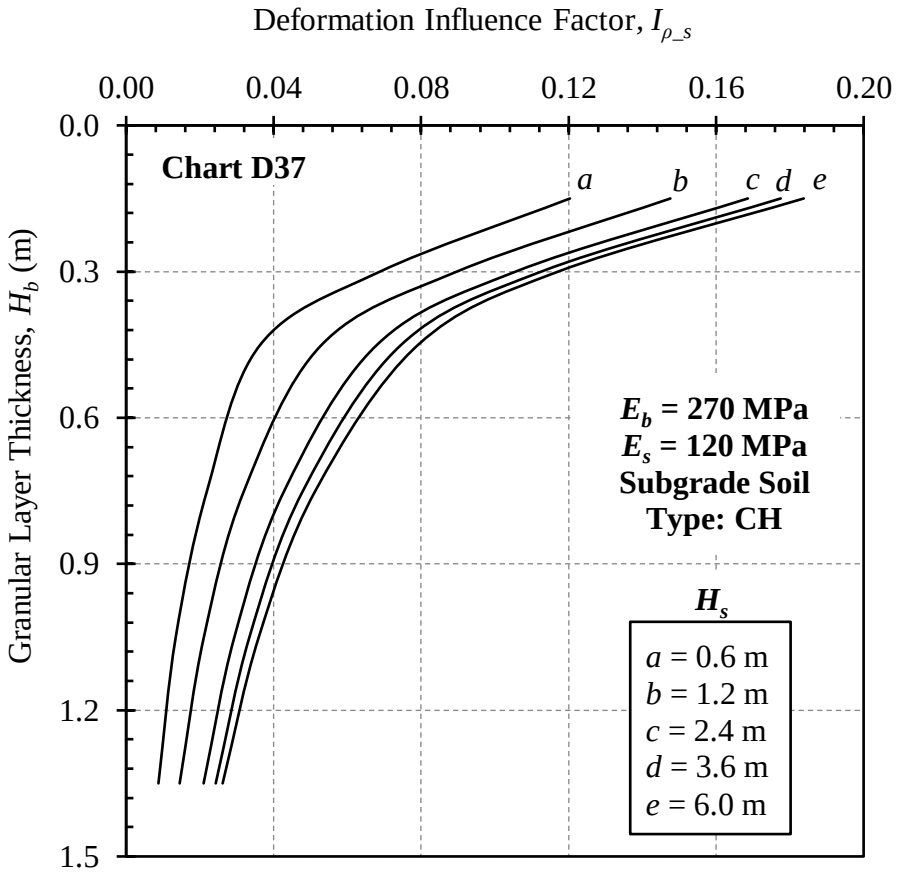
Deformation Influence Factor, I_{ρ_s}
0.00
0.04
0.08
0.12
0.16
0.20
0.0
0.3
0.6
0.9
1.2
1.5
Granular Layer Thickness, H_b (m)
Chart D37
a
b
c
d
e
E_b = 270 MPa
E_s = 120 MPa
Subgrade Soil
Type: CH
H_s
a = 0.6 m
b = 1.2 m
c = 2.4 m
d = 3.6 m
e = 6.0 m

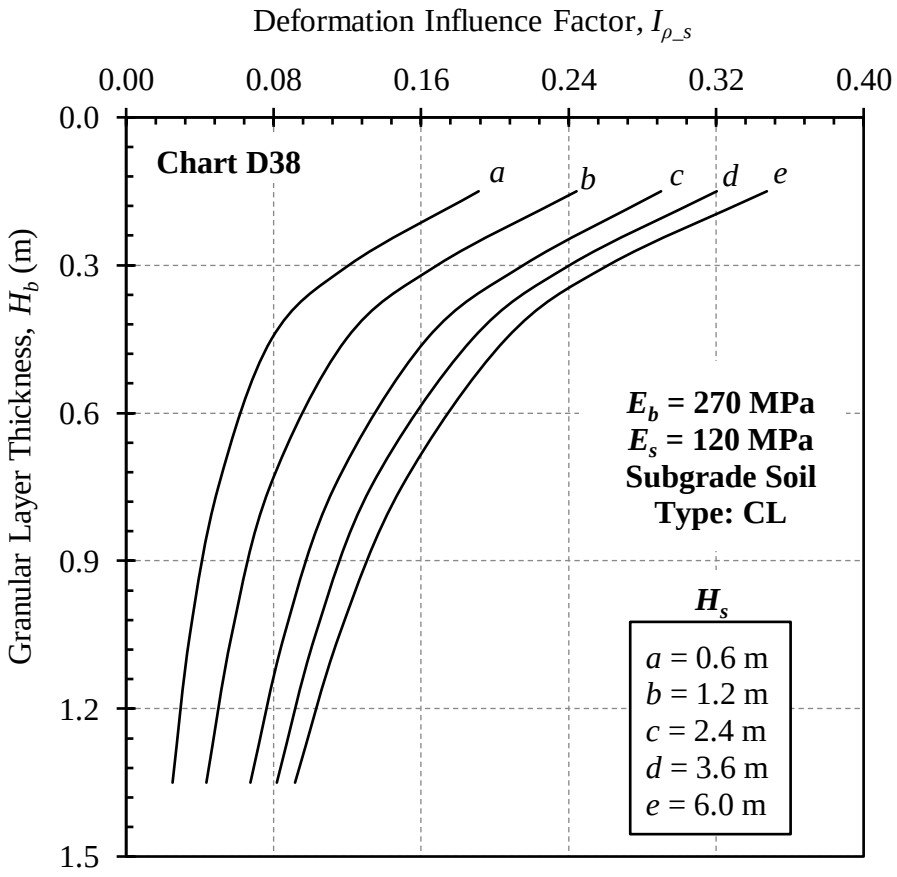
Deformation Influence Factor, I_{ρ_s}
0.00
0.08
0.16
0.24
0.32
0.40
0.0
0.3
0.6
0.9
1.2
1.5
Granular Layer Thickness, H_b (m)
Chart D38
a
b
c
d
e
E_b = 270 MPa
E_s = 120 MPa
Subgrade Soil
Type: CL
H_s
a = 0.6 m
b = 1.2 m
c = 2.4 m
d = 3.6 m
e = 6.0 m

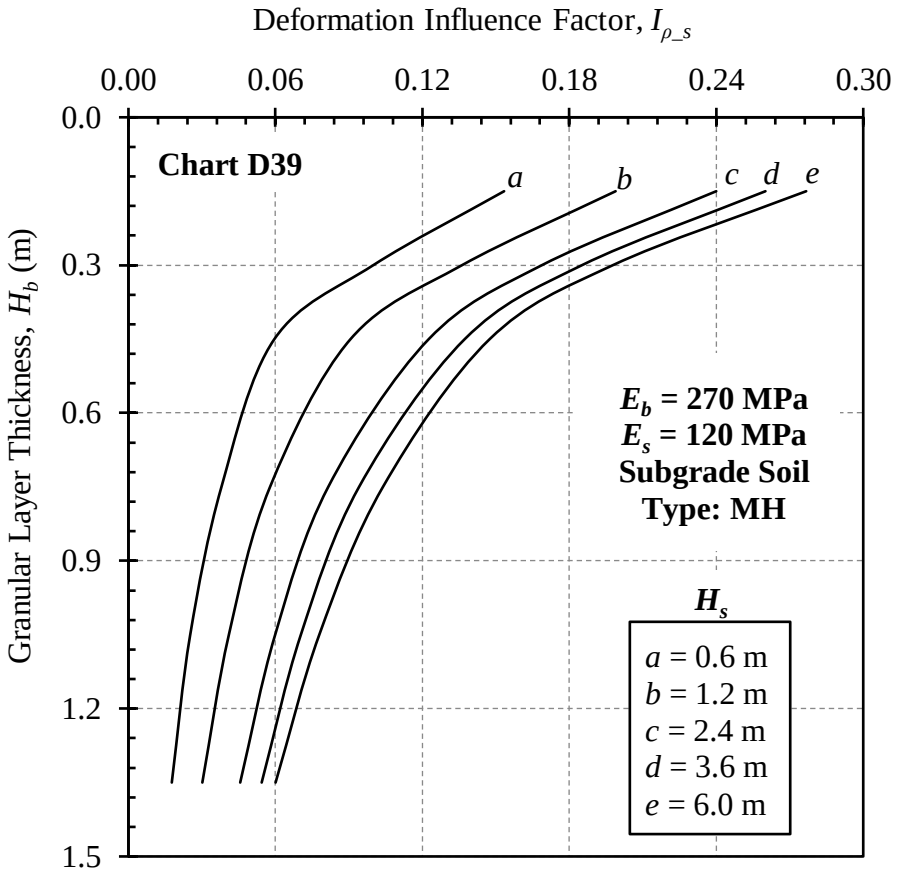
Deformation Influence Factor, I_{ρ_s}
0.00
0.06
0.12
0.18
0.24
0.30
0.0
0.3
0.6
0.9
1.2
1.5
Granular Layer Thickness, H_b (m)
Chart D39
a
b
c
d
e
E_b = 270 MPa
E_s = 120 MPa
Subgrade Soil
Type: MH
H_s
a = 0.6 m
b = 1.2 m
c = 2.4 m
d = 3.6 m
e = 6.0 m

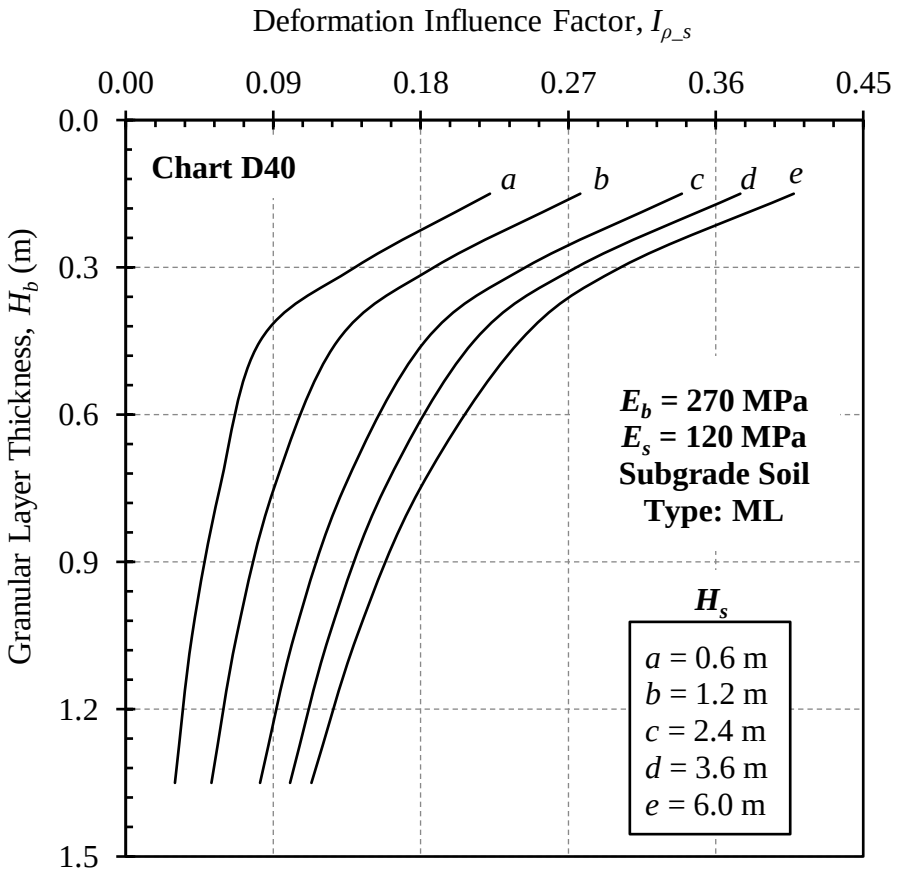
Deformation Influence Factor, I_{ρ_s}
0.00
0.09
0.18
0.27
0.36
0.45
0.0
0.3
0.6
0.9
1.2
1.5
Granular Layer Thickness, H_b (m)
Chart D40
a
b
c
d
e
E_b = 270 MPa
E_s = 120 MPa
Subgrade Soil
Type: ML
H_s
a = 0.6 m
b = 1.2 m
c = 2.4 m
d = 3.6 m
e = 6.0 m

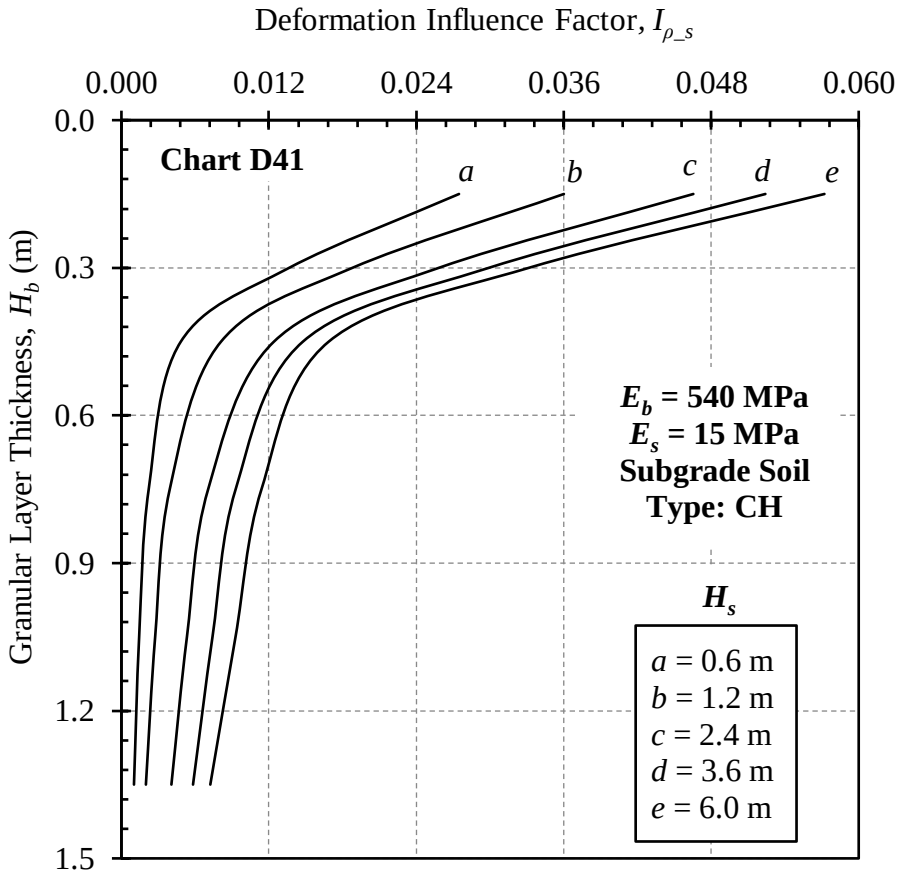
Deformation Influence Factor, I_{ρ_s}
0.000
0.012
0.024
0.036
0.048
0.060
0.0
0.3
0.6
0.9
1.2
1.5
Granular Layer Thickness, H_b (m)
Chart D41
a
b
c
d
e
E_b = 540 MPa
E_s = 15 MPa
Subgrade Soil
Type: CH
H_s
a = 0.6 m
b = 1.2 m
c = 2.4 m
d = 3.6 m
e = 6.0 m

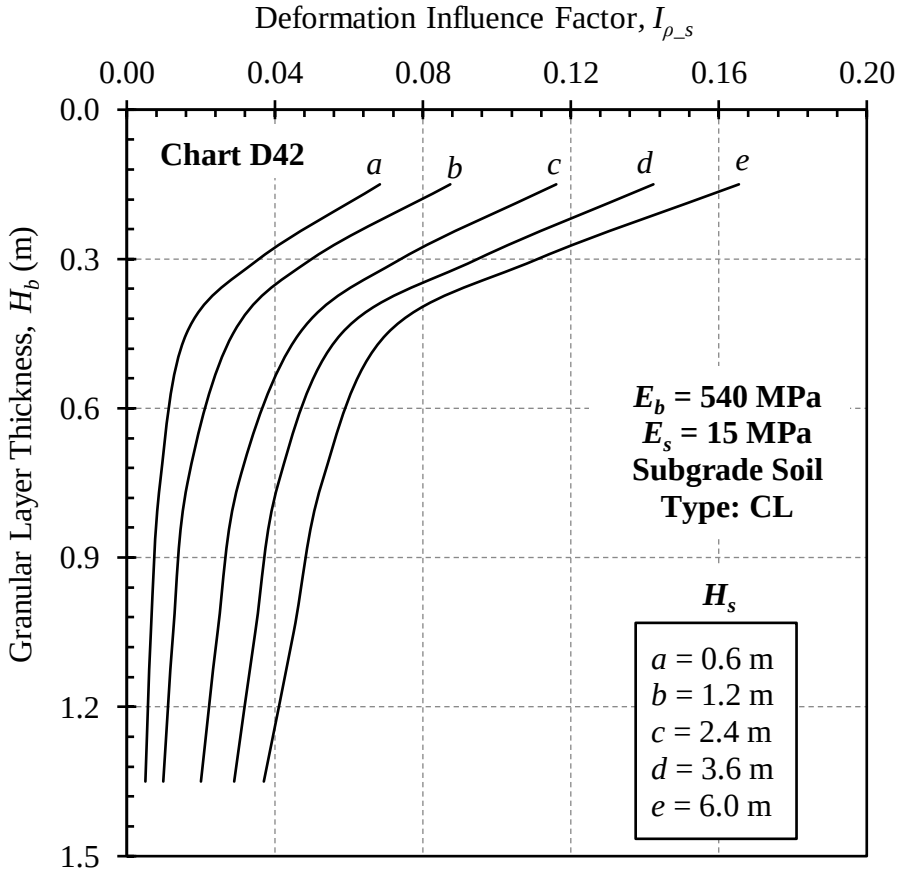
Deformation Influence Factor, I_{ρ_s}
0.00
0.04
0.08
0.12
0.16
0.20
0.0
0.3
0.6
0.9
1.2
1.5
Granular Layer Thickness, H_b (m)
Chart D42
a
b
c
d
e
E_b = 540 MPa
E_s = 15 MPa
Subgrade Soil
Type: CL
H_s
a = 0.6 m
b = 1.2 m
c = 2.4 m
d = 3.6 m
e = 6.0 m

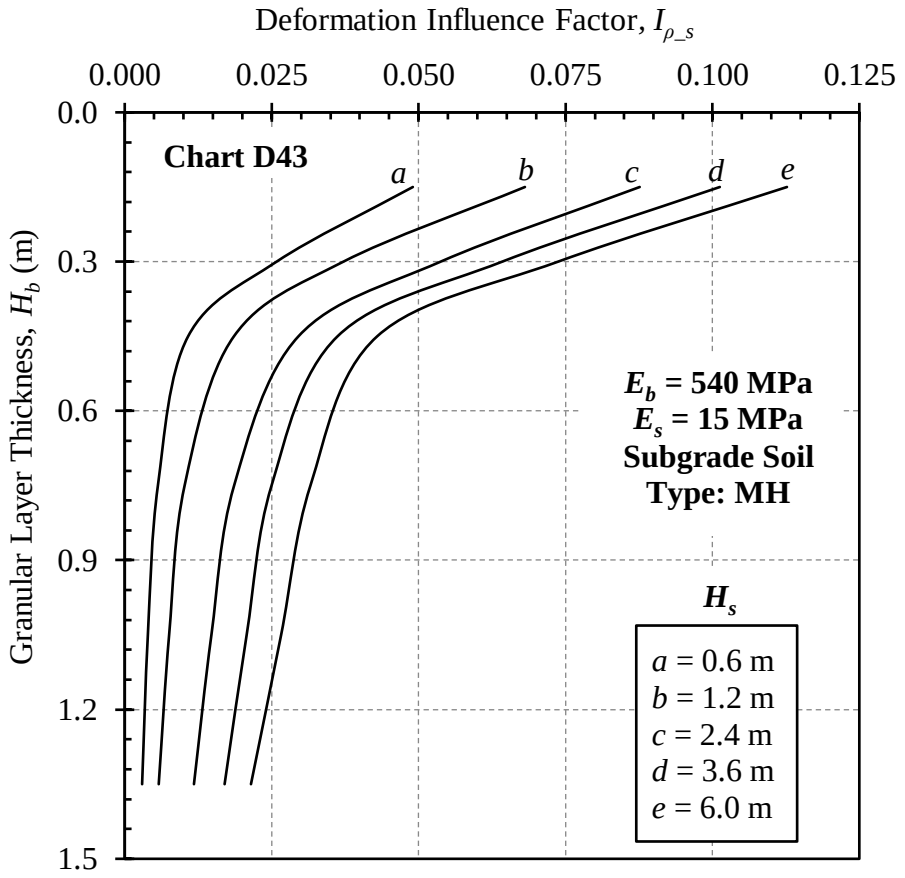
Deformation Influence Factor, I_{ρ_s}
0.000
0.025
0.050
0.075
0.100
0.125
Chart D43
a
b
c
d
e
Granular Layer Thickness, H_b (m)
0.0
0.3
0.6
0.9
1.2
1.5
E_b = 540 MPa
E_s = 15 MPa
Subgrade Soil
Type: MH
H_s
a = 0.6 m
b = 1.2 m
c = 2.4 m
d = 3.6 m
e = 6.0 m

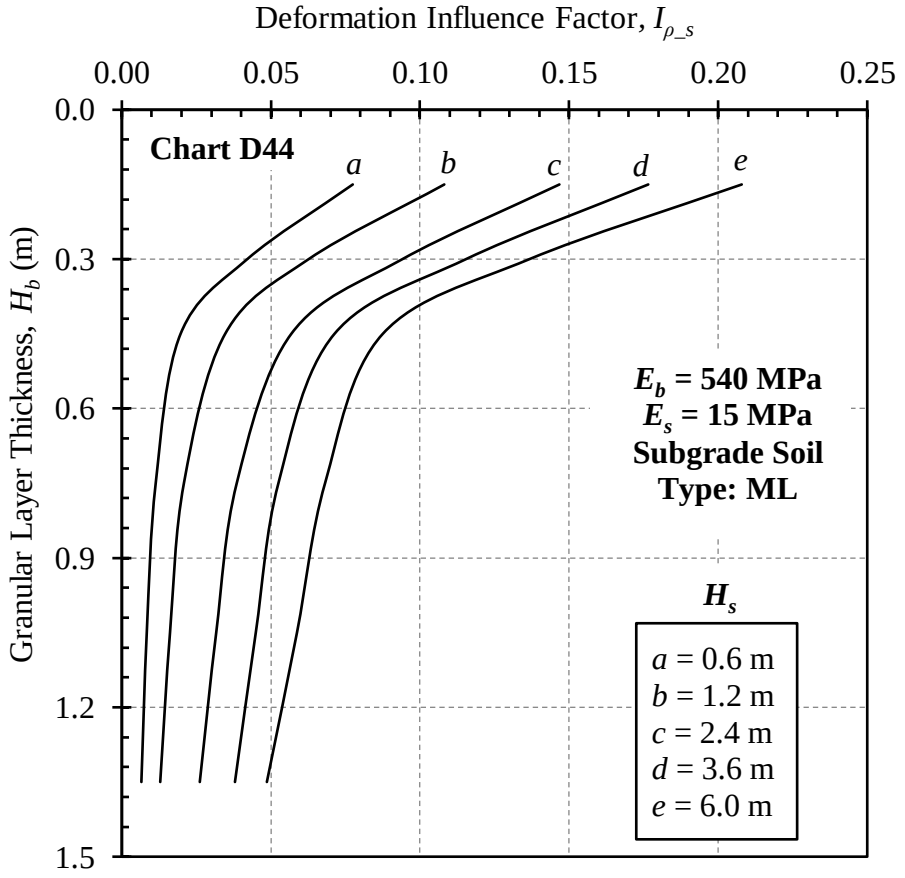
Deformation Influence Factor, I_{ρ_s}
0.00
0.05
0.10
0.15
0.20
0.25
Chart D44
a
b
c
d
e
Granular Layer Thickness, H_b (m)
0.0
0.3
0.6
0.9
1.2
1.5
E_b = 540 MPa
E_s = 15 MPa
Subgrade Soil
Type: ML
H_s
a = 0.6 m
b = 1.2 m
c = 2.4 m
d = 3.6 m
e = 6.0 m

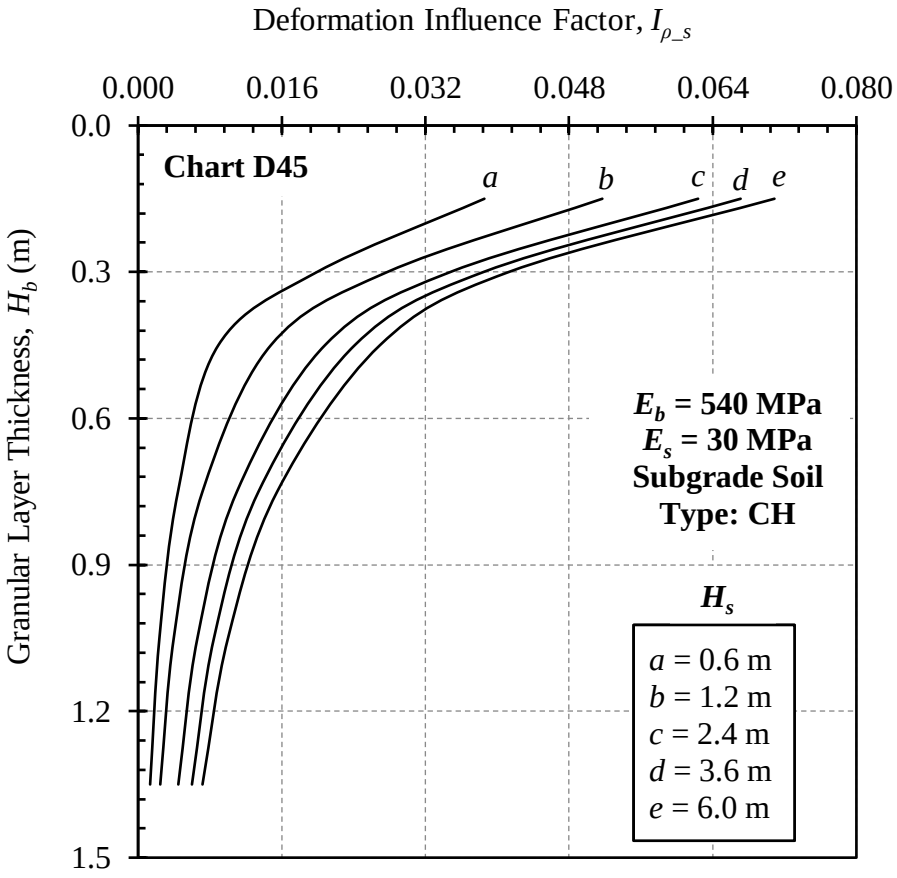
Deformation Influence Factor, I_{ρ_s}
0.000
0.016
0.032
0.048
0.064
0.080
0.0
0.3
0.6
0.9
1.2
1.5
Granular Layer Thickness, H_b (m)
Chart D45
a
b
c
d
e
E_b = 540 MPa
E_s = 30 MPa
Subgrade Soil
Type: CH
H_s
a = 0.6 m
b = 1.2 m
c = 2.4 m
d = 3.6 m
e = 6.0 m

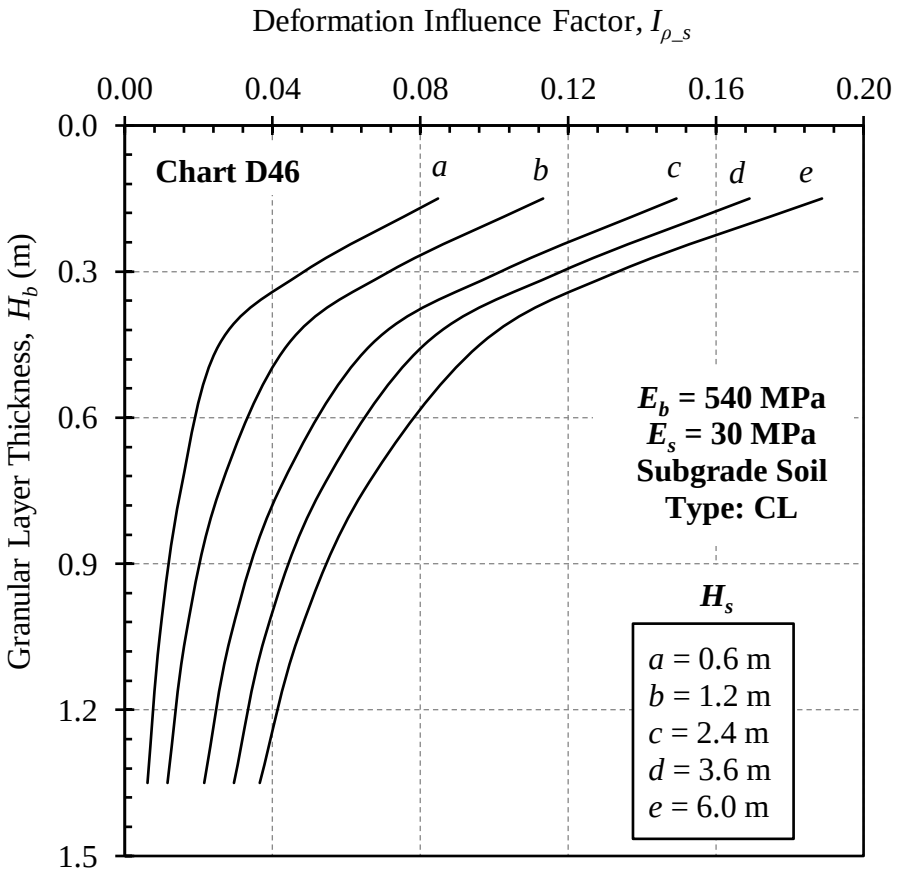
Deformation Influence Factor, I_{ρ_s}
0.00
0.04
0.08
0.12
0.16
0.20
0.0
0.3
0.6
0.9
1.2
1.5
Granular Layer Thickness, H_b (m)
Chart D46
a
b
c
d
e
E_b = 540 MPa
E_s = 30 MPa
Subgrade Soil
Type: CL
H_s
a = 0.6 m
b = 1.2 m
c = 2.4 m
d = 3.6 m
e = 6.0 m

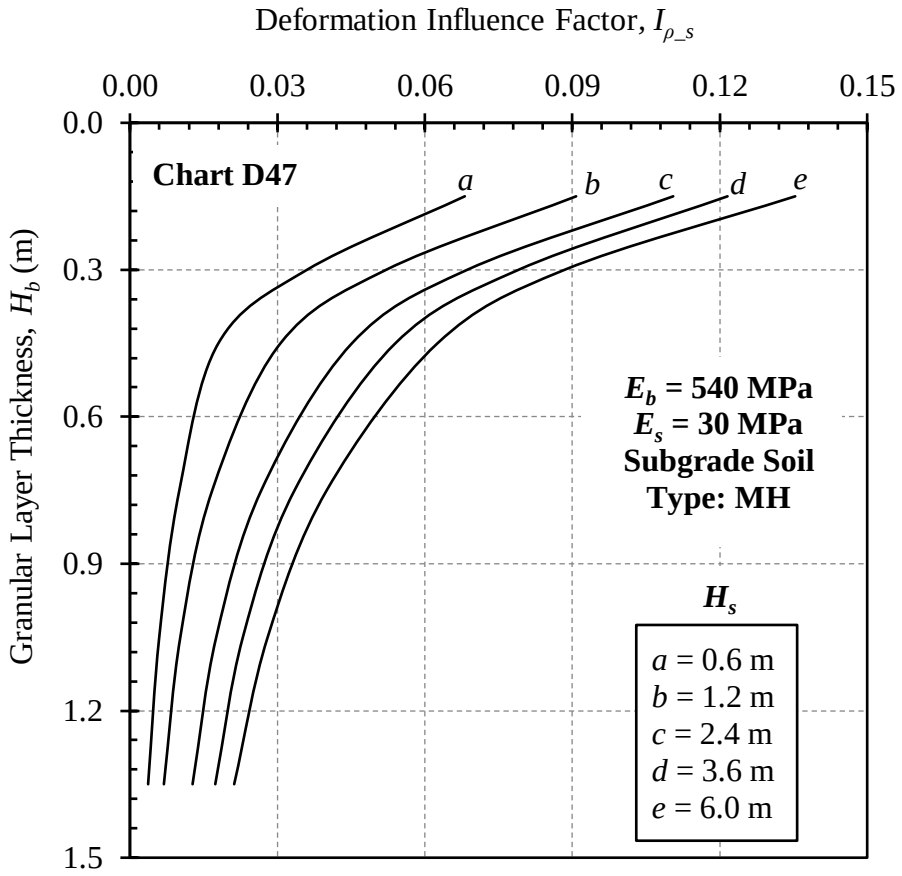
Deformation Influence Factor, I_{ρ_s}
0.00
0.03
0.06
0.09
0.12
0.15
0.0
0.3
0.6
0.9
1.2
1.5
Granular Layer Thickness, H_b (m)
Chart D47
a
b
c
d
e
E_b = 540 MPa
E_s = 30 MPa
Subgrade Soil
Type: MH
H_s
a = 0.6 m
b = 1.2 m
c = 2.4 m
d = 3.6 m
e = 6.0 m

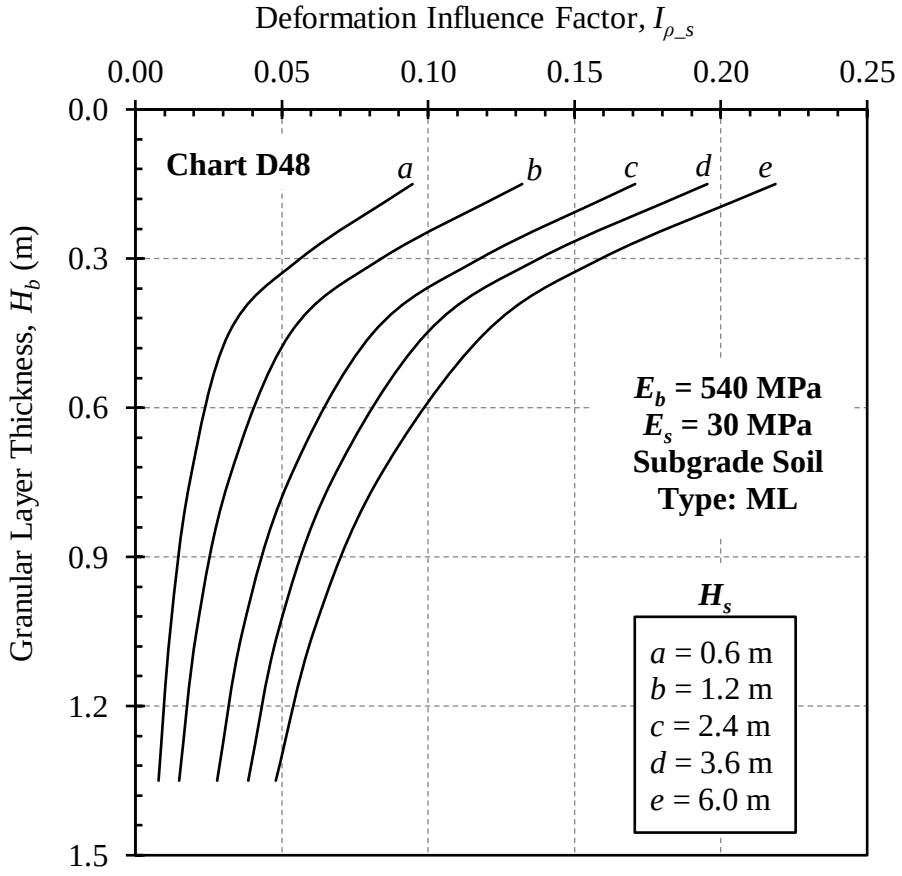
Deformation Influence Factor, I_{ρ_s}
0.00
0.05
0.10
0.15
0.20
0.25
0.0
0.3
0.6
0.9
1.2
1.5
Granular Layer Thickness, H_b (m)
Chart D48
a
b
c
d
e
E_b = 540 MPa
E_s = 30 MPa
Subgrade Soil
Type: ML
H_s
a = 0.6 m
b = 1.2 m
c = 2.4 m
d = 3.6 m
e = 6.0 m

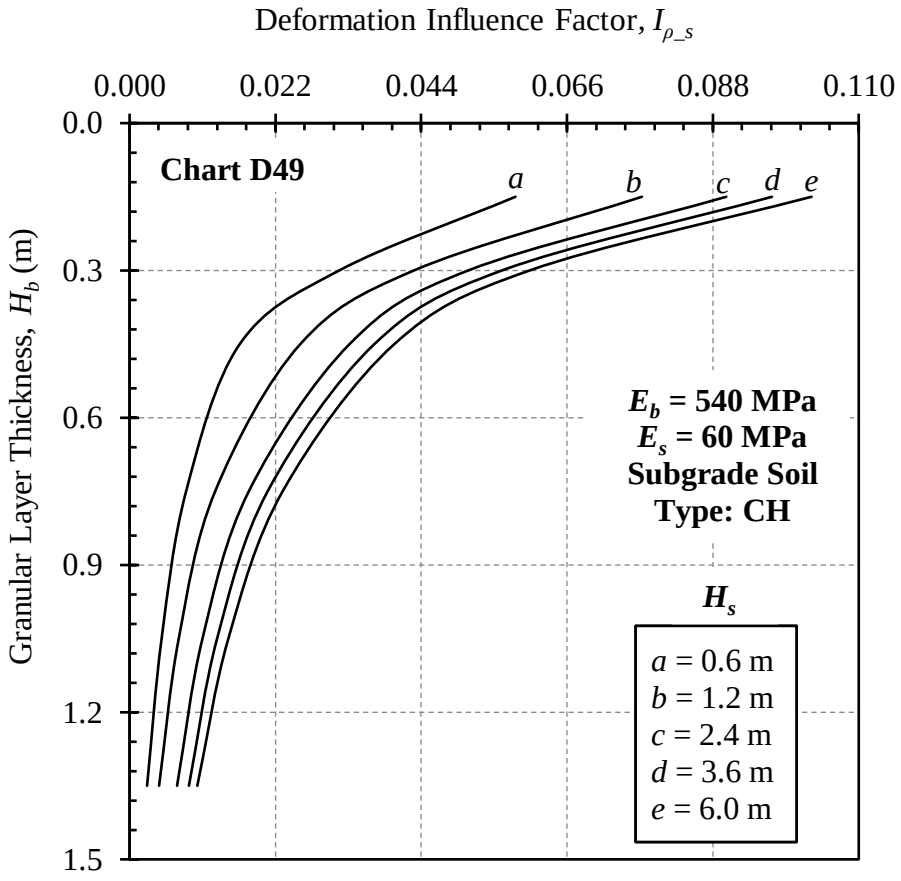
Deformation Influence Factor, I_{ρ_s}
0.000
0.022
0.044
0.066
0.088
0.110
0.0
0.3
0.6
0.9
1.2
1.5
Granular Layer Thickness, H_b (m)
Chart D49
a
b
c
d
e
E_b = 540 MPa
E_s = 60 MPa
Subgrade Soil
Type: CH
H_s
a = 0.6 m
b = 1.2 m
c = 2.4 m
d = 3.6 m
e = 6.0 m

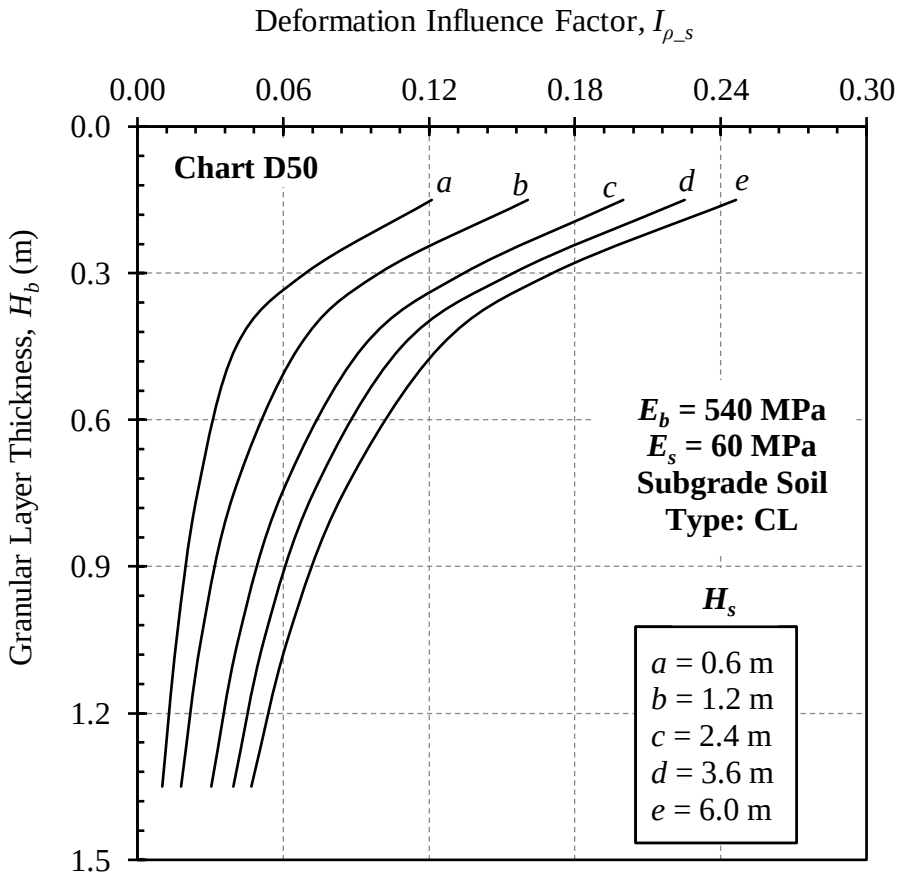
Deformation Influence Factor, I_{ρ_s}
0.00
0.06
0.12
0.18
0.24
0.30
0.0
0.3
0.6
0.9
1.2
1.5
Granular Layer Thickness, H_b (m)
Chart D50
a
b
c
d
e
E_b = 540 MPa
E_s = 60 MPa
Subgrade Soil
Type: CL
H_s
a = 0.6 m
b = 1.2 m
c = 2.4 m
d = 3.6 m
e = 6.0 m

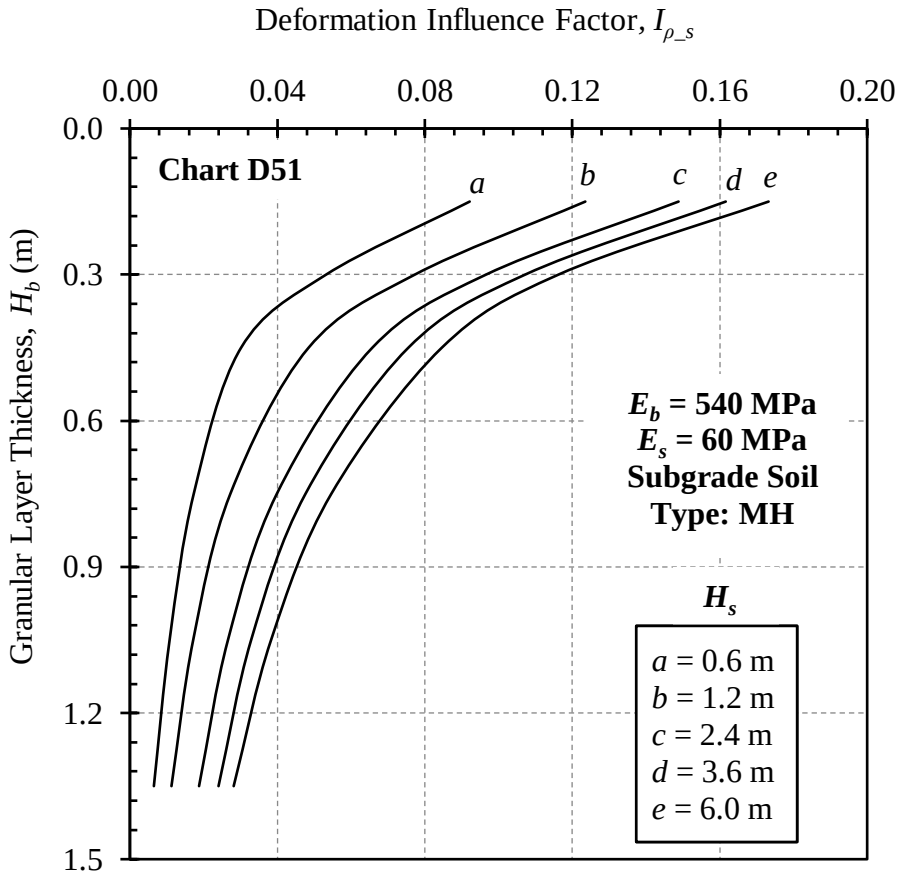
Deformation Influence Factor, I_{ρ_s}
0.00
0.04
0.08
0.12
0.16
0.20
0.0
0.3
0.6
0.9
1.2
1.5
Granular Layer Thickness, H_b (m)
Chart D51
a
b
c
d
e
E_b = 540 MPa
E_s = 60 MPa
Subgrade Soil
Type: MH
H_s
a = 0.6 m
b = 1.2 m
c = 2.4 m
d = 3.6 m
e = 6.0 m

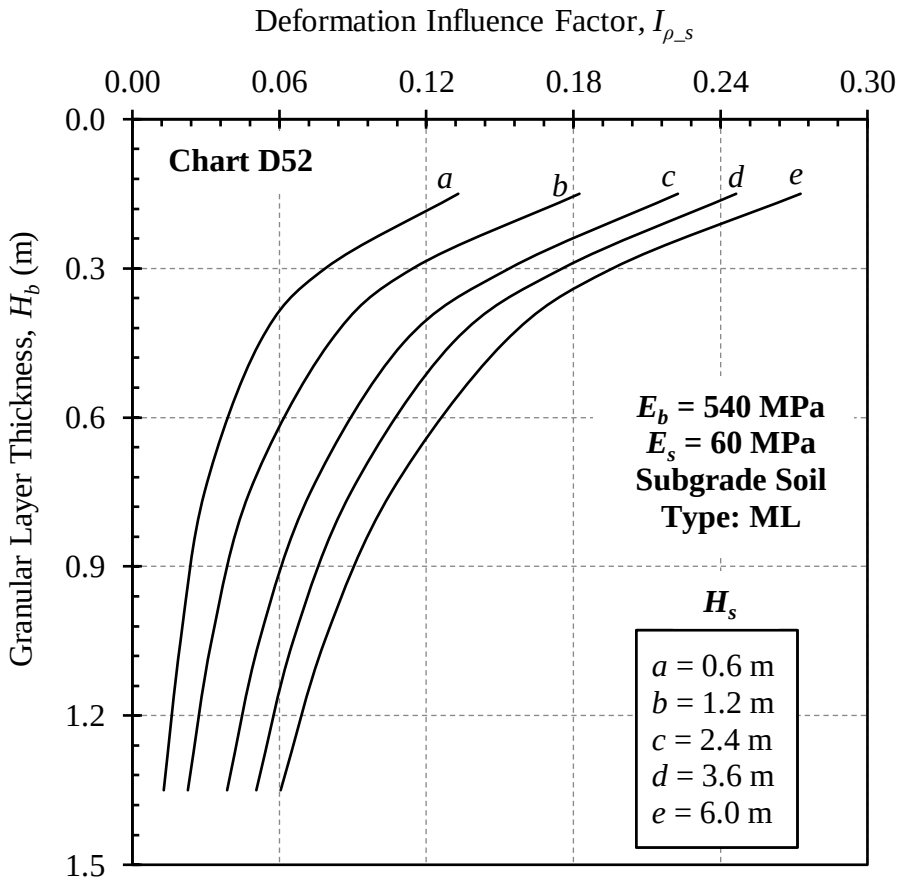
Deformation Influence Factor, I_{ρ_s}
0.00
0.06
0.12
0.18
0.24
0.30
0.0
0.3
0.6
0.9
1.2
1.5
Granular Layer Thickness, H_b (m)
Chart D52
a
b
c
d
e
E_b = 540 MPa
E_s = 60 MPa
Subgrade Soil
Type: ML
H_s
a = 0.6 m
b = 1.2 m
c = 2.4 m
d = 3.6 m
e = 6.0 m

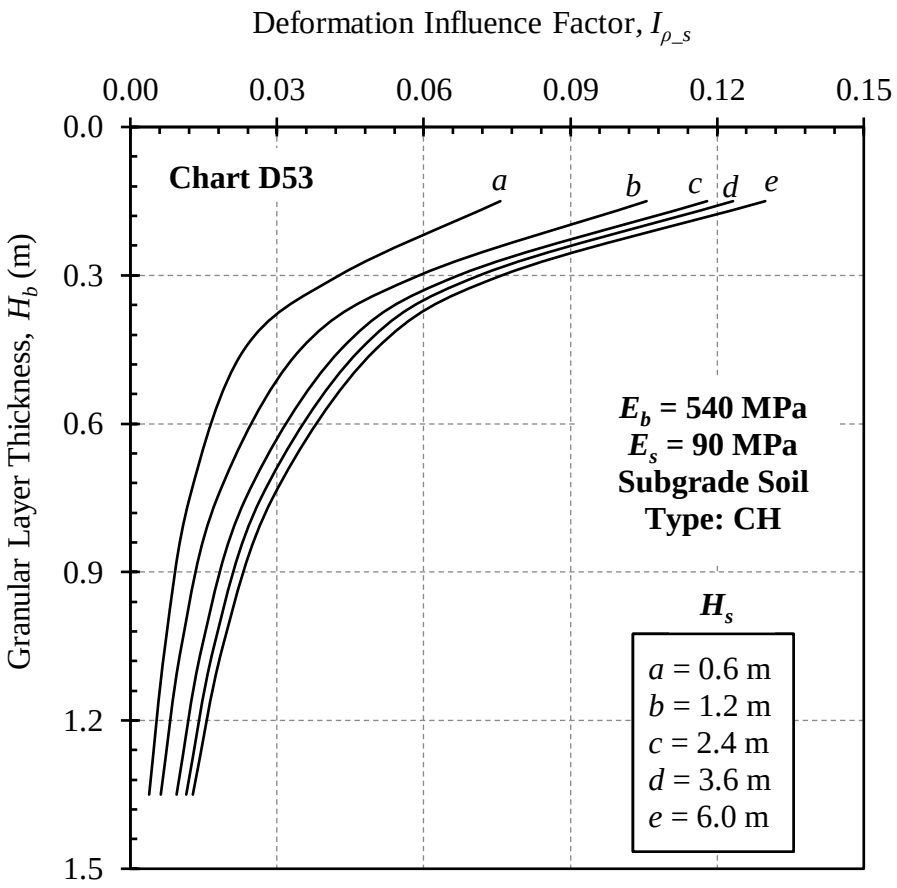
Deformation Influence Factor, I_{ρ_s}
0.00
0.03
0.06
0.09
0.12
0.15
0.0
0.3
0.6
0.9
1.2
1.5
Granular Layer Thickness, H_b (m)
Chart D53
a
b
c
d
e
E_b = 540 MPa
E_s = 90 MPa
Subgrade Soil
Type: CH
H_s
a = 0.6 m
b = 1.2 m
c = 2.4 m
d = 3.6 m
e = 6.0 m

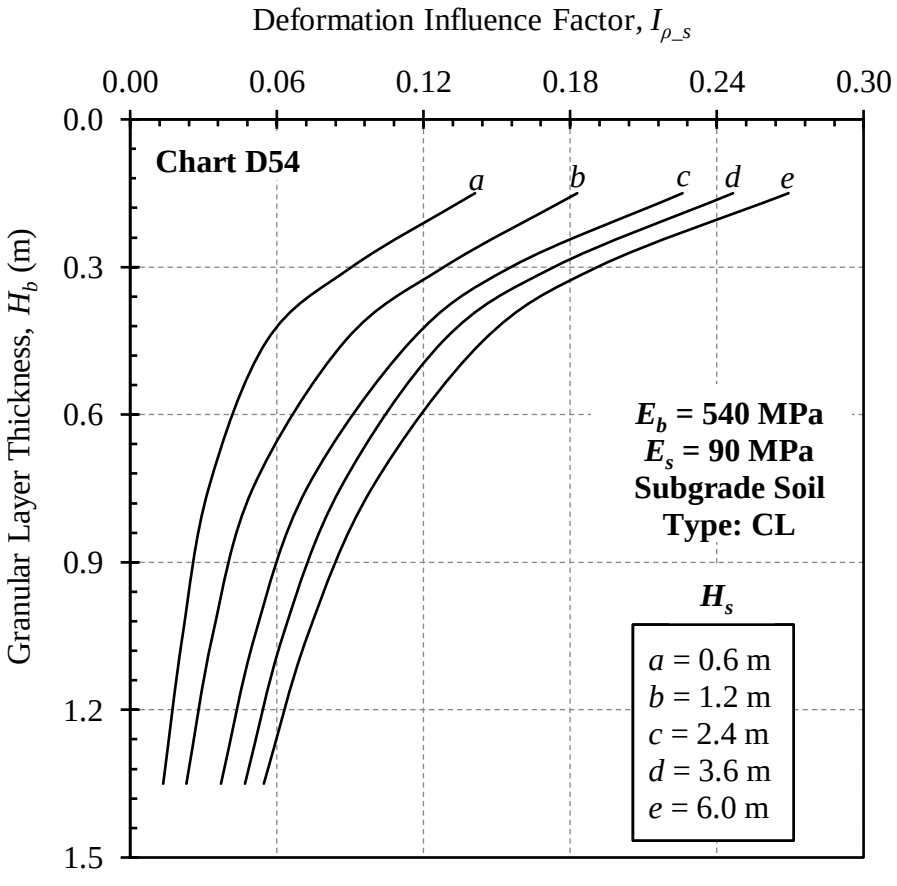
Deformation Influence Factor, I_{ρ_s}
0.00
0.06
0.12
0.18
0.24
0.30
0.0
0.3
0.6
0.9
1.2
1.5
Granular Layer Thickness, H_b (m)
Chart D54
a
b
c
d
e
E_b = 540 MPa
E_s = 90 MPa
Subgrade Soil
Type: CL
H_s
a = 0.6 m
b = 1.2 m
c = 2.4 m
d = 3.6 m
e = 6.0 m

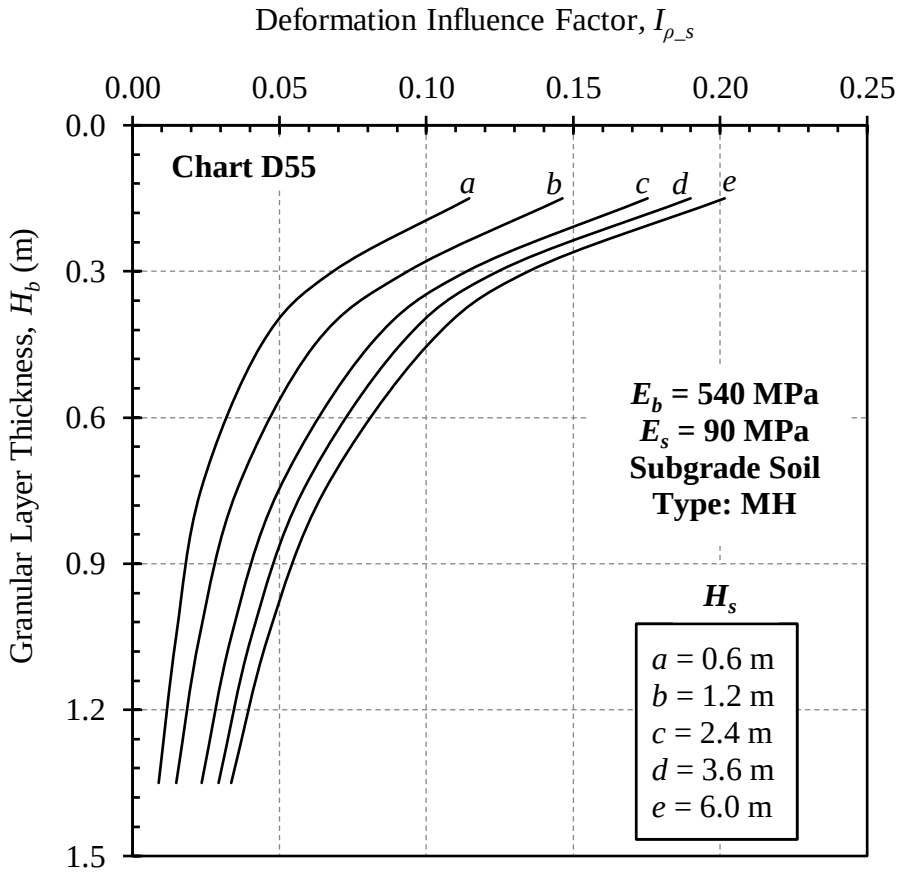
Deformation Influence Factor, I_{ρ_s}
0.00
0.05
0.10
0.15
0.20
0.25
0.0
0.3
0.6
0.9
1.2
1.5
Granular Layer Thickness, H_b (m)
Chart D55
a
b
c
d
e
E_b = 540 MPa
E_s = 90 MPa
Subgrade Soil Type: MH
H_s
a = 0.6 m
b = 1.2 m
c = 2.4 m
d = 3.6 m
e = 6.0 m

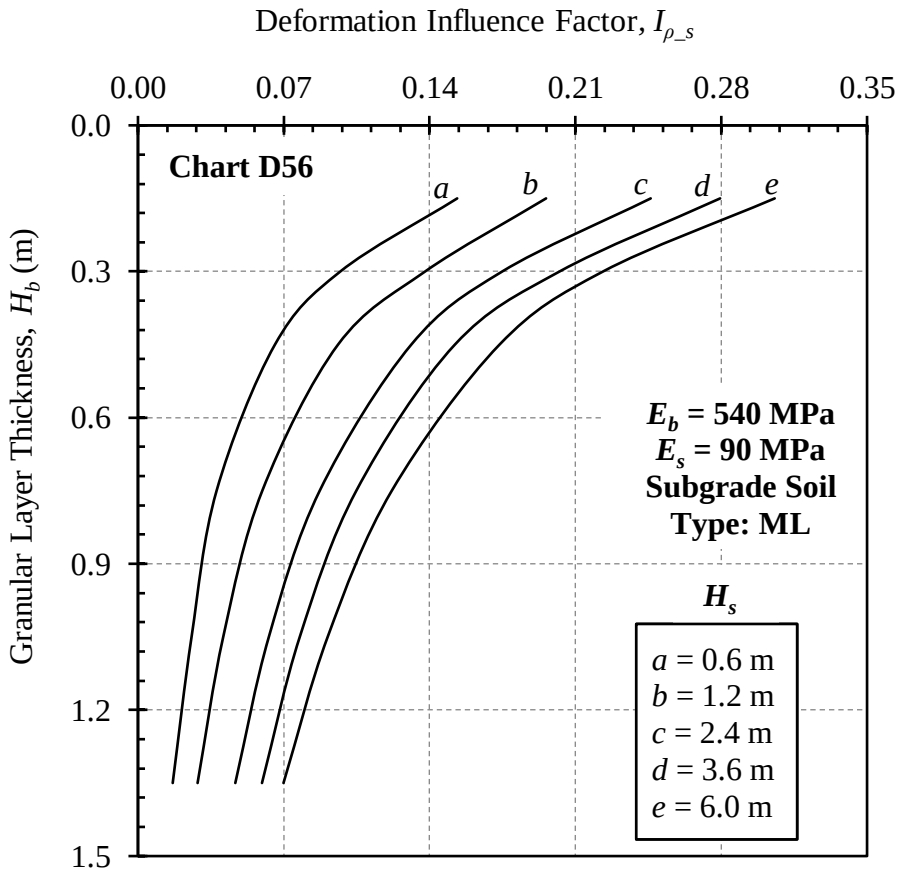
Deformation Influence Factor, I_{ρ_s}
0.00
0.07
0.14
0.21
0.28
0.35
0.0
0.3
0.6
0.9
1.2
1.5
Granular Layer Thickness, H_b (m)
Chart D56
a
b
c
d
e
E_b = 540 MPa
E_s = 90 MPa
Subgrade Soil Type: ML
H_s
a = 0.6 m
b = 1.2 m
c = 2.4 m
d = 3.6 m
e = 6.0 m

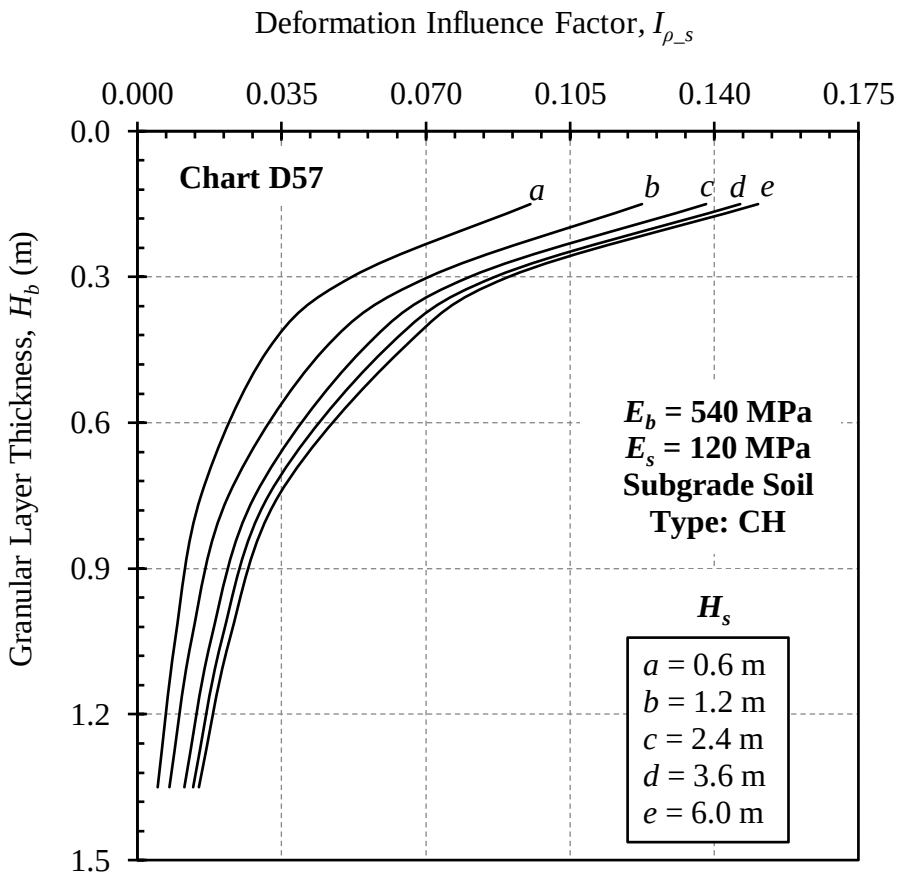
Deformation Influence Factor, I_{ρ_s}
0.000
0.035
0.070
0.105
0.140
0.175
0.0
0.3
0.6
0.9
1.2
1.5
Granular Layer Thickness, H_b (m)
Chart D57
a
b
c
d
e
E_b = 540 MPa
E_s = 120 MPa
Subgrade Soil
Type: CH
H_s
a = 0.6 m
b = 1.2 m
c = 2.4 m
d = 3.6 m
e = 6.0 m

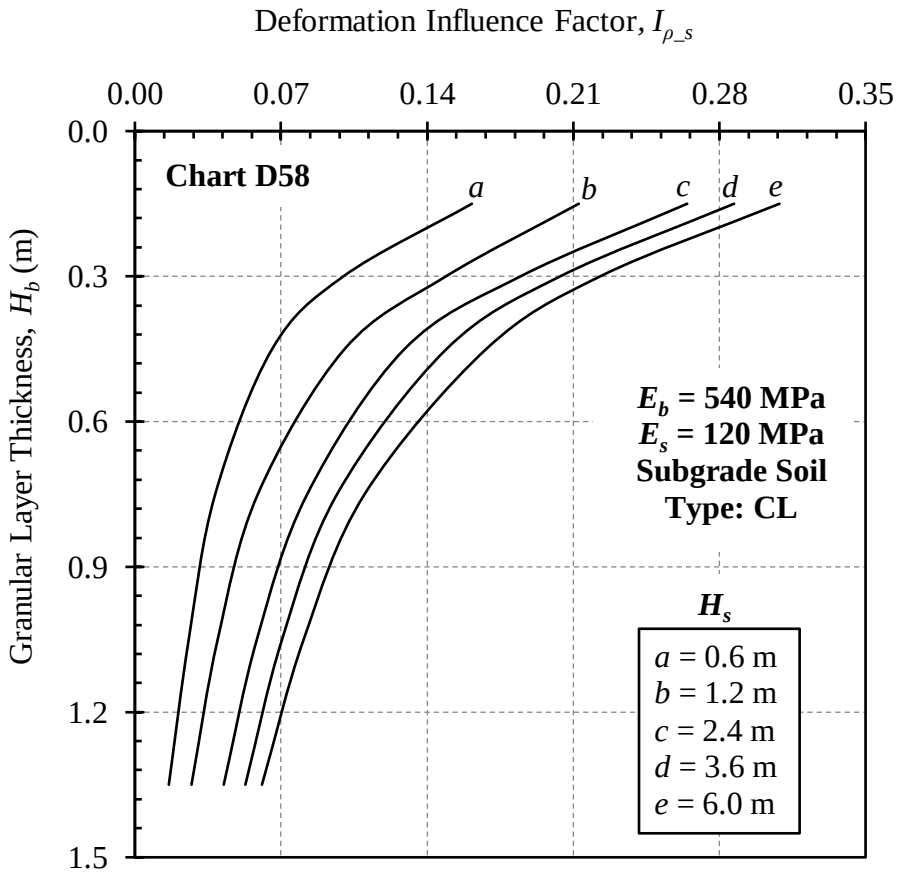
Deformation Influence Factor, I_{ρ_s}
0.00
0.07
0.14
0.21
0.28
0.35
0.0
0.3
0.6
0.9
1.2
1.5
Granular Layer Thickness, H_b (m)
Chart D58
a
b
c
d
e
E_b = 540 MPa
E_s = 120 MPa
Subgrade Soil
Type: CL
H_s
a = 0.6 m
b = 1.2 m
c = 2.4 m
d = 3.6 m
e = 6.0 m

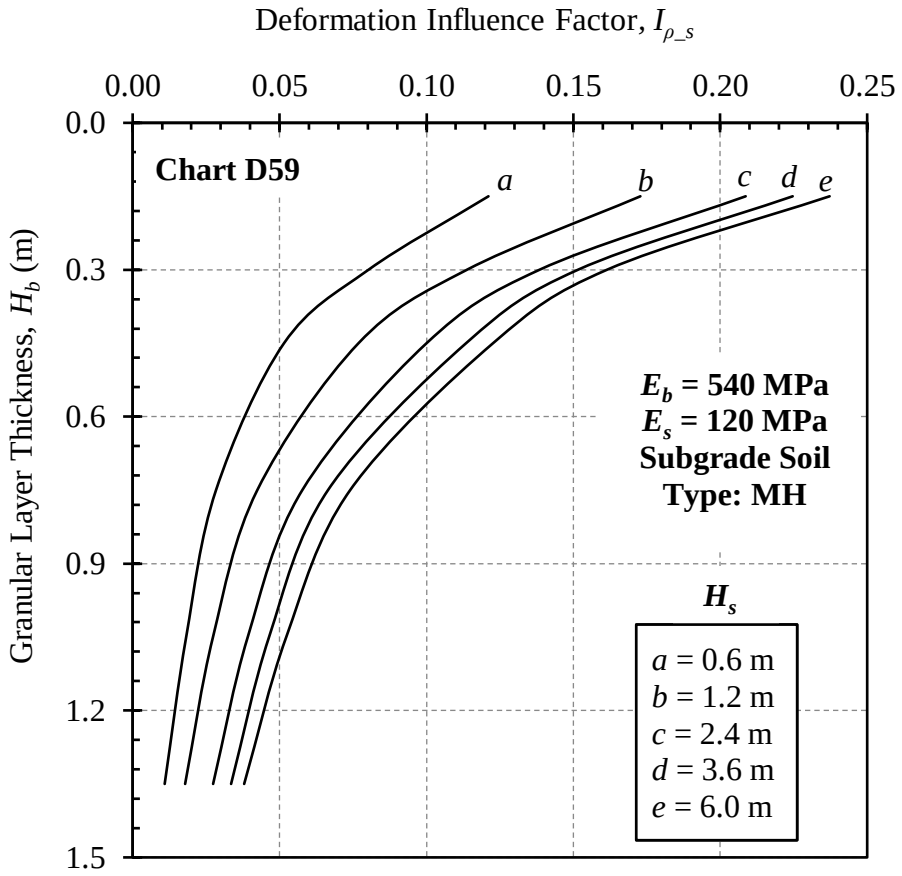
Deformation Influence Factor, I_{ρ_s}
0.00
0.05
0.10
0.15
0.20
0.25
0.0
0.3
0.6
0.9
1.2
1.5
Granular Layer Thickness, H_b (m)
Chart D59
a
b
c
d
e
E_b = 540 MPa
E_s = 120 MPa
Subgrade Soil
Type: MH
H_s
a = 0.6 m
b = 1.2 m
c = 2.4 m
d = 3.6 m
e = 6.0 m

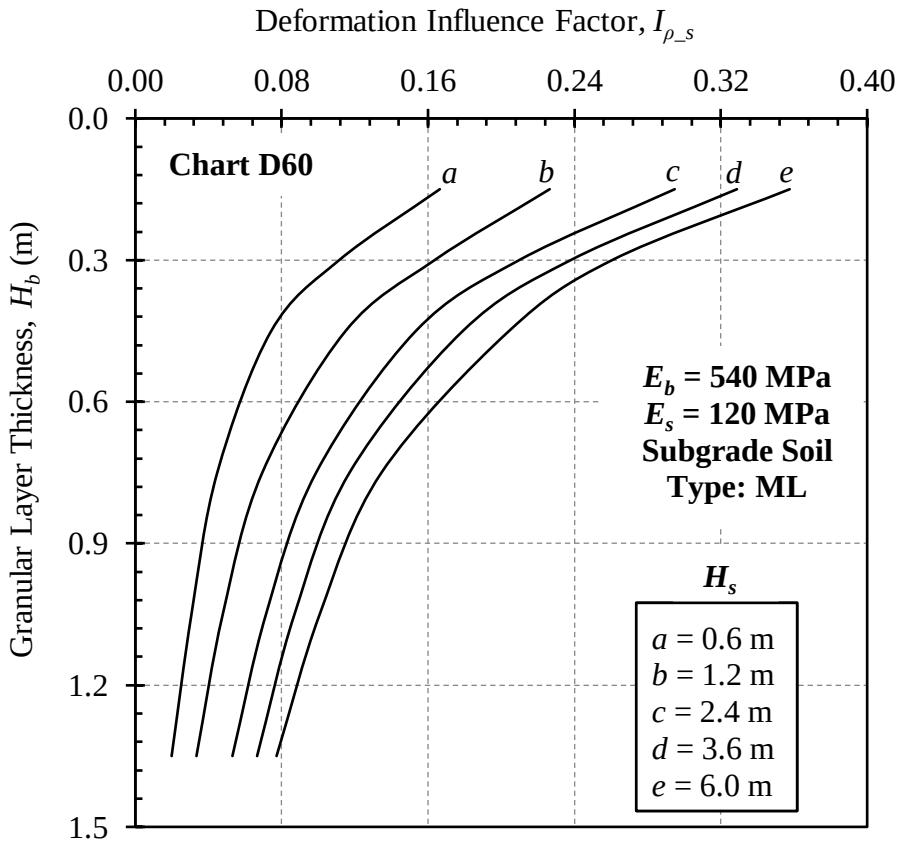
Deformation Influence Factor, I_{ρ_s}
0.00
0.08
0.16
0.24
0.32
0.40
0.0
0.3
0.6
0.9
1.2
1.5
Granular Layer Thickness, H_b (m)
Chart D60
a
b
c
d
e
E_b = 540 MPa
E_s = 120 MPa
Subgrade Soil
Type: ML
H_s
a = 0.6 m
b = 1.2 m
c = 2.4 m
d = 3.6 m
e = 6.0 m